

# Mathematical models for peristaltic motion in a channel



By

**Maryiam Javed**

**Department of Mathematics  
Quaid-i-Azam University  
Islamabad, Pakistan  
2012**

# Mathematical models for peristaltic motion in a channel



By

**Maryiam Javed**

Supervised By

**Prof. Dr. Tasawar Hayat**

**Department of Mathematics  
Quaid-i-Azam University  
Islamabad, Pakistan  
2012**

# Mathematical models for peristaltic motion in a channel



By

**Maryiam Javed**

A THESIS SUBMITTED IN THE PARTIAL FULFILLMENT OF THE REQUIREMENTS FOR  
THE DEGREE OF  
**DOCTOR OF PHILOSOPHY**

IN  
MATHEMATICS

Supervised By

**Prof. Dr. Tasawar Hayat**

**Department of Mathematics  
Quaid-i-Azam University  
Islamabad, Pakistan**

**2012**

# Mathematical models for peristaltic motion in a channel

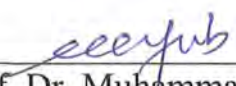
By


Maryyam Javed


## CERTIFICATE

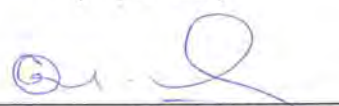
A THESIS SUBMITTED IN THE PARTIAL FULFILLMENT OF THE  
REQUIREMENTS FOR THE DEGREE OF THE DOCTOR OF  
PHILOSOPHY

We accept this thesis as conforming to the required standard

1.   
Prof. Dr. Muhammad Ayub  
(Chairman)

2.   
Prof. Dr. Tasawar Hayat  
(Supervisor)

3.   
Prof. Dr. Tahir Mahmood  
(External Examiner)

4.   
Prof. Dr. Qamar-Ul-Haq  
(External Examiner)

Department of Mathematics  
Quaid-i-Azam University  
Islamabad, Pakistan  
2012



# Dedicated to

*My loving Parents*

*&*

*My Supervisor, Prof. Dr. Tasawar Hayat*

# Acknowledgements

All the praises and appreciations are for omnipotent **Allah**, the most merciful and generous that knows better the hidden truths of the universe and His **Holy Prophet Muhammad** (Peace Be Upon Him) who declared it an obligatory duty of every Muslim to seek and acquire knowledge.

I feel great honor to express my heartiest gratitude and profoundest thanks to my worthy and devoted supervisor, **Prof. Dr. Tasawar Hayat**, for his encouraging discussions, intellectual guidance and enthusiastic interest. Words are too debilitating to express my feeling to a person who sacrifices his health for the betterment of his students and for their tomorrow. Without his generous help and patient guidance, it was not possible for me to complete this work. I am really grateful to him for introducing me to the scientific world of publication. I thank you very much Sir from the core of my heart.

I am highly obliged to **Prof. Dr. Muhammad Ayub**, Chairman Department of Mathematics, Q.A.U. for providing friendly environment for the research work in the department.

*My sincerest thanks goes to all the members of Fluid Mechanics Group especially Dr. Nasir Ali, Dr. Khadija Maqbool, Rahila, Ansa, Humaira Yasmin, Dr. Muhammad Nawaz, Zahid Bhai and Muhammad Awais for their co-operation and suggestions throughout my research work.*

*I express my heartfelt thanks to the **Higher Education Commission** of Pakistan (HEC) for the financial support that really helped me in acquiring this degree.*

*Friendship is almost always the union of a part of one mind with a part of another. I gratefully acknowledge my friends, Rahila and Asia for their prayers for my success.*

*Their company made my stay in the university full of joys and everlasting memories.*

*Each precious second will be treasured in my heart forever.*

*I also thank the office staff of the Mathematics department of Q.A.U. for their whole hearted cooperation.*

*I am also extremely thankful to my examiner, Prof. Dr. Tahir Mahmood for giving a final touch to my PhD thesis after my viva.*

*Acknowledgements are incomplete without paying regards to my family. I express my deep sense of gratitude to my parents for their love and prayers that enabled me to achieve my goals. I have no words to thank my father who developed self confidence in*

*me and my mother who really encouraged me throughout my study life. I owe my heartiest thanks to my loving and caring husband for his prayers, encouragement and moral support during my PhD. Many thanks to my in-laws, my brothers and sisters especially honey for their care, love and prayers. In the last, I cannot forget my cute and loving son, Muhammad Faizan for the love and satisfaction that he gave me in the preparation of my viva.*

*Finally, my sincere thanks to all those who have always pray for me and for my success.*

*08<sup>th</sup> June, 2012*

*Maryiam Jawed*

# Preface

Many nonlinear problems in theory of viscous fluids are governed by the Navier-Stokes equations. Such equations are inadequate for the flow description of non-Newtonian fluids. In literature, many theoretical investigations have been carried out by taking the physiological fluids to behave like a Newtonian fluid which is not true in reality. In such situations, the analysis of rheological characteristics associated with non-Newtonian fluids cannot be ignored. In particular, peristalsis appears extensively in physiological and industrial applications. Especially, the peristaltic motion of magnetohydrodynamic (MHD) flows of electrically conducting fluids has become the subject of growing interest for the researchers in recent times. This is due to the fact that such studies are useful particularly for having a proper understanding of the functioning of different machines used by clinicians for pumping blood and magnetic resonance imaging (MRI). The effect of a magnetic field on the flow of blood in atherosclerotic vessels also finds application in a blood pump used by cardiac surgeons during the surgical procedure. On the other hand, the theoretical study of MHD channel flows have many practical applications in designing cooling systems with liquid metals in many devices such as accelerators, MHD pumps, MHD power generators, electrostatic precipitation, petroleum industry, electrostatic precipitation, purification of crude oil, aerodynamics heating and fluid droplets sprays. The fluid flow in a porous space is significant specifically in geophysical fluid dynamics. The distribution of fatty cholesterol and artery clogging blood clots in the lumen of coronary artery also behave like a porous medium in the pathological situations. Moreover, the process of heat transfer is useful for the analysis of tissues. Thus, the application of heat (hyperthermia), radiation (laser therapy) and coldness (cryosurgery) has attracted the attention of the investigators in thermal modeling for the destruction of undesirable tissues such as cancer.

Keeping in view all the above mentioned facts, the present thesis is arranged as follows:

Chapter one provides the survey regarding the existing relevant literature for peristalsis in viscous/non-Newtonian fluids under various aspects.

The slip effects on the peristaltic transport of viscous fluid are analyzed in chapter two. The flow in an asymmetric channel is considered. Closed form solutions have been established under

the assumption of long wavelength and low Reynolds number. The discussion for pressure rise and frictional forces is provided through numerical integration. The results of this chapter have been published in **Numerical Methods for Partial Differential Equations 5 (2011) 1003-1015**.

The goal of chapter three is to develop a mathematical model in order to examine the slip and heat transfer effects on the MHD peristaltic flow in a channel with compliant walls. The velocity slip condition is imposed in terms of shear stress. Solutions of the axial velocity, stream function, temperature and heat transfer coefficient are derived. Further, some flow quantities of interest are analyzed through graphical results. The contents of this chapter have been published in **Asia-Pacific Journal of Chemical Engineering DOI: 10.1002/apj.470**.

The compliant wall effects on the peristaltic flow of viscous fluid in a curved channel are analyzed in chapter four. In addition, the heat transfer is considered. The series solution have been first computed and then examined by graphical illustrations. This research is published in **Int. J. Heat and Mass Transfer 54 (2011) 1615-1621**.

Chapter five presents the analysis for peristaltic flow of non-Newtonian fluid in a channel with compliant walls. Constitutive equations of a subclass of rate type fluids namely an Oldroyd-B fluid have been used. The flow is induced by the sinusoidal waves on the channel walls. Results are given and discussed for the free pumping case. This research has been published in **Int. J. Numerical Methods in Fluids DOI: 10.1002/flid.2439**.

Chapter six studies the peristaltic transport of Johnson-Segalman fluid in a compliant wall channel. This fluid model is developed to allow non-affine deformations and has been used by many investigators to explain the "spurt" phenomenon. The fluid is electrically conducting in the presence of a constant applied magnetic field. Expressions for mean velocity at the boundaries of the channel, the mean-velocity perturbation function and the time-averaged mean axial velocity distribution are derived. The effects of various emerging flow parameters are shown and discussed through graphs. This work has been published in **Phys. Lett. A 372 (2008) 5026-5036**.

Effects of wall properties on the peristaltic flow of power-law fluid in an asymmetric channel have been investigated in chapter seven. Long wavelength and low Reynolds number approximations have been adopted in the presentation of mathematical developments. Closed

form solutions are constructed for the stream function and velocity. The streamlines pattern and trapping are also discussed. The observations of this chapter are published in **Appl. Math. Mech. (English edition) 31 (2010) 1231-1240**.

The analysis of an electrically conducting Jeffrey fluid with peristalsis is presented in chapter eight. This fluid model is simplest and can describe the rheological characteristics in terms of relaxation and retardation time parameters. The nonlinear differential equations subject to appropriate boundary conditions are solved for the free pumping case. The effects of pertinent parameters on the flow quantities of interest are discussed. The research in this chapter has been published in **Zeitschrift fur Naturforschung A 66a (2011) 106-116**.

Chapter nine discusses the MHD peristaltic transport of Jeffrey fluid in a compliant wall channel with porous space. Heat transfer analysis is also considered. A regular perturbation technique is employed to solve the resulting problem. Solutions are presented in a power of small wave number. Expressions for the stream function, temperature distribution, velocity and heat transfer coefficient are computed. The influence of emerging parameters is shown on velocity, temperature distribution, heat transfer coefficient and trapping. These contents are submitted for publication in **Nonlinear Analysis: Modeling and Control**.

Chapter ten reports the peristaltic transport of compressible Jeffrey fluid in a compliant wall channel. Perturbation approach has been employed when the ratio of the wave amplitude to the radius of the pore is small. Expressions of mean axial velocity distribution, mean velocity at the boundaries and critical values are derived. The effects of various embedded parameters are discussed. This research has been accepted for publication in **Journal of Mechanics in Medicine and Biology**.



# Contents

<b>1</b>	<b>Survey of relevant literature on peristalsis</b>	<b>4</b>
<b>2</b>	<b>Slip effects on peristaltic flow in an asymmetric channel</b>	<b>11</b>
2.1	Problem formulation	11
2.2	Dimensionless formulation	13
2.3	Solution in the wave frame	15
2.4	Results and discussion	17
2.5	Concluding remarks	28
<b>3</b>	<b>Wall properties and slip effects on the magnetohydrodynamic peristaltic motion of viscous fluid with heat transfer and porous space</b>	<b>30</b>
3.1	Mathematical model	30
3.2	Non-dimensionalization	33
3.3	Solution of the problem	35
3.4	Graphical results and discussion	36
3.5	Closing remarks	47
<b>4</b>	<b>Peristaltic transport of viscous fluid in a curved channel with compliant walls</b>	<b>49</b>
4.1	Mathematical model	49
4.2	Dimensionless formulation	51
4.3	Solution of the problem	53
4.4	Graphical results and discussion	54
4.5	Final remarks	62

<b>5</b>	<b>Peristaltic motion of an Oldroyd-B fluid in a channel with compliant walls</b>	<b>63</b>
5.1	Problem definition	63
5.2	Methodology of solution	67
5.3	Discussion	73
5.4	Final remarks	78
<b>6</b>	<b>Peristaltic transport of MHD Johnson-Segalman fluid in a channel with compliant walls</b>	<b>79</b>
6.1	Problem definition	79
6.2	Solution procedure	83
6.3	Results and discussion	91
6.4	Conclusions	96
<b>7</b>	<b>Peristaltic transport of power-law fluid in an asymmetric channel with compliant walls</b>	<b>98</b>
7.1	Mathematical model	98
7.2	Solution of the problem	101
7.3	Discussion	101
7.4	Concluding remarks	107
<b>8</b>	<b>Compliant wall analysis of an electrically conducting Jeffrey fluid with peristalsis</b>	<b>109</b>
8.1	Problem development	109
8.2	Method of solution	112
8.3	Results and discussion	118
8.4	Closing remarks	124
<b>9</b>	<b>Heat transfer analysis on MHD peristaltic motion in a Jeffrey fluid with compliant walls and porous space</b>	<b>125</b>
9.1	Mathematical model	125
9.2	Solution of the problem	129
9.3	Graphical results and discussion	131

9.4	Conclusions . . . . .	146
<b>10</b>	<b>Wall compliance effect on the flow of compressible non-Newtonian fluid</b>	<b>147</b>
10.1	Mathematical model . . . . .	147
10.2	Solution development . . . . .	150
10.3	Graphical results and discussion . . . . .	153
10.4	Conclusions . . . . .	162

## Chapter 1

# Survey of relevant literature on peristalsis

Although peristalsis occur very well in physiology but its appearance is witnessed from the seminal works of Kill [1] and Boyarsky [2]. In view of Kill, the normal renal pelvis and ureter can tolerate a flow of 8-10 ml/ min per ureter without increasing pelvic pressure. Despite extensive research regarding the function of the mammalian kidney, scarce information is available about the functional anatomy of the renal pelvis. Graves and Davidoff [3] have discussed ureteral reflux in normal and abnormal bladders and ureters. Since then, an exhaustive research is undertaken on peristalsis. Latham [4] initiated the step for the analysis of peristaltic transport. The flow of viscous fluid in a flexible tube is examined by Shapiro [5] when the creeping and wave number is small. Burns and Parkes [6] analyzed the flow of a viscous fluid through axially symmetric pipes and symmetrical channels. Analysis in this attempt has been carried out for small Reynolds number. Fung and Yih [7] investigated two-dimensional viscous flow in a channel. Analytic solution is constructed for small amplitude ratio. It is found that the reflux phenomenon is possible at the channel centre. Shapiro et al. [8] presented a mathematical model of peristaltic transport subject to long wavelength and low Reynolds number assumptions. They discussed the viscous flow in both channel and tube. Hanin [9] reported the flow analysis of viscous fluid under the assumptions of large Reynolds number, small amplitude and long wavelength. Meginniss [10] applied the inertial free long wavelength

theory of peristaltic pumping by choosing particular geometry of the tube of a roller pump. Weinberg [11] and Eckstein [12] presented the theoretical and experimental attempts regarding peristaltic pumping. Zein and Ostrach [13] have studied an incompressible viscous fluid in a two dimensional channel under long wavelength approximation. Mathematical analysis in this attempt has been carried out by taking into account the assumption when the wavelength of the peristaltic wave is very small in comparison to half width of the channel. The coupling between the forces of fluid-mechanical origin and the dynamics of the ureteral muscle was investigated by Fung [14]. More realistic model about the uteral waves has been examined by Lykoudis [15]. Jaffrin and Shapiro [16] presented a review article on peristalsis in view of different flow geometry, amplitude ratio, wave number and Reynolds number. Mitra and Prasad [17] studied the peristaltic transport in the presence of pressure gradient. Wilson and Panton [18] discussed the two-dimensional peristaltic transport of a viscous incompressible fluid due to finite amplitude bending and contraction waves. Axisymmetric viscous peristaltic flow is examined analytically by Barton and Raynor [19]. Yin and Fung [20] provided asymptotic solutions to axisymmetric peristaltic flow in powers of the ratio of amplitude to the mean tube radius. Li [21] studied the problem of peristaltic pumping in a circular tube using long wavelength approximation. He further presented a comparison for the two-dimensional flow in channel and axisymmetric flow in a tube. Chow [22] examined the peristaltic transport of an incompressible viscous fluid in a circular cylindrical pipe. Lew and Fung [23] found the results for the flow in valved vessel under small Reynolds number. Tong and Vawter [24] discussed numerically the peristaltic pumping in a circular tube using finite-element method. Manton [25] obtained the asymptotic solution for the low Reynolds number flow in an axisymmetric tube when peristaltic waves of arbitrary shape have been considered. The peristaltic flow through non-uniform channels and tubes with special emphasis regarding the flow of spermatic fluid in vas deferens is considered by Gupta and Seshadri [26]. They discussed the mathematical model for the creeping flow. Liron [27] introduced the idea regarding the efficiency of peristaltic fluid transport. Series solution for peristaltic flow in pipe and channel was constructed by employing double expansion in terms of the Reynolds number and the square of the wave number. Rath [28] looked at the peristaltic flow through a lobe-shaped tube. The interaction of peristaltic motion with pulsatile flow is studied by Srivastava and Srivastava [29]. They considered the peristaltic flow of viscous fluid

in a circular cylindrical tube. An arbitrary periodic pressure gradient is applied and solution is constructed for small amplitude ratio. On the other hand, a numerical technique using boundary integral method has been developed by Pozrikidis [30] just to study the peristaltic transport in an asymmetric channel under Stokes flow conditions. In this study, the creeping flow is studied by boundary integral technique. Takabatake et al. [31] solved the problem of peristaltic pumping in an axisymmetric tube by generalizing the numerical method of Takabatake and Ayukawa [32] to the axisymmetric case. Eytan and Elad [33] have developed a mathematical model for peristaltic flow of viscous fluid in an asymmetric channel. Lubrication approach has been used for the solution of time dependent flow in a fixed frame. They have also calculated the possible particle trajectories in order to examine embryo transport before it gets implanted at the uterine wall. Mishra and Rao [34] examined the flow of a viscous incompressible fluid in an asymmetric channel. Asymmetry is generated through waves propagating on the walls with different amplitudes and phase. Rao and Mishra [35] also investigated the curvature effects on the peristaltic flow of viscous fluid in an asymmetric channel. The problem of peristaltic transport of a viscous incompressible fluid through uniform and non-uniform annulus is studied by Mekheimer [36]. This analysis was examined for long wavelength approximation.

All the above mentioned investigations deal with the peristaltic motion of viscous fluid under different aspects. There is another area, namely, the non-Newtonian fluid mechanics in which peristaltic mechanism was also analyzed previously. Such consideration is very important because many fluids in the physiological world are non-Newtonian. Peristaltic flow of power law fluid in a tube was first studied by Raju and Devanathan [37]. The solution was derived for the stream function in power series of the amplitude of deformation. Devi and Devanathan [38] discussed the peristaltic motion of a micropolar fluid under the assumption of small wave amplitude. Radhakrishnamacharya [39] reported the peristaltic motion of a power law fluid in a two-dimensional channel. The solution for the stream function is derived as an asymptotic expansion in terms of slope parameter. Bohme and Friedrich [40] examined the peristaltic transport of viscoelastic fluids for low Reynolds number. Srivastava and Srivastava [41] have discussed the peristaltic flow by considering a two-fluid model. Mathematical modelling is developed for a Casson fluid and flow is treated creeping. The peristaltic motion of power law fluid in the uniform and non-uniform tubes with reference to the vas deferens and small intestine

is studied by Srivastava and Srivastava [42]. Peristaltic flows for second and third grade fluids have been examined by Siddiqui and Schwarz [43,44]. Usha and Rao [45] analyzed the peristaltic transport of two-layered power-law fluids in axisymmetric tubes. They observed a negative time-mean flow for the free pumping case when one of the peripheral layer and core fluids is non-Newtonian. El Shehawey et al. [46] reported the peristaltic transport of Carreau fluid in non-uniform channel for low Reynolds number and long wavelength approximation. El Shehawey and Sobh [47] carried out the analysis for the peristaltic motion of a viscoelastic fluid in tube. Hakeem et al [48] examined the endoscopic effects on the peristaltic transport of a Carreau fluid. This work was discussed under low Reynolds number and long wavelength. The peristaltic transport of a Couple-Stress fluid in uniform and non-uniform two-dimensional channels has been investigated by Mekheimer [49]. Hayat et al. [50,51] examined the peristaltic transport of Johnson-Segalman and Oldroyd-B fluids in a planar channel. Vajravelu et al. [52,53] studied the peristaltic transport of Herschel-Bulkley fluid in a channel/inclined tube. They constructed expressions of velocity distribution, stream function and volume flow rate. Haroun [54] discussed the peristaltic motion of third order fluid in an asymmetric channel. Analytic solution is developed for small Deborah number.

Recently there are several studies describing the effects of MHD, porosity, heat transfer and slip on the peristaltic transport of viscous and non-Newtonian fluids. For instance, the effect of moving magnetic field on blood flow was studied by Stud et al. [55]. It is noticed that the magnetic field effect accelerates the speed of blood. Srivastava and Agrawal [56] considered the blood as an electrically conducting fluid and constitutes a suspension of red cell in plasma. Agrawal and Anwaruddin [57] studied the influence of magnetic field on blood flow through an equally branched channel with flexible outer walls executing peristaltic waves. Mekheimer [58] studied the peristaltic transport of blood in non-uniform channels when a uniform magnetic field is applied. Tzirtzilakis [59] has illustrated a mathematical model of blood flow under the action of an applied magnetic field. Hayat and Ali [60] discussed the MHD peristaltic transport of third grade fluid in a tube. The peristaltic flow of a Jeffrey fluid in an asymmetric channel is studied by Kothandapani and Srinivas [61] subject to large wavelength and low Reynolds number assumptions. The study of peristaltic flow through a porous medium was presented by El Shehawey et al. [62]. El Shehawey and Husseny [63] studied the effects of porous boundaries



on peristaltic transport in a porous space. El Shehawey et al. [64] analyzed the peristaltic motion of generalized Newtonian fluid through a porous medium. El Shehawey and Husseny [65] also analyzed the peristaltic pumping of a viscous incompressible and electrically conducting fluid in the porous walls of a two-dimensional channel. Sobh [66] studied the peristaltic transport of a MHD viscous fluid saturating a porous medium in uniform channel. Hayat et al. [67] analyzed the peristaltic transport of an incompressible, electrically conducting Maxwell fluid in a planar channel. The effect of Hall current is taken into account and permeability of porous medium is considered uniform. Kothandapani and Srinivas [68] reported the peristaltic transport of viscous fluid in an inclined asymmetric channel with a porous medium. The peristaltic flow of Newtonian/non-Newtonian fluids in the presence of heat transfer has many applications in biomedical science and electronic industry. Radhakrishnamacharya and Murty [69] considered the heat transfer analysis on the peristaltic activity of viscous fluid in a non-uniform channel. Vajravelu et al. [70] discussed the heat transfer effects on peristaltic flow of viscous fluid in a vertical porous annular region between two concentric tubes. Mekheimer and Elmaboud [71] analyzed the heat transfer and magnetic field effects on peristaltic transport of viscous fluid in a vertical annulus. Analysis is performed through low Reynolds number and long-wavelength approximation. Srinivas and Kothandapani [72] have discussed the heat transfer effects on MHD peristaltic flow of viscous fluid in an asymmetric channel. The heat transfer effects on peristaltic motion of viscous fluid in a vertical asymmetric channel with porous medium was studied by Srinivas and Gayathri [73]. Hayat et al. [74] reported the heat transfer effects on MHD peristaltic transport of viscous fluid in an asymmetric channel with porous medium. Mekheimer et al. [75] analyzed the effects of heat transfer and space porosity on the peristaltic transport of a Newtonian fluid in a vertical asymmetric channel. Influence of partial slip/heat transfer on the peristaltic flow are studied by Hayat et al. [76], Ali et al. [77], Ebaid [78], Hayat et al. [79] and Yildirim and Sezer [80].

It is noticed from the available studies that very less attention is focused to the peristaltic flows in curved channel. The peristaltic flow in curved channel or tubes is important in context of its applications in several flows of physiological conduits. Sato et al. [81] examined the peristaltic flow in a two-dimensional rectangular curved channel in the fixed frame of reference. Ali et al. [82] discussed the peristaltic flow of viscous fluid in a curved channel. Closed form

solutions of the stream function, axial velocity and pressure gradient are developed under long wavelength and low Reynolds number assumptions. Ali et al. [83] extended the flow analysis of ref. [82] in view of heat transfer effects. The peristaltic flow of third grade fluid in a curved channel has been discussed by Ali et al. [84].

Although there is a growing body of literature on the peristaltic transport in a channel/tube with non-compliant walls but there are some studies describing the wall properties on the peristaltic motion in a channel/tube. Mention may be made in this direction to the interesting attempts by Mitra and Prasad [85], Camenschi [86], Camenschi and Sandru [87] and Carew and Pedley [88]. Davies and Carpenter [89] examined the stability of plane channel flow with compliant walls. The peristaltic motion in circular cylindrical tubes with compliant feature is discussed by Muthu et al. [90]. Haroun [91] studied the effect of wall properties on peristaltic transport of viscous fluid in an asymmetric channel. Radhakrishnamacharya and Srinivasulu [92] analyzed the wall properties effects on peristaltic transport with heat transfer. Effects of heat transfer and wall properties on MHD peristaltic transport with heat transfer and porous medium was examined by Kothandapani and Srinivas [93]. Muthu et al. [94] reported the peristaltic motion of micropolar fluid in a circular cylindrical flexible tube with viscoelastic or elastic wall properties. Mean axial velocity is given due attention for free pumping situation. Abd Elnaby and Haroun [95] analyzed the effect of wall properties on peristaltic transport of viscous fluid. Ali et al. [96] examined the peristaltic flow of Maxwell fluid in a compliant wall channel. Srinivas et al. [97] studied the peristaltic flow with compliant walls in the presence of slip condition and heat transfer. Hayat and Hina [98] discussed the effects of heat and mass transfer on the magnetohydrodynamic peristaltic flow in a two-dimensional planar channel. The channel walls are taken to be compliant and an incompressible Maxwell fluid occupies a porous space. Slip and heat transfer effects on the peristaltic flow in an asymmetric channel have been examined by Hayat et al. [99]. The closed form solutions of momentum and energy equations are obtained for long wavelength and low Reynolds number approximations. Numerical integration technique has been applied to discuss the pumping and trapping phenomena.

Available literature on the peristaltic transport witnesses that less attention has been given to the case of a compressible fluid. In this regard, few investigations have been presented. For example Tsiklauri and Beresnev [100] discussed the peristaltic motion of compressible Maxwell

fluid. Hayat et al. [101] extended the flow analysis of ref. [100] for a Jeffrey fluid. The peristaltic transport of a compressible viscous fluid through a tapered pore is studied by Elshehawey et al. [102]. Mekheimer and Abdel-Wahab [103] examined the wall properties effect on peristaltic flow of compressible viscous fluid in a microchannel.

## Chapter 2

# Slip effects on peristaltic flow in an asymmetric channel

The magnetohydrodynamic (MHD) peristaltic flow of viscous fluid in an asymmetric channel is theoretically analyzed. The analysis is discussed by taking the slip effects into account. The solutions for stream function, longitudinal pressure gradient and temperature have been constructed in closed form. Long wavelength and low Reynolds number approximations is employed throughout the analysis of computations. A discussion for pressure rise and frictional forces is provided through numerical integration. Finally, the effects of various key parameters are discussed with the help of graphs and tables.

### 2.1 Problem formulation

We consider asymmetric channel of width  $d_1 + d_2$  filled with an incompressible viscous fluid. The fluid is electrically conducting under the influence of a uniform applied magnetic field  $\mathbf{B} = (0, B_0, 0)$  and the induced magnetic field is negligible for small magnetic Reynolds number. The temperatures of the upper and lower walls of the channel are taken as  $T_0$  and  $T_1$  respectively. The imposed travelling waves of small amplitudes on the insulating walls of channel are defined

by

$$\begin{aligned}
Y &= H_1(X, Y, t) = d_1 + a_1 \cos\left(\frac{2\pi}{\lambda}(X - ct)\right), & \text{upper wall,} \\
Y &= H_2(X, Y, t) = -d_2 - b_1 \cos\left(\frac{2\pi}{\lambda}(X - ct) + \Phi\right), & \text{lower wall,}
\end{aligned}$$

where  $a_1^2 + b_1^2 + 2a_1b_1 \cos \Phi \leq (d_1 + d_2)^2$ ,  $\lambda$  is the wavelength,  $c$  is the wave speed,  $\Phi$  ( $0 \leq \Phi \leq \pi$ ) the phase difference,  $a_1$ ,  $b_1$  are the wave amplitudes and  $X$  and  $Y$  are the Cartesian coordinates with  $X$  measured in the direction of the wave propagation and  $Y$  measured in the direction normal to the mean position of the channel walls. Furthermore, for  $\Phi = 0$  and  $\Phi = \pi$  we have symmetric channel with waves out of phase and in phase, respectively. The system in the laboratory frame is represented by the following governing equations

$$\frac{\partial U}{\partial X} + \frac{\partial V}{\partial Y} = 0, \quad (2.1)$$

$$\rho \left( \frac{\partial}{\partial t} + U \frac{\partial}{\partial X} + V \frac{\partial}{\partial Y} \right) U = -\frac{\partial P}{\partial X} + \mu \left( \frac{\partial^2}{\partial X^2} + \frac{\partial^2}{\partial Y^2} \right) U - \sigma B_0^2 U, \quad (2.2)$$

$$\rho \left( \frac{\partial}{\partial t} + U \frac{\partial}{\partial X} + V \frac{\partial}{\partial Y} \right) V = -\frac{\partial P}{\partial Y} + \mu \left( \frac{\partial^2}{\partial X^2} + \frac{\partial^2}{\partial Y^2} \right) V, \quad (2.3)$$

$$\xi \left( \frac{\partial}{\partial t} + U \frac{\partial}{\partial X} + V \frac{\partial}{\partial Y} \right) T = -\frac{k}{\rho} \nabla^2 T + \nu \left[ \left\{ \begin{array}{l} 2 \left( \frac{\partial U}{\partial X} \right)^2 + 2 \left( \frac{\partial V}{\partial Y} \right)^2 \\ + \left( \frac{\partial U}{\partial Y} + \frac{\partial V}{\partial X} \right)^2 \end{array} \right\} \right], \quad (2.4)$$

where  $U$  and  $V$  are the velocity components in the  $X$  and  $Y$  directions respectively and  $\rho$ ,  $t$ ,  $P$ ,  $\mu$ ,  $\nu$ ,  $\sigma$ ,  $\xi$ ,  $k$  and  $T$  are the fluid density, the time, the pressure, the dynamic viscosity, the kinematic viscosity, the electrical conductivity, the specific heat, the thermal conductivity and the temperature respectively.

The transformation between laboratory and wave frames are

$$x = X - ct, \quad y = Y, \quad u = U - ct, \quad v = V, \quad p(x) = P(X, t). \quad (2.5)$$

Upon making use of the above transformations, we have from Eqs. (2.1) – (2.4) as follows

$$\frac{\partial u}{\partial x} + \frac{\partial v}{\partial y} = 0, \quad (2.6)$$

$$\rho \left( u \frac{\partial}{\partial x} + v \frac{\partial}{\partial y} \right) u = -\frac{\partial p}{\partial x} + \mu \left( \frac{\partial^2}{\partial x^2} + \frac{\partial^2}{\partial y^2} \right) u - \sigma B_0^2 u, \quad (2.7)$$

$$\rho \left( u \frac{\partial}{\partial x} + v \frac{\partial}{\partial y} \right) v = -\frac{\partial p}{\partial y} + \mu \left( \frac{\partial^2}{\partial x^2} + \frac{\partial^2}{\partial y^2} \right) v, \quad (2.8)$$

$$\xi \left( u \frac{\partial}{\partial x} + v \frac{\partial}{\partial y} \right) T = -\frac{k}{\rho} \nabla^2 T + \nu \left[ \left\{ \begin{array}{l} 2 \left( \frac{\partial u}{\partial x} \right)^2 + 2 \left( \frac{\partial v}{\partial y} \right)^2 \\ + \left( \frac{\partial u}{\partial y} + \frac{\partial v}{\partial x} \right)^2 \end{array} \right\} \right] \quad (2.9)$$

## 2.2 Dimensionless formulation

Defining

$$\begin{aligned} \bar{x} &= \frac{x}{\lambda}, \quad \bar{y} = \frac{y}{d_1}, \quad \bar{u} = \frac{u}{c}, \quad \bar{v} = \frac{v}{c\delta}, \quad \delta = \frac{d_1}{\lambda}, \quad \bar{p} = \frac{d_1^2 p}{\mu c \lambda}, \\ \bar{t} &= \frac{ct}{\lambda}, \quad h_1 = \frac{H_1}{d_1}, \quad h_2 = \frac{H_2}{d_2}, \quad d = \frac{d_2}{d_1}, \quad a = \frac{a_1}{d_1}, \quad b = \frac{b_1}{d_1}, \\ R &= \frac{cd_1}{\nu}, \quad \bar{\Psi} = \frac{\Psi}{cd_1}, \quad M^2 = \frac{\sigma B_0^2 d_1^2}{\mu}, \quad \theta = \frac{T - T_0}{T_1 - T_0}, \\ \text{Pr} &= \frac{\rho \nu \xi}{k}, \quad E = \frac{c^2}{\xi (T_1 - T_0)} \end{aligned}$$

and setting

$$\bar{u} = \frac{\partial \bar{\Psi}}{\partial \bar{y}}, \quad \bar{v} = -\frac{\partial \bar{\Psi}}{\partial \bar{x}},$$

equation (2.6) is automatically satisfied and Eqs.(2.7)-(2.9) become

$$R\delta \left( -\frac{\partial \bar{\Psi}}{\partial \bar{y}} \frac{\partial^2 \bar{\Psi}}{\partial \bar{x} \partial \bar{y}} - \frac{\partial \bar{\Psi}}{\partial \bar{x}} \frac{\partial^2 \bar{\Psi}}{\partial \bar{y}^2} \right) = -\frac{\partial \bar{p}}{\partial \bar{x}} + \left( \delta^2 \frac{\partial^3 \bar{\Psi}}{\partial \bar{x}^2 \partial \bar{y}} + \frac{\partial^3 \bar{\Psi}}{\partial \bar{y}^3} \right) - M^2 \left( \frac{\partial \bar{\Psi}}{\partial \bar{y}} + 1 \right), \quad (2.10)$$

$$R\delta^3 \left( -\frac{\partial \bar{\Psi}}{\partial \bar{y}} \frac{\partial^2 \bar{\Psi}}{\partial \bar{x}^2} + \frac{\partial \bar{\Psi}}{\partial \bar{x}} \frac{\partial^2 \bar{\Psi}}{\partial \bar{x} \partial \bar{y}} \right) = -\frac{\partial \bar{p}}{\partial \bar{y}} + \delta^2 \left( -\delta^2 \frac{\partial^3 \bar{\Psi}}{\partial \bar{x}^3} - \frac{\partial^3 \bar{\Psi}}{\partial \bar{x} \partial \bar{y}^2} \right), \quad (2.11)$$

$$\begin{aligned} \text{Pr} R\delta \left( \frac{\partial \bar{\Psi}}{\partial \bar{y}} \frac{\partial \theta}{\partial \bar{x}} - \frac{\partial \bar{\Psi}}{\partial \bar{x}} \frac{\partial \theta}{\partial \bar{y}} \right) &= -\left( \delta^2 \frac{\partial^2 \theta}{\partial \bar{x}^2} + \frac{\partial^2 \theta}{\partial \bar{y}^2} \right) + \text{Pr} E \left[ 2\delta^2 \left( \frac{\partial^2 \bar{\Psi}}{\partial \bar{x} \partial \bar{y}} \right)^2 \right. \\ &\quad \left. + 2\delta^2 \left( \frac{\partial^2 \bar{\Psi}}{\partial \bar{x} \partial \bar{y}} \right)^2 + \left( \frac{\partial^2 \bar{\Psi}}{\partial \bar{y}^2} - \delta^2 \frac{\partial^2 \bar{\Psi}}{\partial \bar{x}^2} \right)^2 \right]. \quad (2.12) \end{aligned}$$

Under long wavelength and low Reynolds number, the following equations are obtained

$$\frac{\partial^4 \Psi}{\partial y^4} - M^2 \frac{\partial^2 \Psi}{\partial y^2} = 0, \quad (2.13)$$

$$\frac{dp}{dx} = \frac{\partial^3 \Psi}{\partial y^3} - M^2 \left( \frac{\partial \Psi}{\partial y} + 1 \right), \quad (2.14)$$

$$\frac{1}{Pr} \left( \frac{\partial^2 \theta}{\partial y^2} \right) + E \left( \frac{\partial^2 \Psi}{\partial y^2} \right)^2 = 0, \quad (2.15)$$

in which bars have been suppressed for simplicity,  $\partial p / \partial y = 0$ ,  $\Psi$  is the stream function,  $M$  is the Hartman number,  $Pr$  is the Prandtl number and  $E$  is the Eckert number. Moreover  $\delta$  is the wave number,  $R$  is the Reynolds number and  $a$ ,  $b$ ,  $\Phi$  and  $d$  satisfy [72]

$$a^2 + b^2 + 2ab \cos \Phi \leq (1 + d)^2. \quad (2.16)$$

If  $q$  is the flux in the wave frame, then the dimensionless boundary conditions are

$$\Psi = \frac{q}{2} \quad \text{at } y = h_1(x) = 1 + a \cos 2\pi x, \quad (2.17)$$

$$\Psi = -\frac{q}{2} \quad \text{at } y = h_2(x) = -d - b \cos(2\pi x + \Phi), \quad (2.18)$$

$$\frac{\partial \Psi}{\partial y} + \beta \frac{\partial^2 \Psi}{\partial y^2} = -1 \quad \text{at } y = h_1, \quad (2.19)$$

$$\frac{\partial \Psi}{\partial y} - \beta \frac{\partial^2 \Psi}{\partial y^2} = -1 \quad \text{at } y = h_2, \quad (2.20)$$

$$\theta + \gamma \frac{\partial \theta}{\partial y} = 0 \quad \text{at } y = h_1, \quad (2.21)$$

$$\theta - \gamma \frac{\partial \theta}{\partial y} = 1 \quad \text{at } y = h_2. \quad (2.22)$$

It should be noted that Eqs.(2.19)-(2.22) are the slip conditions for the velocity and temperature respectively and  $\beta = \alpha/d_1$ ,  $\gamma = \eta/d_1$  ( $\alpha$  and  $\eta$  are the dimensional slip parameters corresponding to velocity and thermal slip conditions).



### 2.3 Solution in the wave frame

The solution of Eq. (2.13) is given as

$$\Psi = A_1 + A_2 y + A_3 \cosh My + A_4 \sinh My. \quad (2.23)$$

Using the boundary conditions (2.17)-(2.22), the values of  $A_i$ 's ( $i = 1, 2, 3, 4$ ) are

$$A_1 = \frac{q}{2} - \frac{qh_1}{h_1 - h_2} - \frac{(h_2 - h_1 - q)(h_1 + h_2)(1 - \cosh M(h_1 - h_2) - \beta M \sinh M(h_1 - h_2))}{\left\{ \begin{array}{l} 2 - 2(\cosh M(h_1 - h_2) + \beta M \sinh M(h_1 - h_2)) \\ + M(h_1 - h_2)[\sinh M(h_1 - h_2) + 2\beta M \cosh M(h_1 - h_2) \\ + \beta^2 M^2 \sinh M(h_1 - h_2)] \end{array} \right\}}, \quad (2.24)$$

$$A_2 = \frac{q}{h_1 - h_2} + \frac{(h_2 - h_1 - q)(2 - 2 \cosh M(h_1 - h_2) - 2\beta M \sinh M(h_1 - h_2))}{(h_1 - h_2) \left\{ \begin{array}{l} 2 - 2(\cosh M(h_1 - h_2) + \beta M \sinh M(h_1 - h_2)) \\ + M(h_1 - h_2)[\sinh M(h_1 - h_2) \\ + 2\beta M \cosh M(h_1 - h_2) + \beta^2 M^2 \sinh M(h_1 - h_2)] \end{array} \right\}}, \quad (2.25)$$

$$A_3 = \frac{(h_1 - h_2 + q)(\cosh Mh_1 - \cosh Mh_2 + \beta M(\sinh Mh_1 + \sinh Mh_2))}{\left\{ \begin{array}{l} 2 - 2(\cosh M(h_1 - h_2) + \beta M \sinh M(h_1 - h_2)) \\ + M(h_1 - h_2)[\sinh M(h_1 - h_2) \\ + 2\beta M \cosh M(h_1 - h_2) + \beta^2 M^2 \sinh M(h_1 - h_2)] \end{array} \right\}}, \quad (2.26)$$

$$A_4 = -\frac{(h_1 - h_2 + q)(\sinh Mh_1 - \sinh Mh_2 + \beta M(\cosh Mh_1 + \cosh Mh_2))}{\left\{ \begin{array}{l} 2 - 2(\cosh M(h_1 - h_2) + \beta M \sinh M(h_1 - h_2)) \\ + M(h_1 - h_2)[\sinh M(h_1 - h_2) \\ + 2\beta M \cosh M(h_1 - h_2) + \beta^2 M^2 \sinh M(h_1 - h_2)] \end{array} \right\}}, \quad (2.27)$$

Integration of Eq. (2.15) yields

$$\theta = -\frac{\text{Pr} EM^4}{2} \left[ \frac{A_3^2 - A_4^2 y^2}{2} + \frac{A_3^2 + A_4^2}{4M^2} \cosh 2My + \frac{A_3 A_4}{2M^2} \sinh 2My \right] + C_1 y + C_2. \quad (2.28)$$

Using the boundary conditions (2.21) and (2.22), the expressions of  $C_1$  and  $C_2$  are given by

$$C_1 = \frac{1}{h_2 - h_1 - 2\gamma} + \frac{\text{Pr}EM^4}{2} \left[ \frac{A_3^2 - A_4^2}{2} (h_1 + h_2) + \frac{A_3^2 + A_4^2}{4M^2} (A_5 - 2\gamma MA_7) + \frac{A_3 A_4}{2M^2} (A_6 - 2\gamma MA_8) \right], \quad (2.29)$$

$$C_2 = \frac{h_1 + \gamma}{h_1 - h_2 + 2\gamma} + \frac{\text{Pr}EM^4}{2} \left[ (A_3^2 - A_4^2) \frac{h_1^2}{2} + (A_3^2 + A_4^2) \frac{\cosh 2Mh_1}{4M^2} + A_3 A_4 \frac{\sinh 2Mh_1}{2M^2} \right] + \frac{\gamma \text{Pr}EM^4}{2} \left[ (A_3^2 - A_4^2) h_1 + (A_3^2 + A_4^2) \frac{\sinh 2Mh_1}{2M} + A_3 A_4 \frac{\cosh 2Mh_1}{M} \right] - (h_1 + \gamma) \frac{\text{Pr}EM^4}{2} \left[ \frac{A_3^2 - A_4^2}{2} (h_1 + h_2) + \frac{A_3^2 + A_4^2}{4M^2} (A_5 - 2\gamma MA_7) + \frac{A_3 A_4}{2M^2} (A_6 - 2\gamma MA_8) \right], \quad (2.30)$$

$$A_5 = \frac{\cosh 2Mh_2 - \cosh 2Mh_1}{h_2 - h_1 - 2\gamma}, \quad A_6 = \frac{\sinh 2Mh_2 - \sinh 2Mh_1}{h_2 - h_1 - 2\gamma},$$

$$A_7 = \frac{\sinh 2Mh_1 + \sinh 2Mh_2}{h_2 - h_1 - 2\gamma}, \quad A_8 = \frac{\cosh 2Mh_1 + \cosh 2Mh_2}{h_2 - h_1 - 2\gamma},$$

Putting the values of  $C_1$  and  $C_2$  in Eq. (2.28) and rearranging, we have

$$\theta = -\frac{BrM^4}{2} \left\{ \frac{A_3^2 - A_4^2}{2} ((y^2 - h_1^2) - 2h_1\gamma - (y - h_1 - \gamma)(h_1 + h_2)) + \frac{A_3^2 + A_4^2}{4M^2} (\cosh 2My - \cosh 2Mh_1 - (A_5 - 2\gamma MA_7)(y - h_1 - \gamma) - 2\gamma M \sinh 2Mh_1) + \frac{A_3 A_4}{2M^2} (\sinh 2My - \sinh 2Mh_1 - (A_6 - 2\gamma MA_8)(y - h_1 - \gamma) - 2\gamma M \cosh 2Mh_1) \right\} + \frac{y - h_1 - \gamma}{h_2 - h_1 - 2\gamma}, \quad (2.31)$$

where  $Br = \text{Pr}E$  is the Brinkman number.

The longitudinal velocity is

$$u = \frac{\partial \Psi}{\partial y} = A_2 + A_3 M \sinh My + A_4 M \cosh My. \quad (2.32)$$

Now by Eq. (2.14), the longitudinal pressure gradient is

$$\frac{dp}{dx} = -M^2 (A_2 + 1) \quad (2.33)$$

and the heat transfer coefficient at the upper wall is

$$\begin{aligned}
Z &= h_{1x}\theta_y \\
&= -\frac{h_{1x}BrM^4}{2} \left\{ \frac{A_3^2 - A_4^2}{2} (2y - (h_1 + h_2)) + \frac{A_3^2 + A_4^2}{4M^2} (2M \sinh 2My - (A_5 - 2\gamma M A_7)) \right. \\
&\quad \left. + \frac{A_3 A_4}{2M^2} (2M \cosh 2My - (A_6 - 2\gamma M A_8)) \right\} + \frac{1}{h_2 - h_1 - 2\gamma}.
\end{aligned} \tag{2.34}$$

The dimensionless expressions of pressure rise ( $\Delta P$ ) and frictional forces ( $F_1$ ) and ( $F_2$ ) at the upper and lower walls are

$$\Delta P = \int_0^1 \left( \frac{dp}{dx} \right) dx, \tag{2.35}$$

$$F_1 = \int_0^1 h_1^2 \left( -\frac{dp}{dx} \right) dx, \tag{2.36}$$

$$F_2 = \int_0^1 h_2^2 \left( -\frac{dp}{dx} \right) dx. \tag{2.37}$$

## 2.4 Results and discussion

The expressions for longitudinal velocity, temperature and  $dp/dx$  have been discussed graphically in this section. Also, the pressure rise per wavelength ( $\Delta P$ ) and the frictional forces  $F_i$  ( $i = 1, 2$ ) at the channel walls are analyzed carefully through numerical integration. Figures 2.1a and 2.1b are plotted respectively to see the effects of  $M$  and  $\beta$  on the longitudinal velocity  $u$ . These Figures show that the longitudinal velocity  $u$  increases in the neighborhood of the walls when  $M$  and  $\beta$  are increased. However, it decreases near the centre of the channel. It is evident from these plots that velocity profile is parabolic for fixed values of the parameters at

the inlet  $x = 0$ .

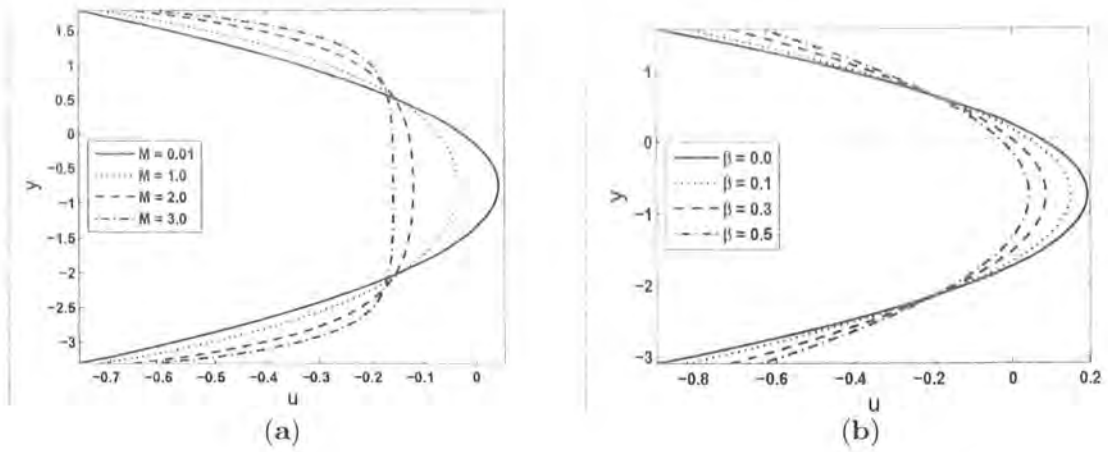


Figure 2.1a: Variation of the longitudinal velocity  $u$  for different values of Hartman number  $M$  when  $a = 0.7$ ,  $b = 1.2$ ,  $d = 2$ ,  $x = 0$ ,  $\beta = 0.5$ ,  $\Phi = 0$  and  $q = -1$ .

Figure 2.1b: Variation of the longitudinal velocity  $u$  for different values of thermal slip parameter  $\beta$  when  $a = 0.7$ ,  $b = 1.2$ ,  $d = 2$ ,  $x = 0$ ,  $M = 0.01$ ,  $\Phi = 0$  and  $q = -1$ .

Here Figures 2.2a and 2.2b indicate the parabolic nature of the temperature profiles. These also show that the temperature decreases by increasing the Hartman number ( $M$ ) at the inlet  $x = 0$ . Note that the temperature decreases in the downstream.

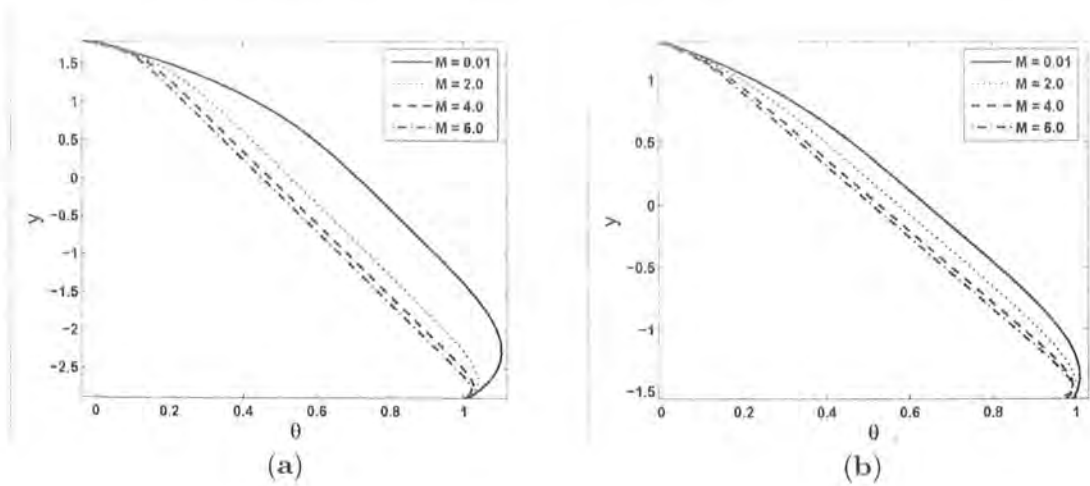


Figure 2.2a: Variation of temperature distribution  $\theta$  for different values of Hartman number

$M$  at the inlet  $x = 0$  when  $a = 0.7$ ,  $b = 1.2$ ,  $d = 2$ ,  $\beta = 0.2$ ,  $\gamma = 0.1$ ,  $\Phi = \pi/4$ ,  $Br = 1$  and  $q = -1$ .

Figure 2.2b: Variation of temperature distribution  $\theta$  for different values of Hartman number  $M$  at the inlet  $x = 0.2$  when  $a = 0.7$ ,  $b = 1.2$ ,  $d = 2$ ,  $\beta = 0.2$ ,  $\gamma = 0.1$ ,  $\Phi = \pi/4$ ,  $Br = 1$  and  $q = -1$ .

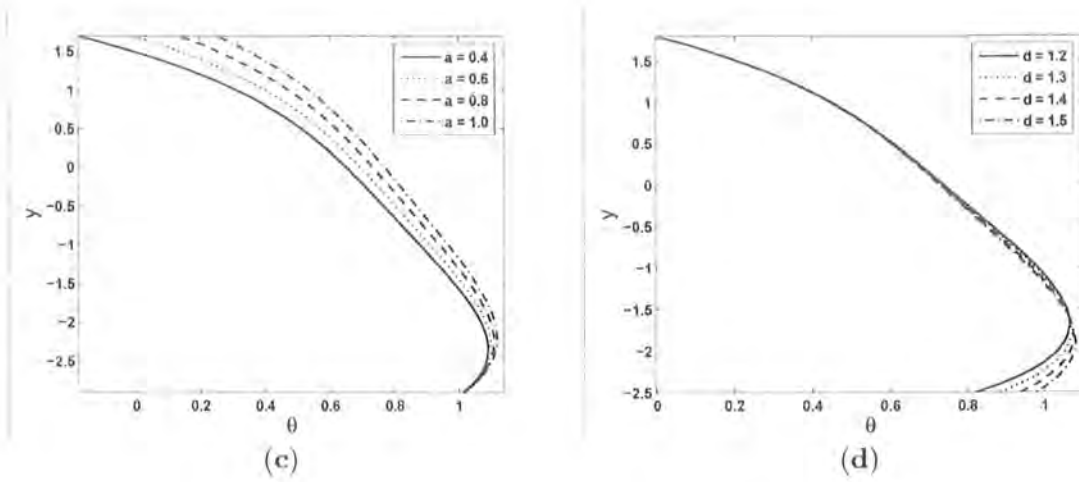


Figure 2.2c: Variation of temperature distribution  $\theta$  for different values of amplitude ratio  $a$  when  $M = 0.01$ ,  $b = 1.2$ ,  $d = 2$ ,  $x = 0.0$ ,  $\beta = 0.2$ ,  $\gamma = 0.1$ ,  $\Phi = \pi/4$ ,  $Br = 1$  and  $q = -1$ .

Figure 2.2d: Variation of temperature distribution  $\theta$  for different values of channel width  $d$  when  $M = 0.01$ ,  $a = 0.7$ ,  $b = 1.2$ ,  $x = 0.0$ ,  $\beta = 0.2$ ,  $\gamma = 0.1$ ,  $\Phi = \pi/4$ ,  $Br = 1$  and  $q = -1$ .

The variations of the amplitude ratio of the upper wall  $a$  and thermal slip parameter  $\gamma$  on the temperature are plotted in the Figures 2.2c and 2.2f. It is obvious from these Figures that temperature is an increasing function of  $a$  and  $\gamma$ . Such variations are significant only near the upper wall. Figure 2.2d elucidates that the temperature increases by increasing  $d$  in the vicinity of lower wall and no significant variation occurs near the upper wall. Figure 2.2e illustrates that the temperature decreases with an increase in the slip parameter  $\beta$ . However, opposite behavior is noted in the case of Brinkman number (Figure 2.2h). Figure 2.2g indicates that by increasing  $\Phi$  no considerable variation occurs near the upper wall of the channel. However we

note that an increase in  $\Phi$  reduces the amplitude of the temperature at the inlet.

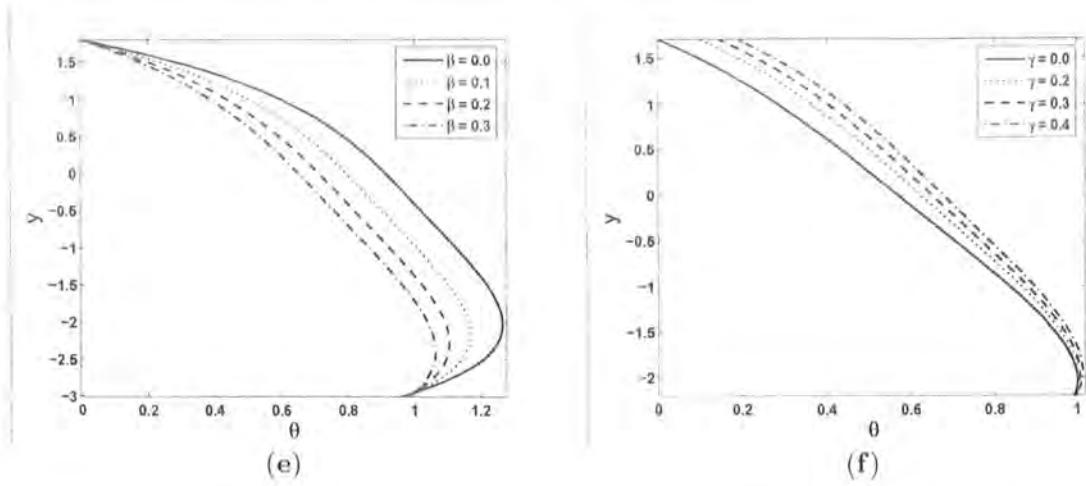


Figure 2.2e: Variation of temperature distribution  $\theta$  for different values of thermal slip parameters  $\beta$  when  $a = 0.7$ ,  $b = 1.2$ ,  $d = 2$ ,  $x = 0.0$ ,  $M = 0.01$ ,  $\gamma = 0.1$ ,  $\Phi = \pi/4$ ,  $Br = 1$  and  $q = -1$ .

Figure 2.2f: Variation of temperature distribution  $\theta$  for different values of thermal slip parameters  $\gamma$  when  $a = 0.7$ ,  $b = 1.2$ ,  $d = 2$ ,  $x = 0.0$ ,  $M = 0.5$ ,  $\beta = 0.5$ ,  $\Phi = 3\pi/2$ ,  $Br = 1$  and  $q = -1$ .

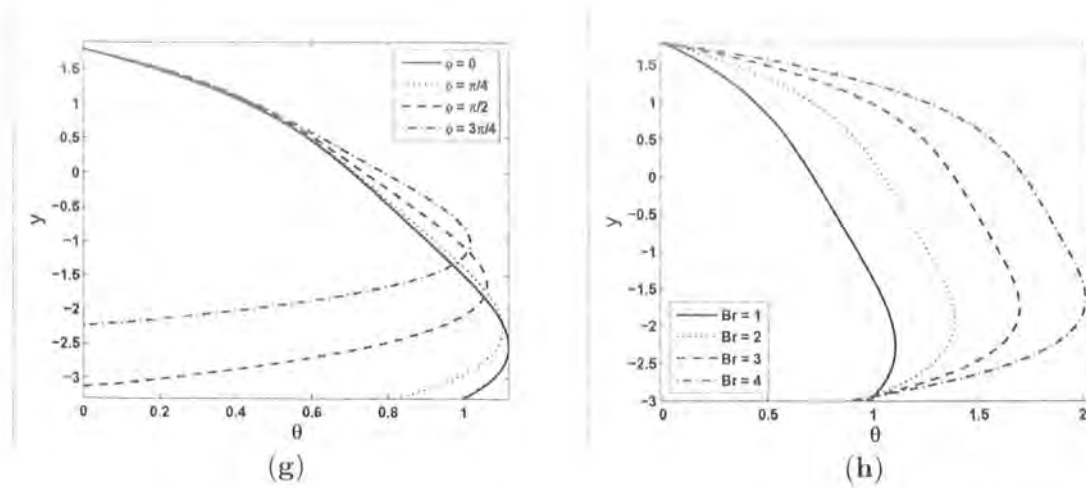


Figure 2.2g: Variation of temperature distribution  $\theta$  for different values of phase difference  $\Phi$  when  $a = 0.7$ ,  $b = 1.2$ ,  $d = 2$ ,  $x = 0.0$ ,  $M = 0.01$ ,  $\beta = 0.2$ ,  $\gamma = 0.1$ ,  $Br = 1$  and  $q = -1$ .

Figure 2.2h: Variation of temperature distribution  $\theta$  for different values of Brinkman number  $Br$  when  $a = 0.7$ ,  $b = 1.2$ ,  $d = 2$ ,  $x = 0.0$ ,  $M = 0.01$ ,  $\beta = 0.2$ ,  $\gamma = 0.1$ ,  $\Phi = \pi/4$  and  $q = -1$ .

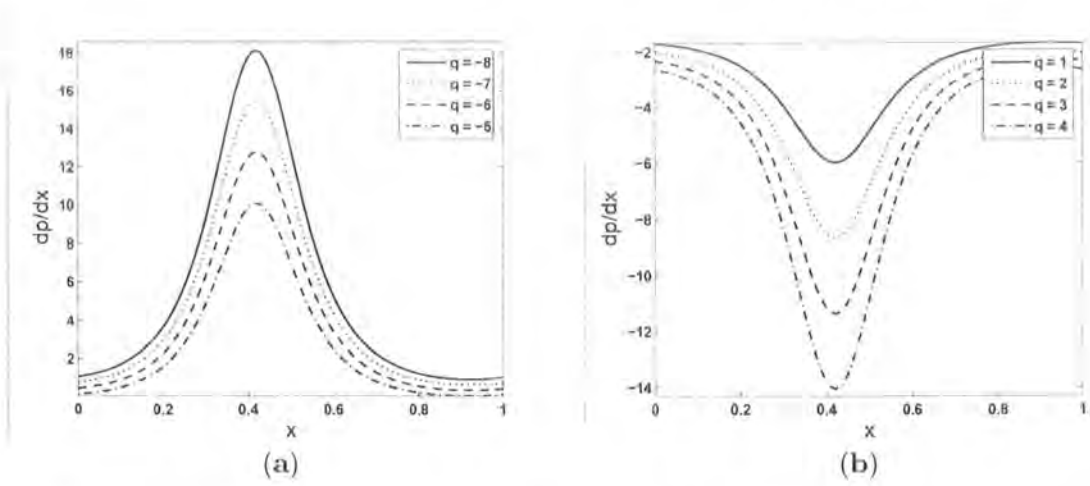


Figure 2.3a: Variation of pressure gradient ( $dp/dx$ ) for different values of flow rate  $q$  when  $a = 0.7$ ,  $b = 1.2$ ,  $d = 2$ ,  $M = 1$ ,  $\beta = 0.5$  and  $\Phi = \pi/4$ .

Figure 2.3b: Variation of pressure gradient ( $dp/dx$ ) for different values of flow rate  $q$  when  $a = 0.7$ ,  $b = 1.2$ ,  $d = 2$ ,  $M = 1$ ,  $\beta = 0.5$  and  $\Phi = \pi/4$ .

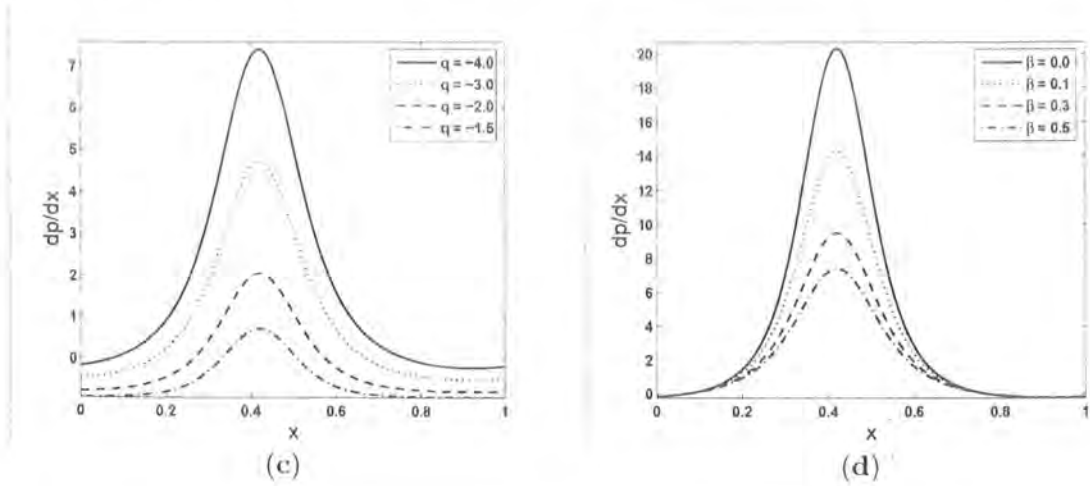


Figure 2.3c: Variation of pressure gradient ( $dp/dx$ ) for different values of flow rate  $q$  when  $a = 0.7$ ,  $b = 1.2$ ,  $d = 2$ ,  $M = 1$ ,  $\beta = 0.5$  and  $\Phi = \pi/4$ .

Figure 2.3d: Variation of pressure gradient ( $dp/dx$ ) for different values of slip parameter  $\beta$



when  $a = 0.7$ ,  $q = -4$ ,  $b = 1.2$ ,  $d = 2$ ,  $M = 1$  and  $\Phi = \pi/4$ .

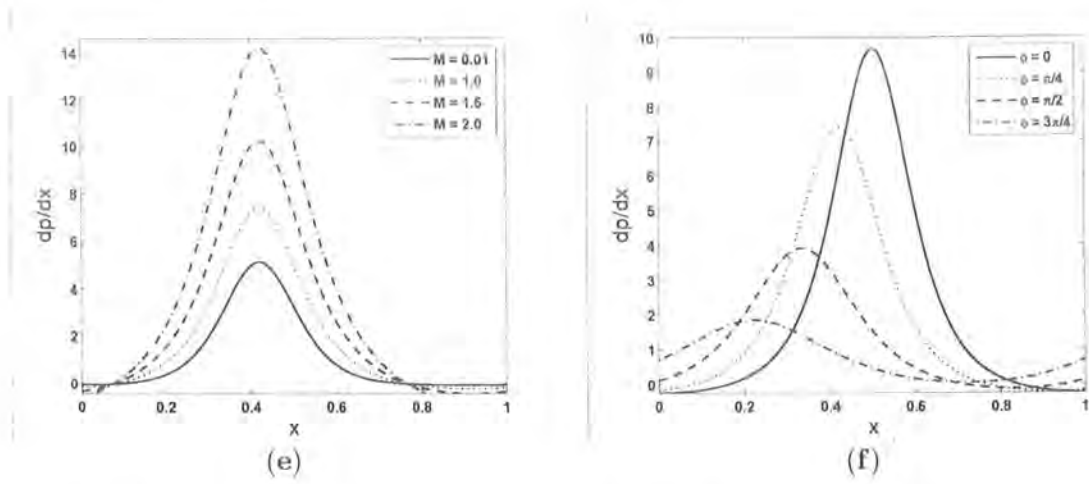


Figure 2.3e: Variation of pressure gradient ( $dp/dx$ ) for different values of Hartman number  $M$  when  $a = 0.7$ ,  $b = 1.2$ ,  $d = 2$ ,  $q = -4$ ,  $\beta = 0.5$  and  $\Phi = \pi/4$ .

Figure 2.3f: Variation of pressure gradient ( $dp/dx$ ) for different values of phase difference  $\Phi$  when  $a = 0.7$ ,  $b = 1.2$ ,  $d = 2$ ,  $M = 1$ ,  $\beta = 0.5$  and  $q = -4$ .

The results presented in Figures 2.3(a – c) show the effect of flow rate  $q$ , slip parameter  $\beta$ , Hartman number  $M$  and the phase difference  $\Phi$  on the pressure gradient  $dp/dx$ . Interestingly  $dp/dx$  is positive for  $q$  from  $-8$  to  $-5$ . In this situation  $dp/dx$  resists the flow in the channel and known as adverse pressure gradient. For  $q \geq 0$ ,  $dp/dx$  is negative in the whole channel and here it assists the flow which is known as favourable pressure gradient. When  $q$  changes from  $-4$  to  $-1.5$ , then  $dp/dx$  is positive in the narrow part of the channel and negative in negative part of the channel and here it assists the flow. Figure 2.3d depicts that  $dp/dx$  decreases with an increase in the velocity slip parameter  $\beta$  in the narrow part of the channel. However  $dp/dx$  exhibits an opposite behavior for  $M$ , where by increasing  $M$ ,  $dp/dx$  increases in the narrow part of the channel  $x \in [0.08, 0.78]$  and decreases in the wider part of the channel  $x \in [0, 0.08]$  and  $x \in [0.78, 1]$  Figures 2.3e and 2.3f display the variation of  $dp/dx$  for different values of  $\Phi$ . Interestingly a small amount of pressure gradient is required to pass the flow in the wider part of the channel in an asymmetric channel when compared to the symmetric channel. However,

an opposite behavior is noted in the wider part of the channel.

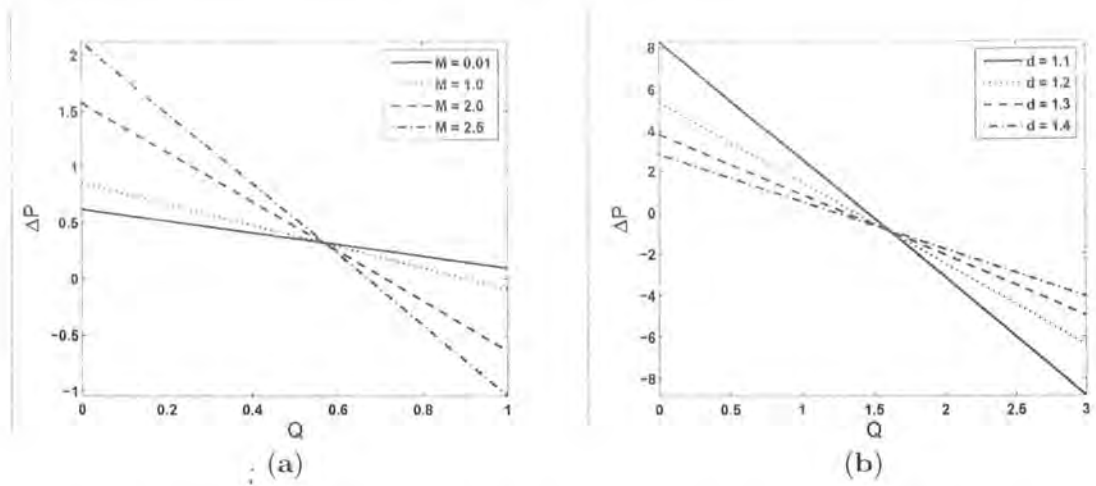


Figure 2.4a: Variation of pressure rise per wavelength ( $\Delta P$ ) for different values of Hartman number  $M$  when  $a = 0.7$ ,  $b = 1.2$ ,  $d = 2$ ,  $\beta = 0.5$  and  $\Phi = \pi/4$ .

Figure 2.4b: Variation of pressure rise per wavelength ( $\Delta P$ ) for different values of channel width  $d$  when  $a = 0.7$ ,  $b = 1.2$ ,  $M = 1$ ,  $\beta = 0.5$  and  $\Phi = \pi/4$ .

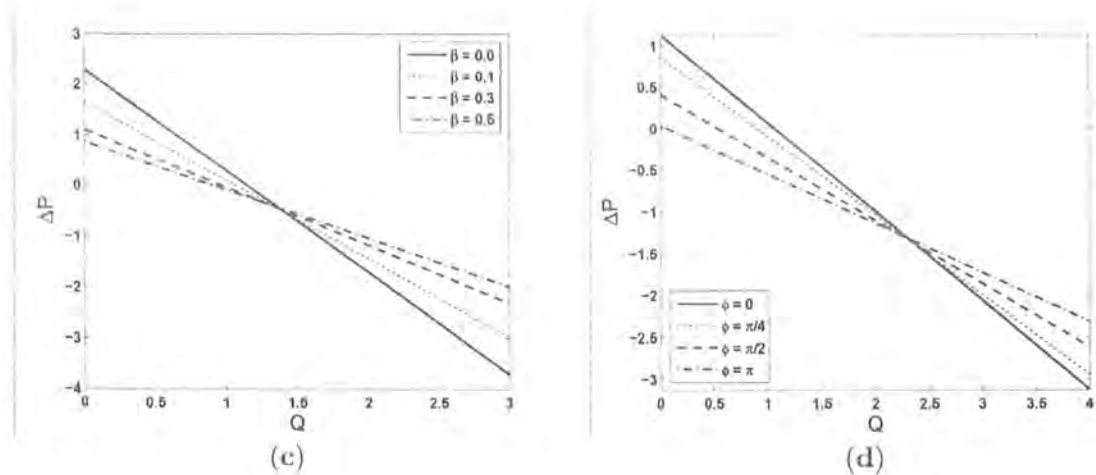


Figure 2.4c: Variation of pressure rise per wavelength ( $\Delta P$ ) for different values of slip parameter  $\beta$  when  $a = 0.7$ ,  $b = 1.2$ ,  $d = 2$ ,  $M = 1$  and  $\Phi = \pi/4$ .

Figure 2.4d: Variation of pressure rise per wavelength ( $\Delta P$ ) for different values of phase difference  $\Phi$  when  $a = 0.7$ ,  $b = 1.2$ ,  $d = 2$ ,  $M = 1$  and  $\beta = 0.5$ .

Figures 2.4(a – d) show the variation of pressure rise per wave length ( $\Delta P$ ) against the average time flux  $Q$  ( $= q + 1 + d$ ). We divide the whole region into three parts for peristaltic pumping. When  $\Delta P > 0$  and  $Q > 0$ , that is the region above the horizontal dotted line and is known as the peristaltic pumping region. The region corresponding to  $\Delta P = 0$  is the free pumping region. The lower part of the Figure below the dotted line represents the augmented pumping region and here  $\Delta P < 0$  and  $Q > 0$ . Figure 2.4a indicates that the pumping rate increases by increasing  $M$  and decreases after a critical value of  $Q = 0.58$  and this behavior remains the same in the free and augmented pumping region. Figures 2.4b and 2.4c show the effect of the channel width  $d$  and slip parameter  $\beta$  on  $\Delta P$ . Here pressure rise decreases with an increase in  $d$  and  $\beta$  in the free and peristaltic pumping region and after a critical value of  $Q$ , it increases in the augmented pumping region. Figure 2.4d explains the effect of the phase difference  $\Phi$  on  $\Delta P$ . The solid line curve shows the case of the symmetric channel. Here pressure rise decreases with an increase in  $\Phi$  in the free and peristaltic pumping region and after a critical value of  $Q$ , it increases in the augmented pumping region. However a wider peristaltic pumping region is observed in this case.

The effects of  $d$ ,  $M$ ,  $\beta$  and  $\Phi$  on  $F_i$  ( $i = 1, 2$ ) are plotted in the Figures 2.5(a – d) and 2.6(a – d). Figures 2.5(a – d) represents the variation of  $F_1$  (*i.e.* the frictional force at the upper wall of the channel) and Figures 2.6(a – d) indicate the variation of  $F_2$  (*i.e.* the frictional force at the lower wall of the channel) with  $Q$ . The phenomenon presented in these Figures is quite opposite to the pumping characteristic. By increasing  $d$ ,  $F_1$  decreases while  $F_2$  increases when  $Q > 0$ . Figures 2.5b and 2.6b display the same behavior. Here  $F_1$  and  $F_2$  increase by increasing the Hartman number  $M$ . Both  $F_1$  and  $F_2$  decrease with an increase in the slip parameter  $\beta$  after a certain critical value of  $Q$ . Figures 2.5d and 2.6d represent that  $F_1$  and  $F_2$  decrease with

an increase in the phase difference  $\Phi$  and increase by increasing  $\Phi$  after a certain value of  $Q$ .

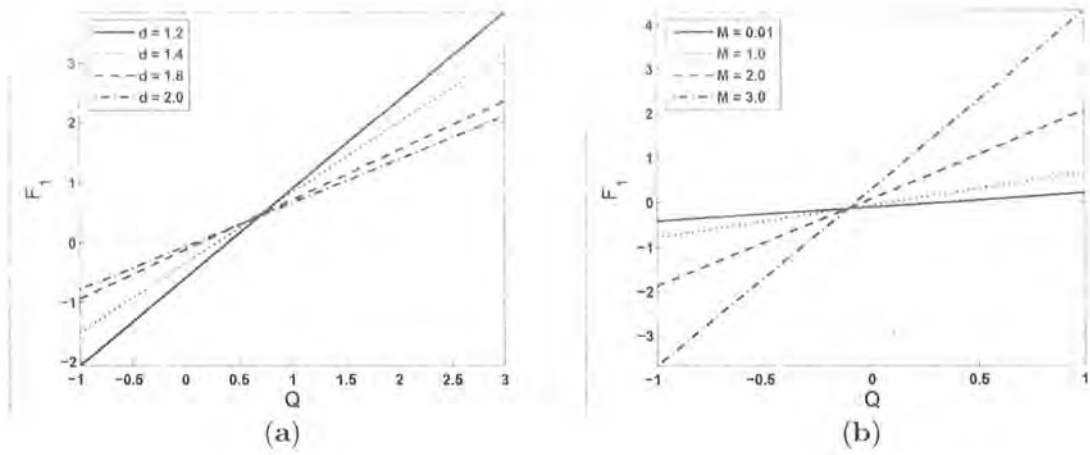


Figure 2.5a: Variation of frictional force  $F_1$  for different values of channel width  $d$  when  $a = 0.7$ ,  $b = 1.2$ ,  $M = 1$ ,  $\beta = 0.5$  and  $\Phi = 3\pi/2$ .

Figure 2.5b: Variation of frictional force  $F_1$  for different values of Hartman number  $M$  when  $a = 0.7$ ,  $b = 1.2$ ,  $d = 2$ ,  $\beta = 0.5$  and  $\Phi = 3\pi/2$ .

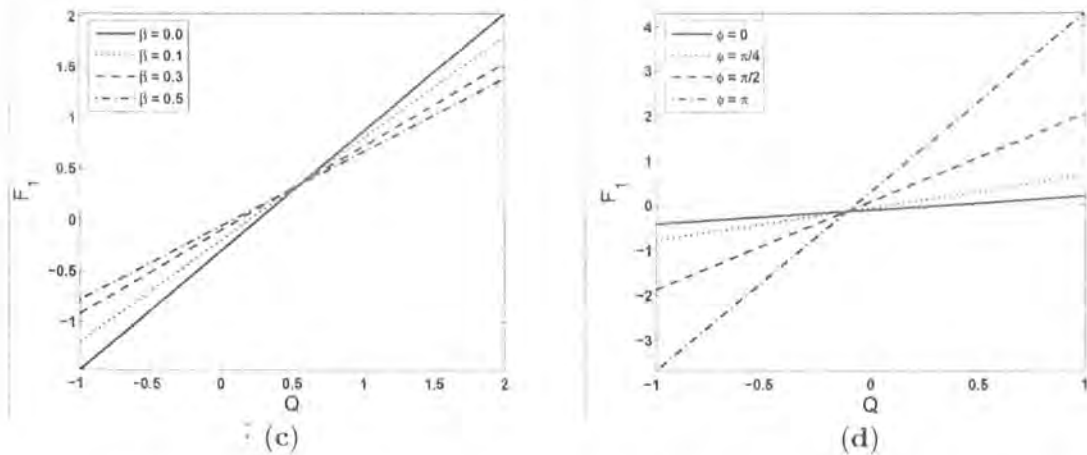


Figure 2.5c: Variation of frictional force  $F_1$  for different values of slip parameter  $\beta$  when  $a = 0.7$ ,  $b = 1.2$ ,  $d = 2$ ,  $M = 1$  and  $\Phi = 3\pi/2$ .

Figure 2.5d: Variation of frictional force  $F_1$  for different values of phase difference  $\Phi$  when

$a = 0.7, b = 1.2, d = 2, M = 1$  and  $\beta = 0.5$ .

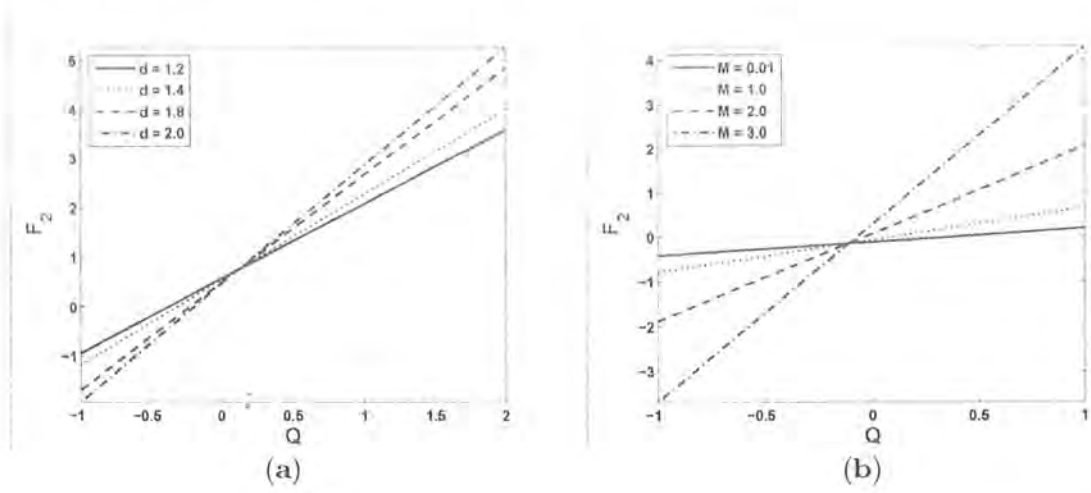


Figure 2.6a: Variation of frictional force  $F_2$  for different values of channel width  $d$  when  $a = 0.7, b = 1.2, M = 1, \beta = 0.5$  and  $\Phi = 3\pi/2$ .

Figure 2.6b: Variation of frictional force  $F_2$  for different values of Hartman number  $M$  when  $a = 0.7, b = 1.2, d = 2, \beta = 0.5$  and  $\Phi = 3\pi/2$ .

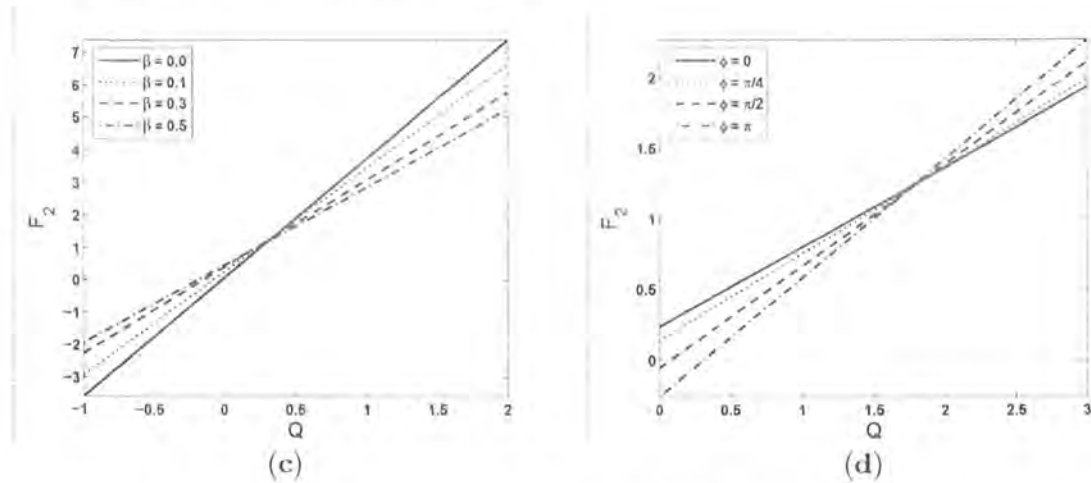


Figure 2.6c: Variation of frictional force  $F_2$  for different values of slip parameter  $\beta$  when  $a = 0.7, b = 1.2, d = 2, M = 1$  and  $\Phi = 3\pi/2$ .

Figure 2.6d: Variation of frictional force  $F_2$  for different values of phase difference  $\Phi$  when  $a = 0.7, b = 1.2, d = 2, M = 1$  and  $\beta = 0.5$ .

Variations of the heat transfer coefficient ( $Z$ ) at the upper wall are given in the Tables 2.1(a)-(f). These Tables show that the heat transfer coefficient decreases with an increase in the Hartman number  $M$ , flow rate  $q$  and the slip parameters  $\beta$  and  $\gamma$ . However, it increases by increasing the amplitude ratio  $a$  and the Eckert number  $E$ .

$x$	$M$			
	0.01	2	3	4
0.1	1.8556	1.5370	1.4384	1.3687
0.2	2.05882	1.9149	1.8487	1.8041
0.3	2.4314	2.3851	2.3518	2.3248

Table 2.1a: Variation of the heat transfer coefficient ( $Z$ ) at the upper wall for different values of Hartman number  $M$  when  $a = 0.74$ ,  $b = 1.2$ ,  $d = 2$ ,  $\beta = 0.35$ ,  $\gamma = 0.18$ ,  $\Phi = \pi/4$ ,  $\text{Pr} = 1$ ,  $E = 1$  and  $q = -2$ .

$x$	$E$			
	1	2	3	4
0.1	0.9517	1.2444	1.5370	1.8296
0.2	1.6068	1.7609	1.9149	2.0690
0.3	2.2246	2.3049	2.3851	2.4653

Table 2.1b: Variation of the heat transfer coefficient ( $Z$ ) at the upper wall for different values of Eckert number  $E$  when  $a = 0.5$ ,  $b = 0.6$ ,  $d = 1.5$ ,  $\beta = 0.5$ ,  $\gamma = 0.18$ ,  $\Phi = \pi/4$ ,  $\text{Pr} = 1$ ,  $M = 2$  and  $q = -2$ .

$x$	$q$			
	-0.5	-1	-1.5	-2
0.1	3.6302	2.7950	2.0972	1.5370
0.2	6.1657	4.2547	2.8378	1.9149
0.3	6.0646	3.4817	2.2552	2.3851

Table 2.1c: Variation of the heat transfer coefficient ( $Z$ ) at the upper wall for different values of flow rate  $q$  when  $a = 0.5$ ,  $b = 0.6$ ,  $d = 1.5$ ,  $\beta = 0.5$ ,  $\gamma = 0.18$ ,  $\Phi = \pi/4$ ,  $\text{Pr} = 1$ ,  $E = -3$  and

$M = 2$ .

$x$	$a$			
	0.5	0.7	0.9	1.1
0.1	0.6447	0.9006	1.1561	1.4114
0.2	1.0943	1.5218	1.9452	2.3652
0.3	1.4266	2.0851	2.8132	3.6284

Table 2.1d: Variation of the heat transfer coefficient ( $Z$ ) at the upper wall for different values of amplitude ratio  $a$  when  $b = 0.6$ ,  $d = 1.5$ ,  $\beta = 0.5$ ,  $\gamma = 0.18$ ,  $\Phi = \pi/4$ ,  $\text{Pr} = E = 1$ ,  $M = 2$  and  $q = -2$ .

$x$	$\gamma$			
	0.1	0.15	0.2	0.25
0.1	1.5634	1.5467	1.5307	1.5155
0.2	1.9955	1.9441	1.8961	1.8510
0.3	2.5655	2.4494	2.3443	2.2488

Table 2.1e: Variation of the heat transfer coefficient ( $Z$ ) at the upper wall for different values of slip parameter  $\gamma$  when  $a = 0.5$ ,  $b = 0.6$ ,  $d = 1.5$ ,  $\beta = 0.5$ ,  $\Phi = \pi/4$ ,  $\text{Pr} = 1$ ,  $E = 3$ ,  $M = 2$  and  $q = -2$ .

$x$	$\beta$			
	0.3	0.4	0.5	0.6
0.1	1.6732	1.4265	1.2599	1.1423
0.2	1.9927	1.8528	1.7610	1.6975
0.3	2.4317	2.3490	2.2975	2.2632

Table 2.1f: Variation of the heat transfer coefficient ( $Z$ ) at the upper wall for different values of slip parameter  $\beta$  when  $a = 0.5$ ,  $b = 0.6$ ,  $d = 1.5$ ,  $\gamma = 0.18$ ,  $\Phi = \pi/4$ ,  $\text{Pr} = 1$ ,  $E = 3$ ,  $M = 2$  and  $q = -2$ .

## 2.5 Concluding remarks

In the present chapter, we have analyzed the slip effects on the magnetohydrodynamic peristaltic flow of a viscous fluid. The influence of heat transfer is also seen. Closed form solutions are

derived for the velocity and temperature. The main observations of the presented analysis are as follows.

- The longitudinal velocity increases in the neighborhood of the walls and decreases near the centre of the channel when the velocity slip parameter is increased.
- An increase in velocity slip parameter leads to a decrease in the temperature.
- Due to increase in thermal slip parameter, the temperature increases.
- The effects of Brinkman number and velocity slip parameter on the temperature are quite opposite. However, the variations of Brinkman number and thermal slip parameter on the temperature are similar in a qualitative sense.
- Frictional forces on the upper and lower walls are the increasing functions of Hartman number.
- There is a decrease in the heat transfer coefficient at the upper wall when velocity and thermal slip parameters are increased.
- The effects of Hartman number and flow rate on the heat transfer coefficient at the upper wall are quite opposite to that of amplitude ratio and Eckert number.
- The variations of velocity and thermal slip parameters on the heat transfer coefficient at the upper wall are opposite when compared with the variations of amplitude ratio and the Eckert number.



## Chapter 3

# Wall properties and slip effects on the magnetohydrodynamic peristaltic motion of viscous fluid with heat transfer and porous space

This chapter explores the effects of slip conditions and wall properties on the MHD peristaltic flow of viscous fluid filling the porous space in a channel. The heat transfer analysis is also presented. The solutions of the stream function, velocity and temperature distributions are constructed in closed form under long wavelength and low Reynolds number approximations. The effects of various influential key parameters are reported and discussed.

### 3.1 Mathematical model

We consider a channel of width  $2d$ . The channel is filled with an incompressible and magnetohydrodynamic (MHD) viscous fluid. A uniform magnetic field  $\mathbf{B} = (0, B_0, 0)$  is applied in the  $y$ -direction. The induced magnetic field is negligible under the assumption of small magnetic Reynolds number consideration. The fluid fills the porous space. The temperatures of the lower and upper walls of the channel are maintained at  $T_0$  and  $T_1$  respectively. The imposed

travelling waves of small amplitudes on the insulating walls of the channel are given by the following expressions

$$y = \pm\eta = \pm \left[ d + u \sin \left( \frac{2\pi}{\lambda} (x - ct) \right) \right],$$

where  $\lambda$  is the wavelength,  $c$  is the wave speed,  $u$  is the wave amplitude and  $x$  and  $y$  are the Cartesian coordinates with  $x$  measured in the direction of the wave propagation and  $y$  measured in the direction normal to the mean position of the channel walls.

The equations which can govern the motion for the present flow are

$$\frac{\partial u}{\partial x} + \frac{\partial v}{\partial y} = 0, \quad (3.1)$$

$$\rho \left( \frac{\partial}{\partial t} + u \frac{\partial}{\partial x} + v \frac{\partial}{\partial y} \right) u = -\frac{\partial p}{\partial x} + \mu \left( \frac{\partial^2}{\partial x^2} + \frac{\partial^2}{\partial y^2} \right) u - \sigma B_0^2 u - \frac{\mu}{k} u, \quad (3.2)$$

$$\rho \left( \frac{\partial}{\partial t} + u \frac{\partial}{\partial x} + v \frac{\partial}{\partial y} \right) v = -\frac{\partial p}{\partial y} + \mu \left( \frac{\partial^2}{\partial x^2} + \frac{\partial^2}{\partial y^2} \right) v - \frac{\mu}{k} v, \quad (3.3)$$

$$\zeta \left( \frac{\partial}{\partial t} + u \frac{\partial}{\partial x} + v \frac{\partial}{\partial y} \right) T = \frac{\kappa}{\rho} \nabla^2 T + \nu \left[ \left\{ 2 \left( \frac{\partial u}{\partial x} \right)^2 + 2 \left( \frac{\partial v}{\partial y} \right)^2 + \left( \frac{\partial u}{\partial y} + \frac{\partial v}{\partial x} \right)^2 \right\} \right] \quad (3.4)$$

subjected to the boundary conditions

$$u \pm \alpha \frac{\partial u}{\partial y} = 0 \quad \text{at } y = \pm\eta = \pm \left[ d + u \sin \left( \frac{2\pi}{\lambda} (x - ct) \right) \right], \quad (3.5)$$

$$\begin{aligned} \frac{\partial}{\partial x} L(\eta) = \frac{\partial p}{\partial x} = \mu \left( \frac{\partial^2 u}{\partial y^2} + \frac{\partial^2 u}{\partial y^2} \right) - \rho \left( \frac{\partial u}{\partial t} + u \frac{\partial u}{\partial x} + v \frac{\partial u}{\partial y} \right) - \sigma B_0^2 u \\ - \frac{\mu}{k} u \quad \text{at } y = \pm\eta, \end{aligned} \quad (3.6)$$

$$T - \xi \frac{\partial T}{\partial y} = T_0 \quad \text{on } y = -\eta, \quad (3.7)$$

$$T + \xi \frac{\partial T}{\partial y} = T_1 \quad \text{on } y = \eta, \quad (3.8)$$

where  $u$  and  $v$  are the velocity components in  $x$  and  $y$  directions respectively and  $\rho$ ,  $t$ ,  $p$ ,  $\mu$ ,  $\nu$ ,  $\sigma$ ,  $\zeta$ ,  $\kappa$  and  $T$  are the fluid density, the time, the pressure, the dynamic viscosity, the kinematic viscosity, the electrical conductivity, the specific heat, the thermal conductivity and the temperature respectively. Furthermore,  $L = -\tau \frac{\partial^2}{\partial x^2} + m \frac{\partial^2}{\partial t^2} + C \frac{\partial}{\partial t}$ ,  $\tau$  is the elastic tension in the membrane,  $m$  is the mass per unit area and  $C$  is the coefficient of viscous damping.

On setting

$$u = \frac{\partial \Psi}{\partial y} \quad \text{and} \quad v = -\frac{\partial \Psi}{\partial x}$$

equation (3.1) is automatically satisfied and Eqs.(3.2)-(3.8) are reduced as follows

$$\rho \left( \frac{\partial}{\partial t} + \frac{\partial \Psi}{\partial y} \frac{\partial}{\partial x} - \frac{\partial \Psi}{\partial x} \frac{\partial}{\partial y} \right) \frac{\partial \Psi}{\partial y} = -\frac{\partial p}{\partial x} + \mu \left( \frac{\partial^2}{\partial x^2} + \frac{\partial^2}{\partial y^2} \right) \frac{\partial \Psi}{\partial y} - \sigma B_0^2 \frac{\partial \Psi}{\partial y} - \frac{\mu}{k} \frac{\partial \Psi}{\partial y}, \quad (3.9)$$

$$\rho \left( \frac{\partial}{\partial t} + \frac{\partial \Psi}{\partial y} \frac{\partial}{\partial x} - \frac{\partial \Psi}{\partial x} \frac{\partial}{\partial y} \right) \left( -\frac{\partial \Psi}{\partial x} \right) = -\frac{\partial p}{\partial y} + \mu \left( \frac{\partial^2}{\partial x^2} + \frac{\partial^2}{\partial y^2} \right) \left( -\frac{\partial \Psi}{\partial x} \right) + \frac{\mu}{k} \frac{\partial \Psi}{\partial x}, \quad (3.10)$$

$$\zeta \left( \frac{\partial}{\partial t} + \frac{\partial \Psi}{\partial y} \frac{\partial}{\partial x} - \frac{\partial \Psi}{\partial x} \frac{\partial}{\partial y} \right) T = \frac{\kappa}{\rho} \nabla^2 T + \nu \left[ \left\{ 4 \left( \frac{\partial^2 \Psi}{\partial x \partial y} \right)^2 + \left( \frac{\partial^2 \Psi}{\partial y^2} - \frac{\partial^2 \Psi}{\partial x^2} \right)^2 \right\} \right], \quad (3.11)$$

$$\frac{\partial \Psi}{\partial y} \pm \alpha \frac{\partial^2 \Psi}{\partial y^2} = 0 \quad \text{at} \quad y = \pm \eta = \pm \left[ d + a \sin \left( \frac{2\pi}{\lambda} (x - ct) \right) \right], \quad (3.12)$$

$$\frac{\partial}{\partial x} L(\eta) = \frac{\partial p}{\partial x} = \left[ E_1 \frac{\partial^3}{\partial x^3} + E_2 \frac{\partial^3}{\partial x \partial t^2} + E_3 \frac{\partial^2}{\partial x \partial t} \right] \eta \quad (3.13)$$

$$= \mu \left( \frac{\partial^2}{\partial x^2} + \frac{\partial^2}{\partial y^2} \right) \frac{\partial \Psi}{\partial y} - \rho \left( \frac{\partial}{\partial t} + \frac{\partial \Psi}{\partial y} \frac{\partial}{\partial x} - \frac{\partial \Psi}{\partial x} \frac{\partial}{\partial y} \right) \frac{\partial \Psi}{\partial y} \quad (3.14)$$

$$- \sigma B_0^2 \frac{\partial \Psi}{\partial y} - \frac{\mu}{k} \frac{\partial \Psi}{\partial y} \quad \text{at} \quad y = \pm \eta, \quad (3.15)$$

$$T - \xi \frac{\partial T}{\partial y} = T_0 \quad \text{on} \quad y = -\eta, \quad (3.16)$$

$$T + \xi \frac{\partial T}{\partial y} = T_1 \quad \text{on} \quad y = \eta. \quad (3.17)$$

## 3.2 Non-dimensionalization

Defining the following non-dimensional variables and parameters

$$\begin{aligned}
 x^* &= \frac{x}{\lambda}, \quad y^* = \frac{y}{d}, \quad \Psi^* = \frac{\Psi}{cd}, \quad t^* = \frac{ct}{\lambda}, \quad \eta^* = \frac{\eta}{d}, \quad p^* = \frac{d^2 p}{\mu c \lambda}, \\
 K^* &= \frac{k}{d^2}, \quad \epsilon = \frac{a}{d}, \quad \delta = \frac{d}{\lambda}, \quad M^2 = \frac{\sigma B_0^2 d^2}{\mu}, \quad E_1 = -\frac{\tau d^3}{\lambda^3 \mu c}, \\
 E_2 &= \frac{mcd^3}{\lambda^3 \mu}, \quad E_3 = \frac{Cd^3}{\lambda^2 \mu}, \quad \text{Pr} = \frac{\rho \nu \zeta}{\kappa}, \quad E = \frac{c^2}{\zeta (T_1 - T_0)}, \\
 R &= \frac{cd}{\nu}, \quad \theta = \frac{T - T_0}{T_1 - T_0},
 \end{aligned}$$

equations (3.9)-(3.17) take the form

$$\begin{aligned}
 R\delta \left( \frac{\partial}{\partial t} + \frac{\partial \Psi}{\partial y} \frac{\partial}{\partial x} - \frac{\partial \Psi}{\partial x} \frac{\partial}{\partial y} \right) \frac{\partial \Psi}{\partial y} &= -\frac{\partial p}{\partial x} + \left( \delta^2 \frac{\partial^2}{\partial x^2} + \frac{\partial^2}{\partial y^2} \right) \frac{\partial \Psi}{\partial y} \\
 &- \left( M^2 + \frac{1}{K} \right) \frac{\partial \Psi}{\partial y}, \tag{3.18}
 \end{aligned}$$

$$\begin{aligned}
 R\delta^3 \left( \frac{\partial}{\partial t} + \frac{\partial \Psi}{\partial y} \frac{\partial}{\partial x} - \frac{\partial \Psi}{\partial x} \frac{\partial}{\partial y} \right) \left( -\frac{\partial \Psi}{\partial x} \right) &= -\frac{\partial p}{\partial y} + \delta^2 \left( \delta^2 \frac{\partial^2}{\partial x^2} + \frac{\partial^2}{\partial y^2} \right) \left( -\frac{\partial \Psi}{\partial x} \right) \\
 &+ \frac{1}{K} \delta^2 \frac{\partial \Psi}{\partial x}, \tag{3.19}
 \end{aligned}$$

$$\begin{aligned}
 R\delta \left( \frac{\partial}{\partial t} + \frac{\partial \Psi}{\partial y} \frac{\partial}{\partial x} - \frac{\partial \Psi}{\partial x} \frac{\partial}{\partial y} \right) \theta &= \frac{1}{\text{Pr}} \left( \delta^2 \frac{\partial^2}{\partial x^2} + \frac{\partial^2}{\partial y^2} \right) \theta + E \left[ 4\delta^2 \left( \frac{\partial^2 \Psi}{\partial x \partial y} \right)^2 \right. \\
 &\left. + \left( \frac{\partial^2 \Psi}{\partial y^2} - \delta^2 \frac{\partial^2 \Psi}{\partial x^2} \right)^2 \right], \tag{3.20}
 \end{aligned}$$

$$\frac{\partial \Psi}{\partial y} \pm \beta \frac{\partial^2 \Psi}{\partial y^2} = 0 \quad \text{at } y = \pm \eta = \pm [1 + \epsilon \sin(2\pi(x-t))], \quad (3.21)$$

$$\begin{aligned} \frac{\partial p}{\partial x} &= -8\epsilon\pi^3 \left[ (E_1 + E_2) \cos 2\pi(x-t) - \frac{E_3 \sin 2\pi(x-t)}{2\pi} \right] \\ &= \mu \left( \frac{\partial^2}{\partial x^2} + \frac{\partial^2}{\partial y^2} \right) \frac{\partial \Psi}{\partial y} - \rho \left( \frac{\partial}{\partial t} + \frac{\partial \Psi}{\partial y} \frac{\partial}{\partial x} - \frac{\partial \Psi}{\partial x} \frac{\partial}{\partial y} \right) \frac{\partial \Psi}{\partial y} \\ &\quad - \sigma B_0^2 \frac{\partial \Psi}{\partial y} - \frac{\mu}{k} \frac{\partial \Psi}{\partial y}, \quad \text{at } y = \pm \eta, \end{aligned} \quad (3.22)$$

$$\theta - \gamma \frac{\partial \theta}{\partial y} = 0 \quad \text{at } y = -\eta, \quad (3.23)$$

$$\theta + \gamma \frac{\partial \theta}{\partial y} = 1 \quad \text{at } y = \eta. \quad (3.24)$$

Invoking long wavelength and low Reynolds number assumptions, one obtains from Eqs.(3.18)-(3.24), the expressions as follows:

$$\frac{\partial^3 \Psi}{\partial y^3} - N^2 \frac{\partial \Psi}{\partial y} - \frac{\partial p}{\partial x} = 0, \quad (3.25)$$

$$\frac{1}{\text{Pr}} \left( \frac{\partial^2 \theta}{\partial y^2} \right) + E \left( \frac{\partial^2 \Psi}{\partial y^2} \right)^2 = 0, \quad (3.26)$$

$$\frac{\partial^3 \Psi}{\partial y^3} - N^2 \frac{\partial \Psi}{\partial y} = \left[ E_1 \frac{\partial^3}{\partial x^3} + E_2 \frac{\partial^3}{\partial x \partial t^2} + E_3 \frac{\partial^2}{\partial x \partial t} \right] \eta \quad \text{at } y = \pm \eta, \quad (3.27)$$

$$\frac{\partial \Psi}{\partial y} \pm \beta \frac{\partial^2 \Psi}{\partial y^2} = 0 \quad \text{at } y = \pm \eta = \pm [1 + \epsilon \sin 2\pi(x-t)], \quad (3.28)$$

$$\theta - \gamma \frac{\partial \theta}{\partial y} = 0 \quad \text{at } y = -\eta, \quad (3.29)$$

$$\theta + \gamma \frac{\partial \theta}{\partial y} = 1 \quad \text{at } y = \eta. \quad (3.30)$$

In above equations, the asterisks have been suppressed for simplicity,  $\partial p / \partial y = 0$  which means that  $p \neq p(y)$ ,  $\Psi$  is a stream function,  $N = \sqrt{M^2 + 1/K}$ ,  $M$  is the Hartman number,  $K$  is the porosity parameter,  $\text{Pr}$  is the Prandtl number and  $E$  is the Eckert number. Furthermore, Eqs. (3.28)-(3.30) are the slip conditions for the velocity and temperature respectively and  $\beta = \alpha/d$ ,  $\gamma = \xi/d$  ( $\alpha$  and  $\xi$  are the dimensional slip parameters corresponding to velocity and temperature).

### 3.3 Solution of the problem

From Eq. (3.25) we have

$$\Psi(y) = A_1 \cosh Ny + A_2 \sinh Ny - L^2 y. \quad (3.31)$$

Employing boundary conditions (3.28), we can write

$$\begin{aligned} A_1 &= 0, \\ A_2 &= \frac{L^2}{N (\cosh N\eta + \beta N \sinh N\eta)} \end{aligned}$$

and now Eq. (3.31) becomes

$$\begin{aligned} \Psi &= L^2 \left[ \frac{\sinh Ny}{N (\cosh N\eta + \beta N \sinh N\eta)} - y \right], \\ L^2 &= \frac{8\epsilon\pi^3}{N^2} \left[ \frac{E_3 \sin 2\pi(x-t)}{2\pi} - (E_1 + E_2) \cos 2\pi(x-t) \right]. \end{aligned} \quad (3.32)$$

Using the expression of stream function in Eq. (3.26) and integrating the resulting expression twice, we have

$$\theta = -\frac{BrL^4N^2}{2(\cosh N\eta + \beta N \sinh N\eta)^2} \left( \frac{\cosh 2Ny}{4N^2} - \frac{y^2}{2} \right) + B_1 y + B_2. \quad (3.33)$$

Through Eqs. (3.29) and (3.30), one has

$$\begin{aligned} B_1 &= \frac{1}{2(\eta + \gamma)}, \\ B_2 &= \frac{1}{2} + \frac{BrL^4N^2}{2(\cosh N\eta + \beta N \sinh N\eta)^2} \left[ -\gamma\eta + \frac{\gamma \sinh 2N\eta}{2N} + \frac{\cosh 2N\eta}{4N^2} - \frac{\eta^2}{2} \right]. \end{aligned}$$

Putting the above expressions in Eq. (3.33) and rearranging, we get

$$\begin{aligned} \theta &= \frac{BrL^4N^2}{8(\cosh N\eta + \beta N \sinh N\eta)^2} \left[ \frac{\cosh 2N\eta - \cosh 2Ny}{N^2} \right. \\ &\quad \left. + 2(y^2 - \eta^2) + 4\gamma \left( \frac{\sin 2N\eta}{2N} - \eta \right) \right] + \frac{y + \eta + \gamma}{2(\eta + \gamma)}, \end{aligned} \quad (3.34)$$

where  $Br = Pr E$  is the Brinkman number and the longitudinal velocity is

$$\begin{aligned} u &= \frac{\partial \Psi}{\partial y} \\ &= L^2 \left[ \frac{\cosh Ny}{(\cosh N\eta + \beta N \sinh N\eta)} - 1 \right]. \end{aligned} \quad (3.35)$$

The heat transfer coefficient at the upper wall is

$$\begin{aligned} Z &= \eta_x \theta_y \\ &= \frac{\eta_x Br L^4 N^2}{8 (\cosh N\eta + \beta N \sinh N\eta)^2} \left[ \frac{-2}{N} \sinh N\eta + 4\eta \right] + \frac{\eta_x}{2(\eta + \gamma)}. \end{aligned} \quad (3.36)$$

### 3.4 Graphical results and discussion

The object of this section is to analyze the longitudinal velocity, stream function, temperature and heat transfer coefficient for various parameters of interest. Hence we displayed Figures 3.1 (a – d)-3.7 (a – d). Figure 3.1 is plotted to examine the effect of various parameters on the longitudinal velocity  $u$ . One observes from Figure 3.1b that the longitudinal velocity  $u$  increases when the porosity parameter  $K$  increases while it decreases when the Hartman number  $M$  is increased (Figure 3.1a). Figures 3.1c and 3.1d record the behavior of velocity slip parameter  $\beta$  and the occlusion parameter  $\epsilon$  on the velocity respectively. These Figures depict an increase in the velocity when  $M$  and  $\epsilon$  are increased. The effect of the elastic parameters  $E_1$ ,  $E_2$  and  $E_3$  are evident in Figure 3.1e. It may be of interest to note from this Figure that by increasing the elastic parameters, the velocity increases. It is also interesting to observe that the velocity profile is parabolic for fixed values of the parameters and its magnitude is maximum near the centre of the channel. Moreover, it is found that the elastic tension  $E_1$  has a significant effect on the axial velocity in comparison to the mass characterizing parameter  $E_2$  and the damping nature of the wall  $E_3$ .

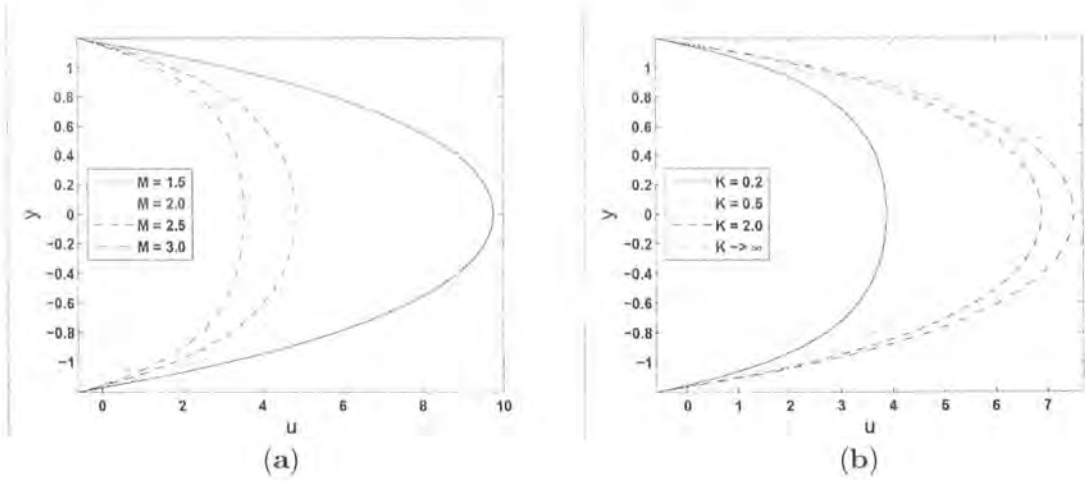


Figure 3.1a: Variations of the longitudinal velocity  $u$  for different values of Hartman number  $M$  when  $E_1 = 0.5$ ,  $E_2 = 0.2$ ,  $E_3 = 0.1$ ,  $\epsilon = 0.2$ ,  $K = 5$ ,  $\beta = 0.2$ ,  $x = 0.2$  and  $t = 0.2$ .

Figure 3.1b: Variations of the longitudinal velocity  $u$  for different values of porosity parameter  $K$  when  $E_1 = 1.0$ ,  $E_2 = 0.5$ ,  $E_3 = 0.1$ ,  $\epsilon = 0.1$ ,  $M = 2$ ,  $\beta = 0.2$ ,  $x = 0.2$  and  $t = 0.2$ .

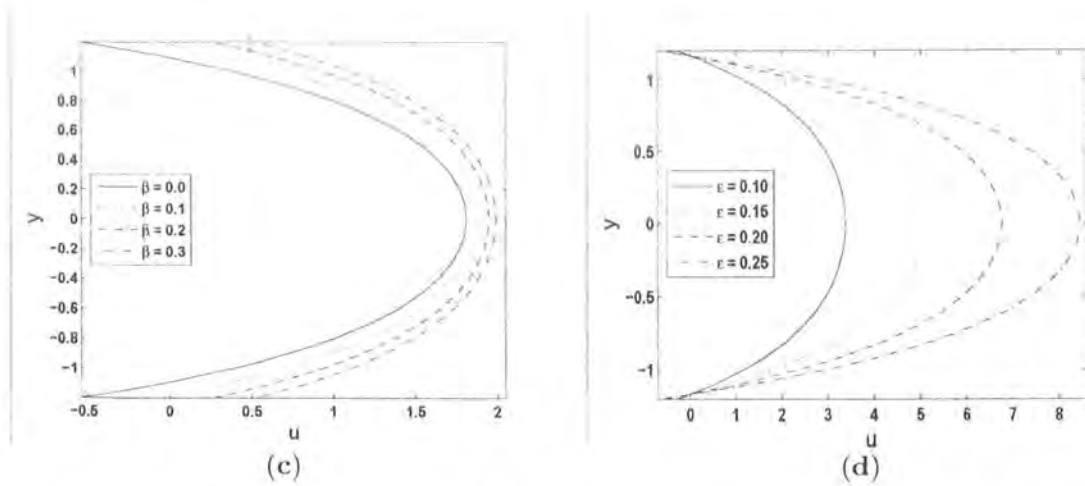


Figure 3.1c: Variations of the longitudinal velocity  $u$  for different values of velocity slip parameter  $\beta$  when  $E_1 = 1$ ,  $E_2 = 0.5$ ,  $E_3 = 0.5$ ,  $\epsilon = 0.1$ ,  $K = 5$ ,  $M = 2$ ,  $x = 0.3$  and  $t = 0.1$ .



Figure 3.1d: Variations of the longitudinal velocity  $u$  for different values of amplitude ratio  $\epsilon$  when  $E_1 = 0.5$ ,  $E_2 = 0.2$ ,  $E_3 = 0.1$ ,  $M = 2$ ,  $K = 5$ ,  $\beta = 0.2$ ,  $x = 0.2$  and  $t = 0.2$ .

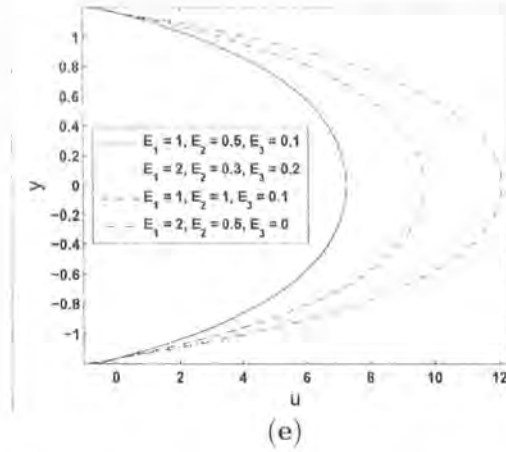


Figure 3.1e: Variations of the longitudinal velocity  $u$  for different values of wall parameters when  $\epsilon = 0.1$ ,  $M = 2$ ,  $K = 5$ ,  $\beta = 0.2$ ,  $x = 0.2$  and  $t = 0.2$ .

In Figures 3.2 (a – g), the nature of the temperature profile is of parabolic character. Here the temperature decreases by increasing the Hartman number  $M$  (Figure 3.2a) and the velocity slip parameter  $\beta$  (Figure 3.2c). Note that the temperature decreases in the downstream. However, Figures 3.2b and 3.2d illustrate that the temperature increases by increasing the permeability parameter  $K$  and the thermal slip parameter  $\gamma$ . The variations of the Brinkman number  $Br$  and the occlusion parameter  $\epsilon$  on the temperature are sketched in the Figures 3.2e and 3.2f. It is noted from these Figures that the temperature is an increasing function of  $Br$  and  $\epsilon$ . Figure 3.2g elucidates the effect of the elastic parameters  $E_1$ ,  $E_2$  and  $E_3$  on the temperature. This Figure reveals that the amplitude of temperature increases with an increase in  $E_1$ ,  $E_2$  and

$E_3$ . It is further observed that the effect of  $E_1$  on temperature is quite significant.

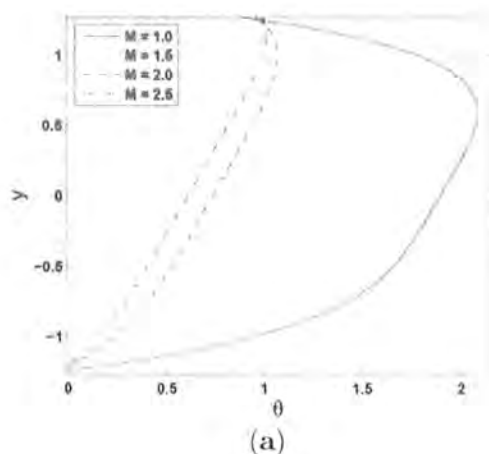


Figure 3.2a: Variations of temperature distribution  $\theta$  for different values of Hartman number  $M$  when  $E_1 = 0.4$ ,  $E_2 = 0.2$ ,  $E_3 = 0.1$ ,  $\epsilon = 0.1$ ,  $K = 5$ ,  $\beta = 0.2$ ,  $\gamma = 0.1$ ,  $x = 0.4$ ,  $Br = 1$  and  $t = 0.1$ .

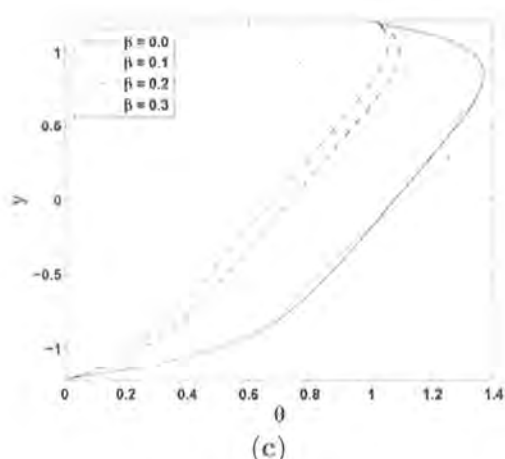
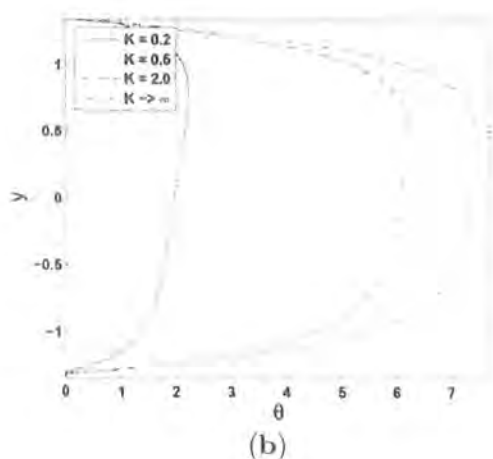


Figure 3.2b: Variations of temperature distribution  $\theta$  for different values of porosity parameter  $K$  when  $E_1 = 1$ ,  $E_2 = 0.2$ ,  $E_3 = 0.1$ ,  $\epsilon = 0.2$ ,  $M = 2$ ,  $\beta = 0.2$ ,  $\gamma = 0.1$ ,  $x = 0.4$ ,  $Br = 2$  and  $t = 0.2$ .

Figure 3.2c: Variations of temperature distribution  $\theta$  for different values of velocity slip parameter  $\beta$  when  $E_1 = 0.8$ ,  $E_2 = 0.2$ ,  $E_3 = 0.1$ ,  $\epsilon = 0.1$ ,  $M = 2$ ,  $K = 5$ ,  $\gamma = 0.1$ ,  $x = 0.3$ ,

$Br = 2$  and  $t = 0.1$ .

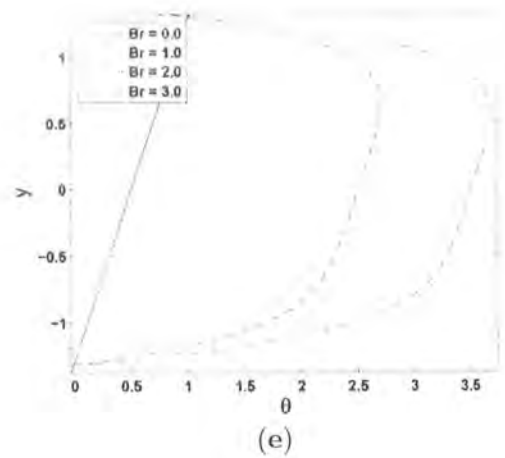
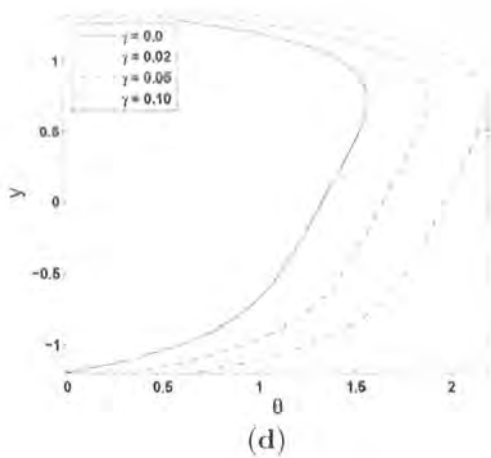


Figure 3.2d: Variations of temperature distribution  $\theta$  for different values of thermal slip parameter  $\gamma$  when  $E_1 = 0.8$ ,  $E_2 = 0.2$ ,  $E_3 = 0.1$ ,  $\epsilon = 0.2$ ,  $M = 2$ ,  $K = 5$ ,  $x = 0.3$ ,  $Br = 2$  and  $t = 0.08$ .

Figure 3.2e: Variations of temperature distribution  $\theta$  for different values of Brinkman number  $Br$  when  $E_1 = 0.5$ ,  $E_2 = 0.2$ ,  $E_3 = 0.1$ ,  $\epsilon = 0.2$ ,  $M = 2$ ,  $K = 5$ ,  $\beta = 0.2$ ,  $\gamma = 0.1$ ,  $x = 0.3$  and  $t = 0.1$ .

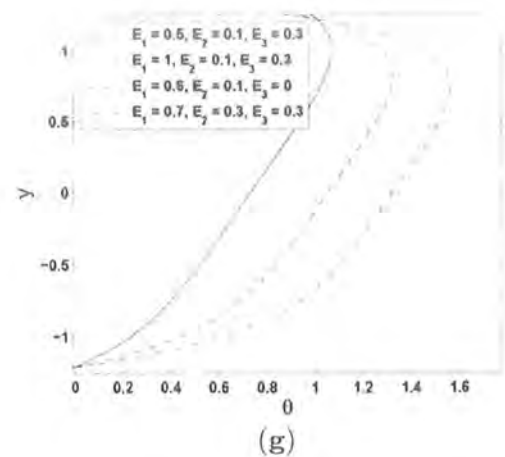
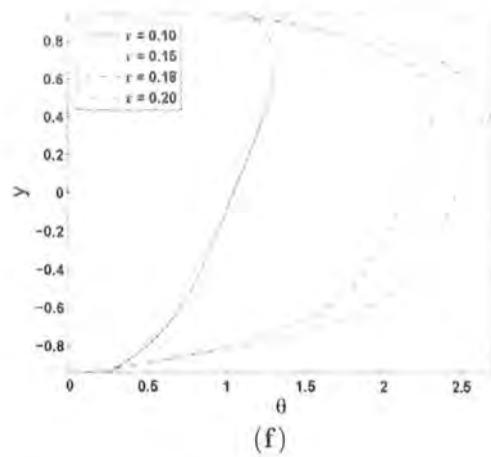


Figure 3.2f: Variations of temperature distribution  $\theta$  for different values of amplitude ratio  $\epsilon$  when  $E_1 = 0.5$ ,  $E_2 = 0.2$ ,  $E_3 = 0.1$ ,  $M = 2$ ,  $K = 5$ ,  $\beta = 0.2$ ,  $\gamma = 0.1$ ,  $Br = 2$ ,  $x = 0.1$  and  $t = 0.1$ .

$t = 0.3$ .

Figure 3.2g: Variations of temperature distribution  $\theta$  for different values of wall parameters when  $\epsilon = 0.1$ ,  $M = 2$ ,  $K = 5$ ,  $\beta = 0.2$ ,  $\gamma = 0.1$ ,  $Br = 2$ ,  $x = 0.3$  and  $t = 0.1$ .

The results presented in Figures 3.3 (a – f) indicate the behavior of  $M$ ,  $K$ ,  $\beta$ ,  $\gamma$ ,  $Br$ ,  $E_1$ ,  $E_2$  and  $E_3$  on the heat transfer coefficient  $Z$ . These Figures show the typical oscillatory behavior of heat transfer which is in view of consideration of the peristaltic motion. Figures 3.3b and 3.3d-3.3f, depict that the absolute value of the heat transfer coefficient increases by increasing  $K$ ,  $\gamma$ ,  $Br$ ,  $E_1$ ,  $E_2$  and  $E_3$  respectively, while the behavior is quite opposite in the cases of  $M$  and  $\beta$  (Figures 3.3a and 3.3c). The damping nature of the wall  $E_3$  has a very insignificant effect on the heat transfer.

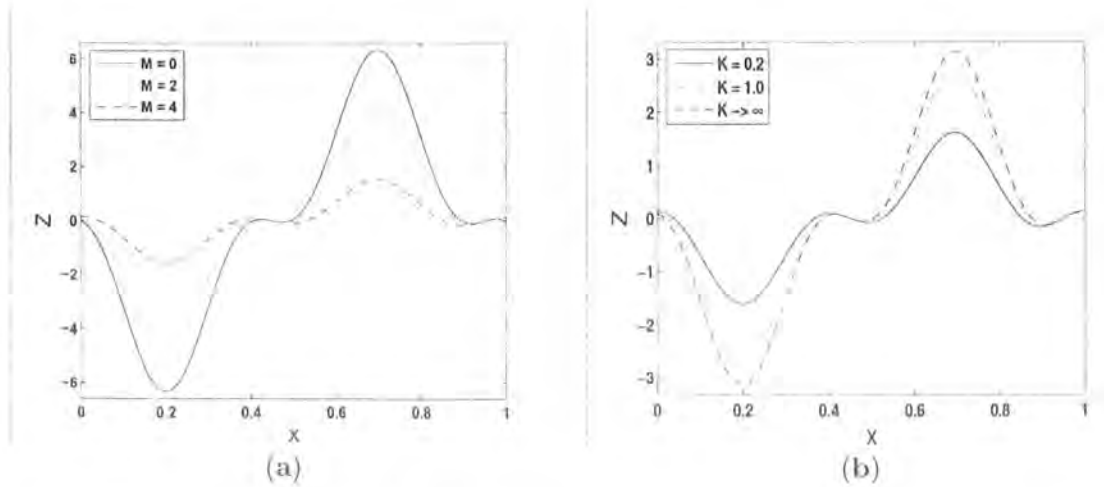


Figure 3.3a: Variations of heat transfer coefficient  $Z$  for different values of Hartman number  $M$  when  $E_1 = 1$ ,  $E_2 = 0.2$ ,  $E_3 = 0.1$ ,  $\epsilon = 0.2$ ,  $K = 0.05$ ,  $\beta = 0.2$ ,  $\gamma = 0.1$ ,  $Br = 1$  and  $t = 0.2$ .

Figure 3.3b: Variations of heat transfer coefficient  $Z$  for different values of porosity parameter  $K$  when  $E_1 = 0.3$ ,  $E_2 = 0.2$ ,  $E_3 = 0.1$ ,  $\epsilon = 0.2$ ,  $M = 4$ ,  $\beta = 0.2$ ,  $\gamma = 0.1$ ,  $Br = 2$  and

$t = 0.1$ .

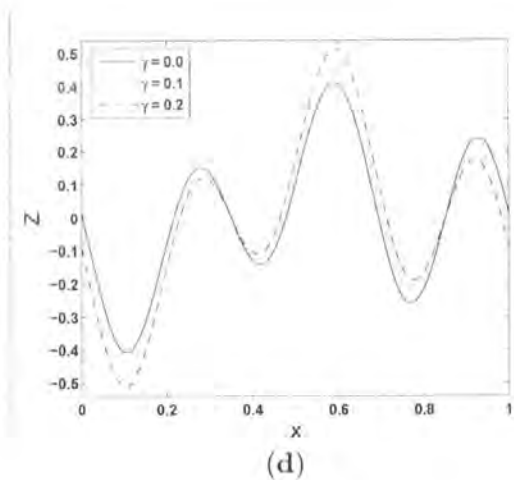
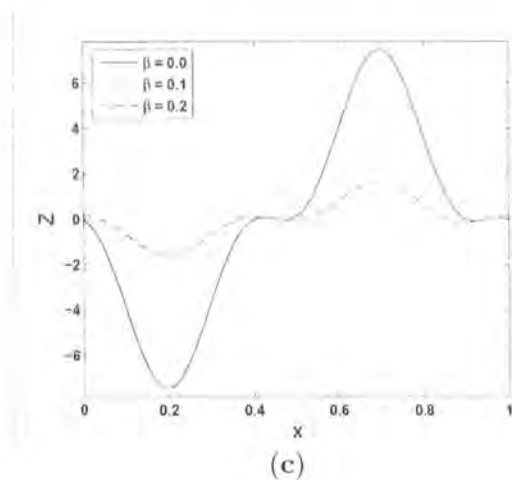


Figure 3.3c: Variations of heat transfer coefficient  $Z$  for different values of velocity slip parameter  $\beta$  when  $E_1 = 0.3$ ,  $E_2 = 0.2$ ,  $E_3 = 0.1$ ,  $\epsilon = 0.2$ ,  $M = 4$ ,  $K = 0.2$ ,  $\gamma = 0.1$ ,  $Br = 2$  and  $t = 0.2$ .

Figure 3.3d: Variations of heat transfer coefficient  $Z$  for different values of thermal slip parameter  $\gamma$  when  $E_1 = 0.8$ ,  $E_2 = 0.1$ ,  $E_3 = 0.1$ ,  $\epsilon = 0.2$ ,  $M = 2$ ,  $K = 0.02$ ,  $\beta = 0.2$ ,  $Br = 2$  and  $t = 0.2$ .

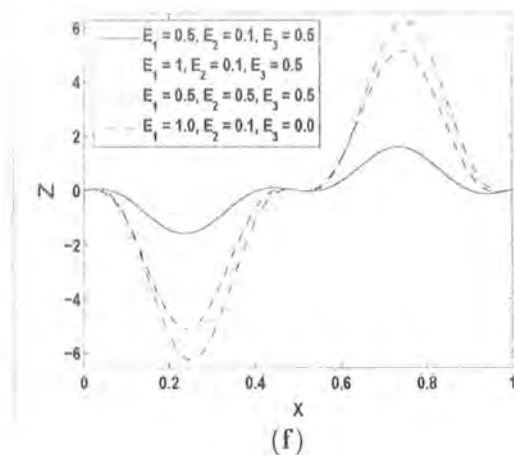
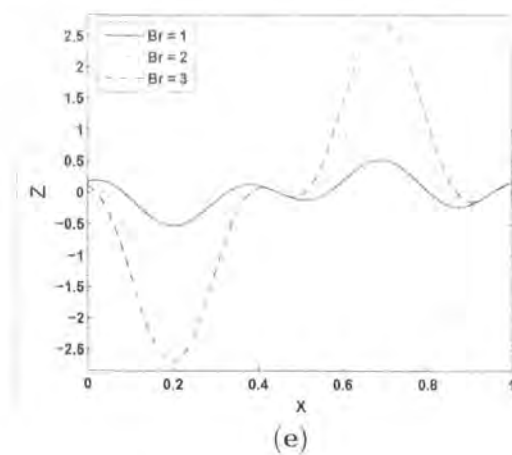
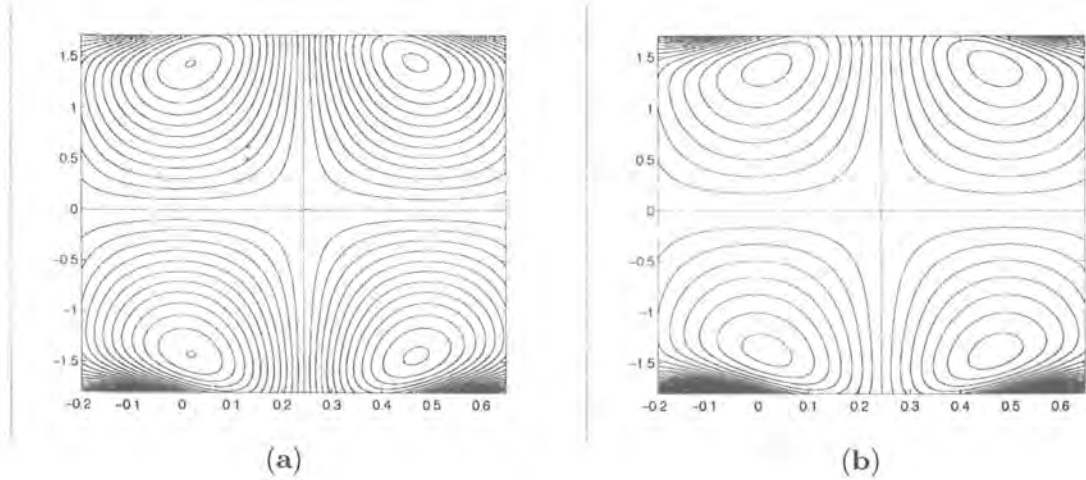
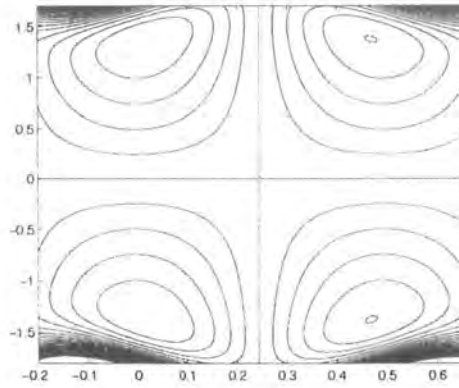


Figure 3.3e: Variations of heat transfer coefficient  $Z$  for different values of Brinkman number  $Br$  when  $E_1 = 0.3$ ,  $E_2 = 0.2$ ,  $E_3 = 0.1$ ,  $\epsilon = 0.2$ ,  $M = 4$ ,  $K = 0.2$ ,  $\beta = 0.2$ ,  $\gamma = 0.1$  and  $t = 0.2$ .

Figure 3.3f: Variations of heat transfer coefficient  $Z$  for different values of wall parameters when  $\epsilon = 0.15$ ,  $M = 1$ ,  $K = 0.05$ ,  $Br = 3$ ,  $\beta = 0.2$ ,  $\gamma = 0.1$  and  $t = 0.25$ .

The formation of an internally circulating bolus of fluid by closed streamlines is shown in Figures 3.4(a-c)-3.7(a-d). Figures 3.4(a-c) display the effect of the Hartman number  $M$  on the streamlines for fixed value of the other parameters. These Figures show that the size of the trapping bolus decreases with an increase in the Hartman number  $M$ , while the behavior is quite opposite in the case of the permeability parameter  $K$  (Figures 3.5(a-c)). Figures 3.6(a-c) reveal that the behavior of velocity for slip parameter  $\beta$  on the streamlines. Here we observed that the number of the streamlines increases by increasing  $\beta$ . The effect of the elastic parameters on the streamlines is plotted in Figures 3.7(a-d). The number of the trapped bolus increases with an increase in  $E_1$ ,  $E_2$  and  $E_3$ . We also note that the damping seems less effective in the trapping phenomenon.

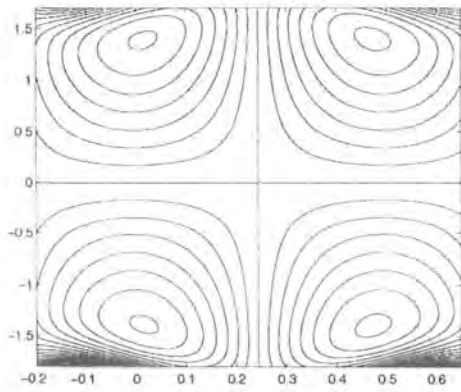




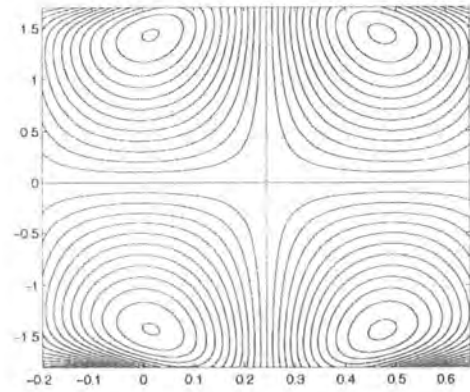
(c)

Figure 3.4: Streamlines for (a)  $M = 0$ , (b)  $M = 4$ , (c)  $M = 6$ .

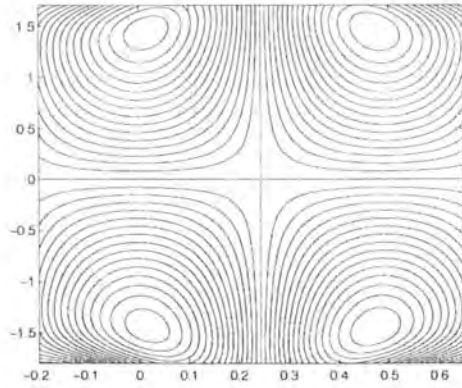
The other parameters chosen are ( $\epsilon = 0.2$ ,  $\beta = 0.1$ ,  $E_1 = 0.3$ ,  $E_2 = 0.1$ ,  $E_3 = 0.1$ ,  $K = 0.04$  and  $t = 0$ ).



(a)



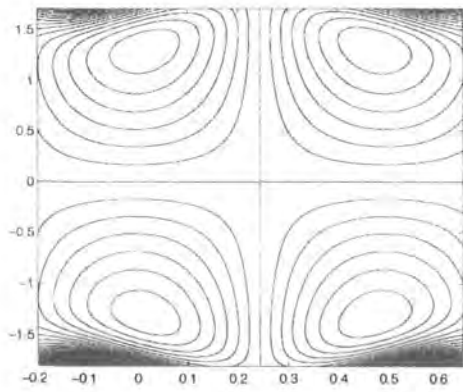
(b)



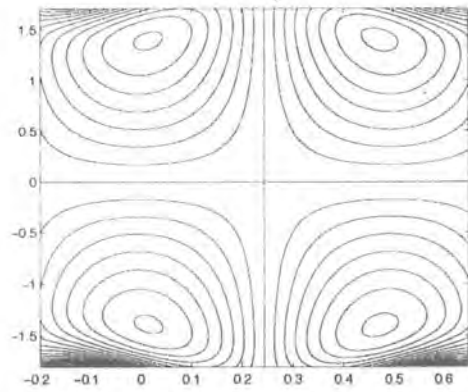
(c)

Figure 3.5: Streamlines for (a)  $K = 0.05$ , (b)  $K = 0.2$ , (c)  $K \rightarrow \infty$ .

The other parameters chosen are ( $\epsilon = 0.17$ ,  $\beta = 0.1$ ,  $E_1 = 0.3$ ,  $E_2 = 0.1$ ,  $E_3 = 0.1$ ,  $M = 4$  and  $t = 0$ ).

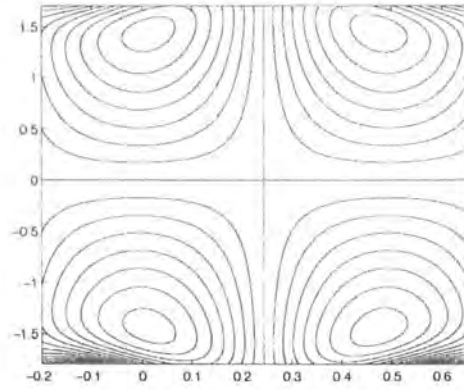


(a)



(b)





(c)

Figure 3.6: Streamlines for (a)  $\beta = 0$ , (b)  $\beta = 0.1$ , (c)  $\beta = 0.2$ .

The other parameters chosen are ( $\epsilon = 0.17$ ,  $E_1 = 0.3$ ,  $E_2 = 0.1$ ,  $E_3 = 0.1$ ,  $M = 4$ ,  $K = 0.05$  and  $t = 0$ ).

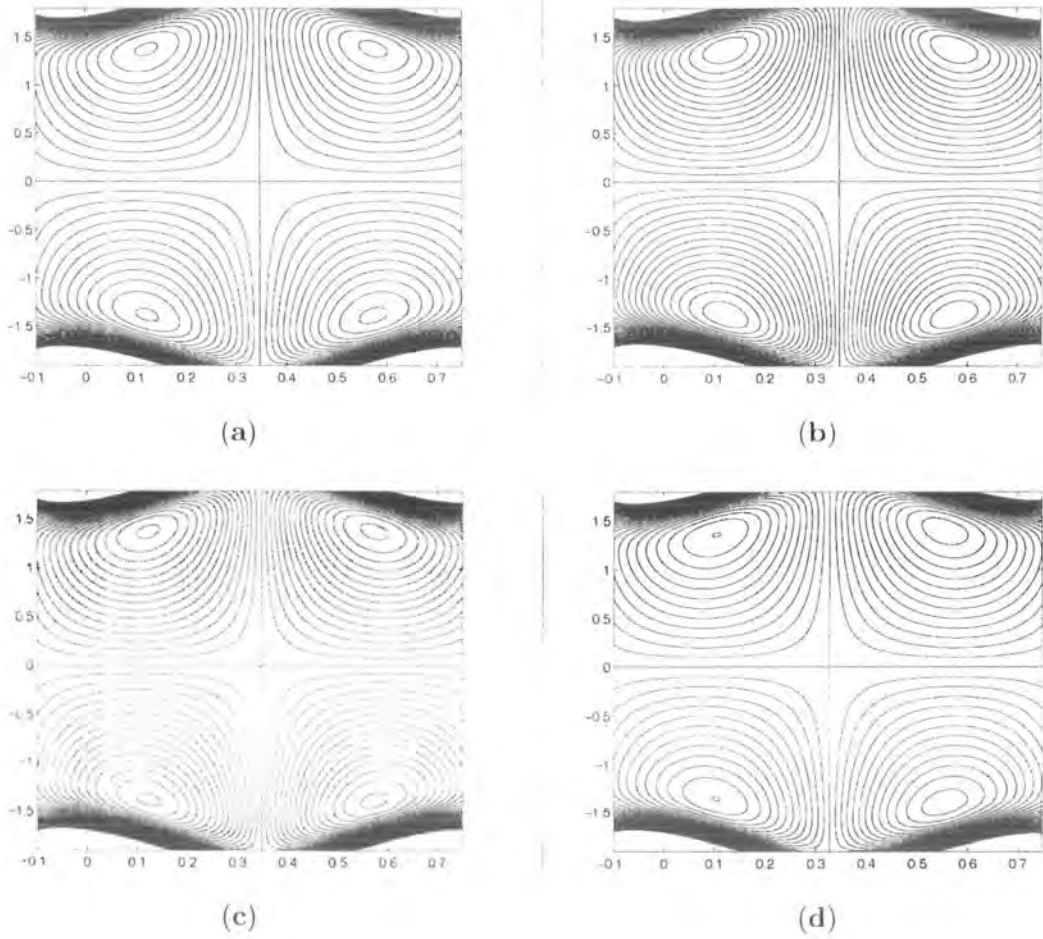


Figure 3.7: Streamlines for ( $\epsilon = 0.2$ ,  $\beta = 0.1$ ,  $K = 0.04$ ,  $M = 5$  and  $t = 0.1$ ).

(a)  $E_1 = 0.5$ ,  $E_2 = 0.3$ ,  $E_3 = 0.1$ .

(b)  $E_1 = 0.8$ ,  $E_2 = 0.3$ ,  $E_3 = 0.1$ .

(c)  $E_1 = 0.5$ ,  $E_2 = 0.5$ ,  $E_3 = 0.1$ .

(d)  $E_1 = 0.5$ ,  $E_2 = 0.3$ ,  $E_3 = 0.7$ .

### 3.5 Closing remarks

Theoretical study for the slip effects in the magnetohydrodynamic peristaltic flow of viscous fluid through a porous medium is presented in the presence of heat transfer. The main findings

are summed up below.

- There is an increase in the longitudinal velocity in the neighborhood of the walls when velocity slip parameter increases. Further such behavior is maintained at the channel centre.
- Temperature decreases in view of increasing velocity slip parameter.
- The behavior of velocity and thermal slip parameters on the temperature are opposite.
- Brinkman number and velocity slip parameter has reverse effects on the temperature. On the other hand, the variations of Brinkman number and thermal slip parameter are similar qualitatively.
- Heat transfer coefficient at the upper wall is decreasing function of velocity slip parameter.
- The influence of Hartman number on the heat transfer coefficient at the upper wall is quite opposite to that of a Brinkman number.
- The absolute value of the heat transfer coefficient increases in the upper part of the channel when the elastic parameters increase.

## Chapter 4

# Peristaltic transport of viscous fluid in a curved channel with compliant walls

This chapter looks at the influence of compliant wall properties and heat transfer on the peristaltic flow of an incompressible viscous fluid in a curved channel. The equations are first modelled and then solved for stream function, velocity and temperature profiles. The variations of various interesting parameters are shown and examined very carefully.

### 4.1 Mathematical model

We consider a curved channel of thickness  $2d$  filled with an incompressible viscous fluid. The channel is coiled in a circle with centre  $O$  and radius  $R^*$ . The flow in the channel is induced by sinusoidal waves of small amplitude  $a$ . Moreover the channel walls are of compliant nature. The temperatures of the lower and upper walls of the channel are  $T_0$  and  $T_1$  respectively. The displacements of the channel walls are considered as follows:

$$r = \pm\eta = \pm \left[ d + a \sin \left( \frac{2\pi}{\lambda} (x - ct) \right) \right],$$

where  $\lambda$  is the wavelength and  $c$  is the wave speed. Let  $v$  and  $u$  denote the velocity components in the radial ( $r$ ) and axial ( $x$ ) directions respectively.

The governing equations in the absence of body forces can be written as

$$\frac{\partial [(r + R^*)v]}{\partial r} + R^* \frac{\partial u}{\partial x} = 0, \quad (4.1)$$

$$\begin{aligned} \rho \left( \frac{\partial v}{\partial t} + v \frac{\partial v}{\partial r} + \frac{uR^*}{r + R^*} \frac{\partial v}{\partial x} - \frac{u^2}{r + R^*} \right) &= -\frac{\partial p}{\partial r} + \frac{2\mu}{r + R^*} \frac{\partial}{\partial r} \left[ (r + R^*) \frac{\partial v}{\partial r} \right] \\ + \frac{R^*\mu}{r + R^*} \frac{\partial}{\partial x} \left[ \frac{\partial u}{\partial r} + \frac{R^*}{r + R^*} \frac{\partial v}{\partial x} - \frac{u}{r + R^*} \right] &- \left( \frac{2\mu}{r + R^*} \right) \left( \frac{R^*}{r + R^*} \frac{\partial u}{\partial x} + \frac{v}{r + R^*} \right), \end{aligned} \quad (4.2)$$

$$\begin{aligned} \rho \left( \frac{\partial u}{\partial t} + v \frac{\partial u}{\partial r} + \frac{R^*}{r + R^*} u \frac{\partial u}{\partial x} + \frac{uv}{r + R^*} \right) &= -\frac{R^*}{r + R^*} \frac{\partial p}{\partial x} + \frac{\mu}{(r + R^*)^2} \frac{\partial}{\partial r} \left[ (r + R^*)^2 \frac{\partial u}{\partial r} \right] \\ + \frac{\mu}{(r + R^*)^2} \frac{\partial}{\partial r} \left[ (r + R^*)^2 \left( \frac{R^*}{r + R^*} \frac{\partial v}{\partial x} - \frac{u}{r + R^*} \right) \right] \\ + \left( \frac{2\mu R^*}{r + R^*} \right) \frac{\partial}{\partial x} \left( \frac{R^*}{r + R^*} \frac{\partial u}{\partial x} + \frac{v}{r + R^*} \right), \end{aligned} \quad (4.3)$$

$$\begin{aligned} \rho C_p \left( \frac{\partial T}{\partial t} + v \frac{\partial T}{\partial r} + \frac{uR^*}{r + R^*} \frac{\partial T}{\partial x} \right) &= \kappa \left[ \frac{\partial^2 T}{\partial r^2} + \frac{1}{r + R^*} \frac{\partial T}{\partial r} + \left( \frac{R^*}{r + R^*} \right)^2 \frac{\partial^2 T}{\partial x^2} \right] \\ + \mu \left[ 2 \left( \frac{\partial v}{\partial r} \right)^2 + \left( \frac{\partial u}{\partial r} + \frac{R^*}{r + R^*} \frac{\partial v}{\partial x} - \frac{u}{r + R^*} \right) \left( \frac{R^*}{r + R^*} \frac{\partial v}{\partial x} - \frac{u}{r + R^*} \right) \right] \\ + \mu \frac{\partial u}{\partial r} \left[ \left( \frac{\partial u}{\partial r} + \frac{R^*}{r + R^*} \frac{\partial v}{\partial x} - \frac{u}{r + R^*} \right) \right] &+ 2\mu \left( \frac{R^*}{r + R^*} \frac{\partial u}{\partial x} + \frac{v}{r + R^*} \right)^2. \end{aligned} \quad (4.4)$$

The boundary conditions are taken in the forms given below

$$u = 0 \quad \text{at} \quad r = \pm\eta = \pm \left[ d + a \sin \left( \frac{2\pi}{\lambda} (x - ct) \right) \right], \quad (4.5)$$

$$\begin{aligned} \frac{R^*}{r + R^*} \frac{\partial}{\partial x} L(\eta) &= \frac{R^*}{r + R^*} \frac{\partial p}{\partial x} \\ = \frac{\mu}{(r + R^*)^2} \frac{\partial}{\partial r} \left[ (r + R^*)^2 \left( \frac{\partial u}{\partial r} + \frac{R^*}{r + R^*} \frac{\partial v}{\partial x} - \frac{u}{r + R^*} \right) \right] &+ \left( \frac{2\mu R^*}{r + R^*} \right) \frac{\partial}{\partial x} \left( \frac{R^*}{r + R^*} \frac{\partial u}{\partial x} + \frac{v}{r + R^*} \right) \\ - \rho \left( \frac{\partial u}{\partial t} + v \frac{\partial u}{\partial r} + \frac{R^*}{r + R^*} u \frac{\partial u}{\partial x} + \frac{uv}{r + R^*} \right) &\text{at } r = \pm\eta, \end{aligned} \quad (4.6)$$

$$T = T_0 \quad \text{on } r = -\eta, \quad (4.7)$$

$$T = T_1 \quad \text{on } r = \eta. \quad (4.8)$$

Here  $\rho$ ,  $t$ ,  $p$ ,  $\mu$ ,  $C_p$ ,  $\kappa$  and  $T$  are the fluid density, the time, the pressure, the dynamic viscosity, the specific heat, the thermal conductivity and the temperature respectively. Further,

$L = -\sigma \frac{\partial^2}{\partial x^2} + m \frac{\partial^2}{\partial t^2} + C \frac{\partial}{\partial t}$ ,  $\sigma$  is the longitudinal tension per unit width,  $m$  is the mass per unit area and  $C$  is the coefficient of viscous damping.

## 4.2 Dimensionless formulation

On setting

$$u = -\frac{\partial \Psi}{\partial r}, \quad v = \delta \frac{k}{r+k} \frac{\partial \Psi}{\partial x}$$

and defining the following non-dimensional variables

$$\begin{aligned} x^* &= \frac{x}{\lambda}, \quad r^* = \frac{r}{d}, \quad u = \frac{u^*}{c}, \quad v = \frac{v^*}{c}, \quad \Psi^* = \frac{\Psi}{cd}, \quad t^* = \frac{ct}{\lambda}, \\ \eta^* &= \frac{\eta}{d}, \quad p^* = \frac{d^2 p}{\mu c \lambda}, \quad k = \frac{R^*}{d}, \quad R = \frac{cd}{\nu}, \quad \epsilon = \frac{a}{d}, \quad \delta = \frac{d}{\lambda}, \\ E_1 &= -\frac{\sigma d^3}{\lambda^3 \mu c}, \quad E_2 = \frac{mcd^3}{\lambda^3 \mu}, \quad E_3 = \frac{Cd^3}{\lambda^2 \mu}, \quad \text{Pr} = \frac{\rho \nu C_p}{\kappa}, \\ E &= \frac{c^2}{C_p (T_1 - T_0)}, \quad \theta = \frac{T - T_0}{T_1 - T_0}, \end{aligned}$$

equation (4.1) is satisfied identically and equations (4.2 to 4.8) now are expressed as

$$\begin{aligned} R\delta \left[ \delta^2 \left( \frac{k}{r+k} \right) \Psi_{xt} + \delta^2 \left( \frac{k}{r+k} \right)^2 \Psi_{rx} - \delta^2 \left( \frac{k}{r+k} \right)^2 \Psi_r \Psi_{xx} - \frac{1}{(r+k)^2} \Psi_r^2 \right] &= -\frac{\partial p}{\partial r} \\ + \frac{\delta}{r+k} \frac{\partial}{\partial r} [(r+k) S_{rr}] + k\delta^2 \frac{\partial S_{rx}}{\partial x} - \frac{\delta}{(r+k)} S_{xx}, \end{aligned} \quad (4.9)$$

$$\begin{aligned} R \left[ -\delta \Psi_{rt} - \delta \left( \frac{k}{r+k} \right) \Psi_x \Psi_{rr} + \delta \left( \frac{k}{r+k} \right) \Psi_r \Psi_{rx} - \delta \frac{k}{(r+k)^2} \Psi_r \Psi_x \right] &= -\left( \frac{k}{r+k} \right) \frac{\partial p}{\partial x} \\ + \frac{1}{(r+k)^2} \frac{\partial}{\partial r} [(r+k)^2 S_{rx}] + \delta \left( \frac{k}{r+k} \right) \frac{\partial S_{xx}}{\partial x}, \end{aligned} \quad (4.10)$$

$$S_{rr} = 2\delta \left( \frac{k}{r+k} \right) \Psi_{rx}, \quad (4.11)$$

$$S_{rx} = -\Psi_{rr} + \delta^2 \left( \frac{k}{r+k} \right)^2 \Psi_{xx} + \frac{1}{(r+k)} \Psi_r, \quad (4.12)$$

$$S_{xx} = 2 \left[ -\delta \left( \frac{k}{r+k} \right) \Psi_{rx} + \delta \frac{k}{(r+k)^2} \Psi_x \right], \quad (4.13)$$

$$\Psi_r = 0 \quad \text{at} \quad r = \pm \eta = \pm [1 + \epsilon \sin 2\pi(x-t)], \quad (4.14)$$

$$\frac{k}{r+k} \left[ E_1 \frac{\partial^3 \eta}{\partial x^3} + E_2 \frac{\partial^3 \eta}{\partial t^2 \partial x} + E_3 \frac{\partial^2 \eta}{\partial t \partial x} \right] = \frac{1}{(r+k)^2} \frac{\partial}{\partial r} \left[ (r+k)^2 S_{rx} \right] + \delta \left( \frac{k}{r+k} \right) \frac{\partial S_{xx}}{\partial x} - R \left[ -\delta \Psi_{rt} - \delta \left( \frac{k}{r+k} \right) \Psi_x \Psi_{rr} + \delta \left( \frac{k}{r+k} \right) \Psi_r \Psi_{rx} - \delta \frac{k}{(r+k)^2} \Psi_r \Psi_x \right] \text{ at } r = \pm \eta, \quad (4.15)$$

$$\text{Pr } R \delta \left[ \frac{\partial \theta}{\partial t} + \delta \left( \frac{k}{r+k} \right) \Psi_x \frac{\partial \theta}{\partial r} - \frac{\delta}{r+k} \Psi_r \frac{\partial \theta}{\partial x} \right] = \frac{\partial^2 \theta}{\partial r^2} + \frac{1}{r+k} \frac{\partial \theta}{\partial r} + \delta^2 \left( \frac{k}{r+k} \right)^2 \frac{\partial^2 \theta}{\partial x^2} + Br \left[ 2\delta^2 \left( \frac{k}{r+k} \right)^2 \Psi_{rx}^2 + \left( -\Psi_{rr} + \frac{\Psi_r}{r+k} + \delta^2 \left( \frac{k}{r+k} \right)^2 \Psi_{xx} \right) \left( \frac{\Psi_r}{r+k} + \delta^2 \frac{k}{(r+k)^2} \Psi_{xx} \right) - \Psi_{rr} \left( -\Psi_{rr} + \frac{\Psi_r}{r+k} + \delta^2 \left( \frac{k}{r+k} \right)^2 \Psi_{xx} \right) + 2\delta^2 \left( -\left( \frac{k}{r+k} \right) \Psi_{rx} + \frac{k}{(r+k)^2} \Psi_x \right)^2 \right], \quad (4.16)$$

$$\theta = 0 \text{ at } r = -\eta, \quad (4.17)$$

$$\theta = 1 \text{ at } r = \eta. \quad (4.18)$$

The above equations after employing long wavelength and low Reynolds number approximations give

$$-\frac{k}{r+k} \frac{\partial p}{\partial x} + \frac{1}{(r+k)^2} \frac{\partial}{\partial r} \left[ (r+k)^2 \left( -\Psi_{rr} + \frac{\Psi_r}{r+k} \right) \right] = 0, \quad (4.19)$$

$$\frac{\partial^2 \theta}{\partial r^2} + \frac{1}{r+k} \frac{\partial \theta}{\partial r} + Br \left[ \frac{\Psi_r}{r+k} \left( -\Psi_{rr} + \frac{\Psi_r}{r+k} \right) + \Psi_{rr}^2 - \frac{\Psi_r \Psi_{rr}}{r+k} \right] = 0, \quad (4.20)$$

$$\Psi_r = 0 \text{ at } r = \pm \eta = \pm [1 + \epsilon \sin 2\pi(x-t)], \quad (4.21)$$

$$\frac{1}{(r+k)^2} \frac{\partial}{\partial r} \left[ (r+k)^2 \left( -\Psi_{rr} + \frac{\Psi_r}{r+k} \right) \right] = \frac{k}{r+k} \left[ E_1 \frac{\partial^3 \eta}{\partial x^3} + E_2 \frac{\partial^3 \eta}{\partial t^2 \partial x} + E_3 \frac{\partial^2 \eta}{\partial t \partial x} \right] \text{ at } r = \pm \eta, \quad (4.22)$$

$$\theta = 0 \text{ at } r = -\eta, \quad (4.23)$$

$$\theta = 1 \text{ at } r = \eta, \quad (4.24)$$

where for brevity, the asterisks are omitted,  $\Psi$  is the stream function, Pr is the Prandtl number,  $E$  is the Eckert number and  $Br = \text{Pr } E$  is the Brinkman number.

### 4.3 Solution of the problem

The closed form solution of equation (4.19) is given by

$$\begin{aligned}\Psi &= \frac{G}{4} (r+k)^2 \left[ \ln(r+k) - \frac{1}{2} \right] + \frac{C_1}{2} \ln(r+k) + \frac{C_2}{2} (r+k)^2 + C_3, \\ G &= 8\epsilon\pi^3 k \left[ \frac{E_3 \sin 2\pi(x-t)}{2\pi} - (E_1 + E_2) \cos 2\pi(x-t) \right],\end{aligned}\quad (4.25)$$

Using the boundary conditions (4.21) and (4.22), the values of the constants are

$$\begin{aligned}C_1 &= \frac{G}{4k\eta} (k^2 - \eta^2)^2 \ln\left(\frac{k+\eta}{k-\eta}\right), \\ C_2 &= -\frac{G}{8k\eta} \left[ (k+\eta)^2 \ln(k+\eta) - (k-\eta)^2 \ln(k-\eta) \right], \\ C_3 &= -\frac{G}{4} k^2 \left[ \ln(r+k) - \frac{1}{2} \right] - \frac{C_1}{2} \ln k - \frac{C_2}{2} k^2,\end{aligned}$$

From equation (4.20) we have

$$\theta = -Br \left[ \frac{C_1^2}{4(r+k)^2} - \frac{C_1 G}{2} \ln^2(r+k) + \frac{G^2}{16} (r+k)^2 \right] + D_1 \ln(r+k) + D_2. \quad (4.26)$$

The value of the constants subject to the boundary conditions (4.23) and (4.24) are

$$\begin{aligned}D_1 &= \frac{1}{\ln\left(\frac{k+\eta}{k-\eta}\right)} \left\{ 1 + Br \left[ -\frac{C_1^2 k \eta}{(k+\eta)^2 (k-\eta)^2} + \frac{G^2 k \eta}{4} - \frac{C_1 G}{2} (\ln^2(k+\eta) - \ln^2(k-\eta)) \right] \right\}, \\ D_2 &= \frac{1}{\ln\left(\frac{k-\eta}{k+\eta}\right)} \left\{ \ln(k-\eta) + Br \left[ -\frac{C_1 G}{2} (\ln^2(k+\eta) \ln(k-\eta) - \ln^2(k-\eta) \ln(k+\eta)) \right. \right. \\ &\quad \left. \left. + \frac{C_1^2}{4} \left( \frac{\ln(k-\eta)}{(k+\eta)^2} - \frac{\ln(k+\eta)}{(k-\eta)^2} \right) + \frac{G^2}{16} [\ln(k-\eta)(k+\eta)^2 - \ln(k+\eta)(k-\eta)^2] \right] \right\}.\end{aligned}$$

The longitudinal velocity is

$$\begin{aligned}u &= -\frac{\partial \Psi}{\partial r} \\ &= -\left[ \frac{G}{2} (r+k) \ln(r+k) + \frac{C_1}{2(r+k)} + C_2 (r+k) \right]\end{aligned}\quad (4.27)$$



and the heat transfer coefficient at the upper wall is

$$\begin{aligned} Z &= \eta_x \theta_r(\eta) \\ &= -\eta_x Br \left[ \frac{-C_1^2}{2(k+\eta)^3} - C_1 G \frac{\ln(k+\eta)}{(k+\eta)} + \frac{G^2}{8}(r+k) \right]. \end{aligned} \quad (4.28)$$

#### 4.4 Graphical results and discussion

We study the behavior of the longitudinal velocity, stream function, temperature and heat transfer coefficient in this section. For this purpose, Figures 4.1 (a – c)-4.6 (a – c) have been plotted. Figures 4.1 (a – c) examine the effect of various parameters on the longitudinal velocity  $u$ . It is observed that the longitudinal velocity  $u$  increases with an increase in the curvature  $k$  in the upper half of the channel while the reverse situation is observed in the lower half of the channel. The effect of the occlusion parameter  $\epsilon$  on  $u$  is depicted in Figure 4.1b. We observe that there is an increase in the longitudinal velocity when  $\epsilon$  increases. The variations of the elastic parameters  $E_1$ ,  $E_2$  and  $E_3$  are shown in Figure 4.1c. This Fig. indicates that by increasing the elastic parameters ( $E_1$ ,  $E_2$  and  $E_3$ ), the velocity increases. It is also interesting to note that the velocity profile is parabolic for fixed values of the parameters and its magnitude is maximum near the centre of the channel. Moreover, it is observed that the elastic tension  $E_1$  has a significant effect on the axial velocity when compared with the mass characterizing parameter  $E_2$  and the damping nature of the wall  $E_3$ .

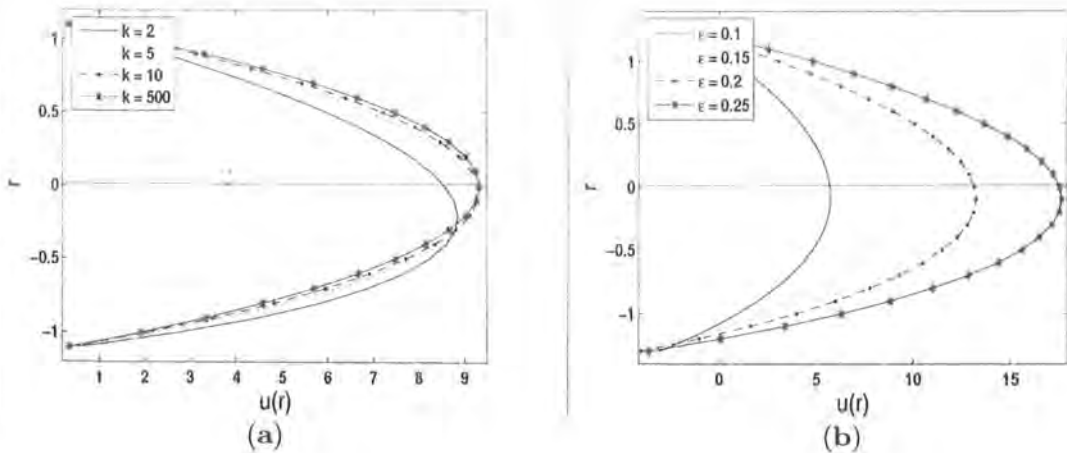


Figure 4.1a: Variations of the longitudinal velocity  $u$  for different values of curvature parameter  $k$  when  $E_1 = 0.5$ ,  $E_2 = 0.2$ ,  $E_3 = 0.1$ ,  $\epsilon = 0.15$ ,  $x = 0.2$  and  $t = 0.05$ .

Figure 4.1b: Variations of the longitudinal velocity  $u$  for different values of occlusion parameter  $\epsilon$  when  $E_1 = 0.5$ ,  $E_2 = 0.2$ ,  $E_3 = 0.1$ ,  $k = 5$ ,  $x = 0.2$  and  $t = 0.05$ .

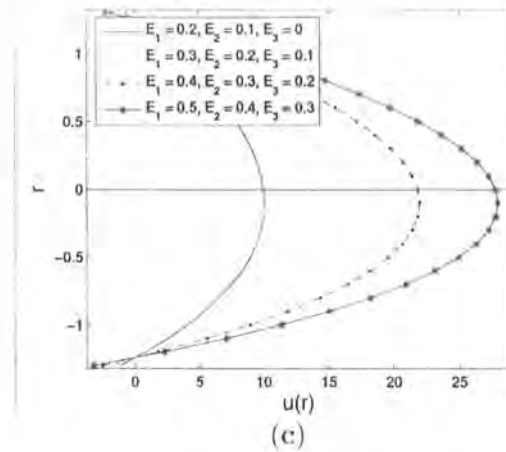


Figure 4.1c: Variations of the longitudinal velocity  $u$  for different values of elastic parameters when  $k = 5$ ,  $\epsilon = 0.3$ ,  $x = 0.2$  and  $t = 0.05$ .

In Figures 4.2(a – d), the nature of the temperature profiles is also parabolic. Here the temperature increases by increasing the Brinkman number  $Br$  (Figure 4.2a) and the occlusion parameter  $\epsilon$  (Figure 4.2c). The variations of the curvature parameter  $k$  is sketched in Figure 4.2b. Obviously the temperature is a decreasing function of  $k$ . A small change has been observed from this figure for large values of  $k$ . Figure 4.2d elucidates the effect of the elastic parameters  $E_1$ ,  $E_2$  and  $E_3$  on the temperature. The amplitude of temperature increases upon increasing  $E_1$ ,  $E_2$  and  $E_3$ . It is further observed that the effect of  $E_1$  on temperature is quite significant.

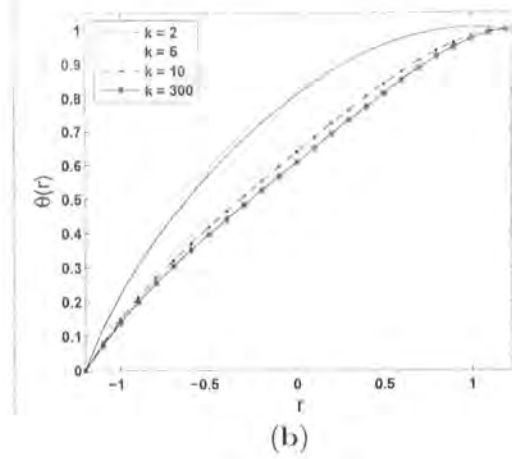
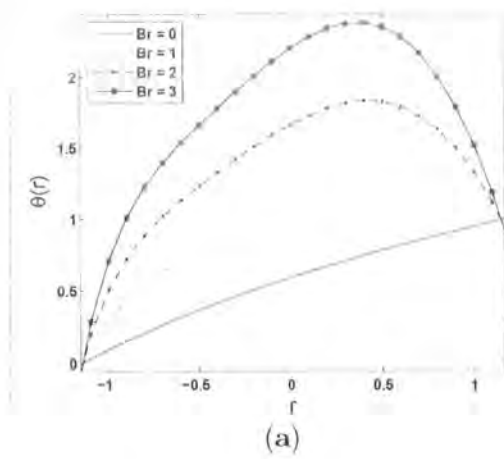


Figure 4.2a: Variations of temperature distribution  $\theta$  for different values of Brinkman number  $Br$  when  $E_1 = 1$ ,  $E_2 = 0.5$ ,  $E_3 = 0.3$ ,  $\epsilon = 0.15$ ,  $k = 3$ ,  $x = 0.3$  and  $t = 0.05$ .

Figure 4.2b: Variations of temperature distribution  $\theta$  for different values of curvature parameter  $k$  when  $E_1 = 1$ ,  $E_2 = 0.5$ ,  $E_3 = 0.1$ ,  $\epsilon = 0.2$ ,  $Br = 1$ ,  $x = 0.3$  and  $t = 0.05$ .

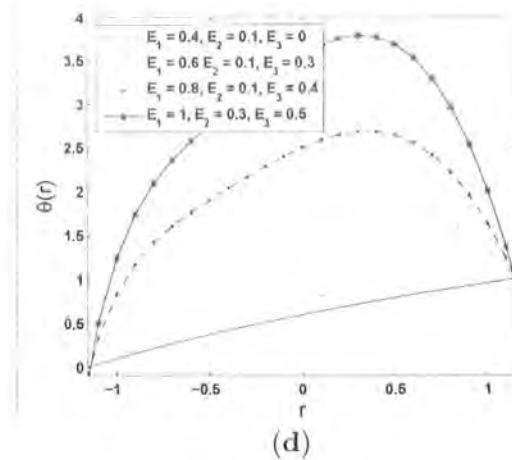
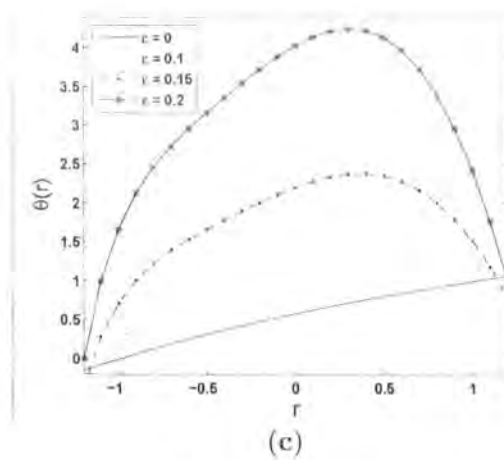


Figure 4.2c: Variations of temperature distribution  $\theta$  for different values of occlusion parameter  $\epsilon$  when  $E_1 = 1$ ,  $E_2 = 0.5$ ,  $E_3 = 0.3$ ,  $Br = 3$ ,  $k = 3$ ,  $x = 0.3$  and  $t = 0.05$ .

Figure 4.2d: Variations of temperature distribution  $\theta$  for different values of elastic param-

ters when  $\epsilon = 0.15$ ,  $Br = 2$ ,  $x = 0.3$ ,  $k = 3$  and  $t = 0.05$ .

The results presented in Figures 4.3 (a – d) indicate the behavior of  $k$ ,  $\epsilon$ ,  $E_1$ ,  $E_2$ ,  $E_3$  and  $Br$  on the heat transfer coefficient  $Z$ . These figures display the typical oscillatory behavior of heat transfer which may be due to the peristaltic phenomenon. Figures 4.3 (a – d) describes the absolute value of the heat transfer coefficient. This coefficient increases by increasing  $k$ ,  $\epsilon$ ,  $E_1$ ,  $E_2$ ,  $E_3$  and  $Br$  respectively.

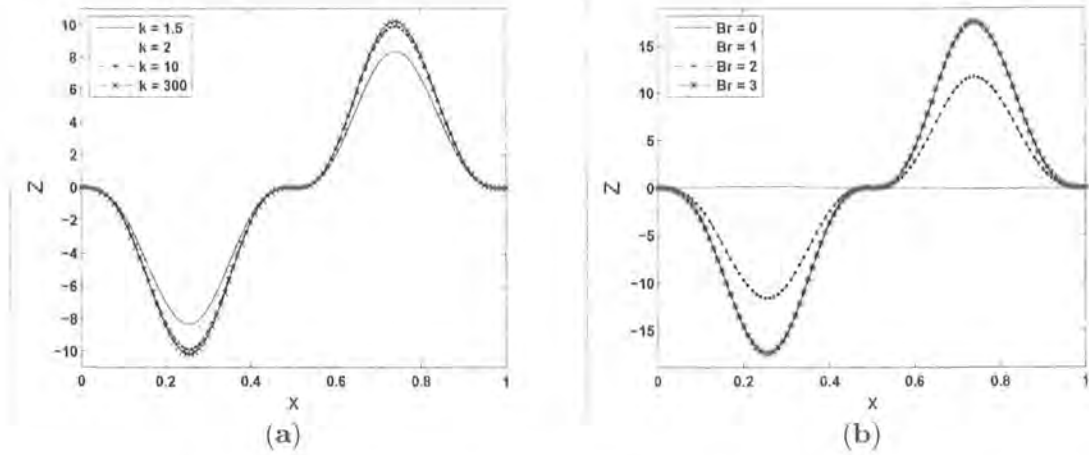


Figure 4.3a: Variations of heat transfer coefficient  $Z$  for different values of curvature parameter  $k$  when  $E_1 = 0.5$ ,  $E_2 = 0.3$ ,  $E_3 = 0.1$ ,  $\epsilon = 0.05$ ,  $Br = 1$  and  $t = 0.25$ .

Figure 4.3b: Variations of heat transfer coefficient  $Z$  for different values of Brinkman number  $Br$  when  $E_1 = 0.5$ ,  $E_2 = 0.15$ ,  $E_3 = 0.1$ ,  $\epsilon = 0.05$ ,  $k = 2$  and  $t = 0.25$ .

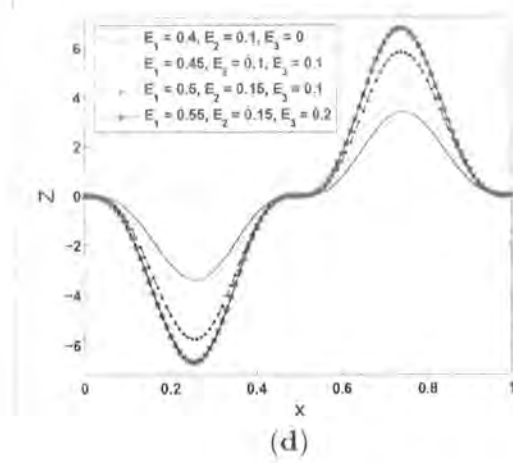
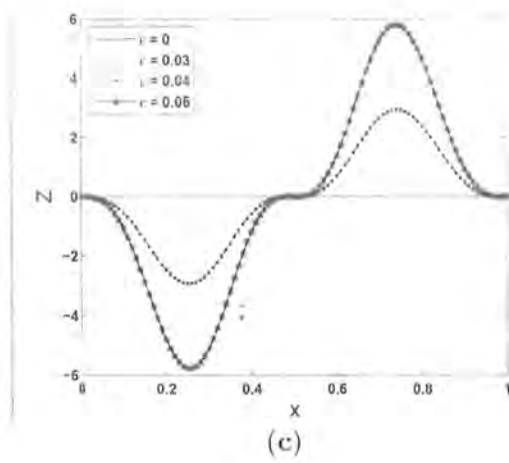


Figure 4.3c: Variations of heat transfer coefficient  $Z$  for different values of occlusion parameter  $\epsilon$  when  $E_1 = 0.5$ ,  $E_2 = 0.15$ ,  $E_3 = 0.1$ ,  $k = 2$ ,  $Br = 1$  and  $t = 0.25$ .

Figure 4.3d: Variations of heat transfer coefficient  $Z$  for different values of elastic parameters when  $\epsilon = 0.05$ ,  $k = 2$ ,  $Br = 1$  and  $t = 0.25$ .

The formation of an internally circulating bolus of fluid by closed streamlines is shown in Figures 4.4(a - c)-4.6(a - c). Figures 4.4(a - c) display the effect of curvature parameter  $k$  on the streamlines for fixed values of the other parameters. This Figure shows that the size of the trapping bolus increases when  $k$  increases. From Figures 4.5(a - c) and 4.6(a - c), we observe that the streamline increases with an increase in the occlusion parameter  $\epsilon$  and the elastic parameters  $E_1$ ,  $E_2$  and  $E_3$  respectively.

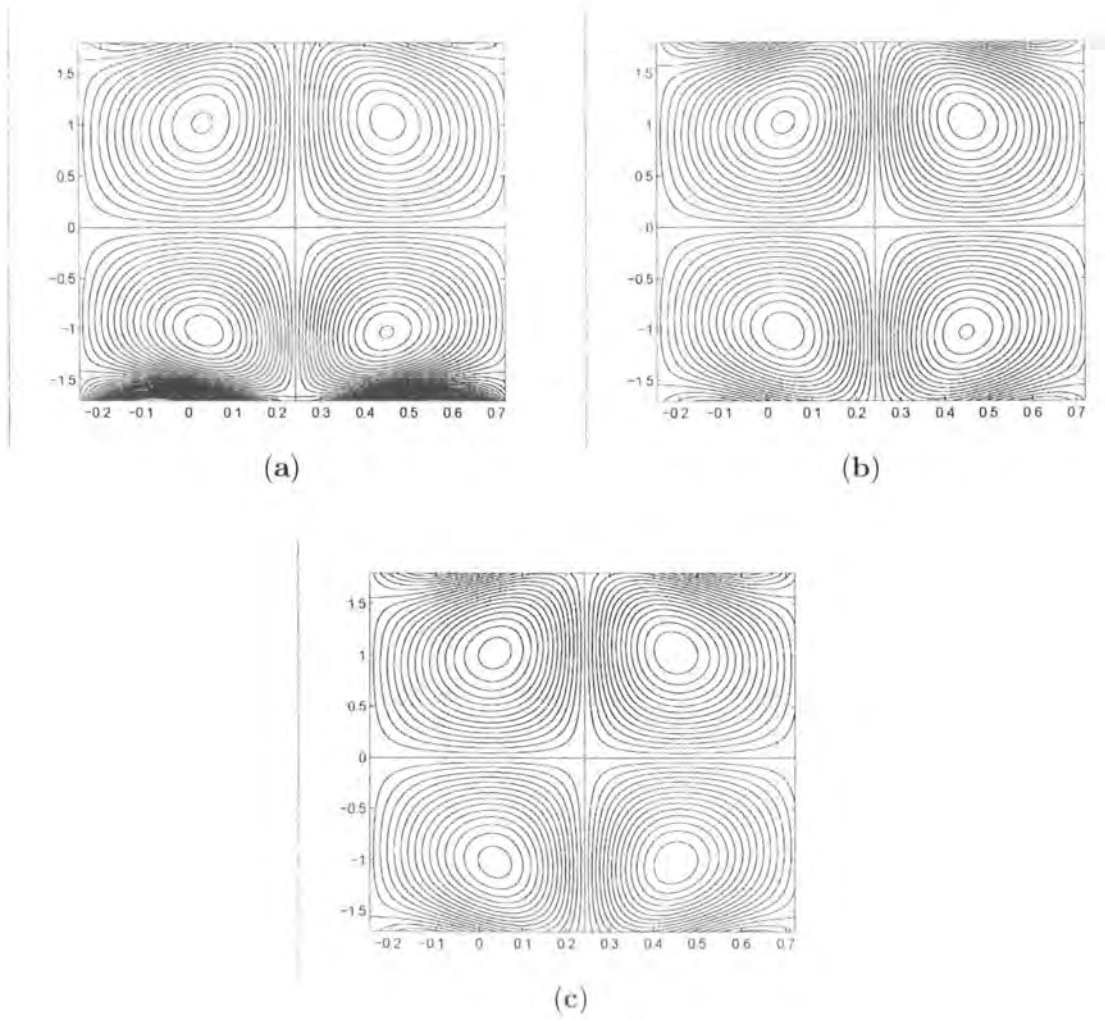


Figure 4.4: Streamlines for (a)  $k = 2$ , (b)  $k = 15$ , (c)  $k = 500$ .  
 The other parameters chosen are  $(\varepsilon = 0.1, E_1 = 0.02, E_2 = 0.15, E_3 = 0.05 \text{ and } t = 0)$ .

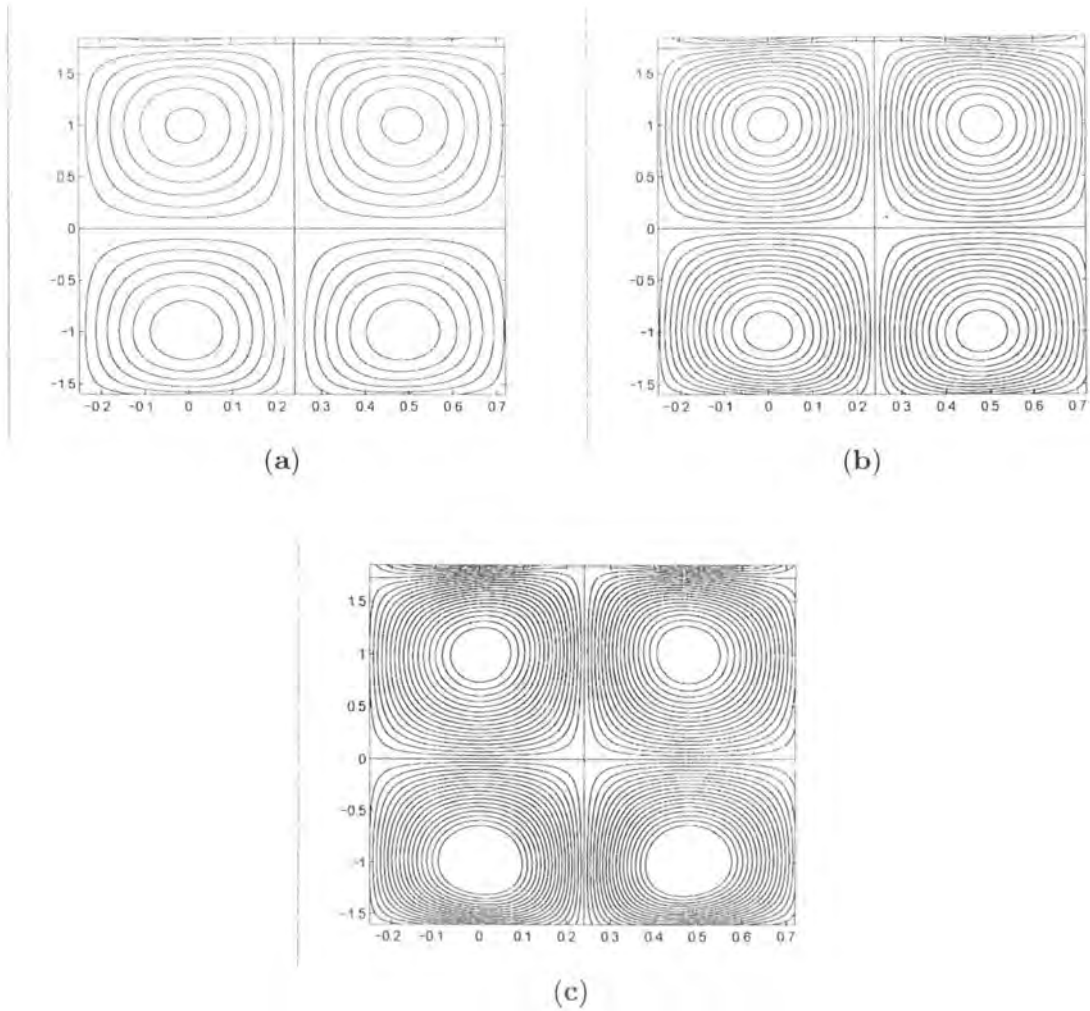


Figure 4.5: Streamlines for (a)  $\epsilon = 0.01$ , (b)  $\epsilon = 0.02$ , (c)  $\epsilon = 0.03$ .

The other parameters chosen are ( $k = 5$ ,  $E_1 = 0.3$ ,  $E_2 = 0.5$ ,  $E_3 = 0.3$  and  $t = 0$ ).

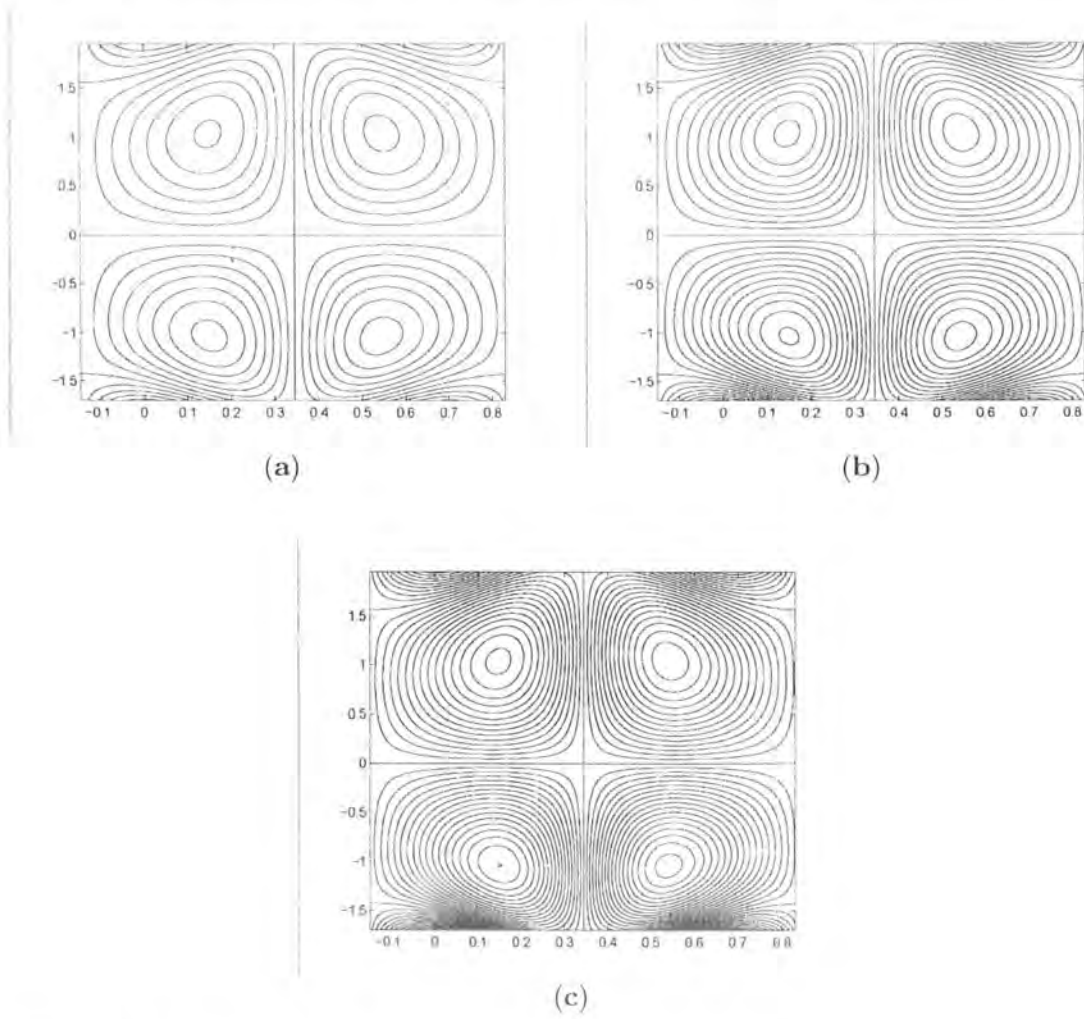


Figure 4.6: Streamlines for

(a)  $E_1 = 0.04$ ,  $E_2 = 0.02$ ,  $E_3 = 0.01$ .

(b)  $E_1 = 0.06$ ,  $E_2 = 0.04$ ,  $E_3 = 0.02$ .

(c)  $E_1 = 0.08$ ,  $E_2 = 0.06$ ,  $E_3 = 0.03$ .

The other parameters chosen are

( $\varepsilon = 0.13$ ,  $k = 3$  and  $t = 0.1$ ).



## 4.5 Final remarks

We studied the compliant wall effects on the peristaltic flow of viscous fluid in a curved channel with heat transfer. The influence of heat transfer is also discussed. The main points of the presented analysis can be summarized as follows:

- In view of increase in occlusion and elastic parameters, the longitudinal velocity increases in the neighborhood of the walls and at the centre of the channel.
- There is an increase in the temperature when the wall parameters are increased.
- The effects of Brinkman number, occlusion and the elastic parameters on the temperature are quite similar, i.e. the temperature increases by increasing such parameters.
- The effect of curvature  $k$  on the temperature is opposite when compared with the other parameters.
- The absolute value of the heat transfer coefficient increases in the upper part of the channel when the curvature parameter is increased.
- Our results for hydrodynamic fluid and no-slip condition are in good agreement with the study in ref. [97] which can be obtained as the limiting cases of present analysis by taking  $k \rightarrow \infty$ .

## Chapter 5

# Peristaltic motion of an Oldroyd-B fluid in a channel with compliant walls

The peristaltic flow of a subclass of rate type fluid in a channel with compliant walls is discussed. Constitutive expressions for an Oldroyd-B fluid are used in the mathematical development of flow equations. The flow is induced by the sinusoidal waves on the channel walls. Series solution of the resulting boundary value problem is derived under small amplitude assumption. Emphasis is given for the analysis of various embedded parameters on the flow quantities of interest.

### 5.1 Problem definition

Consider a two-dimensional channel of uniform width  $2h$  filled with homogenous Oldroyd-B fluid. The fluid motion in the channel is induced by imposing small amplitude sinusoidal waves on the compliant walls of channel. The geometry of the walls is described by the equation

$$y = \pm h \pm \eta \tag{5.1}$$

in which the vertical displacement  $\eta$  of the upper wall from its normal position is defined as

$$\eta = a \cos \frac{2\pi}{\lambda} (x - ct). \quad (5.2)$$

Here  $a$  is the wave amplitude,  $c$  is the constant wave speed,  $\lambda$  is the wavelength, for lower wall  $\eta$  is replaced by  $-\eta$  and in Cartesian coordinate system,  $x$  is measured in the direction of wave propagation and  $y$  is taken in the direction normal to the  $x$ -axis. The equation of the compliant wall is [95]

$$\left[ m \frac{\partial^2}{\partial t^2} + d \frac{\partial}{\partial t} + B \frac{\partial^4}{\partial x^4} - T \frac{\partial^2}{\partial x^2} + K \right] \eta = p - p_0. \quad (5.3)$$

In above equation,  $m$  indicates the plate mass per unit area,  $d$  is the wall damping coefficient,  $B$  is the flexural rigidity of the plate,  $T$  is the longitudinal tension per unit width,  $K$  is the spring stiffness and  $p_0$  is the pressure on the outside surface of the wall. Assuming  $p_0 = 0$  and the channel walls inextensible so that only their lateral motions normal to the undeformed positions occur. The horizontal displacement of the walls is assumed to be zero and so the boundary conditions are

$$\Psi_y = 0 \quad \text{and} \quad \Psi_x = \mp \frac{\partial \eta}{\partial t} \quad \text{at} \quad y = \pm h \pm \eta, \quad (5.4)$$

where the stream function  $\Psi(x, y, t)$  is defined through the following expressions

$$u = \frac{\partial \Psi}{\partial y}, \quad v = -\frac{\partial \Psi}{\partial x}, \quad (5.5)$$

where  $u$  and  $v$  are the  $x$ - and  $y$ - components of the velocity  $\mathbf{V}$  respectively.

The equations governing the flow of an incompressible fluid in absence of body forces are

$$\text{div } \mathbf{V} = 0, \quad (5.6)$$

$$\rho \frac{d\mathbf{V}}{dt} = -\nabla p + \text{div } \mathbf{S}, \quad (5.7)$$

where  $p$  is the pressure,  $\mathbf{S}$  is an extra stress tensor for which an Oldroyd-B fluid satisfies the following constitutive relation

$$\mathbf{S} + \lambda_1 \frac{D\mathbf{S}}{Dt} = \mu \left( 1 + \lambda_2 \frac{D}{Dt} \right) \mathbf{A}_1. \quad (5.8)$$

In above equation,  $\mu$  is the dynamic viscosity,  $\lambda_i$  ( $i = 1 - 2$ ) are material constants associated with Oldroyd-B fluid,  $\mathbf{A}_1$  is the first Rivlin-Ericksen tensor and  $D/Dt$  is the upper convected time derivative. It is pointed out that the model represented by (5.8) reduces to a Maxwell model for  $\lambda_2 = 0$ , a second grade fluid for  $\lambda_1 = 0$  and a viscous fluid model when  $\lambda_1 = \lambda_2 = 0$  as the limiting cases.

In component form, Eqs.(5.6)-(5.8) give

$$\rho \left( \frac{\partial u}{\partial t} + u \frac{\partial u}{\partial x} + v \frac{\partial u}{\partial y} \right) = -\frac{\partial p}{\partial x} + \frac{\partial S_{xx}}{\partial x} + \frac{\partial S_{xy}}{\partial y}, \quad (5.9)$$

$$\rho \left( \frac{\partial v}{\partial t} + u \frac{\partial v}{\partial x} + v \frac{\partial v}{\partial y} \right) = -\frac{\partial p}{\partial y} + \frac{\partial S_{xy}}{\partial x} + \frac{\partial S_{yy}}{\partial y}, \quad (5.10)$$

$$\begin{aligned} & S_{xx} + \lambda_1 \left[ \left( \frac{\partial}{\partial t} + u \frac{\partial}{\partial x} + v \frac{\partial}{\partial y} \right) S_{xx} - 2 \frac{\partial u}{\partial x} S_{xx} - 2 \frac{\partial u}{\partial y} S_{xy} \right] \\ = & 2\mu \frac{\partial u}{\partial x} + 2\mu\lambda_2 \left[ \left( \frac{\partial}{\partial t} + u \frac{\partial}{\partial x} + v \frac{\partial}{\partial y} \right) \frac{\partial u}{\partial x} - 2 \left( \frac{\partial u}{\partial x} \right)^2 - \frac{\partial u}{\partial y} \left( \frac{\partial u}{\partial y} + \frac{\partial v}{\partial x} \right) \right], \end{aligned} \quad (5.11)$$

$$\begin{aligned} & S_{xy} + \lambda_1 \left[ \left( \frac{\partial}{\partial t} + u \frac{\partial}{\partial x} + v \frac{\partial}{\partial y} \right) S_{xy} - \frac{\partial v}{\partial x} S_{xx} - \frac{\partial u}{\partial y} S_{yy} \right] \\ = & \mu\lambda_2 \left[ \left( \frac{\partial}{\partial t} + u \frac{\partial}{\partial x} + v \frac{\partial}{\partial y} \right) \left( \frac{\partial u}{\partial y} + \frac{\partial v}{\partial x} \right) - 2 \left( \frac{\partial u}{\partial x} \frac{\partial v}{\partial x} + \frac{\partial u}{\partial y} \frac{\partial v}{\partial y} \right) \right] \\ & + \mu \left( \frac{\partial u}{\partial y} + \frac{\partial v}{\partial x} \right), \end{aligned} \quad (5.12)$$

$$\begin{aligned} & S_{yy} + \lambda_1 \left[ \left( \frac{\partial}{\partial t} + u \frac{\partial}{\partial x} + v \frac{\partial}{\partial y} \right) S_{yy} - 2 \frac{\partial v}{\partial x} S_{yx} - 2 \frac{\partial v}{\partial y} S_{yy} \right] \\ = & 2\mu \frac{\partial v}{\partial y} + 2\mu\lambda_2 \left[ \left( \frac{\partial}{\partial t} + u \frac{\partial}{\partial x} + v \frac{\partial}{\partial y} \right) \frac{\partial v}{\partial y} - 2 \left( \frac{\partial v}{\partial y} \right)^2 - \frac{\partial v}{\partial x} \left( \frac{\partial v}{\partial x} + \frac{\partial u}{\partial y} \right) \right]. \end{aligned} \quad (5.13)$$

The complete formulation of the problem allows the continuity of stresses which requires that at the interfaces of the walls and the fluid,  $p$  must be the same as that which acts on the fluid at  $y = \pm h \pm \eta$  [95]. Employing Eq.(5.9), we obtain

$$\begin{aligned} & \frac{\partial}{\partial x} \left[ m \frac{\partial^2 \eta}{\partial t^2} + d \frac{\partial \eta}{\partial t} + B \frac{\partial^4 \eta}{\partial x^4} - T \frac{\partial^2 \eta}{\partial x^2} + K \eta \right] \\ = & -\rho (\Psi_{yt} + \Psi_y \Psi_{yx} - \Psi_x \Psi_{yy}) + S_{xx,x} + S_{xy,y}, \end{aligned} \quad (5.14)$$

where subscripts indicate partial differentiation and the incompressibility condition (5.6) is identically satisfied.

The governing equations are non-dimensionalized by the following variables

$$\begin{aligned}\hat{x} &= \frac{x}{h}, \hat{y} = \frac{y}{h}, \hat{u} = \frac{u}{c}, \hat{v} = \frac{v}{c}, \hat{t} = \frac{ct}{h}, \hat{p} = \frac{p}{\rho c^2}, \hat{\eta} = \frac{\eta}{h}, \hat{\Psi} = \frac{\Psi}{ch}, \\ \hat{m} &= \frac{m}{\rho h}, \hat{d} = \frac{dh}{\rho\nu}, \hat{B} = \frac{B}{\rho h\nu^2}, \hat{T} = \frac{Th}{\rho\nu^2}, \hat{K} = \frac{Kh^3}{\rho\nu^2}, \hat{S}_{xx} = \frac{hS_{xx}}{\mu c}, \\ \hat{S}_{xy} &= \frac{hS_{xy}}{\mu c}, \hat{S}_{yy} = \frac{hS_{yy}}{\mu c}, \hat{\lambda}_1 = \frac{c}{h}\lambda_1, \hat{\lambda}_2 = \frac{c}{h}\lambda_2.\end{aligned}\quad (5.15)$$

The resulting non-dimensional governing equations and boundary conditions after dropping the hats are:

$$\frac{\partial}{\partial t}\nabla^2\Psi + \Psi_y\nabla^2\Psi_x - \Psi_x\nabla^2\Psi_y = \frac{1}{R}(S_{xx,xy} + S_{xy,yy} - S_{xy,xx} - S_{yy,xy}), \quad (5.16)$$

$$\begin{aligned}S_{xx} + \lambda_1(S_{xx,t} + \Psi_y S_{xx,x} - \Psi_x S_{xx,y}) - 2\lambda_1(\Psi_{xy} S_{xx} + \Psi_{yy} S_{xy}) \\ = 2\Psi_{xy} + 2\lambda_2(\Psi_{xyt} + \Psi_y\Psi_{xxy} - \Psi_x\Psi_{xyy} - 2\Psi_{xy}^2 - \Psi_{yy}(\Psi_{yy} - \Psi_{xx})),\end{aligned}\quad (5.17)$$

$$\begin{aligned}S_{xy} + \lambda_1(S_{xy,t} + \Psi_y S_{xy,x} - \Psi_x S_{xy,y}) - \lambda_1(\Psi_{yy} S_{yy} - \Psi_{xx} S_{xx}) \\ = (\Psi_{yy} - \Psi_{xx}) + \lambda_2\left(\begin{aligned} &\Psi_{yyt} + \Psi_y\Psi_{xyy} - \Psi_x\Psi_{yyy} - \Psi_{xxt} \\ &- \Psi_y\Psi_{xxx} + \Psi_x\Psi_{xxy} + 2\Psi_{xy}\nabla^2\Psi \end{aligned}\right),\end{aligned}\quad (5.18)$$

$$\begin{aligned}S_{yy} + \lambda_1(S_{yy,t} + \Psi_y S_{yy,x} - \Psi_x S_{yy,y}) + 2\lambda_1(\Psi_{xx} S_{yy} + \Psi_{xy} S_{yy}) \\ = -2\Psi_{xy} + 2\lambda_2(-\Psi_{xyt} - \Psi_y\Psi_{xxy} + \Psi_x\Psi_{xyy} - 2\Psi_{xy}^2 + \Psi_{xx}(\Psi_{yy} - \Psi_{xx})),\end{aligned}\quad (5.19)$$

$$\eta = \epsilon \cos \alpha (x - t), \quad (5.20)$$

$$\Psi_y = 0 \quad \text{and} \quad \Psi_x = \mp \alpha \epsilon \sin \alpha (x - t) \quad \text{at } y = \pm 1 \pm \eta, \quad (5.21)$$

$$\begin{aligned}\frac{\partial}{\partial x}\left[m\frac{\partial^2\eta}{\partial t^2} + \frac{d}{R}\frac{\partial\eta}{\partial t} + \frac{B}{R^2}\frac{\partial^4\eta}{\partial x^4} - \frac{T}{R^2}\frac{\partial^2\eta}{\partial x^2} + \frac{K}{R^2}\eta\right] = \frac{1}{R}(S_{xx,x} + S_{xy,y}) \\ - (\Psi_{yt} + \Psi_y\Psi_{yx} - \Psi_x\Psi_{yy}) \quad \text{at } y = \pm 1 \pm \eta,\end{aligned}\quad (5.22)$$

where  $\epsilon = a/h$  is the amplitude ratio,  $\alpha = 2\pi h/\lambda$  is the wave number,  $R = ch/\nu$  is the Reynolds number and  $\nu = (\mu/\rho)$  is the kinematic viscosity.

## 5.2 Methodology of solution

Following the approach of ref. [7], we expand the flow equations in powers of  $\epsilon$  as

$$\Psi = \Psi_0 + \epsilon\Psi_1 + \epsilon^2\Psi_2 + \dots, \quad (5.23)$$

$$\frac{\partial p}{\partial x} = \left(\frac{\partial p}{\partial x}\right)_0 + \epsilon\left(\frac{\partial p}{\partial x}\right)_1 + \epsilon^2\left(\frac{\partial p}{\partial x}\right)_2 + \dots, \quad (5.24)$$

$$S_{xx} = S_{xx0} + \epsilon S_{xx1} + \epsilon^2 S_{xx2} + \dots, \quad (5.25)$$

$$S_{xy} = S_{xy0} + \epsilon S_{xy1} + \epsilon^2 S_{xy2} + \dots, \quad (5.26)$$

$$S_{yy} = S_{yy0} + \epsilon S_{yy1} + \epsilon^2 S_{yy2} + \dots, \quad (5.27)$$

where the first term on the right-hand side in Eq.(5.24) corresponds to the imposed pressure gradient and the other terms correspond to the peristaltic motion. Invoking the above equations into Eqs. (5.16)-(5.22) and then collecting terms of like powers of  $\epsilon$ , we obtain three sets of coupled differential equations with the corresponding boundary conditions in  $\epsilon_0$ ,  $\epsilon_1$  and  $\epsilon_2$ .

In actual practice  $\epsilon_0$  set of differential equations with steady parallel flow and transverse symmetry assumption when pressure gradient is constant in the  $x$ -direction corresponds to the classical Poiseuille flow, i.e.

$$\begin{aligned} \Psi_0(y) &= K_0 \left[ y - \frac{y^3}{3} \right] + c_1, \\ K_0 &= -\frac{R}{2} \left( \frac{dp}{dx} \right)_0, \end{aligned} \quad (5.28)$$

with  $c_1$  as an arbitrary constant.

The second and third sets of differential equations in  $\Psi_1$  and  $\Psi_2$  can be written in the forms:

$$\Psi_1(x, y, t) = \frac{1}{2} \left[ \Phi_1(y) e^{i\alpha(x-t)} + \Phi_1^*(y) e^{-i\alpha(x-t)} \right], \quad (5.29)$$

$$S_{xx1} = \frac{1}{2} \left[ \Phi_2(y) e^{i\alpha(x-t)} + \Phi_2^*(y) e^{-i\alpha(x-t)} \right], \quad (5.30)$$

$$S_{xy1} = \frac{1}{2} \left[ \Phi_3(y) e^{i\alpha(x-t)} + \Phi_3^*(y) e^{-i\alpha(x-t)} \right], \quad (5.31)$$

$$S_{yy1} = \frac{1}{2} \left[ \Phi_4(y) e^{i\alpha(x-t)} + \Phi_4^*(y) e^{-i\alpha(x-t)} \right], \quad (5.32)$$

$$\Psi_2(x, y, t) = \frac{1}{2} \left[ \Phi_{20}(y) + \Phi_{22}(y) e^{2i\alpha(x-t)} + \Phi_{22}^*(y) e^{-2i\alpha(x-t)} \right], \quad (5.33)$$

$$S_{xx2} = \frac{1}{2} \left[ \Phi_{30}(y) + \Phi_{33}(y) e^{2i\alpha(x-t)} + \Phi_{33}^*(y) e^{-2i\alpha(x-t)} \right], \quad (5.34)$$

$$S_{xy2} = \frac{1}{2} \left[ \Phi_{40}(y) + \Phi_{44}(y) e^{2i\alpha(x-t)} + \Phi_{44}^*(y) e^{-2i\alpha(x-t)} \right], \quad (5.35)$$

$$S_{yy2} = \frac{1}{2} \left[ \Phi_{50}(y) + \Phi_{55}(y) e^{2i\alpha(x-t)} + \Phi_{55}^*(y) e^{-2i\alpha(x-t)} \right] \quad (5.36)$$

in which the asterisk denotes the complex conjugate. Invoking above equations into the differential equations and their corresponding boundary conditions in  $\Psi_1$  and  $\Psi_2$ , we have three sets of coupled linear differential equations with their corresponding boundary conditions which are fourth-order ordinary differential equations with variable coefficients and the boundary conditions are not all homogeneous and the problem is not an eigenvalue problem. For free pumping case  $(\partial p / \partial x)_0 = 0$  which means  $K_0 = 0$  and hence we have

$$i\alpha R \left[ \frac{d^2}{dy^2} - \alpha^2 \right] \Phi_1(y) = i\alpha \Phi_2'(y) + \Phi_3''(y) + \alpha^2 \Phi_3(y) - i\alpha \Phi_4'(y), \quad (5.37)$$

$$(1 - i\alpha\lambda_1) \Phi_2(y) = 2i\alpha (1 - i\alpha\lambda_2) \Phi_1'(y), \quad (5.38)$$

$$\mu (1 - i\alpha\lambda_1) \Phi_3(y) = (1 - i\alpha\lambda_2) (\Phi_1''(y) + \alpha^2 \Phi_1(y)), \quad (5.39)$$

$$\mu (1 - i\alpha\lambda_1) \Phi_4(y) = -2i\alpha (1 - i\alpha\lambda_2) \Phi_1'(y), \quad (5.40)$$

$$\Phi_1'(\pm 1) = 0, \quad (5.41)$$

$$i\alpha R \Phi_1'(\pm 1) + i\alpha \Phi_2(\pm 1) + \Phi_3'(\pm 1) = R\delta, \quad (5.42)$$

$$\delta = -\frac{i\alpha}{R^2} (\alpha^2 R^2 m + i\alpha R d - \alpha^4 B - \alpha^2 T - K),$$

$$\Phi_{40}''(y) = \frac{i\alpha R}{2} [\Phi_1^*(y) \Phi_1''(y) - \Phi_1(y) \Phi_1^{*''}(y)]', \quad (5.43)$$

$$\begin{aligned} \Phi_{30}(y) &= -\frac{i\alpha\lambda_1}{2} [\Phi_1^*(y) \Phi_2(y) - \Phi_1(y) \Phi_2^*(y)]' + i\alpha\lambda_1 [\Phi_1'(y) \Phi_2^*(y) - \Phi_2(y) \Phi_1^{*'}(y)] \\ &+ \lambda_1 [\Phi_1''(y) \Phi_3^*(y) + \Phi_1^{*''}(y) \Phi_3(y)] - \alpha^2\lambda_2 [\Phi_1(y) \Phi_1^{*''}(y) + \Phi_1^*(y) \Phi_1''(y)] \\ &+ 6\Phi_1'(y) \Phi_1^{*'}(y) - \lambda_2 [\Phi_1''(y) (\Phi_1^{*''}(y) + \alpha^2\Phi_1^*(y)) + \Phi_1^{*''}(y) (\Phi_1''(y) + \alpha^2\Phi_1(y))], \end{aligned} \quad (5.44)$$

$$\begin{aligned} \Phi_{40}(y) &= \frac{i\alpha\lambda_1}{2} [\Phi_1(y) \Phi_3^*(y) - \Phi_1^*(y) \Phi_3(y)]' + \frac{\alpha^2\lambda_1}{2} [(\Phi_1(y) \Phi_2^*(y) + \Phi_1^*(y) \Phi_2(y))] \\ &+ \frac{\lambda_1}{2} [\Phi_1''(y) \Phi_4^*(y) + \Phi_1^{*''}(y) \Phi_4(y)] - \frac{i\alpha\lambda_2}{2} [\Phi_1(y) \Phi_1^{*''}(y) - \Phi_1^*(y) \Phi_1''(y)]' \\ &+ i\alpha\lambda_2 [\Phi_1''(y) (\Phi_1^{*''}(y) - \alpha^2\Phi_1^*(y)) - \Phi_1^{*''}(y) (\Phi_1''(y) - \alpha^2\Phi_1(y))] + \Phi_{20}''(y), \end{aligned} \quad (5.45)$$

$$\begin{aligned} \Phi_{50}(y) &= \frac{i\alpha\lambda_1}{2} [\Phi_1^{*'}(y) \Phi_4(y) - \Phi_1'(y) \Phi_4^*(y) - \Phi_1^*(y) \Phi_4'(y) + \Phi_1(y) \Phi_4^{*'}(y)] \\ &+ \alpha^2\lambda_1 [(\Phi_1(y) \Phi_3^*(y) + \Phi_1^*(y) \Phi_3(y))] - 2\alpha^4\lambda_2\Phi_1(y) \Phi_1^*(y) - 2\alpha^2\lambda_2\Phi_1'(y) \Phi_1^{*'}(y), \end{aligned} \quad (5.46)$$

$$\Phi_{20}'(\pm 1) = \mp \frac{1}{2} [\Phi_1''(\pm 1) + \Phi_1^{*''}(\pm 1)], \quad (5.47)$$

$$\begin{aligned} \Phi_{40}'(\pm 1) &= \mp \frac{i\alpha}{2} [\Phi_2'(\pm 1) - \Phi_2^{*'}(\pm 1)] \mp \frac{1}{2} [\Phi_3''(\pm 1) + \Phi_3^{*''}(\pm 1)] \\ &- \frac{i\alpha R}{2} [\Phi_1(\pm 1) \Phi_1^{*''}(\pm 1) - \Phi_1^*(\pm 1) \Phi_1''(\pm 1)] \mp \frac{i\alpha R}{2} [\Phi_1''(\pm 1) - \Phi_1^{*''}(\pm 1)], \end{aligned} \quad (5.48)$$

$$\begin{aligned} 2i\alpha R \left[ \frac{d^2}{dy^2} - 4\alpha^2 \right] \Phi_{22}(y) &= \frac{i\alpha R}{2} [\Phi_1'(y) \Phi_1''(y) - \Phi_1(y) \Phi_1^{*''}(y)] - \Phi_{44}''(y) - 4\alpha^2\Phi_{44}(y) \\ &- 2i\alpha\Phi_{33}'(y) + 2i\alpha\Phi_{55}'(y), \end{aligned} \quad (5.49)$$

$$\begin{aligned} (1 - 2i\alpha\lambda_1) \Phi_{33}(y) &= \frac{i\alpha\lambda_1}{2} (\Phi_1(y) \Phi_2(y))' + \lambda_1\Phi_1'(y) \Phi_3(y) \\ &+ 4i\alpha(1 - 2i\alpha\lambda_2) \Phi_{22}'(y) + \alpha^2\lambda_2 (\Phi_1(y) \Phi_1'(y))' - \lambda_2\Phi_1''(y) (\Phi_1''(y) + \alpha^2\Phi_1(y)), \end{aligned} \quad (5.50)$$

$$\begin{aligned} (1 - 2i\alpha\lambda_1) \Phi_{44}(y) &= \frac{i\alpha\lambda_2}{2} (3\Phi_1'(y) \Phi_1''(y) - \Phi_1(y) \Phi_1^{*''}(y)) \\ &- \frac{i\alpha\lambda_2}{2} [\Phi_1'(y) \Phi_3(y) - \Phi_1(y) \Phi_3'(y)] + (1 - 2i\alpha\lambda_2) \Phi_{22}''(y) + 4\alpha^2(1 - 2i\alpha\lambda_2) \Phi_{22}(y) \\ &+ \frac{\lambda_1}{2} [\Phi_1''(y) \Phi_4(y) + \alpha^2\Phi_1(y) \Phi_2(y)] - i\alpha^3\lambda_2\Phi_1(y) \Phi_1'(y), \end{aligned} \quad (5.51)$$

$$\begin{aligned} (1 - 2i\alpha\lambda_1) \Phi_{55}(y) &= \frac{i\alpha\lambda_1}{2} [\Phi_1(y) \Phi_4'(y) - 3\Phi_1'(y) \Phi_4(y)] + \alpha^2\lambda_1\Phi_1(y) \Phi_3(y) \\ &- 4i\alpha(1 - 2i\alpha\lambda_2) \Phi_{22}'(y) - \alpha^4\lambda_2\Phi_1^2(y) + 3\alpha^2\lambda_2\Phi_1'(y) \Phi_1'(y) - 2\alpha^2\lambda_2\Phi_1(y) \Phi_1''(y), \end{aligned} \quad (5.52)$$

$$\Phi_{22}'(\pm 1) = \mp \frac{1}{2} \Phi_1''(\pm 1), \quad (5.53)$$



$$\begin{aligned}
2\Phi'_{44}(\pm 1) &= +i\alpha R\Phi'_1(\pm 1)\Phi'_1(\pm 1) - 4i\alpha\Phi_{33}(\pm 1) \mp \Phi''_3(\pm 1) \mp i\alpha\Phi'_2(\pm 1) \\
&- 4i\alpha R\Phi'_{22}(\pm 1) \mp i\alpha R\Phi''_1(\pm 1) - i\alpha R\Phi_1(\pm 1)\Phi''_1(\pm 1),
\end{aligned} \tag{5.54}$$

where primes signify differentiation with respect to  $y$ .

The solutions of Eqs. (5.37)-(5.42) are given as

$$\Phi_1(y) = A_1 \sinh \alpha_1 y + B_1 \sinh \beta_1 y, \tag{5.55}$$

$$\Phi_2(y) = A_2 \cosh \alpha_1 y + B_2 \cosh \beta_1 y, \tag{5.56}$$

$$\Phi_3(y) = A_3 \sinh \alpha_1 y + B_3 \sinh \beta_1 y, \tag{5.57}$$

$$\Phi_4(y) = -A_2 \cosh \alpha_1 y - B_2 \cosh \beta_1 y, \tag{5.58}$$

where

$$\begin{aligned}
A_1 &= -\frac{i\delta}{\alpha^2 \cosh \alpha}, & B_1 &= \frac{i\delta}{\alpha\beta \cosh \beta}, \\
A_2 &= 2i\alpha^2 \Gamma A_1, & B_2 &= 2i\alpha\beta \Gamma B_1, \\
A_3 &= 2\alpha^2 \Gamma A_1, & B_3 &= (\alpha^2 + \beta^2) \Gamma B_1, \\
\beta^2 &= \alpha^2 - \frac{i\alpha R}{\Gamma}, & \Gamma &= \frac{1 + i\alpha(\lambda_1 - \lambda_2) + \alpha^2 \lambda_1 \lambda_2}{(1 + \alpha^2 \lambda_1^2)}.
\end{aligned}$$

The solution of Eqs. (5.43)-(5.48) is

$$\Phi'_{20}(y) = F(y) - F(1) + D - C_1(1 - y^2). \tag{5.59}$$

The peristaltic mean flow can be written as

$$\begin{aligned}
\bar{u}(y) &= \frac{\epsilon^2}{2} \Phi'_{20}(y) \\
&= \frac{\epsilon^2}{2} [F(y) - F(1) + D - C_1(1 - y^2)],
\end{aligned} \tag{5.60}$$

where

$$\begin{aligned}
D &= -\frac{1}{2} [(A_1 + A_1^*) \alpha^2 \sinh \alpha + B_1 \beta^2 \sinh \beta + B_1^* \beta^{*2} \sinh \beta^*], \\
C_1 &= \frac{(A_{11} + A_{11}^*)}{2} \sinh \alpha + \frac{B_{11}}{2} \sinh \beta + \frac{B_{11}^*}{2} \sinh \beta^*, \\
A_{11} &= \frac{\alpha^2}{2} [i\alpha R A_1 - iA_2 - \alpha A_3], \quad B_{11} = -\frac{\beta}{2} [i\alpha R \beta B_1 + i\alpha B_2 + \beta B_3], \\
F(y) &= s_1 \cosh 2\alpha y + s_2 \cosh(\alpha + \beta)y + s_3 \cosh(\alpha - \beta)y + s_4 \cosh(\alpha + \beta^*)y \\
&\quad + s_5 \cosh(\alpha - \beta^*)y + s_6 \cosh(\beta + \beta^*)y + s_7 \cosh(\beta - \beta^*)y, \\
s_1 &= \frac{i\alpha\lambda_1}{4} (A_1^* A_3 - A_1 A_3^*),
\end{aligned}$$

$$\begin{aligned}
s_2 &= \frac{-i\alpha R(\alpha - \beta) A_1^* B_1}{4(\alpha + \beta)} + \frac{i\alpha\lambda_1}{4} (A_1^* B_3 - A_3^* B_1) + \frac{\lambda_1}{4} (\beta - \alpha) B_1 A_2^* \\
&\quad - \frac{i\alpha\lambda_2}{4} (\beta - \alpha)^2 A_1^* B_1, \\
s_3 &= \frac{i\alpha R(\alpha + \beta) A_1^* B_1}{4(\alpha - \beta)} - \frac{i\alpha\lambda_1}{4} (A_1^* B_3 - A_3^* B_1) + \frac{\lambda_1}{4} (\alpha + \beta) B_1 A_2^* \\
&\quad + \frac{i\alpha\lambda_2}{4} (\beta + \alpha)^2 A_1^* B_1, \\
s_4 &= \frac{i\alpha R(\alpha - \beta^*) A_1 B_1^*}{4(\alpha + \beta^*)} - \frac{i\alpha\lambda_1}{4} (A_1 B_3^* - B_1^* A_3) + \frac{\lambda_1}{4} (\beta^* - \alpha) B_1^* A_2 \\
&\quad + \frac{i\alpha\lambda_2}{4} (\beta^* - \alpha)^2 A_1 B_1^*, \\
s_5 &= \frac{-i\alpha R(\alpha + \beta^*) A_1 B_1^*}{4(\alpha - \beta^*)} + \frac{i\alpha\lambda_1}{4} (A_1 B_3^* - B_1^* A_3) + \frac{\lambda_1}{4} (\alpha + \beta^*) B_1^* A_2 \\
&\quad - \frac{i\alpha\lambda_2}{4} (\alpha + \beta^*)^2 A_1 B_1^*, \\
s_6 &= \frac{-i\alpha R(\beta^* - \beta) B_1 B_1^*}{4(\beta + \beta^*)} + \frac{i\alpha\lambda_1}{4} (B_3 B_1^* - B_1 B_3^*) + \frac{\lambda_1(\beta^2 - \alpha^2)}{4(\beta + \beta^*)} B_1 B_2^* \\
&\quad + \frac{\lambda_1(\beta^{*2} - \alpha^2)}{4(\beta + \beta^*)} B_1^* B_2 + \frac{i\alpha\lambda_2(\beta - \beta^*) B_1 B_1^*}{4(\beta + \beta^*)} (2\alpha^2 - \beta^2 - \beta^{*2}),
\end{aligned}$$

$$\begin{aligned}
s_7 &= \frac{i\alpha R(\beta^* + \beta) B_1 B_1^*}{4(\beta^* - \beta)} - \frac{i\alpha\lambda_1}{4} (B_3 B_1^* - B_1 B_3^*) + \frac{\lambda_1(\beta^2 - \alpha^2)}{4(\beta - \beta^*)} B_1 B_2^* \\
&\quad + \frac{\lambda_1(\beta^{*2} - \alpha^2)}{4(\beta^* - \beta)} B_1^* B_2 + \frac{i\alpha\lambda_2(\beta^* + \beta) B_1 B_1^*}{4(\beta^* - \beta)} (2\alpha^2 - \beta^2 - \beta^{*2}).
\end{aligned}$$

The critical reflux condition  $\hat{u}$  is zero at  $y = 0$  [95] and so invoking Eq.(5.60), we get

$$T_{\text{critical reflux}} = \frac{H_5 + \sqrt{H_5^2 - 4H_6}}{2}, \quad (5.61)$$

$$H = \left[ \frac{h_1}{\alpha^4 \cosh^2 \alpha} + \frac{(h_2 + h_3)}{4\alpha^3 \beta \cosh \alpha \cosh \beta} + \frac{(h_4 + h_5)}{4\alpha^3 \beta^* \cosh \alpha \cosh \beta^*} + \frac{(h_6 + h_7)}{4\alpha^2 \beta \beta^* \cosh \beta \cosh \beta^*} \right],$$

$$H_1 = \frac{\alpha^2}{2} \left[ 2\alpha \tanh \alpha - \beta \tanh \beta - \beta^* \tanh \beta^* + \alpha^3 (1 - \alpha) (\Gamma + \Gamma^*) \tanh \alpha - \frac{i\alpha}{2} (L_5 \beta \tanh \beta - L_5^* \beta^* \tanh \beta^*) \right],$$

$$H_2 = \frac{1}{2} \left[ (L_4 + L_4^*) \alpha \tanh \alpha - L_4 \beta \tanh \beta - L_4^* \beta^* \tanh \beta^* + \alpha^3 (1 - \alpha) (\Gamma L_4 + \Gamma^* L_4^*) \right],$$

$$H_3 = \frac{i\alpha}{4} \left[ \alpha R (L_4 - L_4^*) \tanh \alpha - L_4 L_5 \beta \tanh \beta - L_4^* L_5^* \beta^* \tanh \beta^* \right], \quad H_4 = H_2 + H_3,$$

$$H_5 = \frac{R^2}{\alpha^6 H} \left[ \frac{2\alpha^4 H L_3}{R^2} + H_1 \right], \quad H_6 = \frac{R^2}{\alpha^6 H} \left[ \frac{\alpha^2 H L_4 L_4^*}{R^2} + H_4 \right],$$

$$L_3 = \alpha^2 R^2 m - \alpha^4 B - K, \quad L_4 = i\alpha R d + L_3, \quad L_5 = \left[ R + 2i\alpha \Gamma - \frac{i\Gamma}{\alpha} (\alpha^2 + \beta^2) \right],$$

$$h_1 = 2i\alpha^3 \lambda_1 (1 - \cosh 2\alpha) (\Gamma - \Gamma^*),$$

$$h_2 = [1 - \cosh (\alpha + \beta)] i\alpha \left\{ \frac{R(\alpha - \beta)}{(\alpha + \beta)} + \lambda_1 [-\Gamma (\alpha^2 + \beta) + 2\alpha^2 \Gamma^*] + 2\alpha \lambda_1 \Gamma^* (\beta - \alpha) + \lambda_2 (\beta - \alpha)^2 \right\},$$

$$h_3 = [1 - \cosh (\alpha - \beta)] i\alpha \left\{ \frac{-R(\alpha + \beta)}{(\alpha - \beta)} - \lambda_1 [-\Gamma (\alpha^2 + \beta^2) + 2\alpha^2 \Gamma^*] + 2\alpha \lambda_1 \Gamma^* (\alpha + \beta) - \lambda_2 (\beta + \alpha)^2 \right\},$$

$$h_4 = [1 - \cosh (\alpha + \beta^*)] i\alpha \left\{ \frac{-R(\alpha - \beta^*)}{(\alpha + \beta^*)} - \lambda_1 [-\Gamma^* (\alpha^2 + \beta^{*2}) + 2\alpha^2 \Gamma] - 2\alpha \lambda_1 \Gamma (\beta^* - \alpha) - \lambda_2 (\beta^* - \alpha)^2 \right\},$$

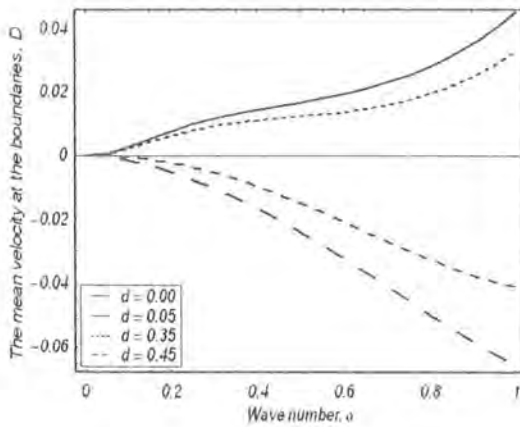
$$\begin{aligned}
h_5 &= [1 - \cosh(\alpha - \beta^*)] i\alpha \left\{ \frac{R(\alpha + \beta^*)}{(\alpha - \beta^*)} + \lambda_1 [-\Gamma^*(\alpha^2 + \beta^{*2}) + 2\alpha^2\Gamma] \right. \\
&\quad \left. - 2\alpha\lambda_1\Gamma(\alpha + \beta^*) + \lambda_2(\alpha + \beta^*)^2 \right\}, \\
h_6 &= [1 - \cosh(\beta + \beta^*)] i\alpha \left\{ \frac{-R(\beta^* - \beta)}{(\beta^* + \beta)} + \lambda_1 [\Gamma(\alpha^2 + \beta^2) - \Gamma^*(\alpha^2 + \beta^{*2})] \right. \\
&\quad \left. - 2\lambda_1\beta^*\Gamma^* \frac{(\beta^2 - \alpha^2)}{(\beta^* + \beta)} + 2\lambda_1\beta\Gamma \frac{(\beta^{*2} - \alpha^2)}{(\beta^* + \beta)} + \lambda_2 \frac{(2\alpha^2 - \beta^2 - \beta^{*2})(\beta - \beta^*)}{(\beta^* + \beta)} \right\}, \\
h_7 &= [1 - \cosh(\beta - \beta^*)] i\alpha \left\{ \frac{R(\beta^* + \beta)}{(\beta^* - \beta)} - \lambda_1 [\Gamma(\alpha^2 + \beta^2) - \Gamma^*(\alpha^2 + \beta^{*2})] \right. \\
&\quad \left. - 2\lambda_1\beta^*\Gamma^* \frac{(\beta^2 - \alpha^2)}{(\beta - \beta^*)} + 2\lambda_1\beta\Gamma \frac{(\beta^{*2} - \alpha^2)}{(\beta^* - \beta)} + \lambda_2 \frac{(2\alpha^2 - \beta^2 - \beta^{*2})(\beta^* + \beta)}{(\beta^* - \beta)} \right\}.
\end{aligned}$$

### 5.3 Discussion

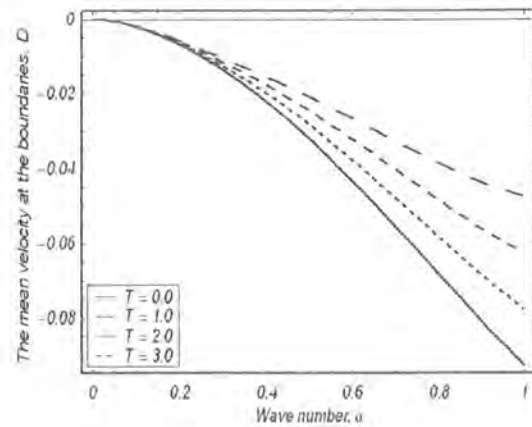
In order to see the variations of various flow parameters, the graphical results are presented in this section. Therefore, the mean velocity at the boundaries of the channel  $D$ , and the time-averaged mean axial velocity distribution  $\bar{u}(y)$  are computed when  $K_0 = 0$ . The constant  $\bar{D}$  which initially arises from the no-slip condition of the axial-velocity on the wall is due to the value of  $\Phi'_{20}(y)$  at the boundary. The mean-velocity at the boundaries of the channel is  $\bar{u}(\pm 1) = \frac{\epsilon^2}{2}\Phi'_{20}(\pm 1) = \frac{\epsilon^2}{2}D$  [95]. Figure 5.1a shows the variation of wall damping  $d$  on the constant  $\bar{D}$ . This figure indicates that  $D$  is a decreasing function of  $d$ . Figure 5.1b is made to see the influence of  $T$  on  $D$ . It is observed that the values of  $D$  increase by increasing  $T$ . Figures 5.1c and 5.1d reveal that the mean velocity at the boundaries decreases by increasing relaxation time  $\lambda_1$  and increases with an increase in the retardation time  $\lambda_2$ . The effects of  $d$ ,  $T$  and  $\lambda_1$  on the mean velocity distribution and reversal flow are presented in the Figures 5.2(a - c). It is found that the possibility of flow reversal increases by increasing these parameters while in case of  $\lambda_2$  the situation is reversed (Figure 5.2d). In the expression (5.60) along with the constant  $D$  and a parabolic distribution  $-C_1(1 - y^2)$  there is a perturbation term  $F(y) - F(1)$ . Following Fung and Yih [7], we define the mean-velocity perturbation function  $G(y)$  as

$$G(y) = -\frac{200}{\alpha^2 R^2} [F(y) - F(1)]. \quad (5.62)$$

The mean velocity perturbation function is plotted with  $\alpha$  for various values of  $d$ ,  $T$ ,  $\lambda_1$  and  $\lambda_2$  in the Figures 5.3(a – d). It is observed from these Figures that  $G(y)$  increases by increasing  $d$ ,  $T$  and  $\lambda_1$ . However, it decreases by increasing  $\lambda_2$ . It is further observed from these Figures that  $G(y)$  is maximum near the centre of the channel and remains constant over a certain range of  $\alpha$ . Figure 5.4a illustrates that critical value of  $T$  decreases with an increase in  $\lambda_1$ . The effects of  $\lambda_2$  on critical value of  $T$  are quite opposite to those of  $\lambda_1$  (Figure 5.4b). We further note that the critical value of  $T$  is very high for small values of the wave number  $\alpha$  when compared with its large values.



(a)

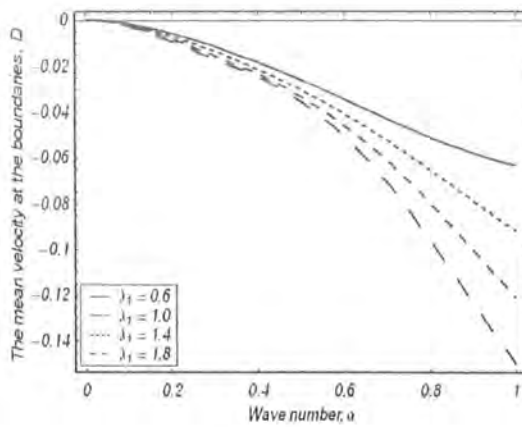


(b)

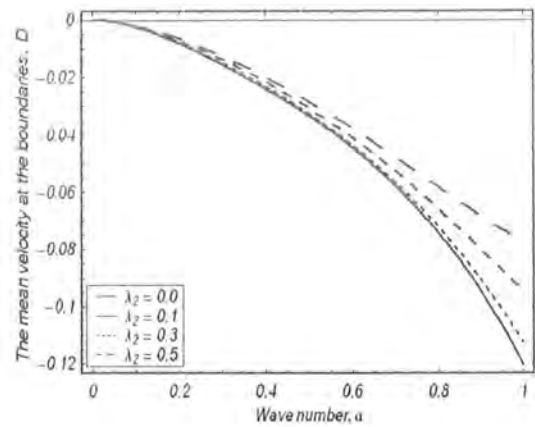
Figure 5.1a. The variation of  $D$  with wave number  $\alpha$  for different values of wall damping  $d$  with  $m = 0.01$ ,  $B = 2$ ,  $T = 1$ ,  $K = 1$ ,  $R = 10$ ,  $\lambda_1 = 0.8$  and  $\lambda_2 = 0.5$ .

Figure 5.1b. The variation of  $D$  with wave number  $\alpha$  for different values of wall tension  $T$

with  $m = 0.01$ ,  $B = 2$ ,  $K = 1$ ,  $R = 10$ ,  $d = 0.5$ ,  $\lambda_1 = 0.8$  and  $\lambda_2 = 0.5$ .



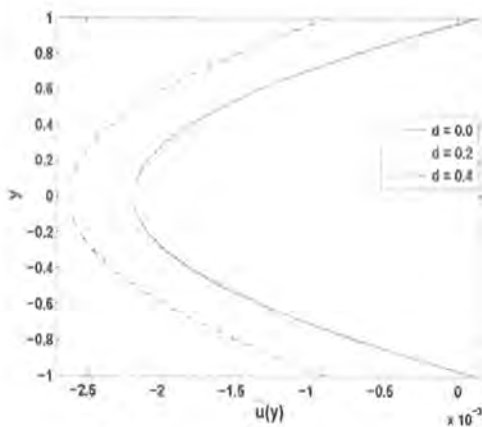
(c)



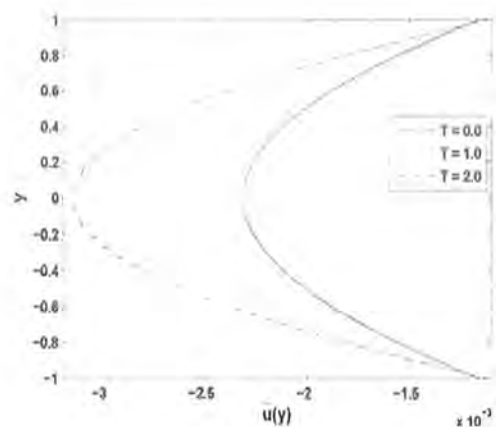
(d)

Figure 5.1c. The variation of  $D$  with wave number  $\alpha$  for different values of relaxation time  $\lambda_1$  with  $m = 0.01$ ,  $B = 2$ ,  $T = 1$ ,  $K = 1$ ,  $R = 10$ ,  $d = 0.5$  and  $\lambda_2 = 0.5$ .

Figure 5.1d. The variation of  $D$  with wave number  $\alpha$  for different values of relaxation time  $\lambda_2$  with  $m = 0.01$ ,  $B = 2$ ,  $T = 1$ ,  $K = 1$ ,  $R = 10$ ,  $d = 0.5$  and  $\lambda_1 = 0.8$ .



(a)



(b)

Figure 5.2a. The variation of mean-velocity distribution and reversal flow for different values of wall damping  $d$  with  $m = 0.01$ ,  $B = 2$ ,  $T = 1$ ,  $K = 1$ ,  $R = 1$ ,  $\alpha = 0.5$ ,  $\epsilon = 0.15$ ,  $\lambda_1 = 0.8$  and  $\lambda_2 = 0.5$ .

Figure 5.2b. The variation of mean-velocity distribution and reversal flow for different values

of wall tension  $T$  with  $m = 0.01$ ,  $B = 2$ ,  $K = 1$ ,  $R = 1$ ,  $d = 0.5$ ,  $\alpha = 0.5$ ,  $\epsilon = 0.15$ ,  $\lambda_1 = 0.8$  and  $\lambda_2 = 0.5$ .

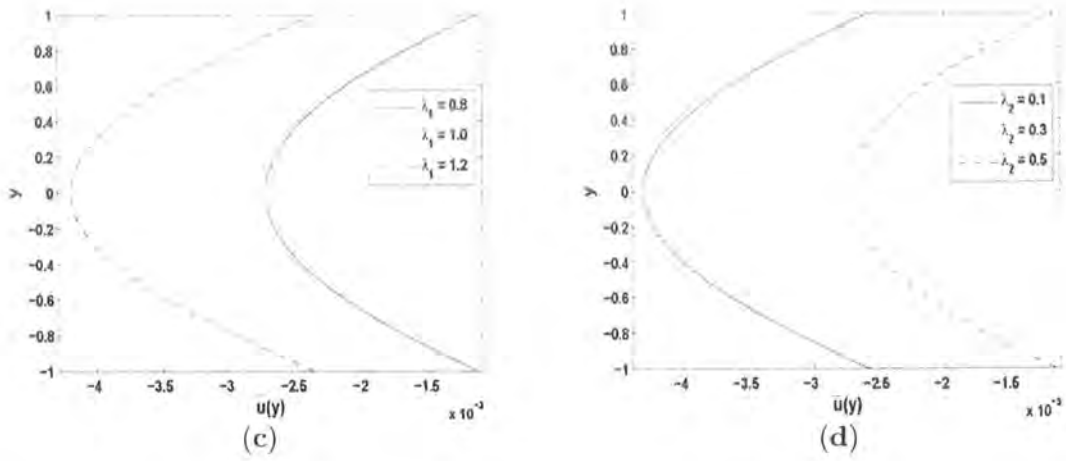


Figure 5.2c. The variation of mean-velocity distribution and reversal flow for different values of relaxation time  $\lambda_1$  with  $m = 0.01$ ,  $B = 2$ ,  $T = 1$ ,  $K = 1$ ,  $R = 1$ ,  $d = 0.5$ ,  $\alpha = 0.5$ ,  $\epsilon = 0.15$  and  $\lambda_2 = 0.5$ .

Figure 5.2d. The variation of mean-velocity distribution and reversal flow for different values of relaxation time  $\lambda_2$  with  $m = 0.01$ ,  $B = 2$ ,  $T = 1$ ,  $K = 1$ ,  $R = 1$ ,  $d = 0.5$ ,  $\alpha = 0.5$ ,  $\epsilon = 0.15$  and  $\lambda_1 = 0.8$ .

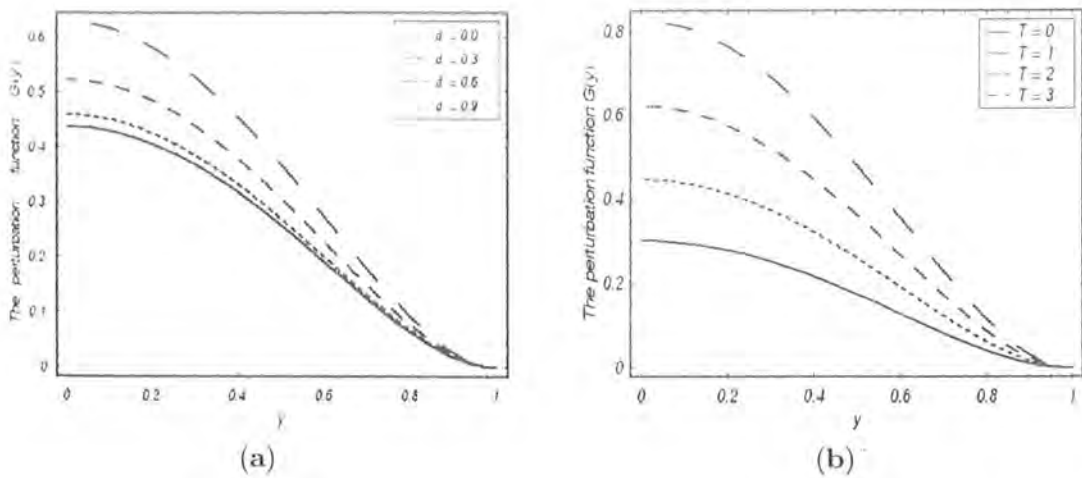


Figure 5.3a. The variation of mean-velocity perturbation function  $G(y)$  for different values

of wall damping  $d$  with  $m = 0.01$ ,  $B = 2$ ,  $T = 1$ ,  $K = 1$ ,  $R = 2$ ,  $\alpha = 0.5$ ,  $\lambda_1 = 0.8$  and  $\lambda_2 = 0.5$ .

Figure 5.3b. The variation of mean-velocity perturbation function  $G(y)$  for different values of wall tension  $T$  with  $m = 0.01$ ,  $B = 2$ ,  $K = 1$ ,  $R = 2$ ,  $d = 0.2$ ,  $\alpha = 0.5$ ,  $\lambda_1 = 0.8$  and  $\lambda_2 = 0.5$ .

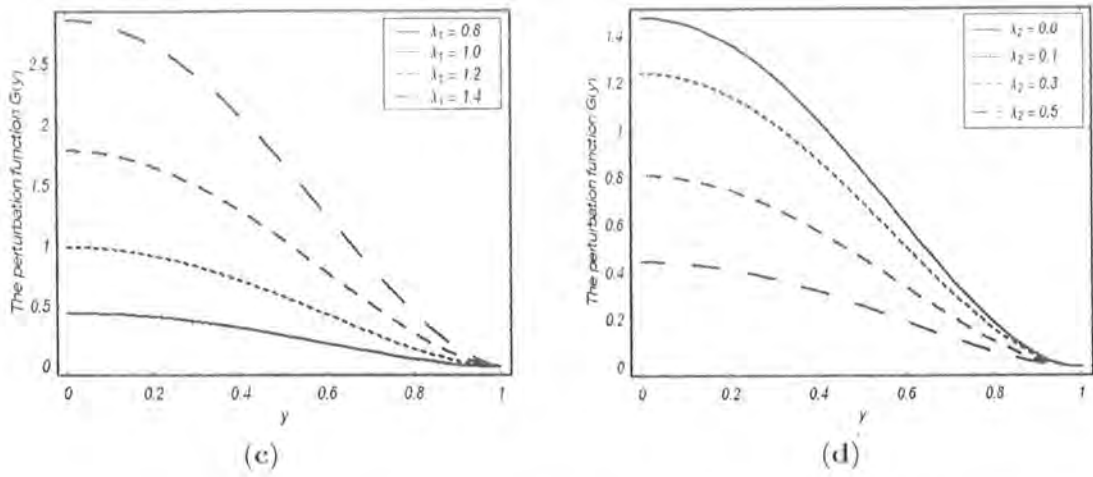


Figure 5.3c. The variation of mean-velocity perturbation function  $G(y)$  for different values of the relaxation time  $\lambda_1$  with  $m = 0.01$ ,  $B = 2$ ,  $T = 1$ ,  $K = 1$ ,  $R = 2$ ,  $d = 0.2$ ,  $\alpha = 0.5$  and  $\lambda_2 = 0.5$ .

Figure 5.3d. The variation of mean-velocity perturbation function  $G(y)$  for different values of the relaxation time  $\lambda_2$  with  $m = 0.01$ ,  $B = 2$ ,  $T = 1$ ,  $K = 1$ ,  $R = 2$ ,  $d = 0.2$ ,  $\alpha = 0.5$  and  $\lambda_1 = 0.8$ .

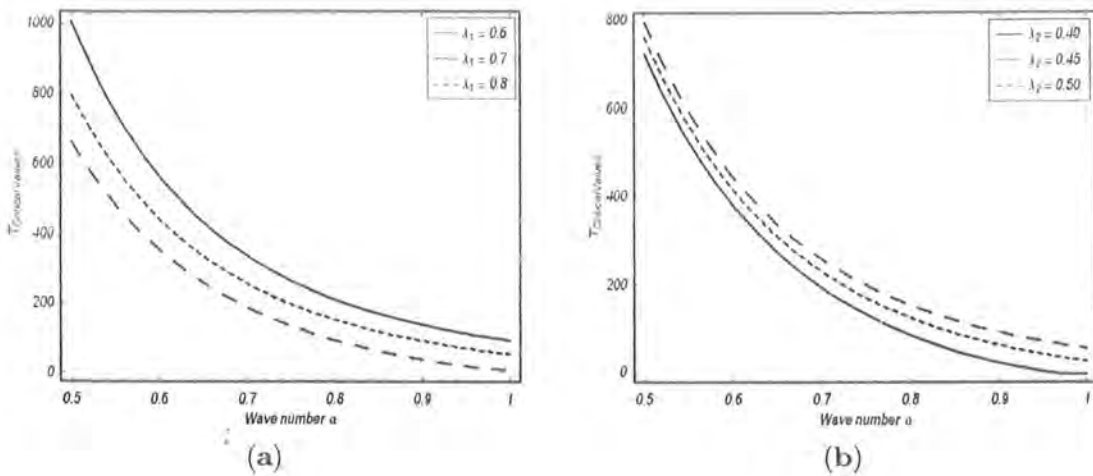




Figure 5.4a. The variation of critical values of the wall tension  $T$  with wave number  $\alpha$  for different values of the relaxation time  $\lambda_1$  with  $m = 0.01$ ,  $B = 2$ ,  $K = 1$ ,  $d = 0.5$ ,  $R = 7$  and  $\lambda_2 = 0.5$ .

Figure 5.4b. The variation of critical values of the wall tension  $T$  with wave number  $\alpha$  for different values of the relaxation time  $\lambda_2$  with  $m = 0.01$ ,  $B = 2$ ,  $K = 1$ ,  $d = 0.5$ ,  $R = 7$  and  $\lambda_1 = 0.7$ .

## 5.4 Final remarks

The presented work in this chapter is focused on the analysis of peristaltic flow of an incompressible Oldroyd-B fluid. The equations for an Oldroyd-B fluid are modeled and free pumping case is considered for the analysis. The performed analysis leads to the following main observations.

- The constant  $D$  decreases with an increase in  $d$  and  $\lambda_1$ .
- The value of  $D$  increases when  $T$  and  $\lambda_2$  are increased.
- The flow reversal decreases by increasing  $\lambda_2$ . However, it increases when  $d$ ,  $T$  and  $\lambda_1$  are increased.
- The corresponding results of viscous fluid [95] can be deduced when  $\lambda_1$  and  $\lambda_2$  are equal to zero.

## Chapter 6

# Peristaltic transport of MHD

# Johnson-Segalman fluid in a channel with compliant walls

This chapter aims to discuss the mathematical model for magnetohydrodynamic (MHD) flow of Johnson-Segalman fluid in a compliant wall channel. The flow is engendered due to sinusoidal waves on the channel walls. A series solution is developed for the case in which the amplitude ratio is small. Our computations show that the mean axial velocity in Johnson-Segalman fluid is smaller than that of a viscous fluid. The variations of various interesting dimensionless parameters are sketched and discussed.

### 6.1 Problem definition

Consider a Johnson-Segalman fluid in a two-dimensional channel of uniform width  $2h$ . The homogeneous fluid is electrically conducting in the presence of a constant applied magnetic field  $B_0$  only. The induced magnetic field is absent. There is no electric field. The motion in a channel is induced by choosing small amplitude sinusoidal waves on the compliant walls of the channel represented by

$$y = \pm h \pm \eta, \tag{6.1}$$

where the vertical displacement  $\eta$  of the upper wall from its normal position can be expressed as follows

$$\eta = a \cos \frac{2\pi}{\lambda} (x - ct). \quad (6.2)$$

In above equation,  $a$  is the amplitude of the wave,  $c$  is the constant wave speed,  $\lambda$  is the wavelength, for lower wall,  $\eta$  is replaced by  $-\eta$  and in Cartesian coordinate system  $x$  is taken in the direction of wave propagation and  $y$  is measured in the direction normal to the  $x$ -axis. If  $\mathbf{V}$  is the velocity, then the respective velocity components in  $x$  and  $y$  directions are denoted by  $u$  and  $v$ . The equation that corresponds to the compliant wall is

$$\left[ \bar{m} \frac{\partial^2}{\partial t^2} + d \frac{\partial}{\partial t} + B \frac{\partial^4}{\partial x^4} - T \frac{\partial^2}{\partial x^2} + K \right] \eta = p - p_0. \quad (6.3)$$

Here  $\bar{m}$  denotes the plate mass per unit area,  $d$  is the wall damping coefficient,  $B$  is the flexural rigidity of the plate,  $T$  is the longitudinal tension per unit width,  $K$  is the spring stiffness and  $p_0$  is the pressure on the outside surface of the wall. Selecting  $p_0 = 0$  and the channel walls inextensible so that only their lateral motions normal to the undeformed positions occur. The horizontal displacement of the walls is assumed to be zero and so the boundary conditions are

$$\Psi_y = 0 \quad \text{and} \quad \Psi_x = \mp \frac{\partial \eta}{\partial t} \quad \text{at} \quad y = \pm h \pm \eta. \quad (6.4)$$

The velocity components in term of stream function  $\Psi(x, y, t)$  are expressed by the following equations

$$u = \frac{\partial \Psi}{\partial y}, \quad v = -\frac{\partial \Psi}{\partial x} \quad (6.5)$$

while the equations governing the MHD flow of an incompressible Johnson-Segalman fluid are:

$$\text{div } \mathbf{V} = 0, \quad (6.6)$$

$$\rho \frac{d\mathbf{V}}{dt} = \text{div } \boldsymbol{\tau} - \sigma B_0^2 \mathbf{V}, \quad (6.7)$$

$$\boldsymbol{\tau} = -p\mathbf{I} + 2\mu\mathbf{D} + \mathbf{S}, \quad (6.8)$$

$$\mathbf{S} + m \left( \frac{d\mathbf{S}}{dt} + \mathbf{S}(\mathbf{W} - l\mathbf{D}) + (\mathbf{W} - l\mathbf{D})^T \mathbf{S} \right) = 2\xi\mathbf{D}, \quad (6.9)$$

in which  $\mu$  and  $\xi$  are the viscosities,  $m$  is the relaxation time,  $l$  is the slip parameter and the tensors  $\mathbf{D}$ ,  $\mathbf{W}$  and  $\mathbf{L}$  are

$$\mathbf{D} = \frac{1}{2} (\mathbf{L} + \mathbf{L}^T), \quad \mathbf{W} = \frac{1}{2} (\mathbf{L} - \mathbf{L}^T), \quad \mathbf{L} = \text{grad } \mathbf{V},$$

where  $\rho$  being the density of the fluid,  $d/dt$  the material time derivative,  $p$  the pressure,  $\sigma$  the electrical conductivity of the fluid,  $\mathbf{I}$  the identity tensor and  $\mathbf{S}$  the extra stress tensor.

Equations (6.7)-(6.9) in scalar forms are represented by the following expressions

$$\rho \left( \frac{\partial u}{\partial t} + u \frac{\partial u}{\partial x} + v \frac{\partial u}{\partial y} \right) = -\frac{\partial p}{\partial x} + \mu \nabla^2 u + \frac{\partial S_{xx}}{\partial x} + \frac{\partial S_{xy}}{\partial y} - \sigma B_0^2 u, \quad (6.10)$$

$$\rho \left( \frac{\partial v}{\partial t} + u \frac{\partial v}{\partial x} + v \frac{\partial v}{\partial y} \right) = -\frac{\partial p}{\partial y} + \mu \nabla^2 v + \frac{\partial S_{xy}}{\partial x} + \frac{\partial S_{yy}}{\partial y}, \quad (6.11)$$

$$S_{xx} + m \left( \frac{\partial S_{xx}}{\partial t} + u \frac{\partial S_{xx}}{\partial x} + v \frac{\partial S_{xx}}{\partial y} \right) + m \left( (1-l) \frac{\partial v}{\partial x} - (1+l) \frac{\partial u}{\partial y} \right) S_{xy} - 2lm \frac{\partial u}{\partial x} S_{xx} = 2\xi \frac{\partial u}{\partial x}, \quad (6.12)$$

$$S_{xy} + m \left( \frac{\partial S_{xy}}{\partial t} + u \frac{\partial S_{xy}}{\partial x} + v \frac{\partial S_{xy}}{\partial y} \right) + \frac{m}{2} \left( (1-l) \frac{\partial u}{\partial y} - (1+l) \frac{\partial v}{\partial x} \right) S_{xx} + \frac{m}{2} \left( (1-l) \frac{\partial v}{\partial x} - (1+l) \frac{\partial u}{\partial y} \right) S_{yy} = \xi \left( \frac{\partial v}{\partial x} + \frac{\partial u}{\partial y} \right), \quad (6.13)$$

$$S_{yy} + m \left( \frac{\partial S_{yy}}{\partial t} + u \frac{\partial S_{yy}}{\partial x} + v \frac{\partial S_{yy}}{\partial y} \right) + m \left( (1-l) \frac{\partial u}{\partial y} - (1+l) \frac{\partial v}{\partial x} \right) S_{xy} - 2lm \frac{\partial v}{\partial y} S_{yy} = 2\xi \frac{\partial v}{\partial y}, \quad (6.14)$$

whence

$$\nabla^2 = \frac{\partial^2}{\partial x^2} + \frac{\partial^2}{\partial y^2}.$$

In order to complete problem formulation, we allow the continuity of stresses requiring that at the interfaces of the walls and the fluid  $p$  must be the same as that which acts on the fluid at

$y = \pm h \pm \eta$ . Utilizing Eq. (6.10), one can write

$$\begin{aligned} & \frac{\partial}{\partial x} \left[ \tilde{m} \frac{\partial^2 \eta}{\partial t^2} + d \frac{\partial \eta}{\partial t} + B \frac{\partial^4 \eta}{\partial x^4} - T \frac{\partial^2 \eta}{\partial x^2} + K \eta \right] \\ &= \mu \nabla^2 \Psi_y - \rho (\Psi_{yt} + \Psi_y \Psi_{yx} - \Psi_x \Psi_{yy}) + S_{xx,x} + S_{xy,y} - \sigma B_0^2 \Psi_y, \end{aligned} \quad (6.15)$$

in which the subscripts denote partial derivative and the Eq. (6.6) is identically satisfied.

Introducing the following dimensionless variables and parameters

$$\begin{aligned} \hat{x} &= \frac{x}{h}, \quad \hat{y} = \frac{y}{h}, \quad \hat{u} = \frac{u}{c}, \quad \hat{v} = \frac{v}{c}, \quad \hat{t} = \frac{ct}{h}, \quad \hat{p} = \frac{p}{\rho c^2}, \quad \hat{\eta} = \frac{\eta}{h}, \\ \hat{\Psi} &= \frac{\Psi}{ch}, \quad \hat{\tilde{m}} = \frac{\tilde{m}}{\rho h}, \quad \hat{d} = \frac{dh}{\rho v}, \quad \hat{B} = \frac{B}{\rho h \nu^2}, \quad \hat{T} = \frac{Th}{\rho \nu^2}, \quad \hat{K} = \frac{Kh^3}{\rho \nu^2}, \\ \hat{S}_{xx} &= \frac{h S_{xx}}{\mu c}, \quad \hat{S}_{xy} = \frac{h S_{xy}}{\mu c}, \quad \hat{S}_{yy} = \frac{h S_{yy}}{\mu c} \end{aligned} \quad (6.16)$$

and then eliminating the pressure gradient and dropping the hats, one arrives at

$$\begin{aligned} & \frac{\partial}{\partial t} \nabla^2 \Psi + \Psi_y \nabla^2 \Psi_x - \Psi_x \nabla^2 \Psi_y = \frac{1}{R} [\nabla^4 \Psi + S_{xx,xy} + S_{xy,yy} - S_{xy,xx} \\ & - S_{yy,xy}] - M^2 \Psi_{yy}, \end{aligned} \quad (6.17)$$

$$\begin{aligned} & S_{xx} + We (S_{xx,t} + \Psi_y S_{xx,x} - \Psi_x S_{xx,y}) - We ((1-l) \Psi_{xx} + (1+l) \Psi_{yy}) S_{xy} \\ & - 2l We \Psi_{xy} S_{xx} = 2 \frac{\xi}{\mu} \Psi_{xy}, \end{aligned} \quad (6.18)$$

$$\begin{aligned} & S_{xy} + We (S_{xy,t} + \Psi_y S_{xy,x} - \Psi_x S_{xy,y}) + \frac{We}{2} ((1+l) \Psi_{xx} + (1-l) \Psi_{yy}) S_{xx} \\ & - \frac{We}{2} ((1-l) \Psi_{xx} + (1+l) \Psi_{yy}) S_{yy} = \frac{\xi}{\mu} (\Psi_{yy} - \Psi_{xx}), \end{aligned} \quad (6.19)$$

$$\begin{aligned} & S_{yy} + We (S_{yy,t} + \Psi_y S_{yy,x} - \Psi_x S_{yy,y}) + We ((1+l) \Psi_{xx} + (1-l) \Psi_{yy}) S_{xy} \\ & + 2l We \Psi_{xy} S_{yy} = -2 \frac{\xi}{\mu} \Psi_{xy}, \end{aligned} \quad (6.20)$$

$$\eta = \epsilon \cos \alpha (x - t), \quad (6.21)$$

$$\Psi_y = 0 \quad \text{and} \quad \Psi_x = \mp \alpha \epsilon \sin \alpha (x - t) \quad \text{at } y = \pm 1 \pm \eta, \quad (6.22)$$

$$\begin{aligned} & \frac{\partial}{\partial x} \left[ \tilde{m} \frac{\partial^2 \eta}{\partial t^2} + d \frac{\partial \eta}{\partial t} + \frac{B}{R^2} \frac{\partial^4 \eta}{\partial x^4} - \frac{T}{R^2} \frac{\partial^2 \eta}{\partial x^2} + \frac{K}{R^2} \eta \right] + M^2 \Psi_y \\ &= \frac{1}{R} [\nabla^2 \Psi_y + S_{xx,x} + S_{xy,y}] - (\Psi_{yt} + \Psi_y \Psi_{yx} - \Psi_x \Psi_{yy}) \quad \text{at } y = \pm 1 \pm \eta. \end{aligned} \quad (6.23)$$

In above equations,  $\epsilon = a/h$  denotes the amplitude ratio,  $\alpha = 2\pi h/\lambda$  shows the wave number,

$R = ch/\nu$  is the Reynold number,  $We = cm/h$  is the Weissenberg number and  $M = \sqrt{\sigma B_0 h/\rho c}$  is the Hartman number and  $\nu = (\mu/\rho)$  and  $\xi/\rho$  are the kinematic viscosities.

## 6.2 Solution procedure

Here the solution of the problem is constructed as expansions with  $\epsilon$  and therefore

$$\Psi = \Psi_0 + \epsilon\Psi_1 + \epsilon^2\Psi_2 + \dots, \quad (6.24)$$

$$\frac{\partial p}{\partial x} = \left(\frac{\partial p}{\partial x}\right)_0 + \epsilon\left(\frac{\partial p}{\partial x}\right)_1 + \epsilon^2\left(\frac{\partial p}{\partial x}\right)_2 + \dots, \quad (6.25)$$

$$S_{xx} = S_{xx0} + \epsilon S_{xx1} + \epsilon^2 S_{xx2} + \dots, \quad (6.26)$$

$$S_{xy} = S_{xy0} + \epsilon S_{xy1} + \epsilon^2 S_{xy2} + \dots, \quad (6.27)$$

$$S_{yy} = S_{yy0} + \epsilon S_{yy1} + \epsilon^2 S_{yy2} + \dots \quad (6.28)$$

adopting the procedure of previous chapter, we have

$$\begin{aligned} \Psi_0(y) &= \frac{2K_0}{RN^2} \left[ y - \frac{\sinh \Gamma y}{\Gamma \cosh \Gamma} \right] + c_1, \\ K_0 &= -\frac{R}{2} \left( \frac{dp}{dx} \right)_0, \end{aligned} \quad (6.29)$$

where  $\Gamma = M\sqrt{\frac{R\mu}{(\mu+\xi)}}$  and  $c_1$  denotes an arbitrary constant.

For second and third sets of differential equations in  $\Psi_1$  and  $\Psi_2$ , we write

$$\Psi_1(x, y, t) = \frac{1}{2} \left[ \Phi_1(y) e^{i\alpha(x-t)} + \Phi_1^*(y) e^{-i\alpha(x-t)} \right], \quad (6.30)$$

$$S_{xx1} = \frac{1}{2} \left[ \Phi_2(y) e^{i\alpha(x-t)} + \Phi_2^*(y) e^{-i\alpha(x-t)} \right], \quad (6.31)$$

$$S_{xy1} = \frac{1}{2} \left[ \Phi_3(y) e^{i\alpha(x-t)} + \Phi_3^*(y) e^{-i\alpha(x-t)} \right], \quad (6.32)$$

$$S_{yy1} = \frac{1}{2} \left[ \Phi_4(y) e^{i\alpha(x-t)} + \Phi_4^*(y) e^{-i\alpha(x-t)} \right], \quad (6.33)$$

$$\Psi_2(x, y, t) = \frac{1}{2} \left[ \Phi_{20}(y) + \Phi_{22}(y) e^{2i\alpha(x-t)} + \Phi_{22}^*(y) e^{-2i\alpha(x-t)} \right], \quad (6.34)$$

$$S_{xx2} = \frac{1}{2} \left[ \Phi_{30}(y) + \Phi_{33}(y) e^{2i\alpha(x-t)} + \Phi_{33}^*(y) e^{-2i\alpha(x-t)} \right], \quad (6.35)$$

$$S_{xy2} = \frac{1}{2} \left[ \Phi_{40}(y) + \Phi_{44}(y) e^{2i\alpha(x-t)} + \Phi_{44}^*(y) e^{-2i\alpha(x-t)} \right], \quad (6.36)$$

$$S_{yy2} = \frac{1}{2} \left[ \Phi_{50}(y) + \Phi_{55}(y) e^{2i\alpha(x-t)} + \Phi_{55}^*(y) e^{-2i\alpha(x-t)} \right]. \quad (6.37)$$

In above expressions, the asterisk is used for the complex conjugate. Upon making use of above equations into the differential equations and boundary conditions in  $\Psi_1$  and  $\Psi_2$ , one obtains three sets of coupled linear differential systems. Note that the resulting ordinary differential equations are fourth order with variable coefficients and the boundary conditions are not all homogeneous and the problem is not an eigenvalue problem. In view of the free pumping case for which  $(\partial p / \partial x)_0 = 0$  meaning that  $K_0 = 0$  and thus one gets

$$\begin{aligned} \left[ \frac{d^2}{dy^2} - \alpha^2 + i\alpha R \right] \left[ \frac{d^2}{dy^2} - \alpha^2 \right] \Phi_1(y) &= RM^2 \Phi_1''(y) + i\alpha \Phi_4'(y) - i\alpha \Phi_2'(y) \\ &- \Phi_3'''(y) - \alpha^2 \Phi_3(y), \end{aligned} \quad (6.38)$$

$$\mu(1 - i\alpha W e) \Phi_2(y) = 2i\alpha \xi \Phi_1'(y), \quad (6.39)$$

$$\mu(1 - i\alpha W e) \Phi_3(y) = \xi (\Phi_1''(y) + \alpha^2 \Phi_1(y)), \quad (6.40)$$

$$\mu(1 - i\alpha W e) \Phi_4(y) = -2i\alpha \xi \Phi_1'(y), \quad (6.41)$$

$$\Phi_1'(\pm 1) = 0, \quad (6.42)$$

$$\begin{aligned} \Phi_1'''(\pm 1) - \alpha^2 \Phi_1'(\pm 1) + i\alpha R \Phi_1'(\pm 1) + i\alpha \Phi_2(\pm 1) + \Phi_3'(\pm 1) \\ - RM^2 \Phi_1'(\pm 1) = R\delta, \end{aligned} \quad (6.43)$$

$$\delta = -\frac{i\alpha}{R^2} (\alpha^2 R^2 \tilde{m} + i\alpha R d - \alpha^4 B - \alpha^2 T - K),$$

$$\Phi_{20}'''(y) + \Phi_{40}''(y) = \frac{i\alpha R}{2} [\Phi_1^*(y) \Phi_1''(y) - \Phi_1(y) \Phi_1^{*''}(y)]' + RN^2 \Phi_{20}''(y), \quad (6.44)$$

$$\begin{aligned} \Phi_{30}(y) = & -\frac{i\alpha W e}{2} [\Phi_1^*(y) \Phi_2(y) - \Phi_1(y) \Phi_2^*(y)]' + i\alpha l W e [\Phi_1'(y) \Phi_2^*(y) \\ & - \Phi_2(y) \Phi_1^{*'}(y)] + \frac{W e}{2} [(1+l)(\Phi_1''(y) \Phi_3^*(y) + \Phi_1^{*''}(y) \Phi_3(y)) \\ & - \alpha^2(1-l)(\Phi_1(y) \Phi_3^*(y) + \Phi_1^*(y) \Phi_3(y))], \end{aligned} \quad (6.45)$$

$$\begin{aligned} \Phi_{40}(y) = & \frac{i\alpha W e}{2} [\Phi_1(y) \Phi_3^*(y) - \Phi_1^*(y) \Phi_3(y)]' - \frac{W e}{4} \left\{ (1-l) \begin{pmatrix} \Phi_1''(y) \Phi_2^*(y) \\ + \Phi_1^{*''}(y) \Phi_2(y) \end{pmatrix} \right. \\ & + \alpha^2(1-l)(\Phi_1(y) \Phi_4^*(y) + \Phi_1^*(y) \Phi_4(y)) - (1+l)(\Phi_1''(y) \Phi_4^*(y) + \Phi_1^{*''}(y) \Phi_4(y)) \\ & \left. - \alpha^2(1+l)(\Phi_1(y) \Phi_2^*(y) + \Phi_1^*(y) \Phi_2(y)) \right\} + \frac{\xi}{\mu} \Phi_{20}''(y), \end{aligned} \quad (6.46)$$

$$\begin{aligned} \Phi_{50}(y) = & \frac{i\alpha W e}{2} [\Phi_1(y) \Phi_4^*(y) - \Phi_1^*(y) \Phi_4(y)]' - \frac{W e}{4} \left\{ (1-l) \begin{pmatrix} \Phi_1''(y) \Phi_3^*(y) \\ + \Phi_1^{*''}(y) \Phi_3(y) \end{pmatrix} \right. \\ & \left. - \alpha^2(1+l)(\Phi_1(y) \Phi_3^*(y) + \Phi_1^*(y) \Phi_3(y)) \right\} + i\alpha l W e \begin{pmatrix} \Phi_1^{*'}(y) \Phi_4(y) \\ - \Phi_1'(y) \Phi_4^*(y) \end{pmatrix}, \end{aligned} \quad (6.47)$$

$$\Phi_{20}'(\pm 1) = \mp \frac{1}{2} [\Phi_1''(\pm 1) + \Phi_1^{*''}(\pm 1)], \quad (6.48)$$

$$\begin{aligned} \Phi_{20}'''(\pm 1) = & -\frac{i\alpha R}{2} [\Phi_1(\pm 1) \Phi_1^{*''}(\pm 1) - \Phi_1^*(\pm 1) \Phi_1''(\pm 1)] \\ & \mp \frac{1}{2} [\Phi_1'''(\pm 1) + \Phi_1^{*''' }(\pm 1)] \pm \frac{\alpha^2}{2} [\Phi_1''(\pm 1) + \Phi_1^{*''}(\pm 1)] + RM^2 \Phi_{20}'(\pm 1) \\ & \mp \frac{i\alpha R}{2} [\Phi_1''(\pm 1) - \Phi_1^{*''}(\pm 1)] \pm \frac{RM^2}{2} [\Phi_1''(\pm 1) + \Phi_1^{*''}(\pm 1)] \\ & \mp \frac{i\alpha}{2} [\Phi_2'(\pm 1) - \Phi_2^{*'}(\pm 1)] - \Phi_{40}'(\pm 1) \mp \frac{1}{2} [\Phi_3''(\pm 1) + \Phi_3^{*''}(\pm 1)], \end{aligned} \quad (6.49)$$



$$\begin{aligned} & \left[ \frac{d^2}{dy^2} - 4\alpha^2 + 2i\alpha R \right] \left[ \frac{d^2}{dy^2} - 4\alpha^2 \right] \Phi_{22}(y) = RM^2 \Phi_{22}''(y) \\ & + \frac{i\alpha R}{2} [\Phi_1'(y) \Phi_1''(y) - \Phi_1(y) \Phi_1'''(y)] - \Phi_{44}''(y) - 4\alpha^2 \Phi_{44}(y) \\ & - 2i\alpha \Phi_{33}'(y) + 2i\alpha \Phi_{55}'(y), \end{aligned} \quad (6.50)$$

$$\begin{aligned} (1 - 2i\alpha We) \Phi_{33}(y) &= 4 \frac{\xi i\alpha}{\mu} \Phi_{22}'(y) - \frac{i\alpha We}{2} [\Phi_1'(y) \Phi_2(y) - \Phi_1(y) \Phi_2'(y)] \\ &+ i\alpha l We \Phi_1'(y) \Phi_2(y) + \frac{We}{4} \{(1+l) \Phi_1''(y) \Phi_3(y) - \alpha^2 (1-l) \Phi_1(y) \Phi_3(y)\}, \end{aligned} \quad (6.51)$$

$$\begin{aligned} (1 - 2i\alpha We) \Phi_{44}(y) &= \frac{\xi}{\mu} (\Phi_{22}''(y) + 4\alpha^2 \Phi_{22}(y)) - \frac{We}{4} \left\{ \begin{array}{l} (1-l) \Phi_1''(y) \Phi_2(y) \\ -\alpha^2 (1+l) \Phi_1(y) \Phi_2(y) \end{array} \right\} \\ &- \frac{i\alpha We}{2} [\Phi_1'(y) \Phi_3(y) - \Phi_1(y) \Phi_3'(y)] + \frac{We}{4} \left\{ \begin{array}{l} (1+l) \Phi_1''(y) \Phi_4(y) \\ -\alpha^2 (1-l) \Phi_1(y) \Phi_{42}(y) \end{array} \right\}, \end{aligned} \quad (6.52)$$

$$\begin{aligned} (1 - 2i\alpha We) \Phi_{55}(y) &= -4 \frac{\xi i\alpha}{\mu} \Phi_{22}'(y) - \frac{i\alpha We}{2} [\Phi_1'(y) \Phi_4(y) - \Phi_1(y) \Phi_4'(y)] \\ &- i\alpha l We \Phi_1'(y) \Phi_4(y) + \frac{We}{4} \{\alpha^2 (1+l) \Phi_1(y) \Phi_3(y) - (1-l) \Phi_1''(y) \Phi_3(y)\}, \end{aligned} \quad (6.53)$$

$$\Phi_{22}'(\pm 1) = \mp \frac{1}{2} \Phi_1''(\pm 1), \quad (6.54)$$

$$\begin{aligned} 2\Phi_{22}'''(\pm 1) &= 4\alpha (2\alpha - iR) \Phi_{22}'(\pm 1) + 2RM^2 \Phi_{22}'(\pm 1) - 2\Phi_{44}'(\pm 1) \mp \Phi_3''(\pm 1) \\ 4i\alpha \Phi_3(\pm 1) &\mp i\alpha \Phi_2'(\pm 1) \mp \Phi_1''''(\pm 1) \mp \alpha (iR - \alpha) \Phi_1''(\pm 1) \pm RM^2 \Phi_1''(\pm 1) \\ &- i\alpha R \Phi_1(\pm 1) \Phi_1''(\pm 1) + i\alpha R \Phi_1'(\pm 1) \Phi_1'(\pm 1), \end{aligned} \quad (6.55)$$

in which prime denotes the derivative with respect to  $y$ .

Solving Eqs. (6.38)-(6.43), one can write

$$\Phi_1(y) = A_1 \sinh \alpha_1 y + B_1 \sinh \beta_1 y, \quad (6.56)$$

$$\Phi_2(y) = A_2 \cosh \alpha_1 y + B_2 \cosh \beta_1 y, \quad (6.57)$$

$$\Phi_3(y) = A_3 \sinh \alpha_1 y + B_3 \sinh \beta_1 y, \quad (6.58)$$

$$\Phi_4(y) = -A_2 \cosh \alpha_1 y - B_2 \cosh \beta_1 y, \quad (6.59)$$

whence

$$A_1 = -\frac{\mu R(1-i\alpha W e)\delta}{\alpha_1(\beta_1^2-\alpha_1^2)[\xi+\mu(1-i\alpha W e)]\cosh\alpha_1},$$

$$B_1 = \frac{\mu R(1-i\alpha W e)\delta}{\beta_1(\beta_1^2-\alpha_1^2)[\xi+\mu(1-i\alpha W e)]\cosh\beta_1},$$

$$A_2 = \frac{2i\alpha\alpha_1\xi}{\mu(1-i\alpha W e)}A_1, \quad B_2 = \frac{2i\alpha\beta_1\xi}{\mu(1-i\alpha W e)}B_1,$$

$$A_3 = \frac{(\alpha^2+\alpha_1^2)\xi}{\mu(1-i\alpha W e)}A_1, \quad B_3 = \frac{(\alpha^2+\beta_1^2)\xi}{\mu(1-i\alpha W e)}B_1,$$

$$\alpha_1^2 = \frac{N+\sqrt{N^2-4\alpha^2\beta^2}}{2}, \quad \beta_1^2 = \frac{N-\sqrt{N^2-4\alpha^2\beta^2}}{2},$$

$$N = \alpha^2 + \beta^2 - \frac{i(\alpha^2 - \beta^2)}{\alpha}M^2,$$

$$\beta^2 = \alpha^2 - \frac{i\alpha R\mu(1-i\alpha W e)}{[\xi+\mu(1-i\alpha W e)]}.$$

From Eqs. (6.44)-(6.49), we have

$$\Phi'_{20}(y) = F(y) + 2C1 \left( \frac{\cosh \Gamma y - \cosh \Gamma}{\Gamma^2 \cosh \Gamma} \right) + (D - F(1)) \left( \frac{\cosh \Gamma y}{\cosh \Gamma} \right) \quad (6.60)$$

and thus the peristaltic mean flow is

$$\bar{u}(y) = \frac{\epsilon^2}{2} \Phi'_{20}(y)$$

$$= \frac{\epsilon^2}{2} \left[ F(y) + 2C1 \left( \frac{\cosh \Gamma y - \cosh \Gamma}{\Gamma^2 \cosh \Gamma} \right) + (D - F(1)) \left( \frac{\cosh \Gamma y}{\cosh \Gamma} \right) \right], \quad (6.61)$$

where

$$\begin{aligned}
D &= -\frac{1}{2} [A_1 \alpha_1^2 \sinh \alpha_1 + A_1^* \alpha_1^{*2} \sinh \alpha_1^* + B_1 \beta_1^2 \sinh \beta_1 + B_1^* \beta_1^{*2} \sinh \beta_1^*], \\
C_1 &= -\frac{\Gamma^2}{2} D + A_{33} \sinh \alpha_1 + A_{33}^* \sinh \alpha_1^* + B_{33} \sinh \beta_1 + B_{33}^* \sinh \beta_1^*, \\
A_{11} &= \frac{A_1 \alpha_1^2 \mu}{2(\mu + \xi)} [\alpha^2 - \alpha_1^2 - i\alpha R], \quad B_{11} = \frac{B_1 \beta_1^2 \mu}{2(\mu + \xi)} [\alpha^2 - \beta_1^2 - i\alpha R], \\
A_{22} &= \frac{\mu \alpha_1 (\alpha_1 A_3 + i\alpha A_2)}{2(\mu + \xi)}, \quad B_{22} = \frac{\mu \beta_1 (\beta_1 B_3 + i\alpha B_2)}{2(\mu + \xi)}, \\
A_{33} &= \frac{A_{11} - A_{22}}{2}, \quad B_{33} = \frac{B_{11} - B_{22}}{2}, \\
F(y) &= s_1 \cosh(\alpha_1 + \alpha_1^*) y + s_2 \cosh(\alpha_1 - \alpha_1^*) y + s_3 \cosh(\alpha_1 + \beta_1^*) y \\
&\quad + s_4 \cosh(\alpha_1 - \beta_1^*) y + s_5 \cosh(\alpha_1^* + \beta_1) y + s_6 \cosh(\alpha_1^* - \beta_1) y \\
&\quad + s_7 \cosh(\beta_1 + \beta_1^*) y + s_8 \cosh(\beta_1 - \beta_1^*) y, \\
s_1 &= \frac{\mu(\alpha_1 + \alpha_1^*)}{4(\mu + \xi) [(\alpha_1 + \alpha_1^*)^2 - \Gamma^2]} [i\alpha R(\alpha_1 - \alpha_1^*) A_1 A_1^* + We(\alpha_1^2 - \alpha^2) A_1 A_2^* \\
&\quad - i\alpha We(\alpha_1 + \alpha_1^*) (A_1 A_3^* - A_1^* A_3) + We(\alpha_1^{*2} - \alpha^2) A_1^* A_2], \\
s_2 &= \frac{\mu(\alpha_1 - \alpha_1^*)}{4(\mu + \xi) [(\alpha_1 - \alpha_1^*)^2 - \Gamma^2]} [-i\alpha R(\alpha_1 + \alpha_1^*) A_1 A_1^* + We(\alpha_1^2 - \alpha^2) A_1 A_2^* \\
&\quad + i\alpha We(\alpha_1 - \alpha_1^*) (A_1 A_3^* - A_1^* A_3) - We(\alpha_1^{*2} - \alpha^2) A_1^* A_2], \\
s_3 &= \frac{\mu(\alpha_1 + \beta_1^*)}{4(\mu + \xi) [(\alpha_1 + \beta_1^*)^2 - \Gamma^2]} [i\alpha R(\alpha_1 - \beta_1^*) A_1 B_1^* + We(\alpha_1^2 - \alpha^2) A_1 B_2^* \\
&\quad - i\alpha We(\alpha_1 + \beta_1^*) (A_1 B_3^* - B_1^* A_3) + We(\beta_1^{*2} - \alpha^2) B_1^* A_2], \\
s_4 &= \frac{\mu(\alpha_1 - \beta_1^*)}{4(\mu + \xi) [(\alpha_1 - \beta_1^*)^2 - \Gamma^2]} [-i\alpha R(\alpha_1 + \beta_1^*) A_1 B_1^* + We(\alpha_1^2 - \alpha^2) A_1 B_2^* \\
&\quad + i\alpha We(\alpha_1 - \beta_1^*) (A_1 B_3^* - B_1^* A_3) + We(\alpha^2 - \beta_1^{*2}) B_1^* A_2], \\
s_5 &= \frac{\mu(\alpha_1^* + \beta_1)}{4(\mu + \xi) [(\alpha_1^* + \beta_1)^2 - \Gamma^2]} [i\alpha R(\beta_1 - \alpha_1^*) B_1 A_1^* + We(\beta_1^2 - \alpha^2) B_1 A_2^* \\
&\quad - i\alpha We(\alpha_1^* + \beta_1) (B_1 A_3^* - A_1^* B_3) - We(\alpha^2 - \alpha_1^{*2}) A_1^* B_2], \\
s_6 &= \frac{\mu(\alpha_1^* - \beta_1)}{4(\mu + \xi) [(\alpha_1^* - \beta_1)^2 - \Gamma^2]} [i\alpha R(\alpha_1^* + \beta_1) B_1 A_1^* - We(\beta_1^2 - \alpha^2) B_1 A_2^* \\
&\quad - i\alpha We(\beta_1 - \alpha_1^*) (B_1 A_3^* - A_1^* B_3) - We(\alpha^2 - \alpha_1^{*2}) A_1^* B_2],
\end{aligned}$$

$$\begin{aligned}
s_7 &= \frac{\mu(\beta_1 + \beta_1^*)}{4(\mu + \xi)[(\beta_1 + \beta_1^*)^2 - \Gamma^2]} \left[ i\alpha R(\beta_1 - \beta_1^*) B_1 B_1^* + We(\beta_1^2 - \alpha^2) B_1 B_2^* \right. \\
&\quad \left. - i\alpha We(\beta_1 + \beta_1^*) (B_1 B_3^* - B_1^* B_3) + We(\beta_1^{*2} - \alpha^2) B_1^* B_2 \right], \\
s_8 &= \frac{\mu(\beta_1^2 - \beta_1^{*2})}{4(\mu + \xi)[(\beta_1 - \beta_1^*)^2 - \Gamma^2]} \left[ -i\alpha R(\beta_1 + \beta_1^*) B_1 B_1^* + We(\beta_1^2 - \alpha^2) B_1 B_2^* \right. \\
&\quad \left. + i\alpha We(\beta_1 - \beta_1^*) (B_1 B_3^* - B_1^* B_3) - We(\beta_1^{*2} - \alpha^2) B_1^* B_2 \right].
\end{aligned}$$

For critical reflux condition,  $\bar{u}$  is zero at  $y = 0$  [95] and therefore by using Eq. (6.61), one can write

$$T_{\text{critical reflux}} = \frac{H_3 + \sqrt{H_3^2 - 4H_4}}{2}, \quad (6.62)$$

with

$$\begin{aligned}
H &= \left[ \frac{(h_1 + h_2)}{\alpha_1 \alpha_1^* \cosh \alpha_1 \cosh \alpha_1^*} + \frac{(h_3 + h_4)}{\alpha_1 \beta_1^* \cosh \alpha_1 \cosh \beta_1^*} \right. \\
&\quad \left. + \frac{(h_5 + h_6)}{\alpha_1^* \beta_1 \cosh \alpha_1^* \cosh \beta_1} + \frac{(h_7 + h_8)}{\beta_1 \beta_1^* \cosh \beta_1 \cosh \beta_1^*} \right], \\
H_1 &= \frac{i\alpha^3}{R^2} [h_9 \alpha_1 \tanh \alpha_1 - h_{10} \alpha_1^* \tanh \alpha_1^* - h_{11} \beta_1 \tanh \beta_1 + h_{12} \beta_1^* \tanh \beta_1^*], \\
H_2 &= i\alpha [L_4 h_9 \alpha_1 \tanh \alpha_1 - L_4^* h_{10} \alpha_1^* \tanh \alpha_1^* - L_4 h_{11} \beta_1 \tanh \beta_1 + L_4^* h_{12} \beta_1^* \tanh \beta_1^*], \\
H_3 &= \frac{R^2}{\alpha^6 H} \left[ \frac{\alpha^4 H (L_4 + L_4^*)}{R^2} + R^2 H_1 \right], \quad H_4 = \frac{R^2}{\alpha^6 H} \left[ \frac{\alpha^2 H L_4 L_4^*}{R^2} + H_2 \right], \\
L_3 &= \alpha^2 R^2 \bar{u} - \alpha^4 B - K, \quad L_4 = i\alpha R d + L_3, \quad L_4^* = -i\alpha R d + L_3,
\end{aligned}$$

$$\begin{aligned}
h_1 &= \frac{(\alpha_1 + \alpha_1^*) g_1}{[(\alpha_1 + \alpha_1^*)^2 - \Gamma^2]} \left[ 1 - \frac{\cosh(\alpha_1 + \alpha_1^*)}{\cosh \Gamma} \right] \left\{ i\alpha R(\alpha_1 - \alpha_1^*) - \frac{2i\alpha \alpha_1^* \xi We(\alpha_1^2 - \alpha^2)}{\mu(1 + i\alpha We)} \right. \\
&\quad \left. - \frac{i\alpha \xi We(\alpha_1 + \alpha_1^*)}{\mu} \left[ \left( \frac{\alpha^2 + \alpha_1^{*2}}{1 + i\alpha We} \right) - \left( \frac{\alpha^2 + \alpha_1^2}{1 - i\alpha We} \right) \right] + \frac{2i\alpha \alpha_1 \xi We(\alpha_1^{*2} - \alpha^2)}{\mu(1 - i\alpha We)} \right\}, \\
h_2 &= \frac{(\alpha_1 - \alpha_1^*) g_1}{[(\alpha_1 - \alpha_1^*)^2 - \Gamma^2]} \left[ 1 - \frac{\cosh(\alpha_1 - \alpha_1^*)}{\cosh \Gamma} \right] \left\{ -i\alpha R(\alpha_1 + \alpha_1^*) - \frac{2i\alpha \alpha_1^* \xi We(\alpha_1^2 - \alpha^2)}{\mu(1 + i\alpha We)} \right. \\
&\quad \left. + \frac{i\alpha \xi We(\alpha_1 - \alpha_1^*)}{\mu} \left[ \left( \frac{\alpha^2 + \alpha_1^{*2}}{1 + i\alpha We} \right) - \left( \frac{\alpha^2 + \alpha_1^2}{1 - i\alpha We} \right) \right] - \frac{2i\alpha \alpha_1 \xi We(\alpha_1^{*2} - \alpha^2)}{\mu(1 - i\alpha We)} \right\},
\end{aligned}$$

$$\begin{aligned}
h_3 &= \frac{(\alpha_1 + \beta_1^*) g_1}{[(\alpha_1 + \beta_1^*)^2 - \Gamma^2]} \left[ 1 - \frac{\cosh(\alpha_1 + \beta_1^*)}{\cosh \Gamma} \right] \left\{ -i\alpha R(\alpha_1 - \beta_1^*) + \frac{2i\alpha\beta_1^* \xi We (\alpha_1^2 - \alpha^2)}{\mu(1 + i\alpha We)} \right. \\
&\quad \left. + \frac{i\alpha \xi We (\alpha_1 + \beta_1^*)}{\mu} \left[ \left( \frac{\alpha^2 + \beta_1^{*2}}{1 + i\alpha We} \right) - \left( \frac{\alpha^2 + \alpha_1^2}{1 - i\alpha We} \right) \right] - \frac{2i\alpha\alpha_1 \xi We (\beta_1^{*2} - \alpha^2)}{\mu(1 - i\alpha We)} \right\}, \\
h_4 &= \frac{(\alpha_1 - \beta_1^*) g_1}{[(\alpha_1 - \beta_1^*)^2 - \Gamma^2]} \left[ 1 - \frac{\cosh(\alpha_1 - \beta_1^*)}{\cosh \Gamma} \right] \left\{ i\alpha R(\alpha_1 + \beta_1^*) + \frac{2i\alpha\beta_1^* \xi We (\alpha_1^2 - \alpha^2)}{\mu(1 + i\alpha We)} \right. \\
&\quad \left. - \frac{i\alpha \xi We (\alpha_1 - \beta_1^*)}{\mu} \left[ \left( \frac{\alpha^2 + \beta_1^{*2}}{1 + i\alpha We} \right) - \left( \frac{\alpha^2 + \alpha_1^2}{1 - i\alpha We} \right) \right] - \frac{2i\alpha\alpha_1 \xi We (\alpha^2 - \beta_1^{*2})}{\mu(1 - i\alpha We)} \right\}, \\
h_5 &= \frac{(\alpha_1^* + \beta_1) g_1}{[(\alpha_1^* + \beta_1)^2 - \Gamma^2]} \left[ 1 - \frac{\cosh(\alpha_1^* + \beta_1)}{\cosh \Gamma} \right] \left\{ -i\alpha R(\beta_1 - \alpha_1^*) + \frac{2i\alpha\alpha_1^* \xi We (\beta_1^2 - \alpha^2)}{\mu(1 + i\alpha We)} \right. \\
&\quad \left. + \frac{i\alpha \xi We (\alpha_1^* + \beta_1)}{\mu} \left[ \left( \frac{\alpha^2 + \alpha_1^{*2}}{1 + i\alpha We} \right) - \left( \frac{\alpha^2 + \beta_1^2}{1 - i\alpha We} \right) \right] + \frac{2i\alpha\beta_1 \xi We (\alpha^2 - \alpha_1^{*2})}{\mu(1 - i\alpha We)} \right\}, \\
h_6 &= \frac{(\alpha_1^* - \beta_1) g_1}{[(\alpha_1^* - \beta_1)^2 - \Gamma^2]} \left[ 1 - \frac{\cosh(\alpha_1^* - \beta_1)}{\cosh \Gamma} \right] \left\{ -i\alpha R(\alpha_1^* + \beta_1) - \frac{2i\alpha\alpha_1^* \xi We (\beta_1^2 - \alpha^2)}{\mu(1 + i\alpha We)} \right. \\
&\quad \left. + \frac{i\alpha \xi We (\beta_1 - \alpha_1^*)}{\mu} \left[ \left( \frac{\alpha^2 + \alpha_1^{*2}}{1 + i\alpha We} \right) - \left( \frac{\alpha^2 + \beta_1^2}{1 - i\alpha We} \right) \right] + \frac{2i\alpha\beta_1 \xi We (\alpha^2 - \alpha_1^{*2})}{\mu(1 - i\alpha We)} \right\}, \\
h_7 &= \frac{(\beta_1 + \beta_1^*) g_1}{[(\beta_1 + \beta_1^*)^2 - \Gamma^2]} \left[ 1 - \frac{\cosh(\beta_1 + \beta_1^*)}{\cosh \Gamma} \right] \left\{ i\alpha R(\beta_1 - \beta_1^*) - \frac{2i\alpha\beta_1^* \xi We (\beta_1^2 - \alpha^2)}{\mu(1 + i\alpha We)} \right. \\
&\quad \left. - \frac{i\alpha \xi We (\beta_1 + \beta_1^*)}{\mu} \left[ \left( \frac{\alpha^2 + \beta_1^{*2}}{1 + i\alpha We} \right) - \left( \frac{\alpha^2 + \beta_1^2}{1 - i\alpha We} \right) \right] + \frac{2i\alpha\beta_1 \xi We (\beta_1^{*2} - \alpha^2)}{\mu(1 - i\alpha We)} \right\}, \\
h_8 &= \frac{(\beta_1 - \beta_1^*) g_1}{[(\beta_1 - \beta_1^*)^2 - \Gamma^2]} \left[ 1 - \frac{\cosh(\beta_1 - \beta_1^*)}{\cosh \Gamma} \right] \left\{ -i\alpha R(\beta_1 + \beta_1^*) - \frac{2i\alpha\beta_1^* \xi We (\beta_1^2 - \alpha^2)}{\mu(1 + i\alpha We)} \right. \\
&\quad \left. + \frac{i\alpha \xi We (\beta_1 - \beta_1^*)}{\mu} \left[ \left( \frac{\alpha^2 + \beta_1^{*2}}{1 + i\alpha We} \right) - \left( \frac{\alpha^2 + \beta_1^2}{1 - i\alpha We} \right) \right] - \frac{2i\alpha\beta_1 \xi We (\beta_1^{*2} - \alpha^2)}{\mu(1 - i\alpha We)} \right\},
\end{aligned}$$

$$\begin{aligned}
h_{10} &= \frac{\mu R(1 - i\alpha We)}{2(\beta_1^2 - \alpha_1^2)[\xi + \mu(1 - i\alpha We)]} \left[ \frac{\mu}{(\mu + \xi)} \left( \frac{1 - \cosh \Gamma}{\Gamma^2 \cosh \Gamma} \right) \left( g_2 + \frac{\xi(\alpha^2 - \alpha_1^2)}{\mu(1 - i\alpha We)} \right) - 1 \right], \\
h_{11} &= \frac{\mu R(1 - i\alpha We)}{2(\beta_1^2 - \alpha_1^2)[\xi + \mu(1 - i\alpha We)]} \left[ \frac{\mu}{(\mu + \xi)} \left( \frac{1 - \cosh \Gamma}{\Gamma^2 \cosh \Gamma} \right) \left( g_3 + \frac{\xi(\alpha^2 - \beta_1^2)}{\mu(1 - i\alpha We)} \right) - 1 \right], \\
h_{10} &= h_9^*, \quad h_{12} = h_{11}^*, \\
y_1 &= \left[ \frac{\mu^3 R^2 (1 + \alpha^2 We^2)}{4(\mu + \xi)(\beta_1^2 - \alpha_1^2)(\beta_1^{*2} - \alpha_1^{*2})[\xi^2 + 2\mu\xi + \mu^2(1 + \alpha^2 We^2)]} \right], \\
g_2 &= [\alpha(\alpha - iR) - \alpha_1^2], \quad g_3 = [\alpha(\alpha - iR) - \beta_1^2].
\end{aligned}$$

### 6.3 Results and discussion

Here our interest is to compute the mean velocity at the boundaries of the channel and the time-averaged mean axial velocity distribution and reversal flow when  $K_0 = 0$ . It is noticed that  $D$  appears in view of the no-slip condition of the axial-velocity on the wall is due to the value of  $\Phi'_{20}(y)$  at the boundary. Mean-velocity at the boundaries of the channel is defined by  $\bar{u}(\pm 1) = \frac{\epsilon^2}{2}\Phi'_{20}(\pm 1) = \frac{\epsilon^2}{2}D$  [7]. Figure 6.1a is prepared for the variation of wall damping  $d$  on the boundaries  $D$ . It is found from this Figure that  $D$  decreases when  $d$  increases. The variation of  $T$  on  $D$  with  $\alpha$  is shown in Figure 6.1b. Here  $D$  is an increasing function of  $T$ . Figure 6.1c lists that the mean velocity at the boundaries increases with increasing wall elastance. Figure 6.1d displays the influence of  $D$  with  $\alpha$  for various values of the Weissenberg number  $We$ . It is worth mentioning here that for large  $\alpha$  the values of  $D$  increase by increasing  $We$ . In order to show the effects of viscosity ratio  $\xi/\mu$  and the magnetic parameter  $M$ , we prepared the Figures 6.1e and 6.1f. As can be seen from these Figures that  $D$  increases when the viscosity ratio and  $M$  are increased. The effects of  $d$  on the mean velocity distribution and reversal flow are presented in Figure 6.2a. It is revealed that the possibility of flow reversal decreases by increasing  $d$  while in case of  $M$  and  $T$ , the situation is reversed (Figures 6.2b and 6.2d). Figure 6.2c illustrates the effects of mean velocity distribution with  $y$  for various values of  $K$ . Here the possibility of flow reversal increases by increasing  $K$ . Figures 6.2e and 6.2f depict that flow reversal decreases by increasing the Weissenberg number  $We$  and the viscosity ratio  $\xi/\mu$ . Figures 6.3a and 6.3b illustrate that the critical value of  $T$  increases with an increase in  $R$  and  $M$  respectively. However, it decreases with an increase in  $We$  and  $\xi/\mu$  (Figures 6.3c

and 6.3d). We further note that the critical value of  $T$  is very high for small values of the wave number  $\alpha$  when compared with its large values.

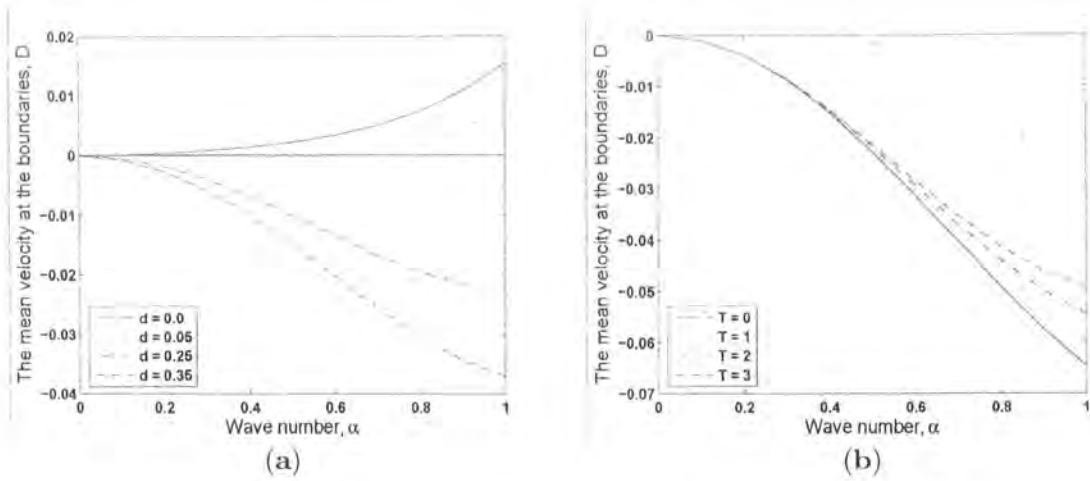


Figure 6.1a. The variation of  $D$  with wave number  $\alpha$  for different values of wall damping  $d$  when  $m = 0.01$ ,  $B = 2$ ,  $T = 1$ ,  $K = 1$ ,  $R = 10$ ,  $M = 1.0$ ,  $We = 0.1$  and  $\xi/\mu = 1.0$ .

Figure 6.1b. The variation of  $D$  with wave number  $\alpha$  for different values of wall tension  $T$  when  $m = 0.01$ ,  $B = 2$ ,  $d = 0.5$ ,  $K = 1$ ,  $R = 10$ ,  $M = 1.0$ ,  $We = 0.1$  and  $\xi/\mu = 1.0$ .

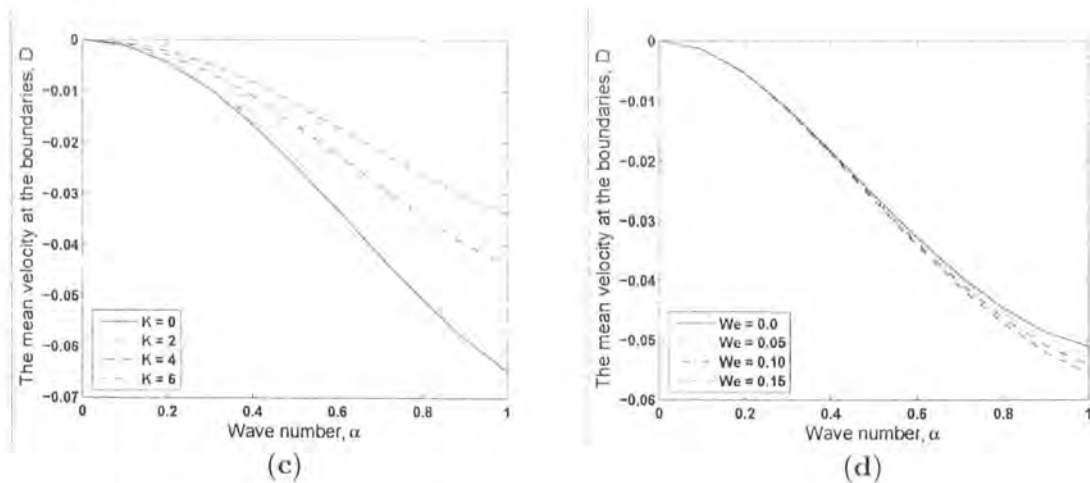


Figure 6.1c. The variation of  $D$  with wave number  $\alpha$  for different values of wall elastance

$K$  when  $m = 0.01$ ,  $B = 2$ ,  $d = 0.5$ ,  $T = 1$ ,  $R = 10$ ,  $M = 1.0$ ,  $We = 0.1$  and  $\xi/\mu = 1.0$ .

Figure 6.1d. The variation of  $D$  with wave number  $\alpha$  for different values of Weissenberg number  $We$  when  $m = 0.01$ ,  $B = 2$ ,  $d = 0.5$ ,  $K = 1$ ,  $R = 10$ ,  $M = 0.5$ ,  $T = 1$  and  $\xi/\mu = 1.0$ .

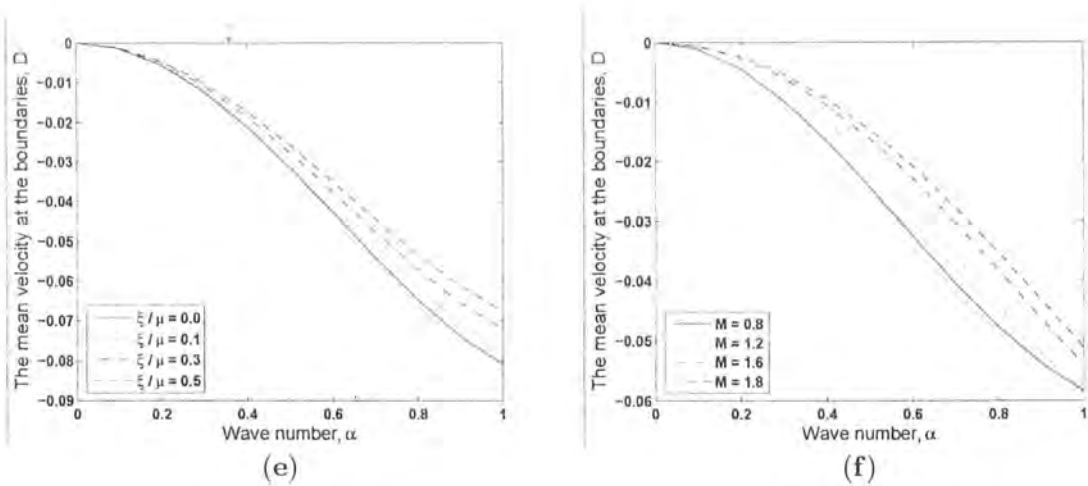


Figure 6.1e. The variation of  $D$  with wave number  $\alpha$  for different values of viscosity ratio  $\xi/\mu$  when  $m = 0.01$ ,  $B = 2$ ,  $T = 1.0$ ,  $d = 0.5$ ,  $K = 1$ ,  $R = 10$ ,  $M = 1.0$  and  $We = 0.1$ .

Figure 6.1f. The variation of  $D$  with wave number  $\alpha$  for different values of magnetic parameter  $M$  when  $m = 0.01$ ,  $B = 2$ ,  $T = 1$ ,  $R = 10$ ,  $d = 0.5$ ,  $K = 1.0$ ,  $\xi/\mu = 1.0$  and  $We = 0.1$ .

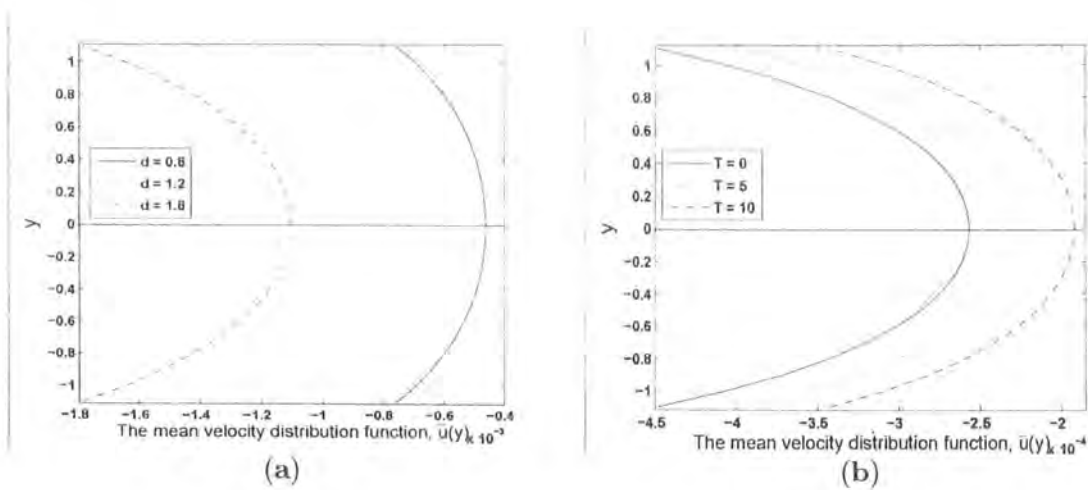




Figure 6.2a. The variation of mean-velocity distribution and reversal flow for different values of wall damping  $d$  when  $m = 0.01$ ,  $B = 2$ ,  $T = 1$ ,  $K = 1$ ,  $R = 10$ ,  $M = 0.5$ ,  $\alpha = 0.5$ ,  $\epsilon = 0.15$ ,  $We = 1.0$  and  $\xi/\mu = 1.0$ .

Figure 6.2b. The variation of mean-velocity distribution and reversal flow for different values of wall tension  $T$  when  $m = 0.01$ ,  $B = 2$ ,  $d = 0.5$ ,  $K = 1$ ,  $R = 10$ ,  $M = 0.6$ ,  $\alpha = 0.5$ ,  $\epsilon = 0.15$ ,  $We = 1.0$  and  $\xi/\mu = 1.0$ .

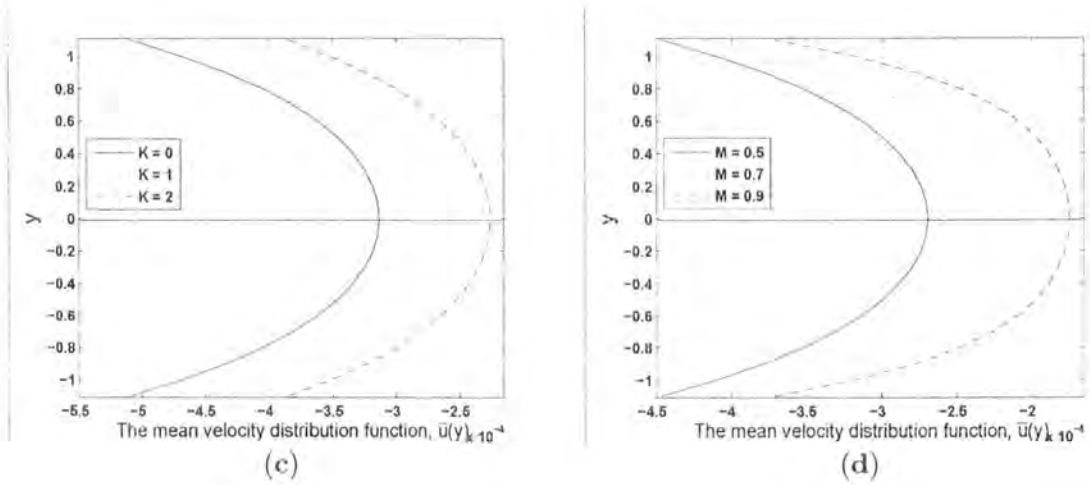


Figure 6.2c. The variation of mean-velocity distribution and reversal flow for different values of wall elastance  $K$  when  $m = 0.01$ ,  $B = 2$ ,  $d = 0.5$ ,  $T = 1$ ,  $R = 10$ ,  $M = 0.5$ ,  $\alpha = 0.5$ ,  $\epsilon = 0.15$ ,  $We = 1.0$  and  $\xi/\mu = 1.0$ .

Figure 6.2d. The variation of mean-velocity distribution and reversal flow for different values of magnetic parameter  $M$  when  $m = 0.01$ ,  $B = 2$ ,  $d = 0.5$ ,  $K = 1$ ,  $R = 10$ ,  $We = 1$ ,  $T = 1$ ,

$\alpha = 0.5$ ,  $\epsilon = 0.15$  and  $\xi/\mu = 1.0$ .

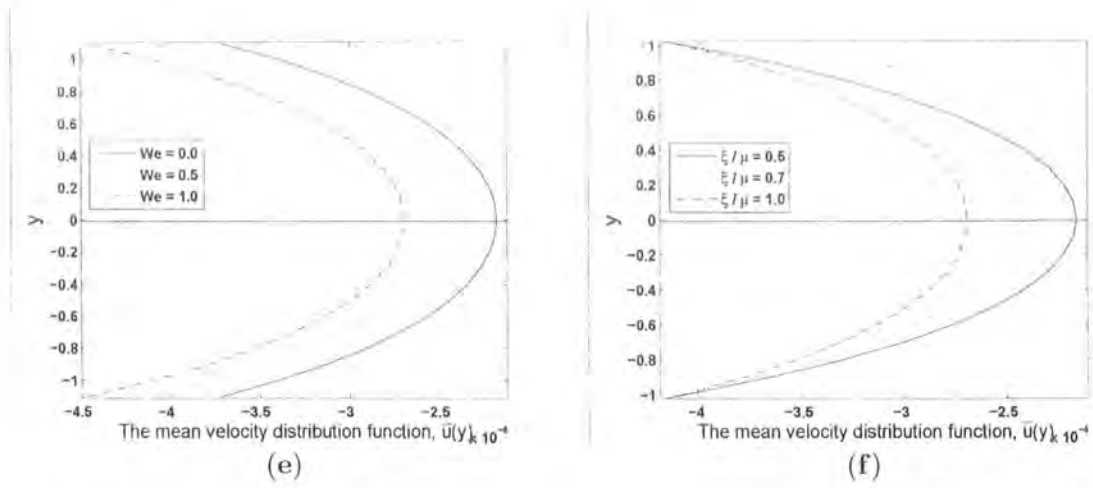


Figure 6.2e. The variation of mean-velocity distribution and reversal flow for different values of Weissenberg number  $We$  when  $m = 0.01$ ,  $B = 2$ ,  $T = 1.0$ ,  $d = 0.5$ ,  $K = 1$ ,  $R = 10$ ,  $\alpha = 0.5$ ,  $\epsilon = 0.15$ ,  $\xi/\mu = 1.0$  and  $M = 0.5$ .

Figure 6.2f. The variation of mean-velocity distribution and reversal flow for different values of viscosity ratio  $\xi/\mu$  when  $m = 0.01$ ,  $B = 2$ ,  $T = 1$ ,  $R = 10$ ,  $d = 0.5$ ,  $M = 0.5$ ,  $K = 1.0$ ,  $\alpha = 0.5$ ,  $\epsilon = 0.15$  and  $We = 1.0$ .

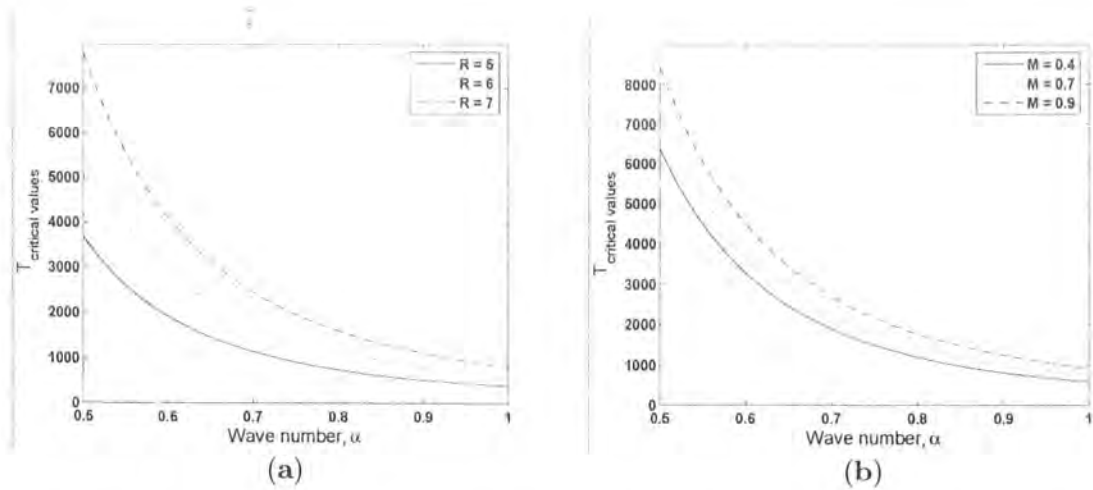


Figure 6.3a. The variation of critical values of the wall tension  $T$  with wave number  $\alpha$  for

different values of the Reynolds number  $R$  when  $m = 0.01$ ,  $B = 2$ ,  $K = 1$ ,  $d = 0.5$ ,  $M = 0.8$ ,  $We = 0.5$ ,  $\xi/\mu = 0.5$  and  $\epsilon = 0.15$ .

Figure 6.3b. The variation of critical values of the wall tension  $T$  with wave number  $\alpha$  for different values of the magnetic parameter  $M$  when  $m = 0.01$ ,  $B = 2$ ,  $d = 0.5$ ,  $K = 1$ ,  $R = 7$ ,  $We = 0.5$ ,  $\xi/\mu = 0.5$  and  $\epsilon = 0.15$ .

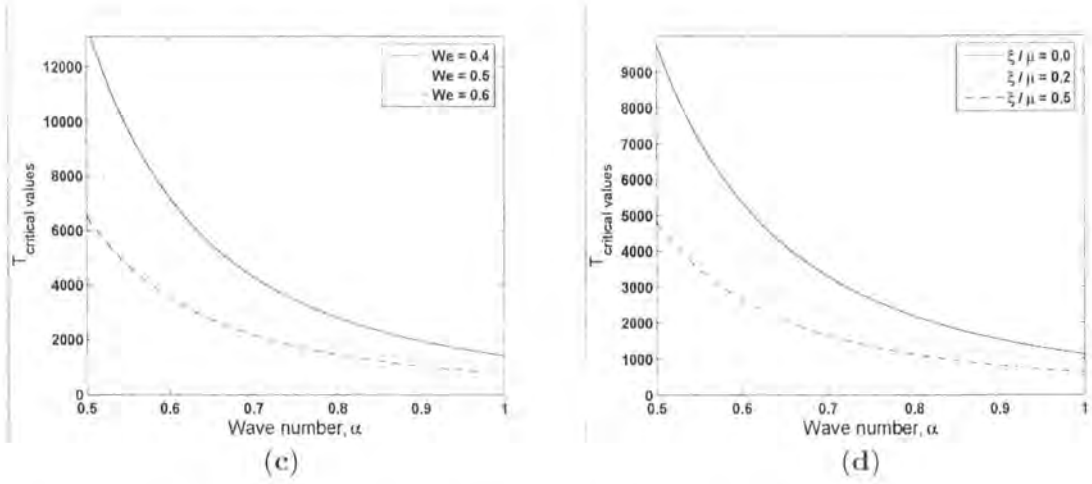


Figure 6.3c. The variation of critical values of the wall tension  $T$  with wave number  $\alpha$  for different values of the Weissenberg number  $We$  when  $m = 0.01$ ,  $B = 2$ ,  $K = 1$ ,  $d = 0.5$ ,  $R = 7$ ,  $M = 1.0$ ,  $\xi/\mu = 0.5$  and  $\epsilon = 0.15$ .

Figure 6.3d. The variation of critical values of the wall tension  $T$  with wave number  $\alpha$  for different values of the viscosity ratio  $\xi/\mu$  when  $m = 0.01$ ,  $B = 2$ ,  $K = 1$ ,  $d = 0.5$ ,  $R = 7$ ,  $M = 1.0$ ,  $\epsilon = 0.15$  and  $We = 0.7$ .

## 6.4 Conclusions

The effects of compliant walls on the MHD peristaltic flow of a Johnson-Segalman fluid are examined. The main observations of this study are listed below.

- Constant  $D$  is decreasing function of  $d$  and  $We$ .
- Effects of  $M$ ,  $T$ ,  $K$  and  $\xi/\mu$  on  $D$  are opposite to that of  $d$  and  $We$ .

- On the other, hand flow reversal is an increasing function of  $M$ ,  $T$  and  $K$ .
- Results of hydrodynamic viscous fluid [95] are recovered when  $M$ ,  $\xi$  and  $We$  are equal to zero.
- Results of hydrodynamic Johnson-Segalman fluid are obtained for  $M = 0$ .

## Chapter 7

# Peristaltic transport of power-law fluid in an asymmetric channel with compliant walls

Effects of compliant wall properties on the peristaltic flow of a non-Newtonian fluid in an asymmetric channel have been investigated in this chapter. The rheological characteristics have been characterized by the constitutive equations of a power-law fluid. Long wavelength and low Reynolds number approximations have been adopted in the presentation of mathematical developments. Exact solutions have been established for the stream function and velocity. The streamlines pattern and trapping are given due attention. The salient features of the key parameters entering into the present flow are displayed and important findings have been pointed out.

### 7.1 Mathematical model

Here we assume that the power-law fluid is confined in an asymmetric channel with width  $d_1 + d_2$ . The channel is filled with an incompressible power law fluid and an infinite wave trains of velocity  $c$  with different amplitudes and phases are travelling along the channel walls which induce asymmetry. Furthermore the channel walls are compliant such as spring-backed plate and constrained to move only in the vertical direction [95]. If  $\eta_1$  and  $\eta_2$  denote the vertical

displacements corresponding to the upper and lower walls, then the walls of asymmetric channel are given by

$$\eta_1 = d_1 + a_1 \cos\left(\frac{2\pi}{\lambda}(x - ct)\right), \quad \eta_2 = d_2 + a_2 \cos\left[\frac{2\pi}{\lambda}(x - ct) + \theta\right],$$

where  $\lambda$  is the wavelength,  $c$  is the wave speed,  $a_1$  and  $a_2$  are the wave amplitudes,  $\theta$  is the phase difference which varies in the range  $0 \leq \theta \leq \pi$  and  $x$  and  $y$  are the Cartesian coordinates with  $x$  in the direction of the wave propagation and  $y$  in a direction normal to the mean position of the channel walls. It should be noted that  $\theta = 0$  corresponds to symmetric channel with waves out of phase,  $\theta = \pi$  with phase, and further  $a_1$ ,  $a_2$ ,  $d_1$ ,  $d_2$  and  $\theta$  satisfy the condition  $a_1^2 + a_2^2 + 2a_1a_2 \cos \theta \leq (d_1 + d_2)^2$ .

The two dimensional flow equations are

$$\frac{\partial u}{\partial x} + \frac{\partial v}{\partial y} = 0, \quad (7.1)$$

$$\rho \left( \frac{\partial}{\partial t} + u \frac{\partial}{\partial x} + v \frac{\partial}{\partial y} \right) u = -\frac{\partial p}{\partial x} + \frac{\partial S_{xx}}{\partial x} + \frac{\partial S_{xy}}{\partial y}, \quad (7.2)$$

$$\rho \left( \frac{\partial}{\partial t} + u \frac{\partial}{\partial x} + v \frac{\partial}{\partial y} \right) v = -\frac{\partial p}{\partial y} + \frac{\partial S_{xy}}{\partial x} + \frac{\partial S_{yy}}{\partial y}, \quad (7.3)$$

$$S_{xx} = 2\mu \left[ 4 \left( \frac{\partial u}{\partial x} \right)^2 + 2 \left( \frac{\partial u}{\partial y} + \frac{\partial v}{\partial x} \right) + 4 \left( \frac{\partial v}{\partial y} \right)^2 \right]^m \frac{\partial u}{\partial x}, \quad (7.4)$$

$$S_{xy} = \mu \left[ 4 \left( \frac{\partial u}{\partial x} \right)^2 + 2 \left( \frac{\partial u}{\partial y} + \frac{\partial v}{\partial x} \right) + 4 \left( \frac{\partial v}{\partial y} \right)^2 \right]^m \left( \frac{\partial u}{\partial y} + \frac{\partial v}{\partial x} \right), \quad (7.5)$$

$$S_{yy} = 2\mu \left[ 4 \left( \frac{\partial u}{\partial x} \right)^2 + 2 \left( \frac{\partial u}{\partial y} + \frac{\partial v}{\partial x} \right) + 4 \left( \frac{\partial v}{\partial y} \right)^2 \right]^m \frac{\partial v}{\partial y}, \quad (7.6)$$

subjected to the boundary conditions

$$u = 0 \quad \text{at } y = \left\{ \begin{array}{l} d_1 + a_1 \cos\left(\frac{2\pi}{\lambda}(x - ct)\right) \\ -d_2 - a_2 \cos\left[\frac{2\pi}{\lambda}(x - ct) + \theta\right] \end{array} \right\}, \quad (7.7)$$

$$\begin{aligned} \frac{\partial p}{\partial x} &= \frac{\partial}{\partial x} \left[ \tilde{m} \frac{\partial^2}{\partial t^2} + C \frac{\partial}{\partial t} + B \frac{\partial^4}{\partial x^4} - \tau \frac{\partial^2}{\partial x^2} + k \right] \left\{ \begin{array}{l} \eta_1 \\ \eta_2 \end{array} \right\} \\ &= \frac{\partial S_{xx}}{\partial x} + \frac{\partial S_{xy}}{\partial y} - \rho \left( \frac{\partial u}{\partial t} + u \frac{\partial u}{\partial x} + v \frac{\partial u}{\partial y} \right), \end{aligned} \quad (7.8)$$

where  $u$  and  $v$  are the velocity components in  $x$  and  $y$  directions respectively and  $\rho$ ,  $t$ ,  $p$  and  $\mu$  are the fluid density, the time, the pressure and the dynamic viscosity respectively. Furthermore,  $L = \bar{m} \frac{\partial^2}{\partial t^2} + C \frac{\partial}{\partial t} + B \frac{\partial^4}{\partial x^4} - \tau \frac{\partial^2}{\partial x^2} + k$ ,  $\tau$  is the elastic tension in the membrane,  $\bar{m}$  is the mass per unit area,  $C$  is the coefficient of viscous damping,  $B$  is the flexural rigidity of the plate and  $k$  is the spring stiffness coefficient. It is further noted that the equations (7.1) to (7.6) describe shear thinning fluids for  $m < 0$ , Newtonian fluids for  $m = 0$  and shear thickening fluids for  $m > 0$ .

On setting

$$u = \frac{\partial \Psi}{\partial y}, \quad v = -\frac{\partial \Psi}{\partial x}$$

and defining the following non-dimensional variables and parameters

$$\begin{aligned} x^* &= \frac{x}{\lambda}, \quad y^* = \frac{y}{d_1}, \quad \Psi^* = \frac{\Psi}{cd_1}, \quad t^* = \frac{ct}{\lambda}, \quad \eta_1^* = \frac{\eta_1}{d_1}, \quad \eta_2^* = \frac{\eta_2}{d_1}, \quad p^* = \frac{d_1}{\mu c \lambda} \left( \frac{d_1^2}{2c^2} \right)^m, \\ \mathbf{S}^* &= \frac{d_1}{\mu c} \left( \frac{d_1^2}{2c^2} \right)^m \mathbf{S}, \quad \delta = \frac{d_1}{\lambda}, \quad E_1 = \frac{\bar{m} c d_1^3}{\lambda^3 \mu} \left( \frac{d_1^2}{2c^2} \right)^m, \quad E_2 = \frac{C d_1^3}{\lambda^2 \mu} \left( \frac{d_1^2}{2c^2} \right)^m, \\ E_3 &= \frac{B d_1^3}{\lambda^5 \mu c} \left( \frac{d_1^2}{2c^2} \right)^m, \quad E_4 = \frac{\tau d_1^3}{\lambda^3 \mu c} \left( \frac{d_1^2}{2c^2} \right)^m, \quad E_5 = \frac{k d_1^3}{\lambda \mu c} \left( \frac{d_1^2}{2c^2} \right)^m, \quad \text{Re} = \frac{cd_1}{\nu} \left( \frac{d_1^2}{2c^2} \right)^m, \end{aligned}$$

incompressibility condition (7.1) is identically satisfied and Eqs.(7.2)-(7.8) under long wavelength and low Reynolds number are reduced to

$$\frac{\partial^2 S_{xy}}{\partial y^2} = 0, \tag{7.9}$$

$$S_{xx} = 0, \tag{7.10}$$

$$S_{xy} = \left( \frac{\partial^2 \Psi}{\partial y^2} \right)^{2m+1}, \tag{7.11}$$

$$S_{yy} = 0, \tag{7.12}$$

$$\frac{\partial S_{xy}}{\partial y} = \frac{\partial}{\partial x} \left[ E_1 \frac{\partial^2}{\partial t^2} + E_2 \frac{\partial}{\partial t} + E_3 \frac{\partial^4}{\partial x^4} - E_4 \frac{\partial^2}{\partial x^2} + E_5 \right] \begin{Bmatrix} \eta_1 \\ \eta_2 \end{Bmatrix} \text{ at } y = \begin{Bmatrix} \eta_1 \\ \eta_2 \end{Bmatrix}, \tag{7.13}$$

$$\frac{\partial \Psi}{\partial y} = 0 \text{ at } y = \pm \begin{Bmatrix} \eta_1 \\ \eta_2 \end{Bmatrix} = \pm \left[ \begin{Bmatrix} 1 + a \cos 2\pi(x-t) \\ h + b \cos [2\pi(x-t) + \theta] \end{Bmatrix} \right], \tag{7.14}$$

in which asterisks have been suppressed for simplicity,  $\Psi$  is a stream function,  $a = a_1/d_1$ ,  $b = a_2/d_1$  and  $h = d_2/d_1$ .

## 7.2 Solution of the problem

Exact solution of Eqs. (7.9)-(7.14) is

$$\Psi = \left(\frac{2m+1}{2m+2}\right) Q_1^{\frac{1}{2m+1}} \left[ \left(\frac{2m+1}{4m+3}\right) \left[ y + \left(\frac{\eta_2 - \eta_1}{2}\right) \right]^{\left(\frac{2m+2}{2m+1}\right)} - y \left(\frac{\eta_1 + \eta_2}{2}\right)^{\left(\frac{2m+2}{2m+1}\right)} \right], \quad (7.15)$$

in which

$$Q_1 = 8a\pi^3 \left\{ \left[ E_1 - E_4 - 4\pi^2 E_3 - \frac{E_5}{4\pi^2} \right] \sin 2\pi(x-t) + \frac{E_2}{2\pi} \cos 2\pi(x-t) \right\}.$$

Expression of longitudinal velocity is now computed by the following expression

$$\begin{aligned} u &= \frac{\partial \Psi}{\partial y} \\ &= \left(\frac{2m+1}{2m+2}\right) Q_1^{\frac{1}{2m+1}} \left\{ \left[ y + \left(\frac{\eta_2 - \eta_1}{2}\right) \right]^{\left(\frac{2m+2}{2m+1}\right)} - \left(\frac{\eta_1 + \eta_2}{2}\right)^{\left(\frac{2m+2}{2m+1}\right)} \right\}. \end{aligned} \quad (7.16)$$

## 7.3 Discussion

Graphical description of the longitudinal velocity and stream function have been analyzed in this section. Effects of various parameters are displayed in the Figures 7.1(a-c)-7.7(a-b). Effect of the phase difference  $\theta$  on the longitudinal velocity  $u$  is plotted in the Figures 7.1(a-c). We observe that velocity decreases in the lower part of the channel when compared with the upper part of the channel. There is an increase in the phase difference  $\theta$  for the shear-thinning, Newtonian and shear-thickening fluids (Figures 7.1(a-c)). However the magnitude of the velocity increases for all the fluids by increasing  $\theta$ . Moreover it is observed that the magnitude of the velocity is maximum for the shear-thinning fluids (Figure 7.1a) when compared with the



shear-thickening fluids (Figure 7.1c).

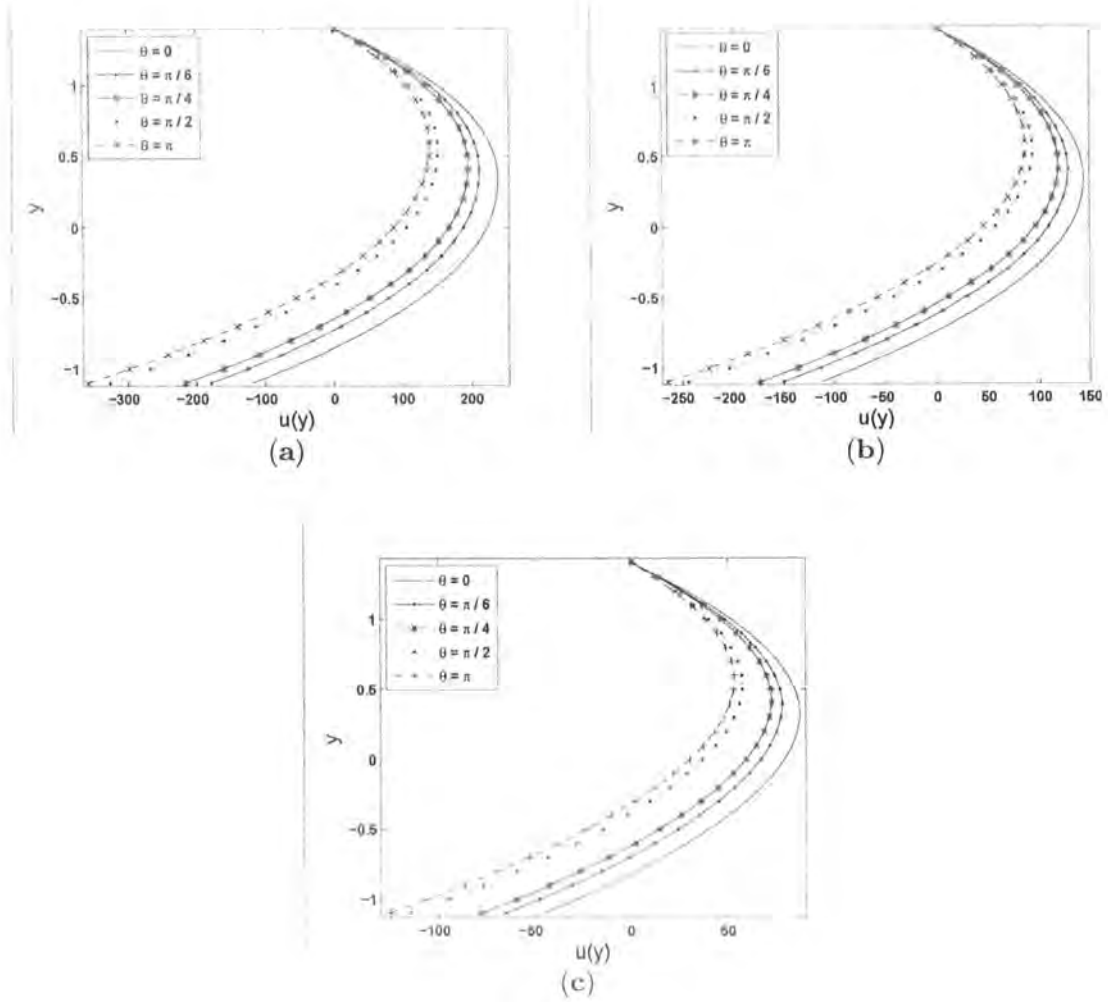


Figure 7.1: Variations of the longitudinal velocity  $u$  for different values of the phase difference  $\theta$  when (a)  $m = -0.05$ , (b)  $m = 0$ , (c)  $m = 0.05$ . The other parameters chosen are  $a = 0.5$ ,  $b = 0.3$ ,  $h = 0.5$ ,  $E_1 = 0.7$ ,  $E_2 = 0.5$ ,  $E_3 = 0.1$ ,  $E_4 = 0.3$ ,  $E_5 = 0.1$ ,  $x = 0.3$  and  $t = 0.2$ .

Effect of the compliant wall parameters  $E_1$ ,  $E_2$ ,  $E_3$ ,  $E_4$  and  $E_5$  are displayed in Figures 7.2(a - c). These Figs. represent an increase in the longitudinal velocity with the increase in these parameters. Here maximum velocity is observed for the shear-thinning fluids (Figure 7.2a) when compared with the Newtonian fluids (Figure 7.2b).

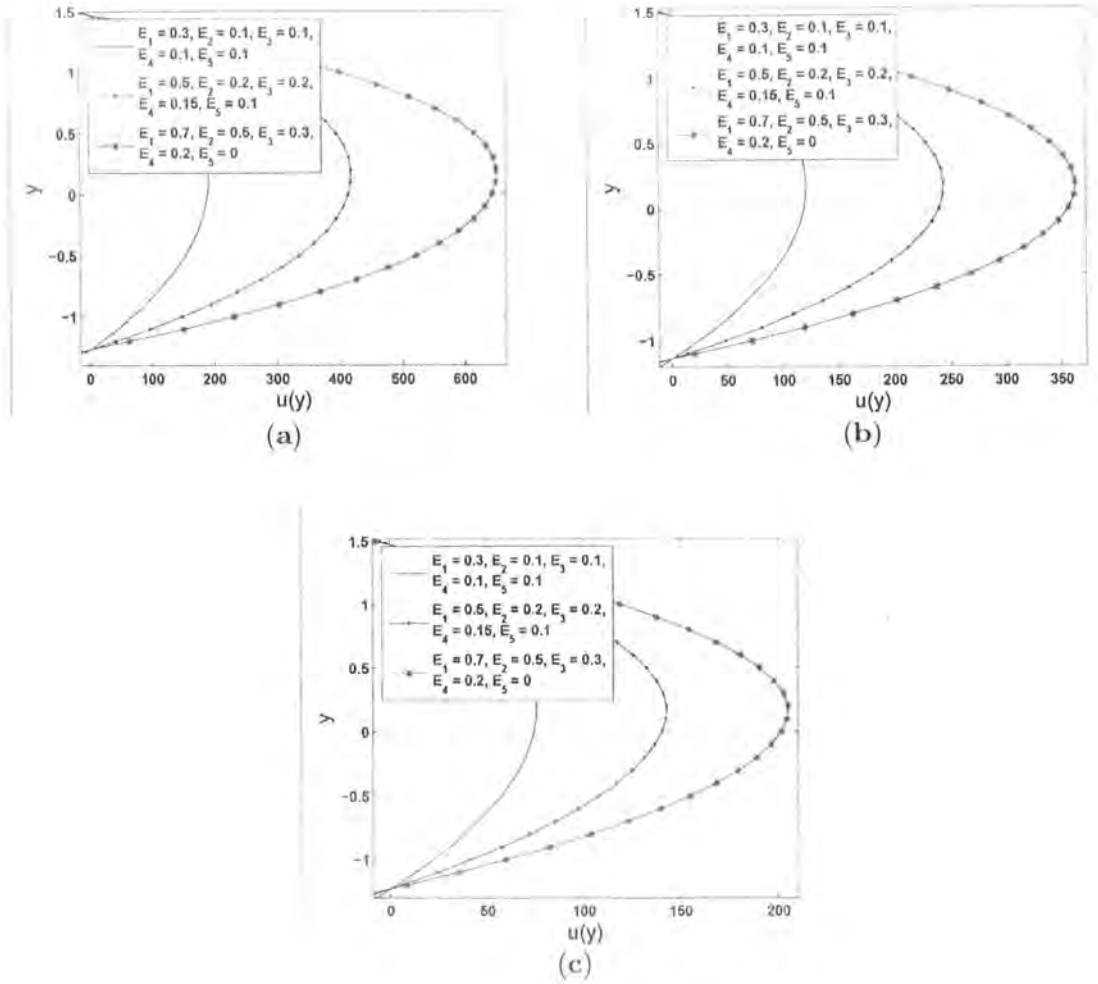


Figure 7.2: Variations of the longitudinal velocity  $u$  for different values of the wall parameters when (a)  $m = -0.05$ , (b)  $m = 0$ , (c)  $m = 0.05$ . The other parameters chosen are  $\theta = \pi/4$ ,  $a = 0.5$ ,  $b = 0.3$ ,  $h = 1$ ,  $x = 0.3$  and  $t = 0.25$ .

Figures 7.3 (a – c) reveal the effect of the power-law exponent  $m$  on the longitudinal velocity for the fixed values of the other parameters. It is observed that the velocity is greater for the shear-thinning fluids than the Newtonian and shear thickening fluids. Moreover velocity is maximum in the lower part of the channel in comparison to the upper part of the channel.

Parabolic behavior of velocity is noticed in all these graphs.

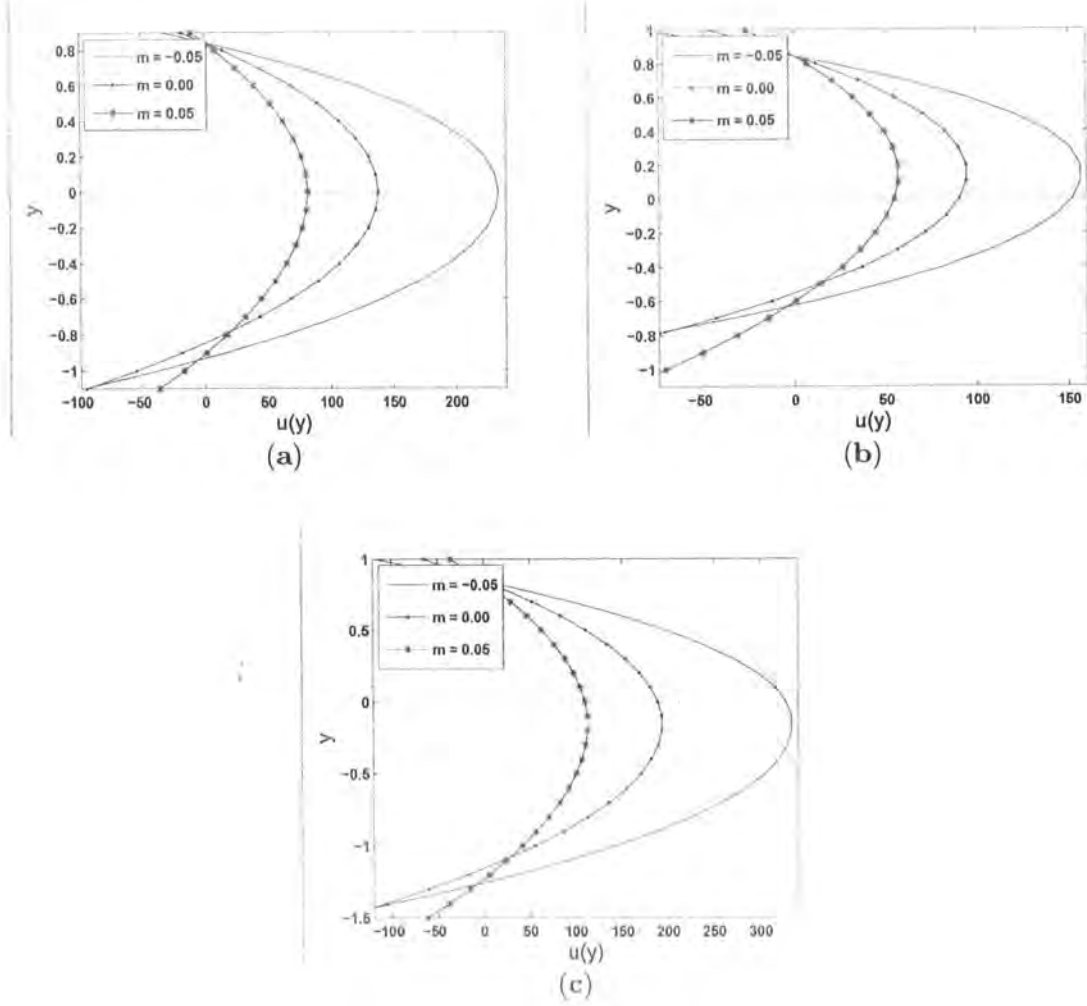


Figure 7.3: Variations of the longitudinal velocity  $u$  for different values of the power-law index  $m$  when (a)  $\theta = 0$ , (b)  $\theta = \pi/4$ , (c)  $\theta = \pi$ . The other parameters chosen are  $a = 0.5$ ,  $b = 0.5$ ,  $h = 1$ ,  $E_1 = 1$ ,  $E_2 = 0.5$ ,  $E_3 = 0.1$ ,  $E_4 = 0.3$ ,  $E_5 = 0.1$ ,  $x = 0.5$  and  $t = 0.2$ .

The phenomenon of trapping is illustrated in the Figures 7.4a – 7.7b. Figures 7.4(a – c) display the effect of power-law exponent  $m$  on the stream function for fixed values of the other parameters. These Figures show that the number of streamlines is larger for the shear-thinning fluids (Figure 7.4a) when compared with the Newtonian and shear-thickening fluids (Figures (7.4b – 7.4c)).

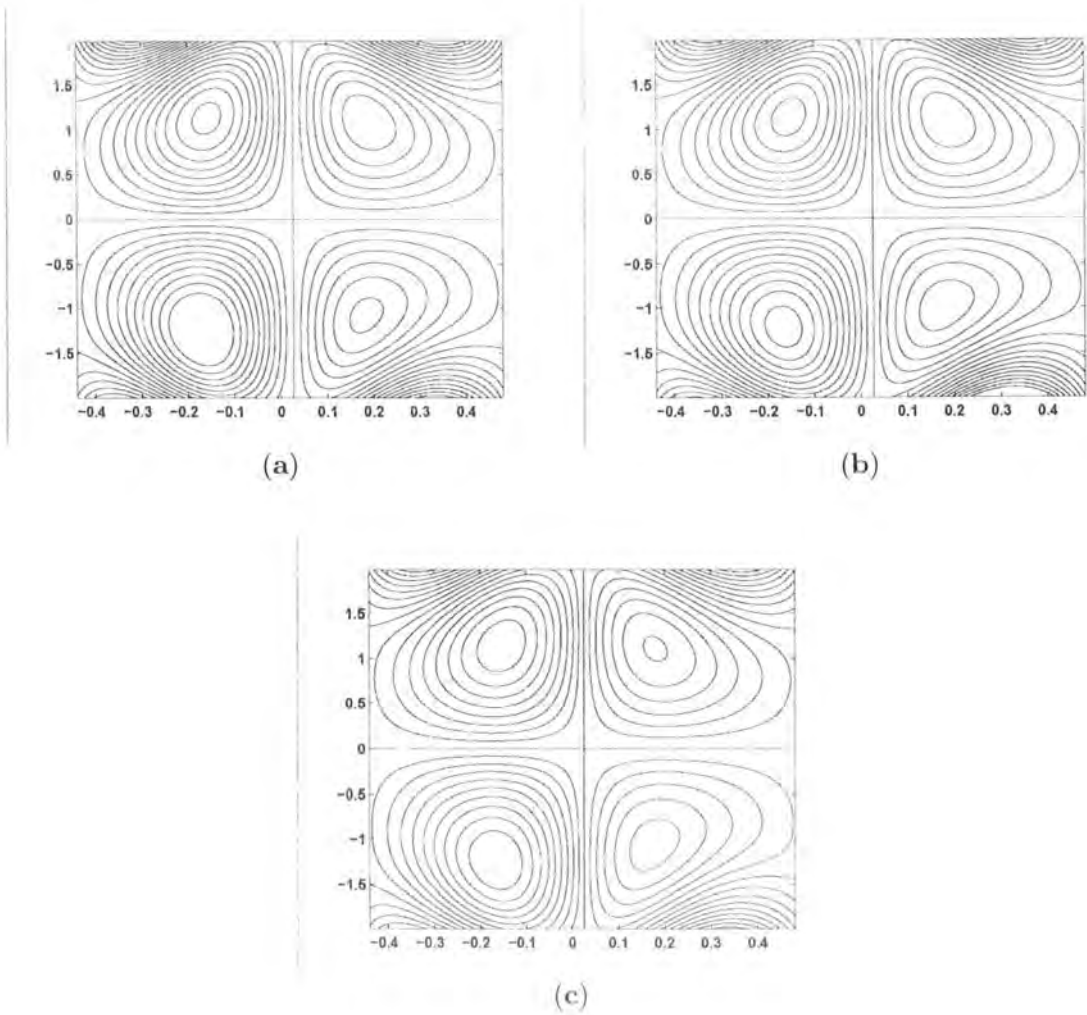
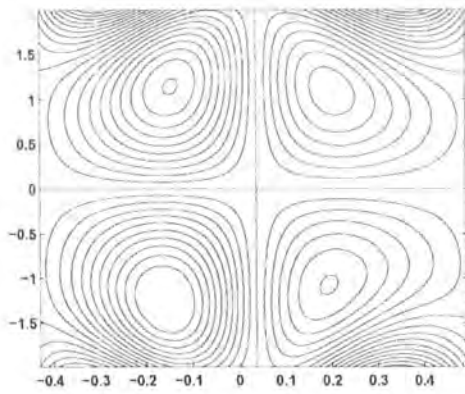
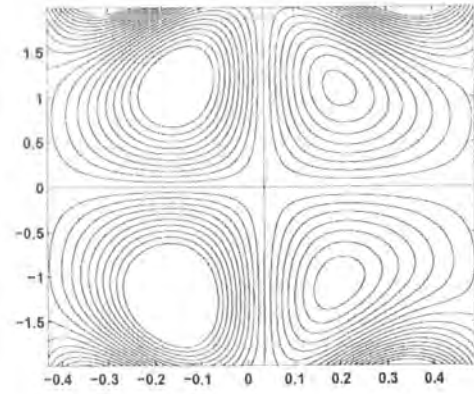


Figure 7.4: Streamlines for (a)  $m = -0.05$ , (b)  $m = 0$ , (c)  $m = 0.05$ . The other parameters chosen are  $a = 0.25$ ,  $b = 0.25$ ,  $h = 1$ ,  $\theta = \pi/6$ ,  $t = 0$ ,  $E_1 = 0.5$ ,  $E_2 = 0.05$ ,  $E_3 = 0.01$ ,  $E_4 = 0.14$  and  $E_5 = 0.5$ .

Effects of the compliant wall parameters for different values of the power-law exponent  $m$  are illustrated in the Figures (7.5a – 7.7b). It is clear from Figures (7.5a – 7.5b) that for the shear-thinning fluids ( $m < 0$ ), the number of the stream lines increases when the wall parameters  $E_1$ ,  $E_2$ ,  $E_3$ ,  $E_4$  and  $E_5$  are increased.



(a)



(b)

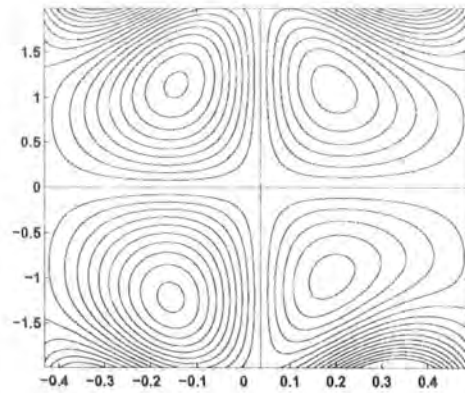
Figure 7.5: Streamlines for

(a)  $E_1 = 0.44$ ,  $E_2 = 0.05$ ,  $E_3 = 0.01$ ,  $E_4 = 0.08$ ,  $E_5 = 0.45$ .

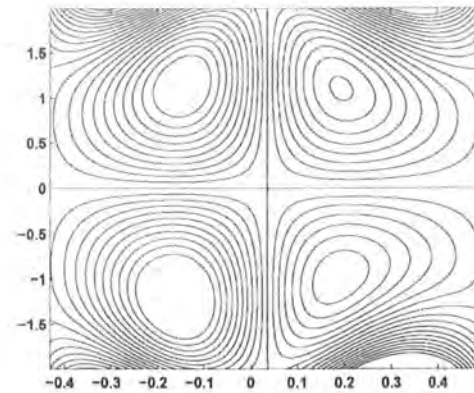
(b)  $E_1 = 0.47$ ,  $E_2 = 0.06$ ,  $E_3 = 0.01$ ,  $E_4 = 0.12$ ,  $E_5 = 0.5$ .

The other parameters chosen are  $\theta = \pi/6$ ,  $m = -0.05$ ,  $a = 0.25$ ,  $b = 0.25$ ,  $h = 1$  and  $t = 0.01$ .

Again an increasing behavior is seen for the Newtonian fluids ( $m = 0$ ) (Figures (7.6a – 7.6b)) and shear-thickening fluids ( $m > 0$ ) (Figures (7.7a – 7.7b)) with increasing elastic parameters.



(a)



(b)

Figure 7.6: Streamlines for

(a)  $E_1 = 0.44, E_2 = 0.05, E_3 = 0.01, E_4 = 0.08, E_5 = 0.45$ .

(b)  $E_1 = 0.47, E_2 = 0.06, E_3 = 0.01, E_4 = 0.12, E_5 = 0.5$ .

The other parameters chosen are  $\theta = \pi/6, m = 0, u = 0.25, b = 0.25, h = 1$  and  $t = 0.01$ .

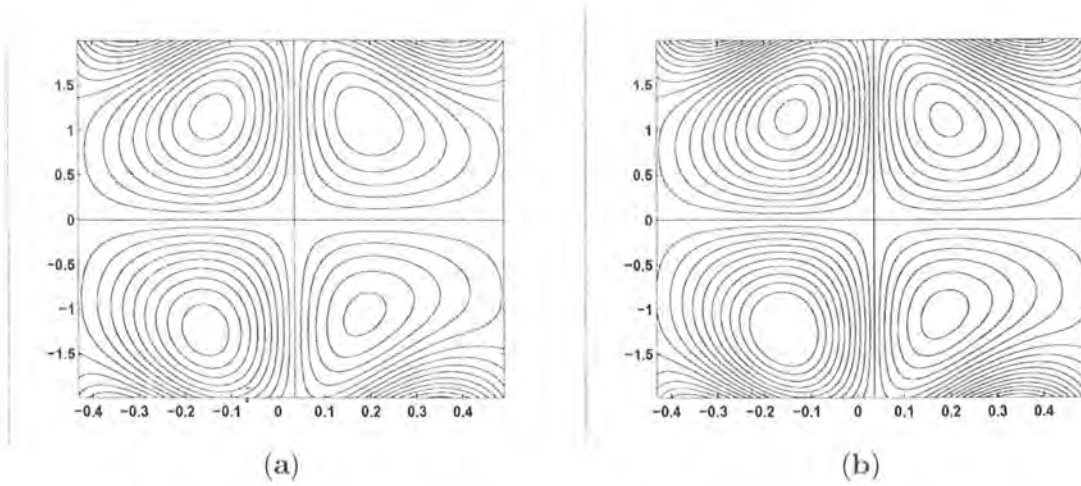


Figure 7.7: Streamlines for

(a)  $E_1 = 0.44, E_2 = 0.05, E_3 = 0.01, E_4 = 0.08, E_5 = 0.45$ .

(b)  $E_1 = 0.47, E_2 = 0.06, E_3 = 0.01, E_4 = 0.12, E_5 = 0.5$ .

The other parameters chosen here are  $\theta = \pi/6, m = 0.05, \bar{a} = 0.25, b = 0.25, h = 1$  and  $t = 0.01$ .

## 7.4 Concluding remarks

We have presented the study for peristaltic flow of a power-law fluid in an asymmetric channel with compliant walls. The closed form solutions of velocity and stream function are computed. The main findings are:

- The magnitude of velocity increases with an increase in the phase difference  $\theta$ .
- Maximum velocity is observed for the shear-thickening fluids when elastic/compliant wall parameters are increased.

- The streamlines increase with the increase in the elastic parameters for all the three fluids.
- Number of stream lines decreases in an asymmetric channel when compared with the symmetric channel.

## Chapter 8

# Compliant wall analysis of an electrically conducting Jeffrey fluid with peristalsis

This chapter looks at the peristaltic flow of magnetohydrodynamic (MHD) Jeffrey fluid in a channel with compliant walls. Conservation laws of mass and linear momentum are employed in the modelling of flow equations. Solution to the arising mathematical problem is derived for small wave amplitude. Graphical results are reported for the interpretation of solution for various flow quantities.

### 8.1 Problem development

We consider a two-dimensional channel of uniform width  $2h$  filled with homogenous Jeffrey fluid. The channel flow is because of small amplitude sinusoidal waves imposed on the compliant walls



of the channel. The physical model of the problem is shown in Figure 8.1.

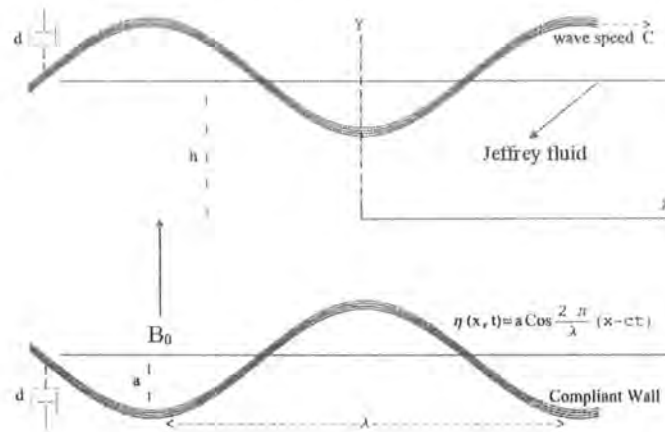


Figure: 8.1

The expressions of Cauchy and extra stress tensors in Jeffrey fluid is

$$\boldsymbol{\tau} = -p\mathbf{I} + \mathbf{S}, \quad (8.1)$$

$$(1 + \lambda_1)\mathbf{S} = 2\mu \left(1 + \lambda_2 \frac{d}{dt}\right) \mathbf{A}_1. \quad (8.2)$$

with  $p$  the pressure,  $\mathbf{I}$  the identity tensor,  $\mu$  the dynamic viscosity,  $\lambda_1$  the ratio of relaxation to retardation times,  $\lambda_2$  the relaxation time and  $\mathbf{A}_1$  the first Rivlin-Ericksen tensor. It should be noted that physical model here is similar to that of chapter 6. In order to avoid repetition, the detail regarding problem formulation is omitted. Hence after using Eqs. (6.1) – (6.7), (8.1) and (8.2), we finally obtain

$$\rho \left( \frac{\partial u}{\partial t} + u \frac{\partial u}{\partial x} + v \frac{\partial u}{\partial y} \right) = -\frac{\partial p}{\partial x} + \frac{\partial S_{xx}}{\partial x} + \frac{\partial S_{xy}}{\partial y} - \sigma B_0^2 u, \quad (8.3)$$

$$\rho \left( \frac{\partial v}{\partial t} + u \frac{\partial v}{\partial x} + v \frac{\partial v}{\partial y} \right) = -\frac{\partial p}{\partial y} + \frac{\partial S_{xy}}{\partial x} + \frac{\partial S_{yy}}{\partial y}, \quad (8.4)$$

$$S_{xx} = \frac{2\mu}{1 + \lambda_1} \left[ 1 + \lambda_2 \left( \frac{\partial}{\partial t} + u \frac{\partial}{\partial x} + v \frac{\partial}{\partial y} \right) \right] \frac{\partial u}{\partial x}, \quad (8.5)$$

$$S_{xy} = \frac{\mu}{1 + \lambda_1} \left[ 1 + \lambda_2 \left( \frac{\partial}{\partial t} + u \frac{\partial}{\partial x} + v \frac{\partial}{\partial y} \right) \right] \left( \frac{\partial u}{\partial y} + \frac{\partial v}{\partial x} \right), \quad (8.6)$$

$$S_{yy} = \frac{2\mu}{1 + \lambda_1} \left[ 1 + \lambda_2 \left( \frac{\partial}{\partial t} + u \frac{\partial}{\partial x} + v \frac{\partial}{\partial y} \right) \right] \frac{\partial v}{\partial y}, \quad (8.7)$$

$$\begin{aligned} & \frac{\partial}{\partial x} \left[ m \frac{\partial^2 \eta}{\partial t^2} + d \frac{\partial \eta}{\partial t} + B \frac{\partial^4 \eta}{\partial x^4} - T \frac{\partial^2 \eta}{\partial x^2} + K \eta \right] \\ &= -\rho (\Psi_{yt} + \Psi_y \Psi_{yx} - \Psi_x \Psi_{yy}) + S_{xx,x} + S_{xy,y} - \sigma B_0^2 \Psi_y, \end{aligned} \quad (8.8)$$

We define the following dimensionless variables

$$\begin{aligned} \hat{x} &= \frac{x}{h}, \quad \hat{y} = \frac{y}{h}, \quad \hat{u} = \frac{u}{c}, \quad \hat{v} = \frac{v}{c}, \quad \hat{t} = \frac{ct}{h}, \quad \hat{p} = \frac{p}{\rho c^2}, \quad \hat{\eta} = \frac{\eta}{h}, \\ \hat{\Psi} &= \frac{\Psi}{ch}, \quad \hat{m} = \frac{m}{\rho h}, \quad \hat{d} = \frac{dh}{\rho \nu}, \quad \hat{B} = \frac{B}{\rho h \nu^2}, \quad \hat{T} = \frac{Th}{\rho \nu^2}, \quad \hat{K} = \frac{Kh^3}{\rho \nu^2}, \\ \hat{S} &= \frac{hS}{\mu c}, \quad \hat{\lambda}_2 = \frac{c}{h} \lambda_2. \end{aligned} \quad (8.9)$$

Now the dimensionless problem takes the form

$$\frac{\partial}{\partial t} \nabla^2 \Psi + \Psi_y \nabla^2 \Psi_x - \Psi_x \nabla^2 \Psi_y = \frac{1}{R} (S_{xx,xy} + S_{xy,yy} - S_{xy,xx} - S_{yy,xy}) - M^2 \Psi_{yy} \quad (8.10)$$

$$S_{xx} = \frac{2}{1 + \lambda_1} (\Psi_{xy} + \lambda_2 (\Psi_{xyt} + \Psi_y \Psi_{xxy} - \Psi_x \Psi_{xyy})), \quad (8.11)$$

$$S_{xy} = \frac{1}{1 + \lambda_1} \left( (\Psi_{yy} - \Psi_{xx}) + \lambda_2 \begin{pmatrix} \Psi_{yyt} + \Psi_y \Psi_{xyy} - \Psi_x \Psi_{yyy} \\ -\Psi_{xxt} - \Psi_y \Psi_{xxx} + \Psi_x \Psi_{xxy} \end{pmatrix} \right), \quad (8.12)$$

$$S_{yy} = \frac{2}{1 + \lambda_1} (-\Psi_{xy} + \lambda_2 (-\Psi_{xyt} - \Psi_y \Psi_{xxy} + \Psi_x \Psi_{xyy})), \quad (8.13)$$

$$\eta = \epsilon \cos \alpha (x - t), \quad (8.14)$$

$$\Psi_y = 0 \quad \text{at } y = \pm 1 \pm \eta, \quad (8.15)$$

$$\begin{aligned} \frac{\partial}{\partial x} \left( m \frac{\partial^2 \eta}{\partial t^2} + \frac{d}{R} \frac{\partial \eta}{\partial t} + \frac{B}{R^2} \frac{\partial^4 \eta}{\partial x^4} - \frac{T}{R^2} \frac{\partial^2 \eta}{\partial x^2} + \frac{K}{R^2} \eta \right) &= \frac{1}{R} (S_{xx,x} + S_{xy,y}) \\ &- (\Psi_{yt} + \Psi_y \Psi_{yx} - \Psi_x \Psi_{yy}) - M^2 \Psi_y \quad \text{at } y = \pm 1 \pm \eta. \end{aligned} \quad (8.16)$$

Here  $\epsilon = a/h$  denotes the amplitude ratio,  $\alpha = 2\pi h/\lambda$  the wave number,  $R = ch/\nu$  the Reynolds number and  $\nu = (\mu/\rho)$  the kinematic viscosity.

## 8.2 Method of solution

Following the methodology of solution of chapter 6, we obtain the following expressions

$$\begin{aligned} \Psi_0(y) &= \frac{2K_0}{RM^2} \left[ y - \frac{\sinh \Gamma y}{\Gamma \cosh \Gamma} \right] + c_1, \\ K_0 &= -\frac{R}{2} \left( \frac{dp}{dx} \right)_0, \\ \Gamma &= M \sqrt{R(1 + \lambda_1)} \end{aligned} \quad (8.17)$$

$$\Psi_1(x, y, t) = \frac{1}{2} \left[ \Phi_1(y) e^{i\alpha(x-t)} + \Phi_1^*(y) e^{-i\alpha(x-t)} \right], \quad (8.18)$$

$$S_{xx1} = \frac{1}{2} \left[ \Phi_2(y) e^{i\alpha(x-t)} + \Phi_2^*(y) e^{-i\alpha(x-t)} \right], \quad (8.19)$$

$$S_{xy1} = \frac{1}{2} \left[ \Phi_3(y) e^{i\alpha(x-t)} + \Phi_3^*(y) e^{-i\alpha(x-t)} \right], \quad (8.20)$$

$$S_{yy1} = \frac{1}{2} \left[ \Phi_4(y) e^{i\alpha(x-t)} + \Phi_4^*(y) e^{-i\alpha(x-t)} \right], \quad (8.21)$$

$$\Psi_2(x, y, t) = \frac{1}{2} \left[ \Phi_{20}(y) + \Phi_{22}(y) e^{2i\alpha(x-t)} + \Phi_{22}^*(y) e^{-2i\alpha(x-t)} \right], \quad (8.22)$$

$$S_{xx2} = \frac{1}{2} \left[ \Phi_{30}(y) + \Phi_{33}(y) e^{2i\alpha(x-t)} + \Phi_{33}^*(y) e^{-2i\alpha(x-t)} \right], \quad (8.23)$$

$$S_{xy2} = \frac{1}{2} \left[ \Phi_{40}(y) + \Phi_{44}(y) e^{2i\alpha(x-t)} + \Phi_{44}^*(y) e^{-2i\alpha(x-t)} \right], \quad (8.24)$$

$$S_{yy2} = \frac{1}{2} \left[ \Phi_{50}(y) + \Phi_{55}(y) e^{2i\alpha(x-t)} + \Phi_{55}^*(y) e^{-2i\alpha(x-t)} \right], \quad (8.25)$$

with asterisk being the complex conjugate and  $c_1$  the arbitrary constant. Letting  $K_0 = 0$ , one has

$$\begin{aligned} i\alpha R \left[ \frac{d^2}{dy^2} - \alpha^2 \right] \Phi_1(y) &= RM^2 \Phi_1''(y) + i\alpha \Phi_4'(y) - \Phi_3''(y) \\ &\quad - \alpha^2 \Phi_3(y) - i\alpha \Phi_2'(y), \end{aligned} \quad (8.26)$$

$$(1 + \lambda_1) \Phi_2(y) = 2i\alpha (1 - i\alpha\lambda_2) \Phi_1'(y), \quad (8.27)$$

$$(1 + \lambda_1) \Phi_3(y) = (1 - i\alpha\lambda_2) (\Phi_1''(y) + \alpha^2 \Phi_1(y)), \quad (8.28)$$

$$(1 + \lambda_1) \Phi_4(y) = -2i\alpha (1 - i\alpha\lambda_2) \Phi_1'(y), \quad (8.29)$$

$$\Phi_1'(\pm 1) = 0, \quad (8.30)$$

$$i\alpha R \Phi_1'(\pm 1) + i\alpha \Phi_2(\pm 1) + \Phi_3'(\pm 1) - RM^2 \Phi_1'(\pm 1) = R\delta, \quad (8.31)$$

$$\delta = -\frac{i\alpha}{R^2} (\alpha^2 R^2 m + i\alpha R d - \alpha^4 B - \alpha^2 T - K),$$

$$\Phi_{40}''(y) = \frac{i\alpha R}{2} [\Phi_1^*(y) \Phi_1''(y) - \Phi_1(y) \Phi_1^{*''}(y)]' + RM^2 \Phi_{20}''(y), \quad (8.32)$$

$$\Phi_{30}(y) = -\frac{\alpha^2 \lambda_2}{1 + \lambda_1} [\Phi_1(y) \Phi_1^{*''}(y) + \Phi_1^*(y) \Phi_1''(y) + 2\Phi_1'(y) \Phi_1^{*'}(y)], \quad (8.33)$$

$$\Phi_{40}(y) = \frac{1}{1 + \lambda_1} \Phi_{20}''(y) - \frac{i\alpha \lambda_2}{2(1 + \lambda_1)} [\Phi_1(y) \Phi_1^{*''}(y) - \Phi_1^*(y) \Phi_1''(y)]', \quad (8.34)$$

$$\Phi_{50}(y) = \frac{\alpha^2 \lambda_2}{1 + \lambda_1} [\Phi_1(y) \Phi_1^{*''}(y) + \Phi_1^*(y) \Phi_1''(y) + 2\Phi_1'(y) \Phi_1^{*'}(y)], \quad (8.35)$$

$$\Phi_{20}'(\pm 1) = \mp \frac{1}{2} [\Phi_1''(\pm 1) + \Phi_1^{*''}(\pm 1)], \quad (8.36)$$

$$\begin{aligned} \Phi_{40}'(\pm 1) &= -\frac{i\alpha R}{2} [\Phi_1(\pm 1) \Phi_1^{*''}(\pm 1) - \Phi_1^*(\pm 1) \Phi_1''(\pm 1)] + RM^2 \Phi_{20}'(\pm 1) \\ &\mp \frac{i\alpha R}{2} [\Phi_1''(\pm 1) - \Phi_1^{*''}(\pm 1)] \pm \frac{RM^2}{2} [\Phi_1''(\pm 1) + \Phi_1^{*''}(\pm 1)] \\ &\mp \frac{i\alpha}{2} [\Phi_2'(\pm 1) - \Phi_2^{*'}(\pm 1)] \mp \frac{1}{2} [\Phi_3''(\pm 1) + \Phi_3^{*''}(\pm 1)], \end{aligned} \quad (8.37)$$

$$\begin{aligned} 2i\alpha R \left[ \frac{d^2}{dy^2} - 4\alpha^2 \right] \Phi_{22}(y) &= RM^2 \Phi_{22}''(y) + \frac{i\alpha R}{2} [\Phi_1'(y) \Phi_1''(y) - \Phi_1(y) \Phi_1'''(y)] \\ &- \Phi_{44}''(y) - 4\alpha^2 \Phi_{44}(y) - 2i\alpha \Phi_{33}'(y) + 2i\alpha \Phi_{55}'(y), \end{aligned} \quad (8.38)$$

$$(1 + \lambda_1) \Phi_{33}(y) = \frac{\alpha^2 \lambda_2}{(1 + \lambda_1)} [\Phi_1(y) \Phi_1''(y) - \Phi_1'^2(y)] + \frac{4i\alpha(1 - 2i\alpha\lambda_2)}{(1 + \lambda_1)} \Phi_{22}'(y), \quad (8.39)$$

$$\begin{aligned} (1 + \lambda_1) \Phi_{44}(y) &= \frac{i\alpha \lambda_2}{2} [\Phi_1'(y) \Phi_1''(y) - \Phi_1(y) \Phi_1'''(y)] + \frac{(1 - 2i\alpha\lambda_2)}{(1 + \lambda_1)} \Phi_{22}''(y) \\ &\frac{4\alpha^2(1 - 2i\alpha\lambda_2)}{(1 + \lambda_1)} \Phi_{22}(y), \end{aligned} \quad (8.40)$$

$$(1 + \lambda_1) \Phi_{55}(y) = -\frac{\alpha^2 \lambda_2}{(1 + \lambda_1)} [\Phi_1(y) \Phi_1''(y) - \Phi_1'^2(y)] - \frac{4i\alpha(1 - 2i\alpha\lambda_2)}{(1 + \lambda_1)} \Phi_{22}'(y), \quad (8.41)$$

$$\Phi_{22}'(\pm 1) = \mp \frac{1}{2} \Phi_1''(\pm 1), \quad (8.42)$$

$$\begin{aligned} 2\Phi_{44}'(\pm 1) &= i\alpha R \Phi_1'(\pm 1) \Phi_1'(\pm 1) - 4i\alpha R \Phi_{22}'(\pm 1) - 4i\alpha \Phi_{33}(\pm 1) \mp \Phi_3''(\pm 1) \\ &+ 2RM^2 \Phi_{22}'(\pm 1) \mp i\alpha \Phi_2'(\pm 1) \mp i\alpha R \Phi_1''(\pm 1) - i\alpha R \Phi_1(\pm 1) \Phi_1''(\pm 1) \\ &\pm RM^2 \Phi_1''(\pm 1) \end{aligned} \quad (8.43)$$

and the relevant solutions are

$$\Phi_1(y) = A_1 \sinh \alpha_1 y + B_1 \sinh \beta_1 y, \quad (8.44)$$

$$\Phi_2(y) = A_2 \cosh \alpha_1 y + B_2 \cosh \beta_1 y, \quad (8.45)$$

$$\Phi_3(y) = A_3 \sinh \alpha_1 y + B_3 \sinh \beta_1 y, \quad (8.46)$$

$$\Phi_4(y) = -A_2 \cosh \alpha_1 y - B_2 \cosh \beta_1 y, \quad (8.47)$$

where

$$\begin{aligned} A_1 &= -\frac{(1 + \lambda_1) R\delta}{(1 - i\alpha\lambda_2) (\beta_1^2 - \alpha_1^2) \alpha_1 \cosh \alpha_1}, & B_1 &= \frac{(1 + \lambda_1) R\delta}{(1 - i\alpha\lambda_2) (\beta_1^2 - \alpha_1^2) \beta_1 \cosh \beta_1}, \\ A_2 &= \frac{2i\alpha\alpha_1 (1 - i\alpha\lambda_2)}{(1 + \lambda_1)} A_1, & B_2 &= \frac{2i\alpha\beta_1 (1 - i\alpha\lambda_2)}{(1 + \lambda_1)} B_1, \\ A_3 &= \frac{(1 - i\alpha\lambda_2)}{(1 + \lambda_1)} (\alpha^2 + \alpha_1^2) A_1, & B_3 &= \frac{(1 - i\alpha\lambda_2)}{(1 + \lambda_1)} (\alpha^2 + \beta_1^2) B_1, \\ \alpha_1^2 &= \frac{N + \sqrt{N^2 - 4\alpha\beta^2}}{2}, & \beta_1^2 &= \frac{N - \sqrt{N^2 - 4\alpha\beta^2}}{2}, \\ N &= \alpha^2 + \beta^2 - \frac{i(\alpha^2 - \beta^2) M^2}{\alpha}. \end{aligned}$$

From Eqs. (8.32)-(8.37), we obtain

$$\Phi'_{20}(y) = F(y) + 2C_1 \left[ \frac{\cosh \Gamma y - \cosh \Gamma}{\Gamma^2 \cosh \Gamma} \right] + (D - F(1)) \frac{\cosh \Gamma y}{\cosh \Gamma}. \quad (8.48)$$

Result for peristaltic mean flow can be expressed as

$$\begin{aligned} \bar{u}(y) &= \frac{\epsilon^2}{2} \Phi'_{20}(y) \\ &= \frac{\epsilon^2}{2} \left[ F(y) + 2C_1 \left( \frac{\cosh \Gamma y - \cosh \Gamma}{\Gamma^2 \cosh \Gamma} \right) + (D - F(1)) \frac{\cosh \Gamma y}{\cosh \Gamma} \right], \end{aligned} \quad (8.49)$$

$$\begin{aligned}
D &= -\frac{1}{2} \left[ A_1 \alpha_1^2 \sinh \alpha_1 + A_1^* \alpha_1^{*2} \sinh \alpha_1^* + B_1 \beta_1^2 \sinh \beta_1 + B_1^* \beta_1^{*2} \sinh \beta_1^* \right], \\
C_1 &= -\frac{RM^2(1+\lambda_1)}{2} D + A_4 \sinh \alpha_1 + A_4^* \sinh \alpha_1^* + B_4 \sinh \beta_1 + B_4^* \sinh \beta_1^*, \\
A_4 &= -\frac{(1+\lambda_1)}{4} \left[ i\alpha \alpha_1^2 R A_1 + i\alpha \alpha_1 A_2 + A_3 \alpha_1^2 \right], \\
B_4 &= -\frac{(1+\lambda_1)}{4} \left[ i\alpha \beta_1^2 R B_1 + i\alpha \beta_1 B_2 + B_3 \beta_1^2 \right], \\
F(y) &= s_1 \cosh 2\alpha y + s_2 \cosh(\alpha + \beta)y + s_3 \cosh(\alpha - \beta)y + s_4 \cosh(\alpha + \beta^*)y \\
&+ s_5 \cosh(\alpha - \beta^*)y + s_6 \cosh(\beta + \beta^*)y + s_7 \cosh(\beta - \beta^*)y,
\end{aligned}$$

$$\begin{aligned}
s_1 &= \frac{i\alpha A_1 A_1^* (\alpha_1^2 - \alpha_1^{*2})}{4 \left[ (\alpha_1 + \alpha_1^*)^2 - \Gamma^2 \right]} \left[ R(1 + \lambda_1) - \lambda_2 (\alpha_1 + \alpha_1^*)^2 \right], \\
s_2 &= \frac{i\alpha A_1 A_1^* (\alpha_1^2 - \alpha_1^{*2})}{4 \left[ (\alpha_1 - \alpha_1^*)^2 - \Gamma^2 \right]} \left[ -R(1 + \lambda_1) + \lambda_2 (\alpha_1 - \alpha_1^*)^2 \right], \\
s_3 &= \frac{i\alpha A_1 B_1^* (\alpha_1^2 - \beta_1^{*2})}{4 \left[ (\alpha_1 + \beta_1^*)^2 - \Gamma^2 \right]} \left[ R(1 + \lambda_1) - \lambda_2 (\alpha_1 + \beta_1^*)^2 \right], \\
s_4 &= \frac{i\alpha A_1 B_1^* (\alpha_1^2 - \beta_1^{*2})}{4 \left[ (\alpha_1 - \beta_1^*)^2 - \Gamma^2 \right]} \left[ -R(1 + \lambda_1) + \lambda_2 (\alpha_1 - \beta_1^*)^2 \right], \\
s_5 &= \frac{i\alpha B_1 A_1^* (\beta_1^2 - \alpha_1^{*2})}{4 \left[ (\alpha_1^* + \beta_1)^2 - \Gamma^2 \right]} \left[ R(1 + \lambda_1) - \lambda_2 (\alpha_1^* + \beta_1)^2 \right], \\
s_6 &= \frac{i\alpha B_1 A_1^* (\alpha_1^{*2} - \beta_1^2)}{4 \left[ (\alpha_1^* - \beta_1)^2 - \Gamma^2 \right]} \left[ R(1 + \lambda_1) - \lambda_2 (\beta_1 - \alpha_1^*)^2 \right], \\
s_7 &= \frac{i\alpha B_1 B_1^* (\beta_1^2 - \beta_1^{*2})}{4 \left[ (\beta_1 + \beta_1^*)^2 - \Gamma^2 \right]} \left[ R(1 + \lambda_1) - \lambda_2 (\beta_1 + \beta_1^*)^2 \right], \\
s_8 &= \frac{i\alpha B_1 B_1^* (\beta_1^2 - \beta_1^{*2})}{4 \left[ (\beta_1 - \beta_1^*)^2 - \Gamma^2 \right]} \left[ -R(1 + \lambda_1) + \lambda_2 (\beta_1 - \beta_1^*)^2 \right],
\end{aligned}$$

By critical reflux condition i.e.  $\bar{u}(0) = 0$  and Eq. (8.49), one obtains

$$T_{\text{critical reflux}} = \frac{H_1 + \sqrt{H_1^2 - 4H_2}}{2}, \quad (8.50)$$

$$\begin{aligned}
H &= \left[ \frac{(h_1 + h_2)}{\alpha_1 \alpha_1^* \cosh \alpha_1 \cosh \alpha_1^*} + \frac{(h_3 + h_4)}{\alpha_1 \beta_1^* \cosh \alpha_1 \cosh \beta_1^*} \right. \\
&\quad \left. + \frac{(h_5 + h_6)}{\alpha_1^* \beta_1 \cosh \alpha_1^* \cosh \beta_1} + \frac{(h_7 + h_8)}{\beta_1 \beta_1^* \cosh \beta_1 \cosh \beta_1^*} \right], \\
H_1 &= \frac{1}{\alpha^2} [2L_3 + g_3 + g_3^*], \quad H_2 = \frac{1}{\alpha^4} [L_4 L_4^* + L_4 g_3 + L_4^* g_3^*], \\
g &= \frac{i\alpha R^2 (1 + \lambda_1)^2}{4(1 + \alpha^2 \lambda_2^2) (\beta_1^2 - \alpha_1^2) (\beta_1^{*2} - \alpha_1^{*2})}, \\
g_1 &= -\frac{R(1 + \lambda_1)}{2(1 - i\alpha \lambda_2) (\beta_1^2 - \alpha_1^2)} \left[ \left( \frac{1 - \cosh \Gamma}{\Gamma^2 \cosh \Gamma} \right) \left( \begin{array}{c} -i\alpha R(1 + \lambda_1) \\ + (1 - i\alpha \lambda_2) (\alpha^2 - \alpha_1^2) \end{array} \right) - 1 \right], \\
g_2 &= -\frac{R(1 + \lambda_1)}{2(1 - i\alpha \lambda_2) (\beta_1^2 - \alpha_1^2)} \left[ \left( \frac{1 - \cosh \Gamma}{\Gamma^2 \cosh \Gamma} \right) \left( \begin{array}{c} i\alpha R(1 + \lambda_1) \\ + (1 - i\alpha \lambda_2) (\beta_1^2 - \alpha^2) \end{array} \right) - 1 \right], \\
g_3 &= -\frac{iR^2}{\alpha H} [g_1 \alpha_1 \tanh \alpha_1 + g_2 \beta_1 \tanh \beta_1], \\
L_3 &= \alpha^2 R^2 m - \alpha^4 B - K, \quad L_4 = i\alpha R d + L_3,
\end{aligned}$$

$$h_1 = \frac{g(\alpha_1^2 - \alpha_1^{*2})}{[(\alpha_1 + \alpha_1^*)^2 - \Gamma^2]} \left[ 1 - \frac{\cosh(\alpha_1 + \alpha_1^*)}{\cosh \Gamma} \right] [R(1 + \lambda_1) - \lambda_2(\alpha_1 + \alpha_1^*)^2],$$

$$h_2 = \frac{g(\alpha_1^2 - \alpha_1^{*2})}{[(\alpha_1 - \alpha_1^*)^2 - \Gamma^2]} \left[ 1 - \frac{\cosh(\alpha_1 - \alpha_1^*)}{\cosh \Gamma} \right] [-R(1 + \lambda_1) + \lambda_2(\alpha_1 - \alpha_1^*)^2],$$

$$h_3 = \frac{-g(\alpha_1^2 - \beta_1^{*2})}{[(\alpha_1 + \beta_1^*)^2 - \Gamma^2]} \left[ 1 - \frac{\cosh(\alpha_1 + \beta_1^*)}{\cosh \Gamma} \right] [R(1 + \lambda_1) - \lambda_2(\alpha_1 + \beta_1^*)^2],$$

$$h_4 = \frac{-g(\alpha_1^2 - \beta_1^{*2})}{[(\alpha_1 - \beta_1^*)^2 - \Gamma^2]} \left[ 1 - \frac{\cosh(\alpha_1 - \beta_1^*)}{\cosh \Gamma} \right] [-R(1 + \lambda_1) + \lambda_2(\alpha_1 - \beta_1^*)^2],$$

$$h_5 = \frac{-g(\beta_1^2 - \alpha_1^{*2})}{[(\alpha_1^* + \beta_1)^2 - \Gamma^2]} \left[ 1 - \frac{\cosh(\alpha_1^* + \beta_1)}{\cosh \Gamma} \right] [R(1 + \lambda_1) - \lambda_2(\alpha_1^* + \beta_1)^2],$$

$$h_6 = \frac{-g(\alpha_1^{*2} - \beta_1^2)}{[(\alpha_1^* - \beta_1)^2 - \Gamma^2]} \left[ 1 - \frac{\cosh(\alpha_1^* - \beta_1)}{\cosh \Gamma} \right] [R(1 + \lambda_1) - \lambda_2(\beta_1 - \alpha_1^*)^2],$$



$$h_7 = \frac{g(\beta_1^2 - \beta_1^{*2})}{[(\beta_1 + \beta_1^*)^2 - \Gamma^2]} \left[ 1 - \frac{\cosh(\beta_1 + \beta_1^*)}{\cosh \Gamma} \right] \left[ R(1 + \lambda_1) - \lambda_2(\beta_1 + \beta_1^*)^2 \right],$$

$$h_8 = \frac{g(\beta_1^2 - \beta_1^{*2})}{[(\beta_1 - \beta_1^*)^2 - \Gamma^2]} \left[ 1 - \frac{\cosh(\beta_1 - \beta_1^*)}{\cosh \Gamma} \right] \left[ -R(1 + \lambda_1) + \lambda_2(\beta_1 - \beta_1^*)^2 \right].$$

### 8.3 Results and discussion

This section describes the effects of various emerging flow parameters on the flow quantities of interest. For this purpose, the mean-velocity at the boundaries of the channel, the time-averaged mean axial velocity distribution and reversal flow are calculated and the results are discussed through plots when  $K_0 = 0$ . The variation of wall damping  $d$  on  $D$  is shown in Figure 8.2a. We conclude that  $D$  decreases upon increasing  $d$ . The effects of Hartman number  $M$  on the mean velocity at the boundaries have been plotted in Figure 8.2b. It is found from this Figure that the mean velocity at the boundaries increases when Hartman number  $M$  is increased. Figure 8.2c elucidates the effect of the ratio of the relaxation time to the retardation time  $\lambda_1$  on the mean velocity at the boundaries of the channel. It is noticed that  $D$  decreases with an increase in  $\lambda_1$ . However an opposite behavior is observed in Figure 8.2d which shows the effect of the retardation time  $\lambda_2$  on  $D$ . The effects of different fluids on the mean velocity at the boundaries of the channel are depicted in Figure 8.3. This Figure shows that the mean velocity at the boundaries is greater in the case of the Newtonian fluids when compared to a Jeffrey fluid. It is noted that the damping may cause the mean flow reversal at the walls which is not possible in the elastic case. For small  $\alpha$ , the damping occurs which indicate some disturbances during the motion. The variations of  $d$  and  $M$  on the mean velocity distribution and reversal flow are plotted in the Figures 8.4a and 8.4b. Obviously the possibility of flow reversal increases by increasing  $M$  (Figure 8.4b) while in case of  $d$  the situation is reversed (Figure 8.4a). The variations of  $\lambda_1$  and  $\lambda_2$  on the mean velocity distribution and reversal flow are shown in the Figures 8.4c-8.4d. It is noticed that the flow reversal increases by increasing  $\lambda_1$  and  $\lambda_2$  (Figures 8.4c and 8.4d). The behavior of different fluids on the mean velocity distribution and reversal flow is depicted in Figure 8.5. This Figure indicates that the magnitude of the velocity is large for the linear Jeffrey fluid when compared with the Newtonian fluid. Following Fung and

Yih [7], the mean-velocity perturbation function  $G(y)$  is defined by

$$G(y) = -\frac{200}{\alpha^2 R^2} [F(y) - F(1)]. \quad (8.51)$$

Figures 8.6a and 8.6b clearly show that the critical value of  $T$  increases when Reynolds number  $R$  and the Hartman number  $M$  are increased. It is seen from Figure 8.6c that the effect of the ratio of the relaxation time to the retardation time  $\lambda_1$  on critical value of  $T$  is quite opposite to that of  $\lambda_2$  (Figure 8.6d). We further note that the critical value of  $T$  is very high for small values of the wave number  $\alpha$  when compared with its large values. Figure 8.7 shows that the critical reflux is greater in case of the Newtonian fluid when compared with Jeffrey fluid.

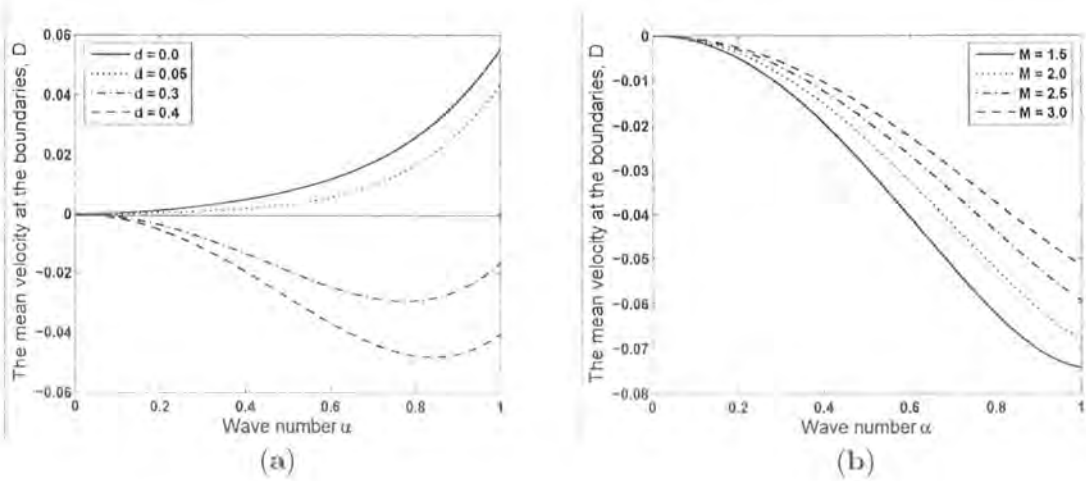


Figure 8.2a. The variation of  $D$  with wave number  $\alpha$  for different values of wall damping  $d$  when  $m = 0.01$ ,  $B = 2$ ,  $T = 1$ ,  $K = 1$ ,  $M = 2$ ,  $R = 10$ ,  $\lambda_1 = 0.8$  and  $\lambda_2 = 0.5$ .

Figure 8.2b. The variation of  $D$  with wave number  $\alpha$  for different values of Hartman number  $M$  when  $m = 0.01$ ,  $B = 2$ ,  $T = 1$ ,  $K = 1$ ,  $R = 10$ ,  $d = 0.5$ ,  $\lambda_1 = 0.8$  and  $\lambda_2 = 0.4$

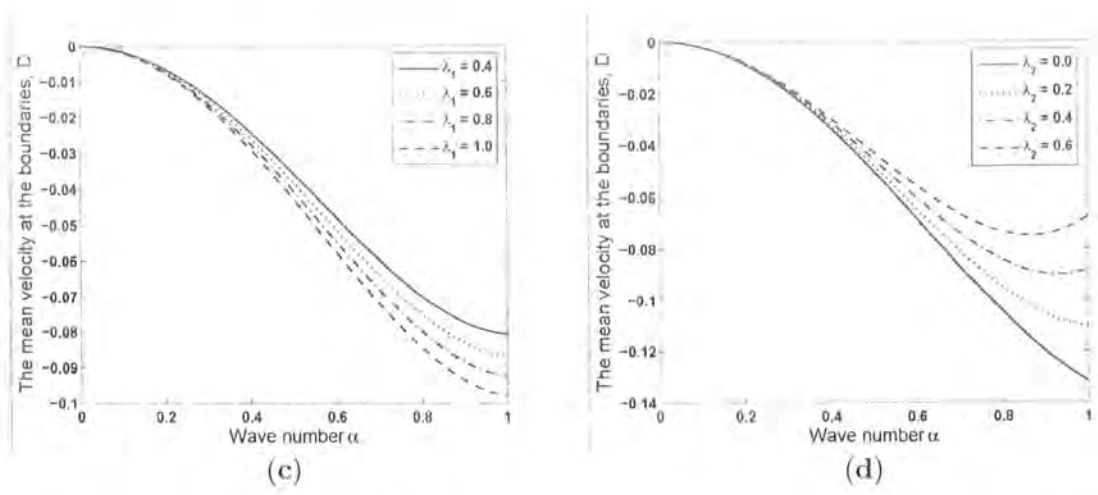


Figure 8.2c. The variation of  $D$  with wave number  $\alpha$  for different values of ratio of the relaxation time to the retardation time  $\lambda_1$  when  $m = 0.01$ ,  $B = 2$ ,  $T = 1$ ,  $K = 1$ ,  $R = 10$ ,  $M = 1$ ,  $d = 0.5$  and  $\lambda_2 = 0.2$ .

Figure 8.2d. The variation of  $D$  with wave number  $\alpha$  for different values of retardation time  $\lambda_2$  when  $m = 0.01$ ,  $B = 2$ ,  $T = 1$ ,  $K = 1$ ,  $R = 10$ ,  $M = 1$ ,  $d = 0.5$  and  $\lambda_1 = 1.5$

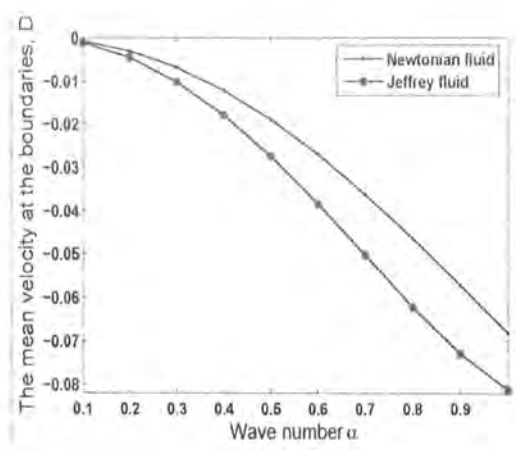


Figure 8.3: The variation of  $D$  with wave number  $\alpha$  for different fluids when  $m = 0.01$ ,  $B = 2$ ,  $T = 1$ ,  $K = 1$ ,  $M = 2$ ,  $R = 10$  and  $d = 0.5$ .

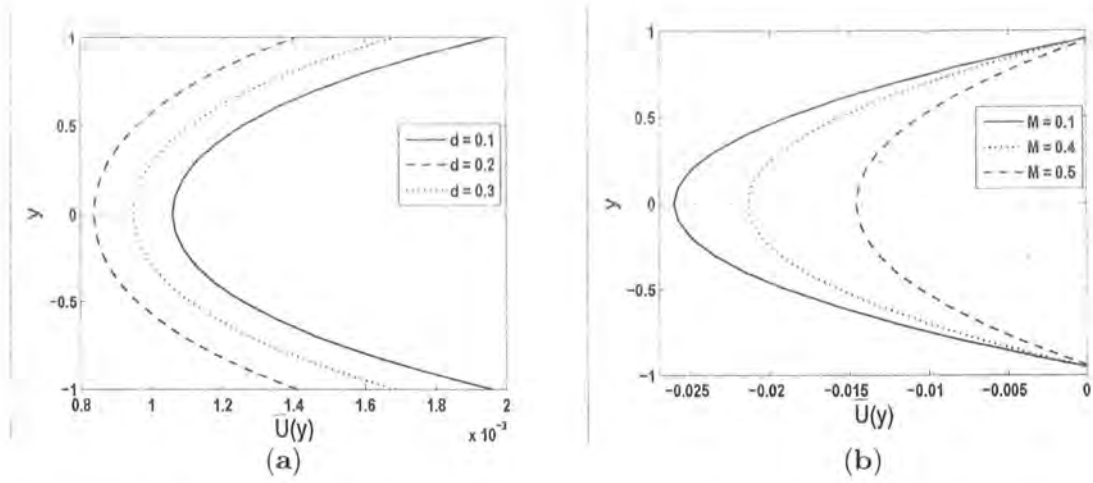


Figure 8.4a. The variation of mean-velocity distribution and reversal flow for different values of wall damping  $d$  when  $m = 0.01$ ,  $B = 2$ ,  $T = 1$ ,  $K = 1$ ,  $R = 1$ ,  $\alpha = 0.5$ ,  $\epsilon = 0.15$ ,  $\lambda_1 = 0.8$  and  $\lambda_2 = 0.4$ .

Figure 8.4b. The variation of mean-velocity distribution and reversal flow for different values of Hartman number  $M$  when  $m = 0.01$ ,  $B = 2$ ,  $K = 1$ ,  $T = 1$ ,  $R = 1$ ,  $d = 0.5$ ,  $\alpha = 0.5$ ,  $\epsilon = 0.15$ ,  $\lambda_1 = 0.8$  and  $\lambda_2 = 0.4$ .

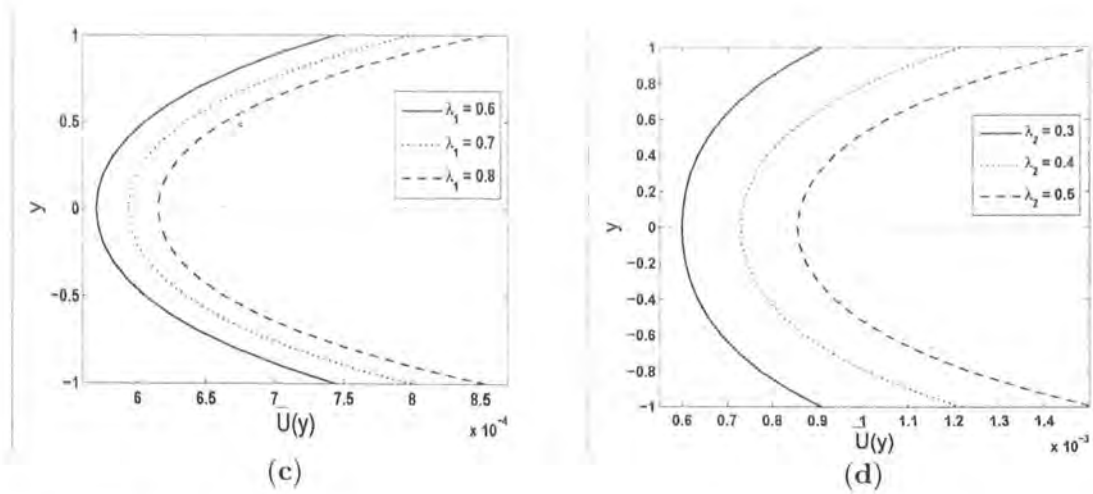


Figure 8.4c. The variation of mean-velocity distribution and reversal flow for different values

of ratio of the relaxation time to the retardation time  $\lambda_1$  when  $m = 0.01$ ,  $B = 2$ ,  $T = 1$ ,  $K = 1$ ,  $R = 1$ ,  $M = 1$ ,  $d = 0.5$ ,  $\alpha = 0.5$ ,  $\epsilon = 0.15$  and  $\lambda_2 = 0.4$ .

Figure 8.4d. The variation of mean-velocity distribution and reversal flow for different values of retardation time  $\lambda_2$  when  $m = 0.01$ ,  $B = 2$ ,  $T = 1$ ,  $K = 1$ ,  $R = 1$ ,  $M = 1$ ,  $d = 0.5$ ,  $\alpha = 0.5$ ,  $\epsilon = 0.15$  and  $\lambda_1 = 0.4$

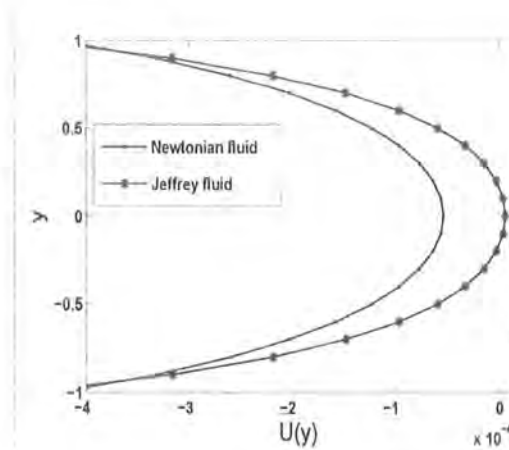


Figure 8.5: The variation of mean-velocity distribution and reversal flow for different fluids when  $m = 0.01$ ,  $B = 2$ ,  $T = 1$ ,  $K = 1$ ,  $M = 1$ ,  $R = 10$ ,  $\alpha = 0.5$ ,  $\epsilon = 0.15$  and  $d = 0.5$ .

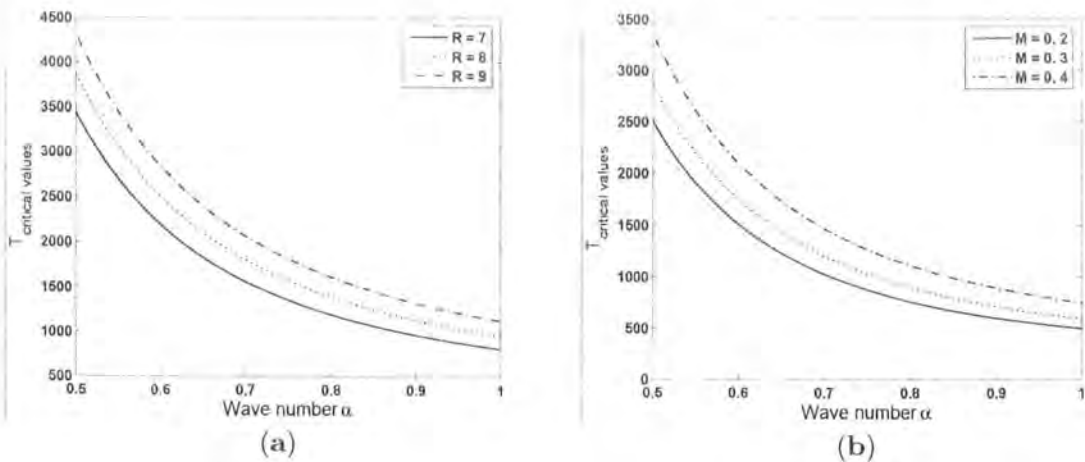


Figure 8.6a. The variation of critical values of wall tension  $T$  with wave number  $\alpha$  for different values of the Reynolds number  $R$  when  $m = 0.01$ ,  $B = 2$ ,  $K = 1$ ,  $d = 0.5$ ,  $M = 0.5$ ,

$\lambda_1 = 0.7$  and  $\lambda_2 = 0.4$ .

Figure 8.6b. The variation of critical values of wall tension  $T$  with wave number  $\alpha$  for different values of Hartman number  $M$  when  $m = 0.01$ ,  $B = 2$ ,  $K = 1$ ,  $d = 0.5$ ,  $R = 8$ ,  $\lambda_2 = 0.4$  and  $\lambda_1 = 0.7$

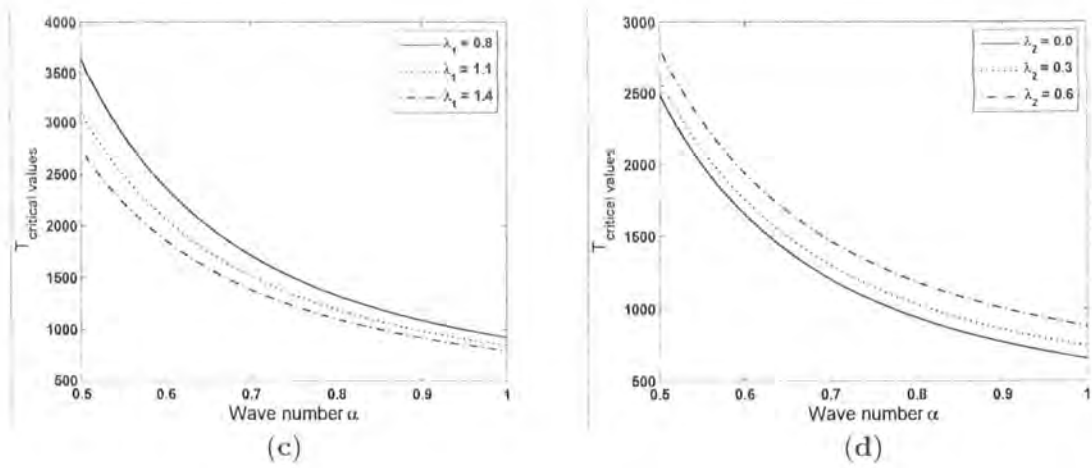


Figure 8.6c. The variation of critical values of wall tension  $T$  with wave number  $\alpha$  for different values of the relaxation time to the retardation time  $\lambda_1$  when  $m = 0.01$ ,  $B = 2$ ,  $K = 1$ ,  $R = 8$ ,  $M = 0.5$ ,  $d = 0.5$  and  $\lambda_2 = 0.4$ .

Figure 8.6d. The variation of critical values of wall tension  $T$  with wave number  $\alpha$  for different values of retardation time  $\lambda_2$  when  $m = 0.01$ ,  $B = 2$ ,  $K = 1$ ,  $R = 8$ ,  $M = 0.5$ ,  $d = 0.5$  and  $\lambda_1 = 1.5$

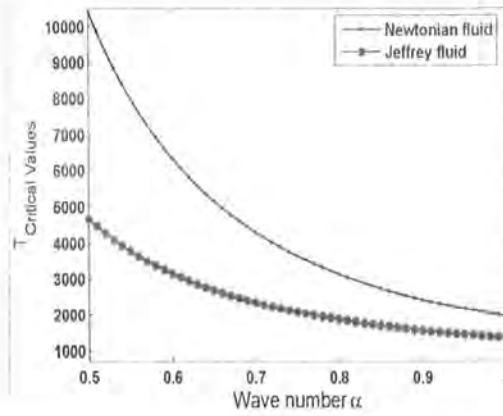


Figure 8.7: The variation of critical values of wall tension  $T$  with wave number  $\alpha$  for different fluids when  $m = 0.01$ ,  $B = 2$ ,  $K = 1$ ,  $M = 0.5$ ,  $R = 10$ ,  $\alpha = 0.5$  and  $d = 0.5$ .

## 8.4 Closing remarks

This study describes the peristaltic flow of an incompressible Jeffrey fluid. The two-dimensional equations are modeled and analysis is performed for free pumping case. It is concluded that:

- There is a decrease in the constant  $D$  when  $\lambda_1$  is increased.
- The role of  $\lambda_2$  on  $D$  is quite opposite to that of  $\lambda_1$ .
- The flow reversal increases by increasing  $\lambda_1$  and  $\lambda_2$  while the flow reversal decreases when  $d$  increases.
- The magnitude of velocity in Jeffrey fluid is greater than that of Newtonian fluid.
- For  $\lambda_1 = \lambda_2 = 0$ , the results of viscous fluid are recovered [95].

## Chapter 9

# Heat transfer analysis on MHD peristaltic motion in a Jeffrey fluid with compliant walls and porous space

This chapter reports the magnetohydrodynamic (MHD) peristaltic flow of Jeffrey fluid in a channel with compliant wall and heat transfer. The fluid fills the porous space. Mathematical modelling is based upon modified Darcy's law. The solutions of stream function, velocity and temperature distributions are derived. Finally, the solution expressions are displayed and analyzed.

### 9.1 Mathematical model

We consider a channel (of thickness  $2d$ ) filled with an incompressible and magnetohydrodynamic (MHD) Jeffrey fluid. A uniform magnetic field  $\mathbf{B} = (0, B_0, 0)$  is applied in the  $y$ -direction. The induced magnetic field is negligible for small magnetic Reynolds number. An incompressible fluid occupies a porous space. The temperatures of the lower and upper walls of the channel are maintained at  $T_0$  and  $T_1$  respectively. Assume an infinite wave train travelling with velocity



$c$  along the walls. The walls of the channel are

$$y = \pm\eta = \pm \left[ d + a \sin \left( \frac{2\pi}{\lambda} (x - ct) \right) \right],$$

where  $\lambda$  is the wavelength,  $c$  is the wave speed and  $a$  is the wave amplitude. The relevant equations can be written as

$$\frac{\partial u}{\partial x} + \frac{\partial v}{\partial y} = 0, \quad (9.1)$$

$$\rho \left( \frac{\partial}{\partial t} + u \frac{\partial}{\partial x} + v \frac{\partial}{\partial y} \right) u = -\frac{\partial p}{\partial x} + \frac{\partial S_{xx}}{\partial x} + \frac{\partial S_{xy}}{\partial y} - \sigma B_0^2 u + R_x, \quad (9.2)$$

$$\rho \left( \frac{\partial}{\partial t} + u \frac{\partial}{\partial x} + v \frac{\partial}{\partial y} \right) v = -\frac{\partial p}{\partial y} + \frac{\partial S_{yx}}{\partial x} + \frac{\partial S_{yy}}{\partial y} + R_y, \quad (9.3)$$

$$S_{xx} + \lambda_1 \frac{\partial}{\partial t} S_{xx} = 2\mu \left( 1 + \lambda_2 \frac{\partial}{\partial t} \right) \frac{\partial u}{\partial x}, \quad (9.4)$$

$$S_{xy} + \lambda_1 \frac{\partial}{\partial t} S_{xy} = \mu \left( 1 + \lambda_2 \frac{\partial}{\partial t} \right) \left( \frac{\partial u}{\partial y} + \frac{\partial v}{\partial x} \right), \quad (9.5)$$

$$S_{yy} + \lambda_1 \frac{\partial}{\partial t} S_{yy} = 2\mu \left( 1 + \lambda_2 \frac{\partial}{\partial t} \right) \frac{\partial v}{\partial y}, \quad (9.6)$$

$$\rho C_p \left( \frac{\partial}{\partial t} + u \frac{\partial}{\partial x} + v \frac{\partial}{\partial y} \right) T = \kappa \nabla^2 T + S_{xx} \frac{\partial u}{\partial x} + S_{xy} \left( \frac{\partial u}{\partial y} + \frac{\partial v}{\partial x} \right) + S_{yy} \frac{\partial v}{\partial y} \quad (9.7)$$

while the boundary conditions are prescribed as follows:

$$u = 0 \quad \text{at} \quad y = \pm\eta = \pm \left[ d + a \sin \left( \frac{2\pi}{\lambda} (x - ct) \right) \right], \quad (9.8)$$

$$\begin{aligned} \frac{\partial}{\partial x} L(\eta) &= \frac{\partial p}{\partial x} \\ &= \frac{\partial S_{xx}}{\partial x} + \frac{\partial S_{xy}}{\partial y} - \rho \left( \frac{\partial}{\partial t} + u \frac{\partial}{\partial x} + v \frac{\partial}{\partial y} \right) u - \sigma B_0^2 u + R_x \quad \text{at} \quad y = \pm\eta, \end{aligned} \quad (9.9)$$

$$T = T_0 \quad \text{on} \quad y = -\eta, \quad (9.10)$$

$$T = T_1 \quad \text{on} \quad y = \eta. \quad (9.11)$$

Here for the convenience of readers, we define  $u$  and  $v$  the velocity components in the  $x$  and  $y$  directions respectively and  $\rho$ ,  $t$ ,  $p$ ,  $\mu$ ,  $\sigma$ ,  $C_p$ ,  $\kappa$  and  $T$  are the fluid density, the time, the pressure, the dynamic viscosity, the electrical conductivity, the specific heat, the thermal conductivity and the temperature respectively. Furthermore,  $L = -\tau \frac{\partial^2}{\partial x^2} + m \frac{\partial^2}{\partial t^2} + C \frac{\partial}{\partial t} + B \frac{\partial^4}{\partial x^4} + k$ ,  $\tau$  is the

longitudinal tension per unit width,  $m$  is the mass per unit area,  $C$  is the coefficient of viscous damping,  $B$  is the flexural rigidity of the plate and  $k$  is the spring stiffness coefficient.

On the basis of Jeffrey fluid model the expression of Darcy's resistance is:

$$\left(1 + \lambda_1 \frac{\partial}{\partial t}\right) \mathbf{R} = -\frac{\mu\Phi}{K} \left(1 + \lambda_2 \frac{\partial}{\partial t}\right) \mathbf{V}, \quad (9.12)$$

where  $\Phi$  ( $0 < \Phi < 1$ ) and  $K$  ( $> 0$ ) are respectively the (constant) porosity and permeability of the porous medium.

Setting

$$u = \frac{\partial \Psi}{\partial y}, \quad v = -\frac{\partial \Psi}{\partial x},$$

$$\begin{aligned} x^* &= \frac{x}{\lambda}, \quad y^* = \frac{y}{d}, \quad \Psi^* = \frac{\Psi}{cd}, \quad t^* = \frac{ct}{\lambda}, \quad \eta^* = \frac{\eta}{d}, \quad p^* = \frac{d^2 p}{\mu c \lambda}, \\ \mathbf{S}^* &= \frac{d}{\mu c} \mathbf{S}, \quad K^* = \frac{K}{\Phi d^2}, \quad M^2 = \frac{\sigma B_0^2 d^2}{\mu}, \quad R = \frac{cd}{\nu}, \quad \epsilon = \frac{a}{d}, \\ \delta &= \frac{d}{\lambda}, \quad E_1 = -\frac{\tau d^3}{\lambda^3 \mu c}, \quad E_2 = \frac{mcd^3}{\lambda^3 \mu}, \quad E_3 = \frac{Cd^3}{\lambda^2 \mu}, \quad E_4 = \frac{Bd^3}{\lambda^5 \mu c}, \\ E_5 &= \frac{kd^3}{\lambda \mu c}, \quad \text{Pr} = \frac{\rho \nu C_p}{\kappa}, \quad E = \frac{c^2}{C_p (T_1 - T_0)}, \quad \theta = \frac{T - T_0}{T_1 - T_0}, \end{aligned}$$

equation (9.1) is automatically satisfied and Eqs. (9.2)-(9.12) become

$$R\delta \left(1 + \delta\lambda_1 \frac{\partial}{\partial t}\right) \left[ \frac{\partial}{\partial t} \left( \delta^2 \frac{\partial^2}{\partial x^2} + \frac{\partial^2}{\partial y^2} \right) \Psi + \Psi_y \left( \delta^2 \frac{\partial^2}{\partial x^2} + \frac{\partial^2}{\partial y^2} \right) \Psi_x - \Psi_x \left( \delta^2 \frac{\partial^2}{\partial x^2} + \frac{\partial^2}{\partial y^2} \right) \right] = \left(1 + \delta\lambda_1 \frac{\partial}{\partial t}\right) \left[ \left( \frac{\partial^2}{\partial y^2} - \delta^2 \frac{\partial^2}{\partial x^2} \right) S_{xy} + \delta \frac{\partial^2}{\partial x \partial y} (S_{xx} - S_{yy}) \right] - M^2 \left(1 + \delta\lambda_1 \frac{\partial}{\partial t}\right) \Psi_{yy} - \left(1 + \delta\lambda_2 \frac{\partial}{\partial t}\right) \left( \delta^2 \frac{\partial^2}{\partial x^2} + \frac{\partial^2}{\partial y^2} \right) \Psi, \quad (9.13)$$

$$\left(1 + \delta\lambda_1 \frac{\partial}{\partial t}\right) S_{xx} = 2\delta \left(1 + \delta\lambda_2 \frac{\partial}{\partial t}\right) \Psi_{xy}, \quad (9.14)$$

$$\left(1 + \delta\lambda_1 \frac{\partial}{\partial t}\right) S_{xy} = \left(1 + \delta\lambda_2 \frac{\partial}{\partial t}\right) (\Psi_{yy} - \delta^2 \Psi_{xx}), \quad (9.15)$$

$$\left(1 + \delta\lambda_1 \frac{\partial}{\partial t}\right) S_{yy} = -2\delta \left(1 + \delta\lambda_2 \frac{\partial}{\partial t}\right) \Psi_{xy}, \quad (9.16)$$

$$\text{Pr } R\delta \left( \frac{\partial \theta}{\partial t} + \Psi_y \frac{\partial \theta}{\partial x} - \Psi_x \frac{\partial \theta}{\partial y} \right) = \delta Br S_{xx} \Psi_{xy} + Br (\Psi_{yy} - \delta^2 \Psi_{xx}) S_{xy} - \delta Br S_{yy} \Psi_{xy} + \left( \frac{\partial^2 \theta}{\partial y^2} + \delta^2 \frac{\partial^2 \theta}{\partial x^2} \right), \quad (9.17)$$

$$\frac{\partial \Psi}{\partial y} = 0 \quad \text{at} \quad y = \pm \eta = \pm [1 + \epsilon \sin 2\pi(x - t)], \quad (9.18)$$

$$\theta = 0 \quad \text{at} \quad y = -\eta, \quad (9.19)$$

$$\theta = 1 \quad \text{at} \quad y = \eta. \quad (9.20)$$

$$\begin{aligned} \left(1 + \delta\lambda_1 \frac{\partial}{\partial t}\right) \frac{\partial p}{\partial x} &= \left(1 + \delta\lambda_1 \frac{\partial}{\partial t}\right) \left[ E_1 \frac{\partial^3}{\partial x^3} + E_2 \frac{\partial^3}{\partial x \partial t^2} + E_3 \frac{\partial^2}{\partial x \partial t} + E_4 \frac{\partial^5}{\partial x^5} + E_5 \frac{\partial}{\partial x} \right] \eta \\ &= \left(1 + \delta\lambda_1 \frac{\partial}{\partial t}\right) \left( \delta \frac{\partial}{\partial x} S_{xx} + \frac{\partial}{\partial y} S_{xy} \right) - M^2 \left(1 + \delta\lambda_1 \frac{\partial}{\partial t}\right) \Psi_y \\ &\quad - R\delta \left(1 + \delta\lambda_1 \frac{\partial}{\partial t}\right) \left[ \frac{\partial}{\partial t} + \Psi_y \frac{\partial}{\partial x} - \Psi_x \frac{\partial}{\partial y} \right] \Psi_y \\ &\quad - \frac{1}{K} \left(1 + \delta\lambda_2 \frac{\partial}{\partial t}\right) \Psi_y \quad \text{at} \quad y = \pm \eta, \end{aligned} \quad (9.21)$$

where  $N = \sqrt{M^2 + 1/K}$ ,  $M$  is the Hartman number,  $K$  is the porosity parameter,  $\text{Pr}$  is the Prandtl number and  $E$  is the Eckert number.

## 9.2 Solution of the problem

In order to carry out the analysis of perturbation solution, we expand

$$\Psi = \Psi_0 + \delta\Psi_1 + \dots, \quad (9.22)$$

$$\theta = \theta_0 + \delta\theta_1 + \dots, \quad (9.23)$$

$$S_{xx} = S_{xx0} + \delta S_{xx1} + \dots, \quad (9.24)$$

$$S_{xy} = S_{xy0} + \delta S_{xy1} + \dots, \quad (9.25)$$

$$S_{yy} = S_{yy0} + \delta S_{yy1} + \dots, \quad (9.26)$$

$$Z = Z_0 + \delta Z_1 + \dots, \quad (9.27)$$

Employing Eqs. (9.22)-(9.27) into (9.13)-(9.21), and then computing the solutions upto first order, we have

$$\begin{aligned} \Psi = & \delta (B_1 y + B_3 \sinh Ny + L_1 y \cosh Ny + L_2 y^2 \sinh Ny) \\ & + L \left( \frac{\sinh Ny}{N \cosh N\eta} - y \right), \end{aligned} \quad (9.28)$$

$$\begin{aligned} \theta = & \frac{1}{8\eta \cosh^2 N\eta} [\eta Br L^2 (2N^2 y^2 - \cosh 2Ny) + \eta Br L^2 (\cosh 2N\eta - 2N^2 \eta^2) \\ & + 4(y + \eta) \cosh^2 N\eta] + \delta \left[ \frac{L_{19}}{N^2} y^2 \cosh Ny - L_{31} y \sinh Ny + \frac{L_{20}}{4N^2} y^2 \cosh 2Ny \right. \\ & + L_{32} y \sinh 2Ny + \frac{L_{24}}{N^2} y \cosh Ny + \frac{L_{21}}{9N^2} \cosh 3Ny + L_{33} \cosh 2Ny + L_{34} \cosh Ny \\ & \left. + L_{35} \sinh Ny + \frac{L_{28}}{12} y^4 + \frac{L_{29}}{6} y^3 + \frac{L_{30}}{2} y^2 + B_4 y + B_5 \right], \end{aligned} \quad (9.29)$$

$$L = \frac{8\epsilon\pi^3}{N^2} \left[ \frac{E_3 \sin 2\pi(x-t)}{2\pi} - (E_1 + E_2) \cos 2\pi(x-t) + \left( 4\pi^2 E_4 + \frac{E_5}{4\pi^2} \right) \cos 2\pi(x-t) \right],$$

where  $Br = Pr E$  is the Brinkman number and the longitudinal velocity is

$$\begin{aligned} u = & \frac{\partial \Psi}{\partial y} \\ = & L \left( \frac{\cosh Ny}{\cosh N\eta} - 1 \right) + \delta (B_1 + B_3 N \cosh Ny + L_1 \cosh Ny + L_1 y N \sinh Ny \\ & + 2L_2 y \sinh Ny + L_2 y^2 N \cosh Ny). \end{aligned} \quad (9.30)$$

The heat transfer coefficient at the upper wall is

$$\begin{aligned}
Z &= \eta_x \theta_y \\
&= \frac{\eta_x}{8\eta \cosh^2 N\eta} \left[ \eta Br L^2 (4N^2\eta - 2N \sinh 2N\eta) + 4 \cosh^2 N\eta \right] + \delta\eta_x \left[ \frac{L_{19}}{N} \eta^2 \sinh N\eta \right. \\
&\quad + \frac{2L_{19}}{N^2} \eta \cosh N\eta - L_{31} \sinh N\eta - L_{31} N\eta \cosh N\eta + \frac{L_{20}}{2N^2} \eta \cosh 2N\eta \\
&\quad + \frac{L_{20}}{2N} \eta^2 \sinh 2N\eta + L_{32} \sinh 2N\eta + 2N\eta L_{32} \cosh 2N\eta + \frac{L_{24}}{N^2} \cosh N\eta \\
&\quad + \frac{L_{24}}{N} \eta \sinh N\eta + \frac{L_{21}}{3N} \sinh 3N\eta + 2N L_{33} \sinh 2N\eta + L_{34} N \sinh N\eta \\
&\quad \left. + N L_{35} \cosh N\eta + \frac{L_{28}}{3} \eta^3 + \frac{L_{29}}{2} \eta^2 + L_{30} \eta + B_4 \right], \tag{9.31}
\end{aligned}$$

$$B_1 = \frac{1}{N^2} \left[ \lambda_1 L_x N^2 - 2L_x \left( \lambda_1 M^2 + \frac{\lambda_2}{K} \right) - R L_x - L L_x \left( \frac{1 + \cosh^2 N\eta}{\cosh^2 N\eta} \right) \right],$$

$$B_3 = - \frac{[B_1 + (L_1 + L_2 N\eta^2) \cosh N\eta + (L_1 N + 2L_2) \eta \sinh N\eta]}{N \cosh N\eta},$$

$$B_4 = - \left( \frac{L_{35} \sinh N\eta}{\eta} + \frac{L_{29} \eta^2}{6} \right),$$

$$\begin{aligned}
B_5 &= - \left[ \frac{L_{19}}{N^2} \eta^2 \cosh N\eta - L_{31} \eta \sinh N\eta + \frac{L_{20}}{4N^2} \eta^2 \cosh 2N\eta + L_{32} \eta \sinh 2N\eta \right. \\
&\quad \left. + \frac{L_{24}}{N^2} \eta \cosh N\eta + \frac{L_{21}}{9N^2} \cosh 3N\eta + L_{33} \cosh 2N\eta + L_{34} \cosh N\eta + \frac{L_{28}}{12} \eta^4 + \frac{L_{30}}{2} \eta^2 \right],
\end{aligned}$$

$$L_1 = \frac{2L_x [(\lambda_2 - \lambda_1) M^2 - (3L + 1) R] - R L L_x N}{4N^2 \cosh N\eta}, \quad L_2 = \frac{R L L_x}{4 \cosh N\eta}, \quad L_3 = \frac{2L L_x \eta Br + \eta_x Br L^2}{8\eta \cosh^2 N\eta},$$

$$L_4 = \frac{(\eta_x Br L^2 + 2L L_x \eta Br) (\cosh 2N\eta - 2N^2 \eta^2) + \eta Br L^2 (2N\eta_x \sinh 2N\eta - 4N^2 \eta \eta_x)}{8\eta \cosh^2 N\eta}, \quad L_5 = \frac{\eta_x}{2\eta},$$

$$L_6 = \frac{N\eta_x \sinh 2N\eta}{2\eta \cosh^2 N\eta}, \quad L_7 = \frac{\eta_x (\cosh N\eta + 2\eta N \sinh N\eta)}{8\eta^2 \cosh^3 N\eta}, \quad L_8 = \eta Br L^2,$$

$$\begin{aligned}
L_9 &= \eta Br L^2 (\cosh 2N\eta - 2N^2\eta^2), & L_{10} &= 4 \cosh^2 N\eta, & L_{11} &= L_3 - L_7 L_8, \\
L_{12} &= L_4 + L_5 - L_7 L_8, & L_{13} &= L_6 - L_7 L_{10}, & L_{14} &= \frac{N^2 L^2 Br}{2 \cosh^2 N\eta}, \\
L_{15} &= -\frac{NL^2 Br}{4 \cosh^2 N\eta}, & L_{16} &= \frac{1}{2\eta}, & L_{17} &= B_3 N^2 + 2NL_1 + 2L_2, \\
L_{18} &= L_1 N^2 + 4L_2 N, & L_{19} &= \frac{2 \text{Pr} RL N^2 L_{11}}{\cosh N\eta}, \\
L_{20} &= -\frac{Br LL_2 N^3}{\cosh N\eta}, & L_{21} &= -\frac{\text{Pr} R (NLL_{11} + L_x L_{15})}{2N \cosh N\eta}, \\
L_{22} &= \frac{\text{Pr} R (L_x L_{15} - NLL_{11} + 2(L_{12} + L_{13}\eta))}{2N \cosh N\eta},
\end{aligned}$$

$$\begin{aligned}
L_{23} &= \left( \text{Pr} R (L + 1) L_{13} - \frac{LL_{17} N Br}{\cosh N\eta} + \frac{LL_x (\lambda_2 - \lambda_1) N^2 Br}{2 \cosh^2 N\eta} \right), \\
L_{24} &= \frac{\text{Pr} RLL_{13}}{\cosh N\eta}, & L_{25} &= \frac{\text{Pr} RL_x L_{15} \cosh N\eta - LL_{21} N Br}{\cosh N\eta}, \\
L_{26} &= -\frac{\text{Pr} RL_x L_{17}}{N \cosh N\eta}, & L_{27} &= -\frac{\text{Pr} RL_x L_{16}}{N \cosh N\eta}, \\
L_{28} &= \frac{\text{Pr} R \cosh N\eta [L_x L_{14} - 2N^2 (L + 1) L_{11}] + LL_2 N^3 Br}{\cosh N\eta}, \\
L_{29} &= \text{Pr} R [L_x L_{16} - (L + 1) L_{13}], \\
L_{30} &= \left[ Br \left( \frac{LL_{17} N}{\cosh N\eta} - \frac{LL_x (\lambda_2 - \lambda_1) N^2}{2 \cosh^2 N\eta} \right) - \text{Pr} R (L + 1) (L_{12} + L_{13}\eta) \right]
\end{aligned}$$

$$\begin{aligned}
L_{31} &= \frac{4L_{22} + L_{29} N}{N^3}, & L_{32} &= \frac{2L_{25} N - 4L_{20}}{8N^3}, & L_{33} &= \frac{3L_{20} - 2NL_{25} + 2N^2 L_{23}}{8N^4}, \\
L_{34} &= \frac{6L_{19} + N^2 L_{22} - 2NL_{26}}{N^4}, & L_{35} &= \frac{L_{27} N - 2L_{24}}{N^3}.
\end{aligned}$$

### 9.3 Graphical results and discussion

The behaviors of the longitudinal velocity, stream function, temperature and heat transfer coefficient are addressed in this section. In order to achieve this objective, the Figures 9.1(a-g)-9.10(a-d) are displayed. Figures 9.1(a-g) are plotted to examine the effect of various parameters on the longitudinal velocity  $u$ . It is observed from Figure 9.1a that the longitudinal velocity  $u$  decreases when the Hartman number  $M$  increases while it increases when the porosity

parameter  $K$  is increased (Figure 9.1b). Figures 9.1c and 9.1d show the effect of Weissenberg numbers  $\lambda_1$  and  $\lambda_2$  respectively. These Figures depict that there is an increase in the velocity when  $\lambda_1$  and  $\lambda_2$  are increased. Figure 9.1e shows the effect of the wave number  $\delta$  on the longitudinal velocity. We observed that the velocity increases with increasing wave number. A similar effect is seen for the occlusion parameter  $\epsilon$  on  $u$  (Figure 9.1f). The effect of the elastic parameters  $E_1, E_2, E_3, E_4$  and  $E_5$  are evident in Figure 9.1g. It may be of interest to note from this Figure that by increasing the elastic parameters ( $E_1, E_2, E_3$  and  $E_5$ ), the velocity decreases while it increases when  $E_4$  is increased. It is also interesting to note that the velocity profile is parabolic for fixed values of the parameters and its magnitude is maximum near the centre of the channel. Moreover, it is noticed that the elastic tension  $E_1$  and the flexural rigidity  $E_4$  has a significant effect on the axial velocity when compared with the mass characterizing parameter  $E_2$  and the damping nature of the wall  $E_3$ . Figure 9.2 is plotted to see the effect of different fluids on the velocity. From this Figure we observed that the velocity for the Jeffrey fluid is greater than the Maxwell and Newtonian fluids. In Figures 9.3 ( $a - g$ ), the nature of the temperature profile is also parabolic. Here the temperature decreases by increasing the Hartman number  $M$  (Figure 9.3a) and the Weissenberg number  $\lambda_2$  (Figure 9.3d). Note that the temperature decreases in the downstream. However, Figures 9.3b and 9.3c illustrate that the temperature increases by increasing the permeability parameter  $K$  and the Weissenberg number  $\lambda_1$ . The variations of the Brinkman number  $Br$  and the wave number  $\delta$  on the temperature are sketched in the Figures 9.3e and 9.3f. It is noted from these Figures that the temperature is an increasing function of  $Br$  and  $\delta$ . Figure 9.3g shows the effect of the elastic parameters  $E_1, E_2, E_3, E_4$  and  $E_5$  on the temperature. This Figure reveals that the amplitude of temperature increases with an increase in  $E_1, E_2, E_3, E_4$  and  $E_5$ . It is further observed that the effect of  $E_1$  and  $E_4$  on temperature are quite significant. In Figure 9.4 the effect of temperature profile is seen for different fluids. It is quite obvious from this Figure that the Maxwell fluid possesses very large temperature when compared with the other fluids. The results presented in Figures 9.5 ( $a - h$ ) indicate the variations of  $M, K, \lambda_1, \lambda_2, Br, \delta, \epsilon, E_1, E_2, E_3, E_4$  and  $E_5$  on the heat transfer coefficient  $Z$ . This Figure shows the typical oscillatory behavior of heat transfer which may be due to the peristaltic phenomena. Figures 9.5b, 9.5e, 9.5f, 9.5g, 9.5h depict that the absolute value of the heat transfer coefficient increases by increasing  $K, Br, \delta, \epsilon, E_1, E_2,$

$E_3$ ,  $E_4$  and  $E_5$  respectively, while the behavior is quite opposite in the case of  $M$  (Figure 9.5a). Figure 9.5c displays the effect of the Weissenberg number  $\lambda_1$  on the heat transfer coefficient  $Z$ . It is observed that when  $x$  ranges from 0 to 0.5,  $\lambda_1$  decreases while it increases when  $x \in [0.5, 1]$ . The effect of the Weissenberg number  $\lambda_2$  on  $Z$  is quite opposite to the effect of  $\lambda_1$  on  $Z$  (Figure 9.5d). In Figure 9.6 we have plotted the heat transfer coefficient for different fluids. It is obvious from this Figure that when  $x$  ranges from 0 to 0.5, the heat transfer coefficient for Jeffrey fluid is larger than the Maxwell and viscous fluids and the effect is opposite when  $x \in [0.5, 1]$ .

The formation of an internally circulating bolus of fluid by closed streamlines is sketched in the Figures 9.7 (a – c)-9.10 (a – d). Figures 9.7 (a – c) display the effect of Hartman number  $M$  on the streamlines for fixed values of the other parameters. This Figure shows that the size of trapping bolus decreases with an increase in the Hartman number  $M$  while the behavior is quite opposite in the case of the permeability parameter  $K$  (Figures 9.8 (a – c)). Figures 9.9 (a – c) witness that the behavior of wave number  $\delta$  on the streamlines. Here we observed that the number of the streamlines increases by increasing  $\delta$ . The effect of the elastic parameters on the streamlines is plotted in Figures 9.10 (a – d). The trapped bolus increases with an increase in  $E_1$ ,  $E_2$ ,  $E_3$ ,  $E_4$  and  $E_5$ . It is worth mentioning to point out that the damping is not much effective in the trapping.

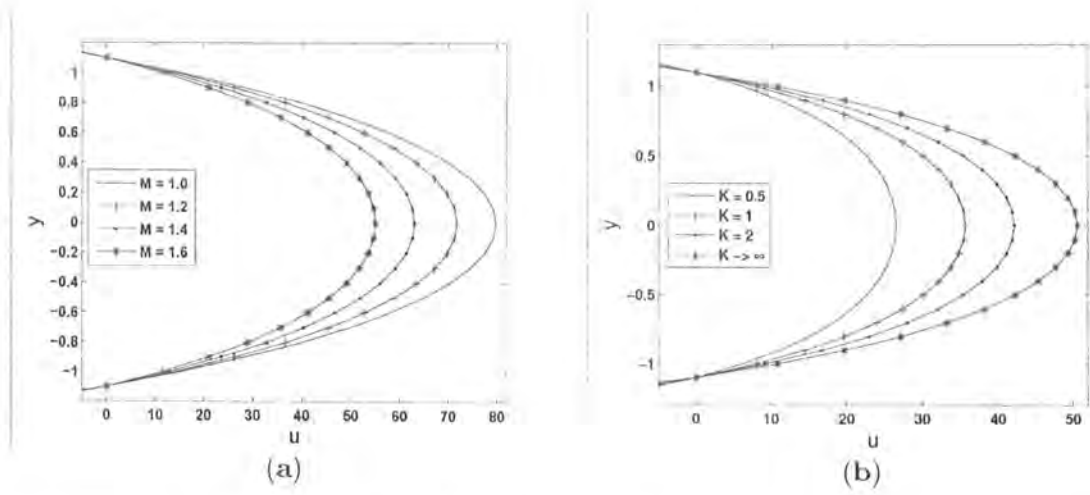


Figure 9.1a: Variations of the longitudinal velocity  $u$  for different values of Hartman number



$M$  when  $E_1 = 1$ ,  $E_2 = 0.4$ ,  $E_3 = 0.5$ ,  $E_4 = 0.3$ ,  $E_5 = 0.2$ ,  $\epsilon = 0.1$ ,  $R = 1$ ,  $\delta = 0.1$ ,  $K = 2$ ,  $\lambda_1 = 1.5$ ,  $\lambda_2 = 0.8$ ,  $x = 0.3$  and  $t = 0.05$ .

Figure 9.1b: Variations of the longitudinal velocity  $u$  for different values of porosity parameter  $K$  when  $E_1 = 1$ ,  $E_2 = 0.4$ ,  $E_3 = 0.5$ ,  $E_4 = 0.3$ ,  $E_5 = 0.2$ ,  $\epsilon = 0.1$ ,  $R = 1$ ,  $\delta = 0.1$ ,  $M = 2$ ,  $\lambda_1 = 1.5$ ,  $\lambda_2 = 0.8$ ,  $x = 0.3$  and  $t = 0.05$ .

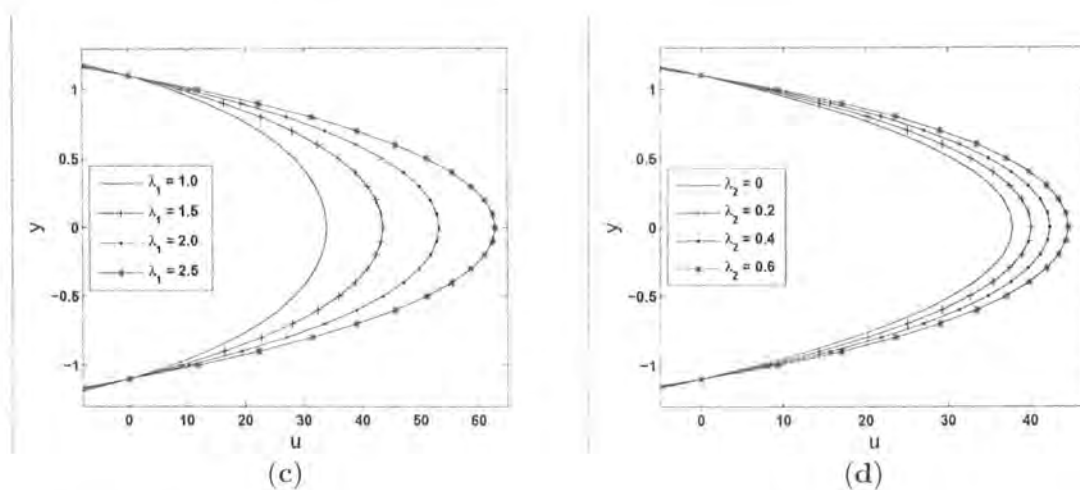


Figure 9.1c: Variations of the longitudinal velocity  $u$  for different values of Weissenberg number  $\lambda_1$  when  $E_1 = 1$ ,  $E_2 = 0.4$ ,  $E_3 = 0.5$ ,  $E_4 = 0.3$ ,  $E_5 = 0.2$ ,  $\epsilon = 0.1$ ,  $R = 1$ ,  $\delta = 0.1$ ,  $M = 2$ ,  $K = 5$ ,  $\lambda_2 = 0.5$ ,  $x = 0.3$  and  $t = 0.05$ .

Figure 9.1d: Variations of the longitudinal velocity  $u$  for different values of Weissenberg number  $\lambda_2$  when  $E_1 = 1$ ,  $E_2 = 0.4$ ,  $E_3 = 0.5$ ,  $E_4 = 0.3$ ,  $E_5 = 0.2$ ,  $\epsilon = 0.1$ ,  $R = 1$ ,  $\delta = 0.1$ ,

$M = 2, K = 5, \lambda_1 = 1.5, x = 0.3$  and  $t = 0.05$ .

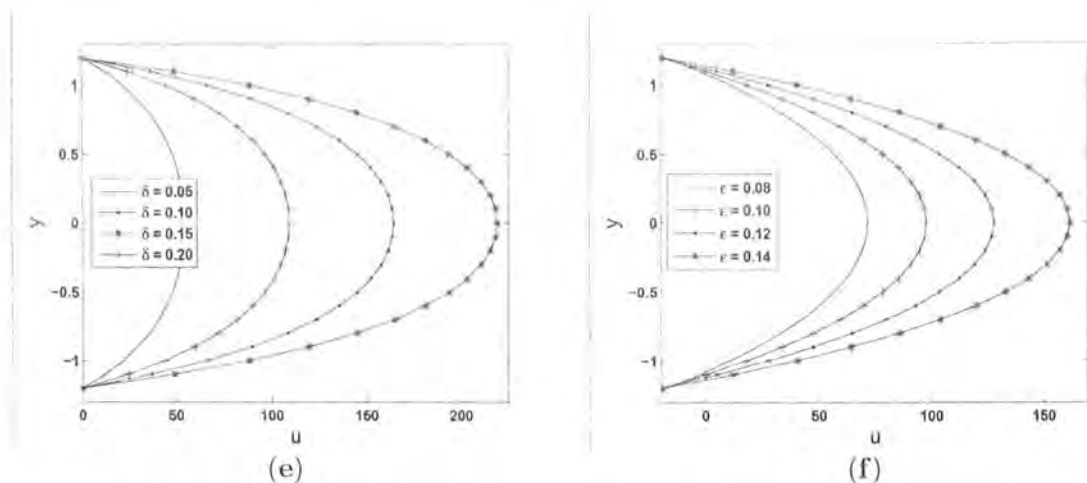


Figure 9.1e: Variations of the longitudinal velocity  $u$  for different values of wave number  $\delta$  when  $E_1 = 1, E_2 = 0.4, E_3 = 0.5, E_4 = 0.3, E_5 = 0.2, \epsilon = 0.2, R = 1, M = 2, K = 5, \lambda_1 = 1.5, \lambda_2 = 0.8, x = 0.3$  and  $t = 0.05$ .

Figure 9.1f: Variations of the longitudinal velocity  $u$  for different values of occlusion parameter  $\epsilon$  when  $E_1 = 1, E_2 = 0.4, E_3 = 0.5, E_4 = 0.3, E_5 = 0.2, \delta = 0.1, R = 1, M = 1, K = 5, \lambda_1 = 1.5, \lambda_2 = 0.8, x = 0.3$  and  $t = 0.05$ .

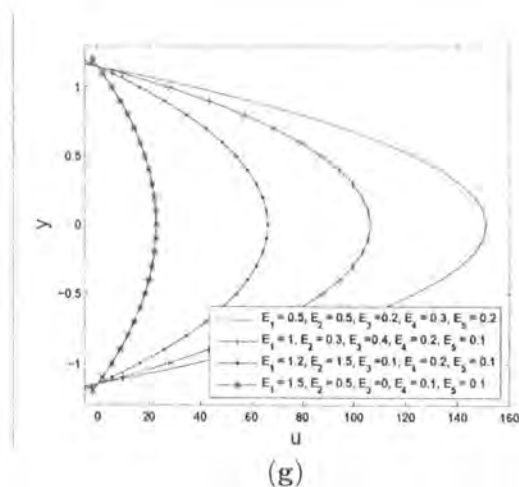


Figure 9.1g: Variations of the longitudinal velocity  $u$  for different values of elastic parameters when  $\epsilon = 0.15, R = 1, \delta = 0.1, M = 1, K = 5, \lambda_1 = 1.5, \lambda_2 = 0.8, x = 0.3$  and  $t = 0.05$ .

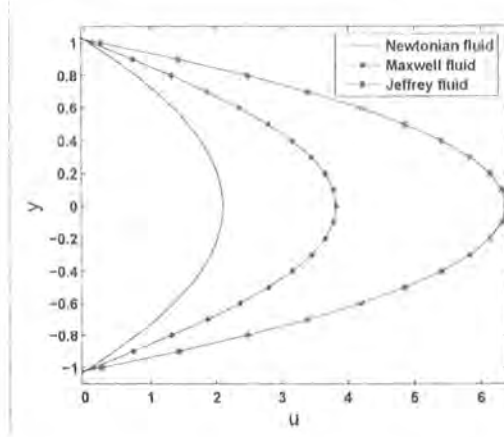


Figure 9.2: Variations of the longitudinal velocity  $u$  for different fluids when  $E_1 = 1$ ,  $E_2 = 0.3$ ,  $E_3 = 0.5$ ,  $E_4 = 0.4$ ,  $E_5 = 0.2$ ,  $\epsilon = 0.02$ ,  $R = 1$ ,  $\delta = 0.05$ ,  $M = 1.2$ ,  $K = 5$ ,  $x = 0.3$  and  $t = 0.05$

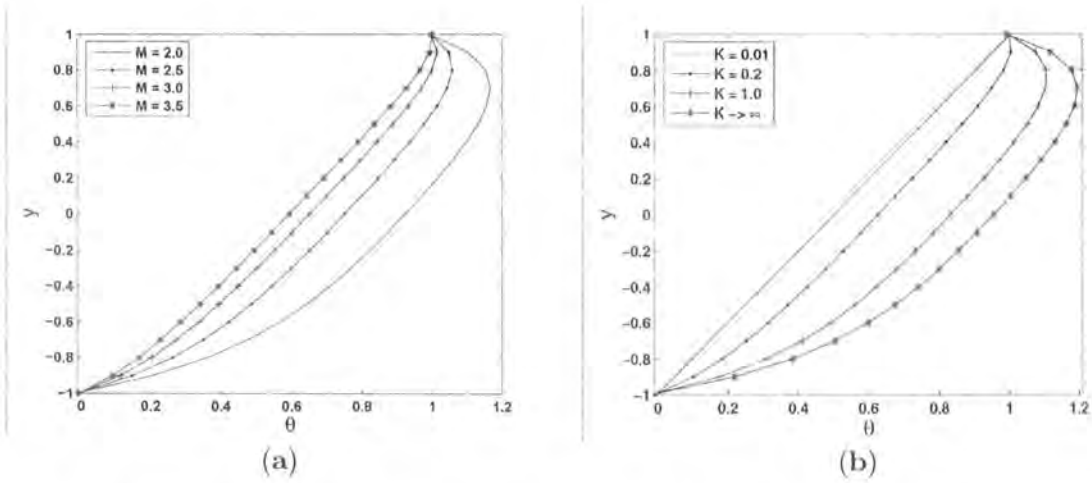


Figure 9.3a: Variations of temperature distribution  $\theta$  for different values of Hartman number  $M$  when  $E_1 = 1$ ,  $E_2 = 0.2$ ,  $E_3 = 0.1$ ,  $E_4 = 0.1$ ,  $E_5 = 0.2$ ,  $\epsilon = 0.01$ ,  $R = 1$ ,  $\delta = 0.07$ ,  $K = 0.5$ ,  $\lambda_1 = 1.5$ ,  $\lambda_2 = 0.5$ ,  $Br = 1$ ,  $Pr = 1$ ,  $x = 0.3$  and  $t = 0.4$ .

Figure 9.3b: Variations of temperature distribution  $\theta$  for different values of porosity parameter  $K$  when  $E_1 = 1$ ,  $E_2 = 0.2$ ,  $E_3 = 0.1$ ,  $E_4 = 0.1$ ,  $E_5 = 0.2$ ,  $\epsilon = 0.01$ ,  $R = 1$ ,  $\delta = 0.07$ ,  $M = 2.5$ ,  $\lambda_1 = 1.5$ ,  $\lambda_2 = 0.5$ ,  $Br = 1$ ,  $Pr = 1$ ,  $x = 0.3$  and  $t = 0.4$ .

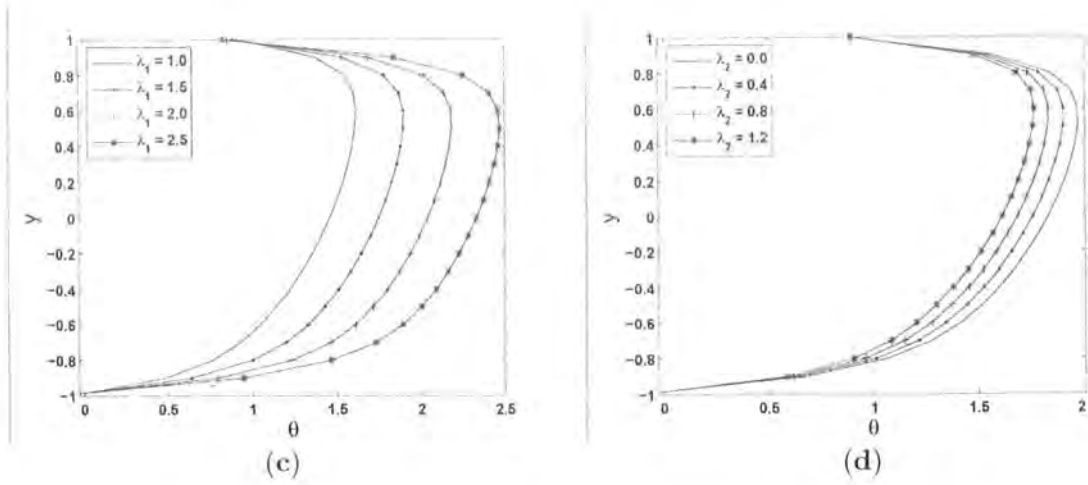


Figure 9.3c: Variations of temperature distribution  $\theta$  for different values of Weissenberg number  $\lambda_1$  when  $E_1 = 1$ ,  $E_2 = 0.2$ ,  $E_3 = 0.1$ ,  $E_4 = 0.1$ ,  $E_5 = 0.2$ ,  $\epsilon = 0.02$ ,  $R = 1$ ,  $\delta = 0.3$ ,  $M = 5$ ,  $K = 5$ ,  $\lambda_2 = 0.4$ ,  $Br = 3$ ,  $Pr = 1$ ,  $x = 0.3$  and  $t = 0.4$ .

Figure 9.3d: Variations of temperature distribution  $\theta$  for different values of Weissenberg number  $\lambda_2$  when  $E_1 = 1$ ,  $E_2 = 0.2$ ,  $E_3 = 0.1$ ,  $E_4 = 0.1$ ,  $E_5 = 0.2$ ,  $\epsilon = 0.02$ ,  $R = 1$ ,  $\delta = 0.3$ ,  $M = 5$ ,  $K = 5$ ,  $\lambda_1 = 1.5$ ,  $Br = 3$ ,  $Pr = 1$ ,  $x = 0.3$  and  $t = 0.4$ .

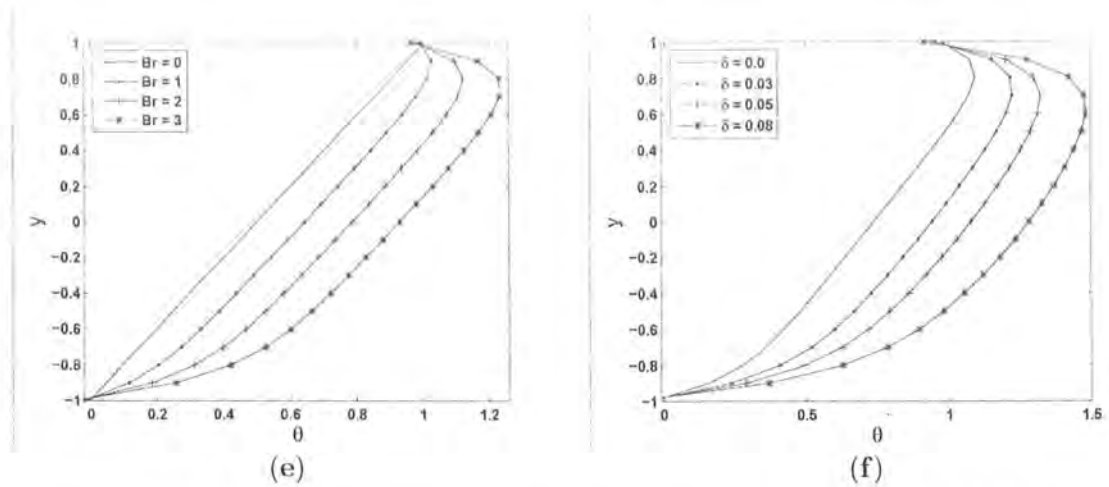


Figure 9.3e: Variations of temperature distribution  $\theta$  for different values of Brinkman num-

ber  $Br$  when  $E_1 = 1, E_2 = 0.2, E_3 = 0.1, E_4 = 0.1, E_5 = 0.2, \epsilon = 0.02, R = 1, \delta = 0.01, M = 4, K = 5, \lambda_1 = 1.5, \lambda_2 = 0.5, Pr = 1, x = 0.3$  and  $t = 0.4$ .

Figure 9.3f: Variations of temperature distribution  $\theta$  for different values of wave number  $\delta$  when  $E_1 = 1, E_2 = 0.3, E_3 = 0.1, E_4 = 0.1, E_5 = 0.2, \epsilon = 0.03, R = 1, M = 4, K = 5, \lambda_1 = 1.5, \lambda_2 = 0.5, Br = 1, Pr = 1, x = 0.3$  and  $t = 0.4$ .

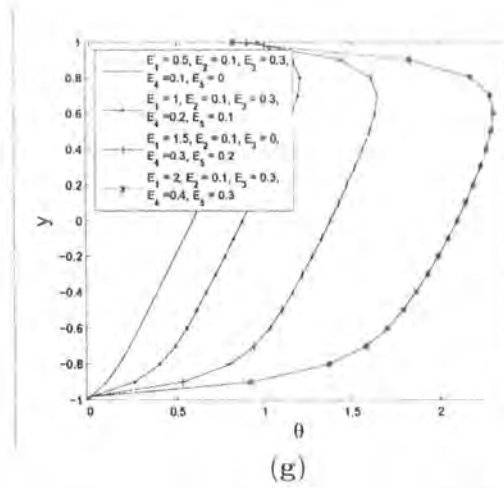


Figure 9.3g: Variations of temperature distribution  $\theta$  for different values of elastic parameters when  $\epsilon = 0.02, R = 1, \delta = 0.01, M = 5, K = 5, \lambda_1 = 1.5, \lambda_2 = 0.5, Br = 1, Pr = 1, x = 0.3$  and  $t = 0.4$ .

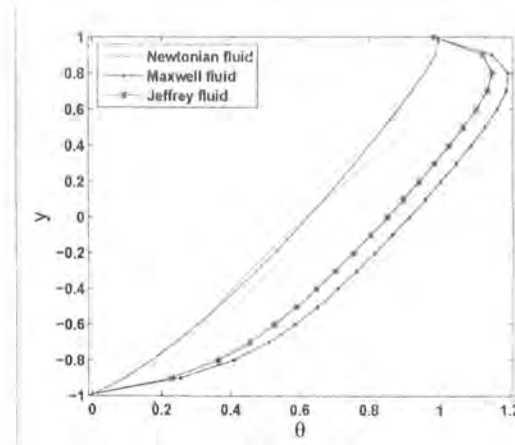


Figure 9.4: Variations of temperature distribution  $\theta$  for different fluids when  $E_1 = 1, E_2 = 0.2, E_3 = 0.1, E_4 = 0.1, E_5 = 0.2, \epsilon = 0.01, R = 1, \delta = 0.4, M = 5, K = 5, Br = 3, Pr = 1,$

$x = 0.3$  and  $t = 0.4$

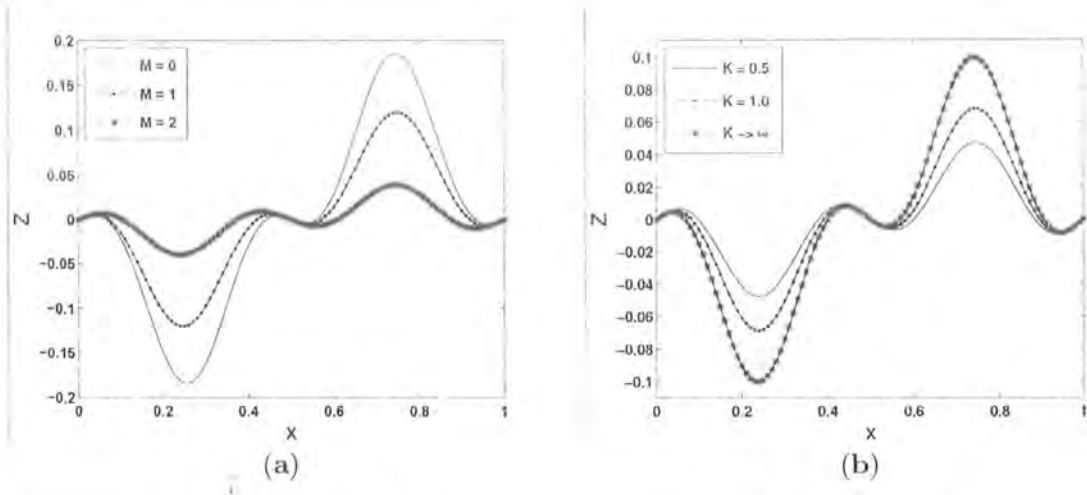


Figure 9.5a: Variations of heat transfer coefficient  $Z$  for different values of Hartman number  $M$  when  $E_1 = 1$ ,  $E_2 = 0.4$ ,  $E_3 = 0.3$ ,  $E_4 = 0.1$ ,  $E_5 = 0.2$ ,  $\epsilon = 0.01$ ,  $R = 1$ ,  $\delta = 0.01$ ,  $K = 0.4$ ,  $\lambda_1 = 1.5$ ,  $\lambda_2 = 0.5$ ,  $Br = 1$ ,  $Pr = 1$  and  $t = 0.25$ .

Figure 9.5b: Variations of heat transfer coefficient  $Z$  for different values of porosity parameter  $K$  when  $E_1 = 1$ ,  $E_2 = 0.4$ ,  $E_3 = 0.3$ ,  $E_4 = 0.1$ ,  $E_5 = 0.2$ ,  $\epsilon = 0.01$ ,  $R = 1$ ,  $\delta = 0.01$ ,  $M = 2$ ,  $\lambda_1 = 1.5$ ,  $\lambda_2 = 0.5$ ,  $Br = 1$ ,  $Pr = 1$  and  $t = 0.25$ .

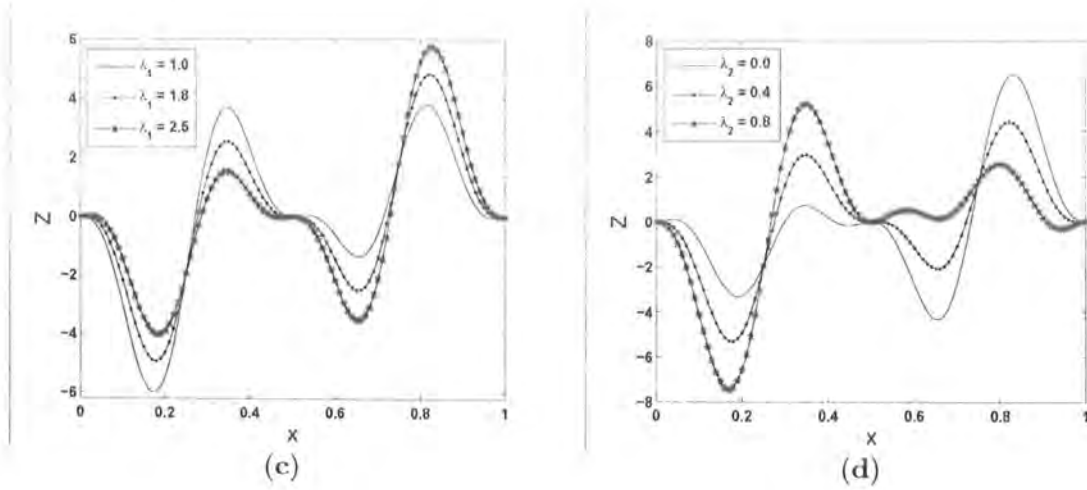


Figure 9.5c: Variations of heat transfer coefficient  $Z$  for different values of Weissenberg number  $\lambda_1$  when  $E_1 = 1$ ,  $E_2 = 0.5$ ,  $E_3 = 0.2$ ,  $E_4 = 0.5$ ,  $E_5 = 0.1$ ,  $\epsilon = 0.01$ ,  $R = 0.5$ ,  $\delta = 0.5$ ,  $M = 1$ ,  $K = 0.1$ ,  $\lambda_2 = 0.4$ ,  $Br = 1$ ,  $Pr = 1$  and  $t = 0.25$ .

Figure 9.5d: Variations of heat transfer coefficient  $Z$  for different values of Weissenberg number  $\lambda_2$  when  $E_1 = 1$ ,  $E_2 = 0.5$ ,  $E_3 = 0.2$ ,  $E_4 = 0.5$ ,  $E_5 = 0.1$ ,  $\epsilon = 0.01$ ,  $R = 0.5$ ,  $\delta = 0.5$ ,  $M = 1$ ,  $K = 0.1$ ,  $\lambda_1 = 1.5$ ,  $Br = 1$ ,  $Pr = 1$  and  $t = 0.25$ .

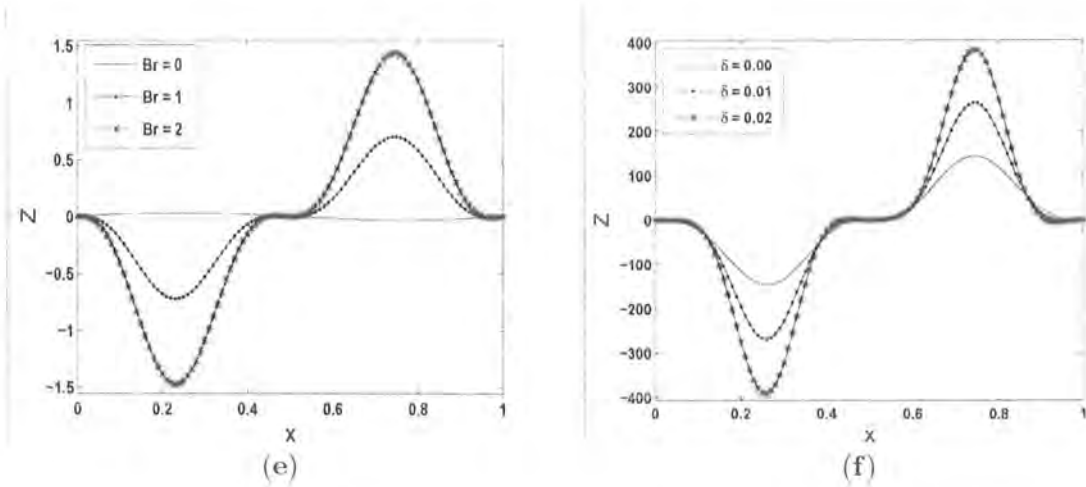


Figure 9.5e: Variations of heat transfer coefficient  $Z$  for different values of Brinkman number  $Br$  when  $E_1 = 1$ ,  $E_2 = 0.4$ ,  $E_3 = 0.3$ ,  $E_4 = 0.3$ ,  $E_5 = 0.2$ ,  $\epsilon = 0.01$ ,  $R = 1$ ,  $\delta = 0.01$ ,  $M = 3$ ,  $K = 5$ ,  $\lambda_1 = 1.5$ ,  $\lambda_2 = 0.5$ ,  $Pr = 1$  and  $t = 0.25$ .

Figure 9.5f: Variations of heat transfer coefficient  $Z$  for different values of wave number  $\delta$  when  $E_1 = 2$ ,  $E_2 = 0.8$ ,  $E_3 = 0.2$ ,  $E_4 = 0.1$ ,  $E_5 = 0.1$ ,  $\epsilon = 0.2$ ,  $R = 1$ ,  $M = 1$ ,  $K = 0.5$ ,  $\lambda_1 = 1.5$ ,  $\lambda_2 = 0.5$ ,  $Br = 0.5$ ,  $Pr = 1$  and  $t = 0.25$ .

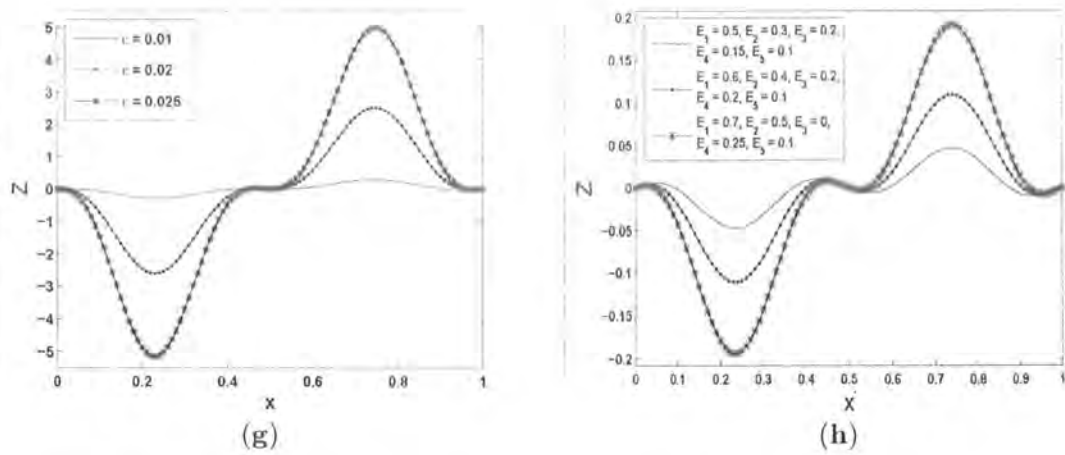


Figure 9.5g: Variations of heat transfer coefficient  $Z$  for different values of occlusion parameter  $\epsilon$  when  $E_1 = 1$ ,  $E_2 = 0.4$ ,  $E_3 = 0.3$ ,  $E_4 = 0.3$ ,  $E_5 = 0.2$ ,  $\delta = 0.01$ ,  $R = 1$ ,  $M = 4$ ,  $K = 5$ ,  $\lambda_1 = 1.5$ ,  $\lambda_2 = 0.5$ ,  $Br = 1$ ,  $Pr = 1$  and  $t = 0.25$ .

Figure 9.5h: Variations of heat transfer coefficient  $Z$  for different values of elastic parameters when  $\epsilon = 0.01$ ,  $R = 1$ ,  $\delta = 0.01$ ,  $M = 4$ ,  $K = 5$ ,  $\lambda_1 = 1.5$ ,  $\lambda_2 = 0.5$ ,  $Br = 1$ ,  $Pr = 1$  and  $t = 0.25$ .

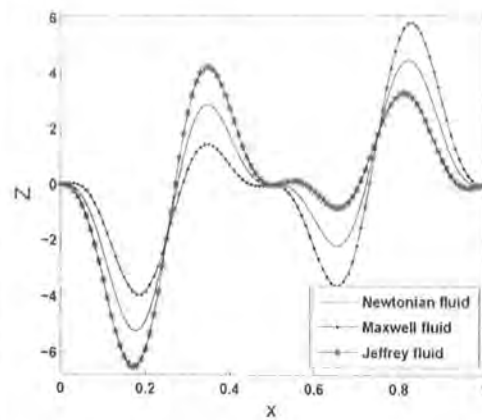
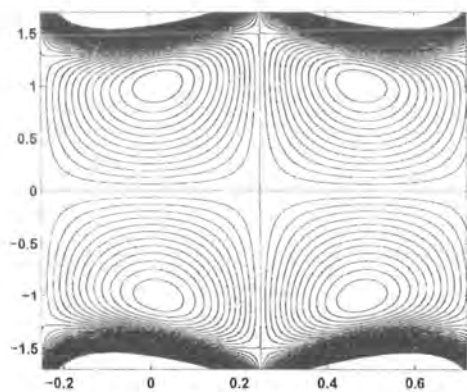
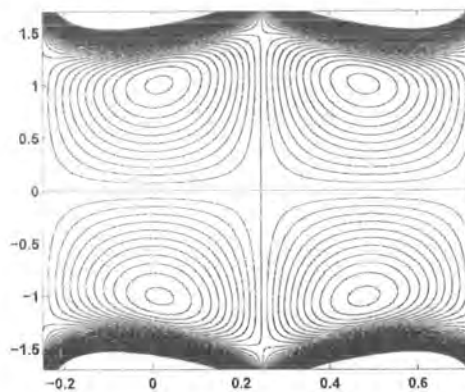


Figure 9.6: Variations of heat transfer coefficient  $Z$  for different fluids. The other parameters chosen are  $E_1 = 1$ ,  $E_2 = 0.5$ ,  $E_3 = 0.2$ ,  $E_4 = 0.5$ ,  $E_5 = 0.1$ ,  $\epsilon = 0.01$ ,  $R = 0.5$ ,  $\delta = 0.5$ ,  $M = 1$ ,  $K = 0.1$ ,  $Br = 1$ ,  $Pr = 1$  and  $t = 0.25$ .

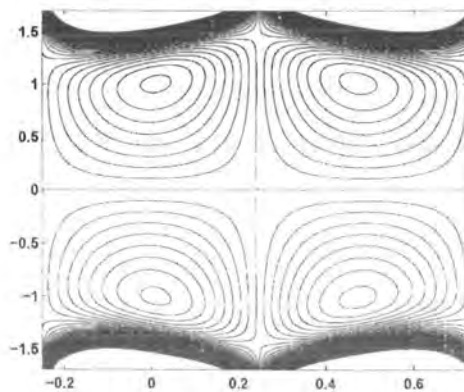




(a)



(b)

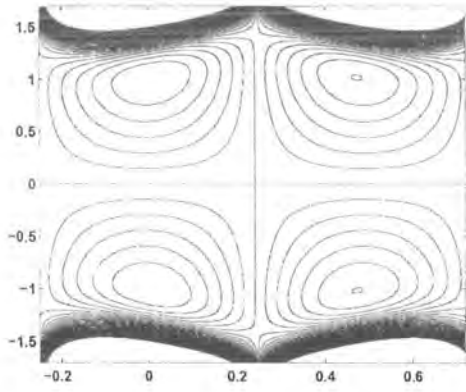


(c)

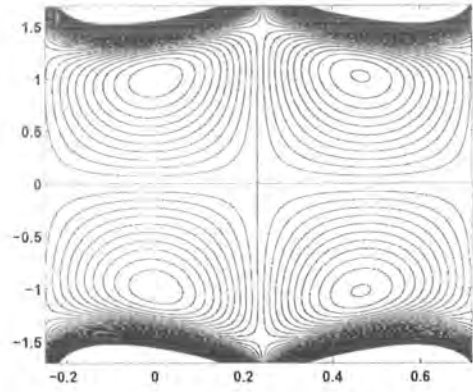
Figure 9.7: Streamlines for (a)  $M = 0$ , (b),  $M = 2$ , (c)  $M = 4$ .

The other chosen parameters are ( $\epsilon = 0.1$ ,  $R = 1$ ,  $\delta = 0.01$ ,  $E_1 = 0.7$ ,  $E_2 = 0.5$ ,

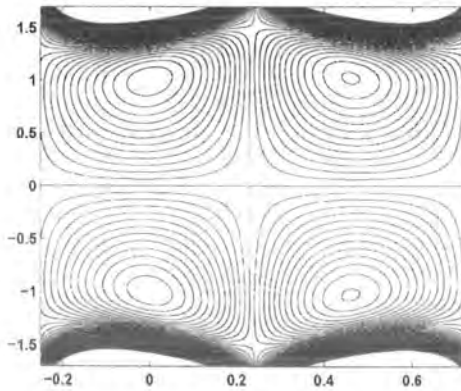
$E_3 = 0.2, E_4 = 0.01, E_5 = 0.1, K = 0.04, \lambda_1 = 1.5, \lambda_2 = 0.5$  and  $t = 0$ ).



(a)



(b)

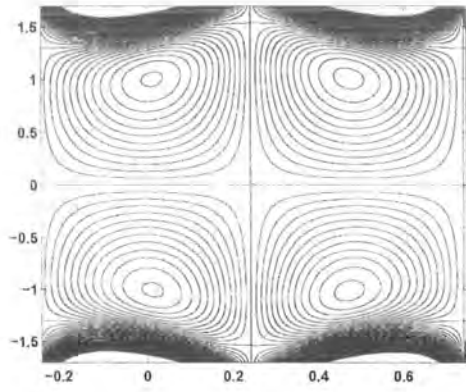


(c)

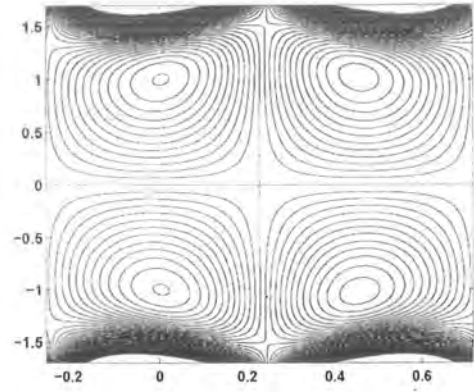
Figure 9.8: Streamlines for (a)  $K = 0.03$ , (b)  $K = 0.2$ , (c)  $K \rightarrow \infty$ .

The other chosen parameters are ( $\epsilon = 0.1, R = 1, \delta = 0.01, E_1 = 0.7, E_2 = 0.5$ ,

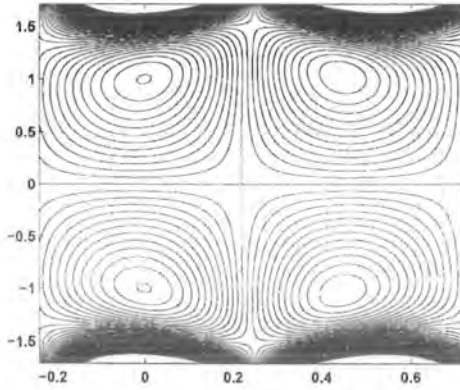
$E_3 = 0.2$ ,  $E_4 = 0.01$ ,  $E_5 = 0.1$ ,  $M = 5$ ,  $\lambda_1 = 1.5$ ,  $\lambda_2 = 0.5$  and  $t = 0$ ).



(a)



(b)



(c)

Figure 9.9: Streamlines for (a)  $\delta = 0$ , (b)  $\delta = 0.03$ , (c)  $\delta = 0.05$ .

The other chosen parameters are ( $\epsilon = 0.12$ ,  $R = 1$ ,  $E_1 = 0.5$ ,  $E_2 = 0.5$ ,

$E_3 = 0.2$ ,  $E_4 = 0.01$ ,  $E_5 = 0.1$ ,  $M = 3$ ,  $K = 0.1$ ,  $\lambda_1 = 1.5$ ,  $\lambda_2 = 0.5$  and  $t = 0$ ).

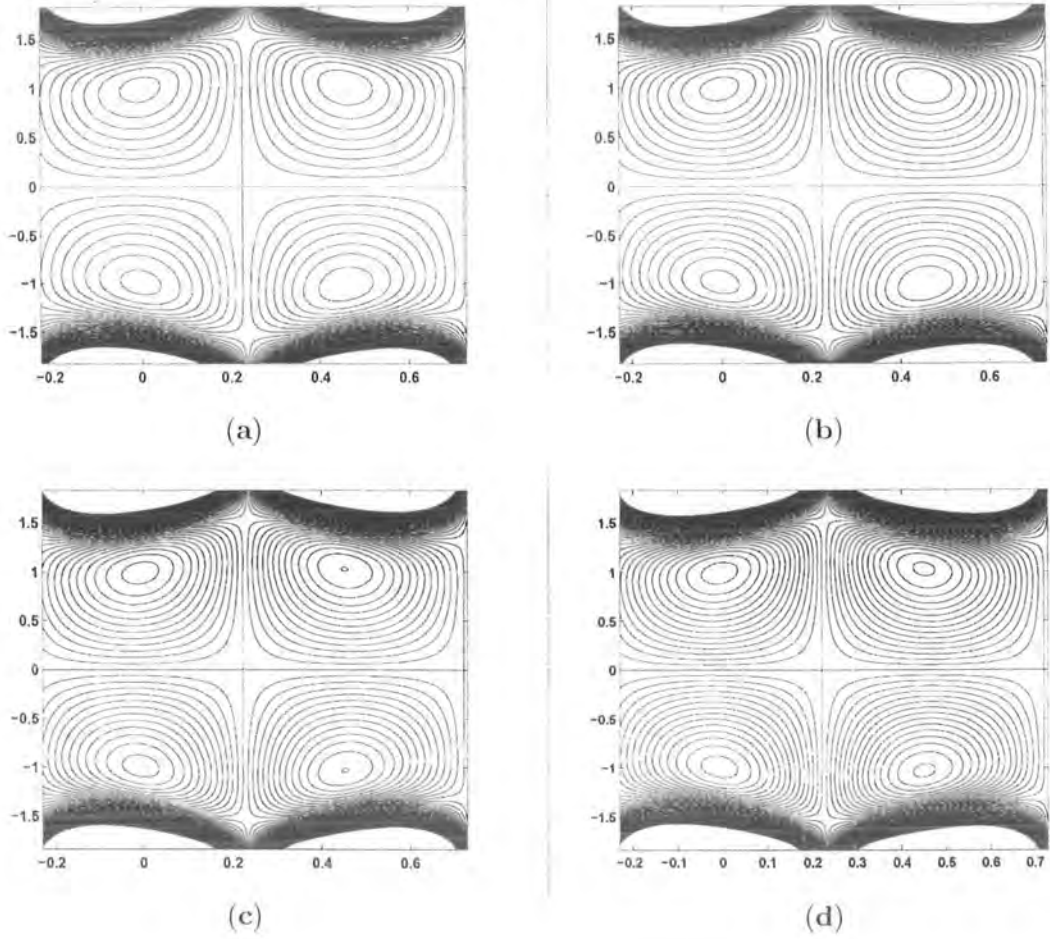


Figure 9.10: Streamlines for

(a)  $E_1 = 0.7$ ,  $E_2 = 0.5$ ,  $E_3 = 0.2$ ,  $E_4 = 0.02$ ,  $E_5 = 0.1$ .

(b)  $E_1 = 0.8$ ,  $E_2 = 0.5$ ,  $E_3 = 0.3$ ,  $E_4 = 0.02$ ,  $E_5 = 0.1$ .

(c)  $E_1 = 0.9$ ,  $E_2 = 0.5$ ,  $E_3 = 0.4$ ,  $E_4 = 0.02$ ,  $E_5 = 0.1$ .

(d)  $E_1 = 1.0$ ,  $E_2 = 0.5$ ,  $E_3 = 0.5$ ,  $E_4 = 0.02$ ,  $E_5 = 0.1$ .

The other chosen parameters are

( $\epsilon = 0.1$ ,  $R = 1$ ,  $\delta = 0.01$ ,  $K = 0.4$ ,  $M = 4$ ,  $\lambda_1 = 1.5$ ,  $\lambda_2 = 0.5$  and  $t = 1$ ).

## 9.4 Conclusions

Influence of heat transfer on the magnetohydrodynamic peristaltic flow of a Jeffrey fluid in a channel with compliant walls is illustrated. The porosity effect on the flow is also examined. The main points are summed up below:

- An increase in the Weissenberg number  $\lambda_1$  shows an increase in the temperature. Temperature decreases when the Weissenberg number  $\lambda_2$  is increased.
- The wall parameters increases the temperature.
- Brinkman number and wave number has similar role on the temperature.
- Hartman number and Brinkman number on the heat transfer coefficient at the upper wall have opposite effects.
- An increase in the absolute value of heat transfer coefficient in the upper part of the channel is observed when the elastic parameters increase.

## Chapter 10

# Wall compliance effect on the flow of compressible non-Newtonian fluid

This chapter discusses the peristaltic flow of Jeffrey fluid in a microchannel with compliant walls. The rheological effects and compressibility of the fluid are given proper attention. Perturbation approach has been employed when the ratio of the wave amplitude to the radius of the pore is small. Expressions of mean axial velocity distribution, mean velocity at the boundaries and critical values are derived. The variations of several pertinent variables are shown and studied.

### 10.1 Mathematical model

Consider a compressible Jeffrey fluid in a symmetric channel of width  $2d$ . The flow in a porous space is due to sinusoidal small amplitude travelling waves on the compliant walls of the channel. We introduce Cartesian coordinates system with the  $x$ -axis along the centre line of the channel and  $y$ -axis normal to it. Let  $v_x$  and  $v_y$  denote the components of velocity along  $x$ - and  $y$ -directions respectively. The compliant wall is modeled as spring-backed plate, it is constrained to move only in the vertical direction. If  $\eta$  and  $-\eta$  denote the vertical displacements corresponding to upper and lower walls, then  $\eta$  is assumed as follows

$$\eta = \left[ a \sin \left( \frac{2\pi}{\lambda} (x - ct) \right) \right],$$

where  $a$  is the wave amplitude,  $\lambda$  is the wavelength and  $c$  is the wave speed.

The equation of motion of the compliant wall is [89]:

$$L = \left[ m \frac{\partial^2}{\partial t^2} + d \frac{\partial}{\partial t} + B \frac{\partial^4}{\partial x^4} - T \frac{\partial^2}{\partial x^2} + K \right] \eta = p - p_0.$$

In above equation,  $m$  is the plate mass per unit area,  $d$  is the wall damping coefficient,  $B$  is the flexural rigidity of the plate,  $T$  is the longitudinal tension per unit width,  $K$  is the spring stiffness and  $p_0$  is the pressure on the outside surface of the wall.

The relevant governing equations for compressible flow are

$$\frac{\partial \rho}{\partial t} + v_x \frac{\partial \rho}{\partial x} + v_y \frac{\partial \rho}{\partial y} + \rho \left( \frac{\partial v_x}{\partial x} + \frac{\partial v_y}{\partial y} \right) = 0, \quad (10.1)$$

$$\begin{aligned} \left( 1 + \lambda_1 \frac{\partial}{\partial t} \right) \left[ \rho \left( \frac{\partial v_x}{\partial t} + v_x \frac{\partial v_x}{\partial x} + v_y \frac{\partial v_x}{\partial y} \right) \right] &= - \left( 1 + \lambda_1 \frac{\partial}{\partial t} \right) \frac{\partial p}{\partial x} \\ + \mu \left( 1 + \lambda_2 \frac{\partial}{\partial t} \right) \left[ \nabla^2 v_x + \frac{1}{3} \frac{\partial}{\partial x} (\nabla \cdot \mathbf{V}) \right], & \end{aligned} \quad (10.2)$$

$$\begin{aligned} \left( 1 + \lambda_1 \frac{\partial}{\partial t} \right) \left[ \rho \left( \frac{\partial v_y}{\partial t} + v_x \frac{\partial v_y}{\partial x} + v_y \frac{\partial v_y}{\partial y} \right) \right] &= - \left( 1 + \lambda_1 \frac{\partial}{\partial t} \right) \frac{\partial p}{\partial y} \\ + \mu \left( 1 + \lambda_2 \frac{\partial}{\partial t} \right) \left[ \nabla^2 v_y + \frac{1}{3} \frac{\partial}{\partial y} (\nabla \cdot \mathbf{V}) \right]. & \end{aligned} \quad (10.3)$$

The appropriate boundary conditions are

$$v_x = \mp A \frac{\partial v_x}{\partial y} \quad \text{at } y = \pm (d + \eta), \quad (\text{slip boundary condition}), \quad (10.4)$$

$$v_y = \pm \frac{\partial \eta}{\partial t} \quad \text{at } y = \pm (d + \eta), \quad (\text{no permeability condition}), \quad (10.5)$$

$$\begin{aligned} \left( 1 + \lambda_1 \frac{\partial}{\partial t} \right) \frac{\partial}{\partial x} L &= - \left( 1 + \lambda_1 \frac{\partial}{\partial t} \right) \left[ \rho \left( \frac{\partial v_x}{\partial t} + v_x \frac{\partial v_x}{\partial x} + v_y \frac{\partial v_x}{\partial y} \right) \right] \\ + \mu \left( 1 + \lambda_2 \frac{\partial}{\partial t} \right) \left[ \frac{\partial^2 v_x}{\partial x^2} + \frac{\partial^2 v_x}{\partial y^2} + \frac{1}{3} \frac{\partial}{\partial x} \left( \frac{\partial v_x}{\partial x} + \frac{\partial v_y}{\partial y} \right) \right] & \quad \text{at } y = \pm (d + \eta), \end{aligned} \quad (10.6)$$

Here  $\rho$  is the fluid density,  $\mu$  is the dynamic viscosity,  $t$  is the time,  $\lambda_1$  is the relaxation time,  $\lambda_2$  is the retardation time. The characteristic response of the fluid to a compression is described as [103]

$$\frac{1}{\rho} \frac{\partial \rho}{\partial p} = k_c,$$

where  $k_c$  is the compressibility of the liquid. The solution of the above equation for the density

as a function of pressure is given by

$$\rho = \rho_o \exp(k_c(p - p_c))$$

in which  $\rho_o$  is the (constant) density at the reference pressure  $p_c$ .

We now non-dimensionalize the relevant equations by introducing the following quantities

$$\begin{aligned} x^* &= \frac{x}{d}, \quad y^* = \frac{y}{d}, \quad v_x^* = \frac{v_x}{c}, \quad v_y^* = \frac{v_y}{c}, \quad \rho^* = \frac{\rho}{\rho_o}, \quad t^* = \frac{ct}{d}, \\ \eta^* &= \frac{\eta}{d}, \quad p^* = \frac{p}{\rho_o c^2}, \quad p_c^* = \frac{p_c}{\rho_o c^2}, \quad R = \frac{\rho_o c d}{\mu}, \quad \epsilon = \frac{a}{d}, \\ T^* &= \frac{T d \rho_o}{\mu^2}, \quad D^* = \frac{D d}{\mu}, \quad B^* = \frac{B d \rho_o}{\mu^2}, \quad K^* = \frac{K d^3 \rho_o}{\mu^2}, \\ m^* &= \frac{m}{d \rho_o}, \quad \lambda_1^* = \frac{c}{d} \lambda_1, \quad \lambda_2^* = \frac{c}{d} \lambda_2. \end{aligned}$$

The non-dimensional equations now are presented as

$$\rho = \exp(\chi(p - p_c)), \tag{10.7}$$

$$\frac{\partial \rho}{\partial t} + v_x \frac{\partial \rho}{\partial x} + v_y \frac{\partial \rho}{\partial y} + \rho \left( \frac{\partial v_x}{\partial x} + \frac{\partial v_y}{\partial y} \right) = 0, \tag{10.8}$$

$$\begin{aligned} &\left( 1 + \lambda_1 \frac{\partial}{\partial t} \right) \left[ \rho \left( \frac{\partial v_x}{\partial t} + v_x \frac{\partial v_x}{\partial x} + v_y \frac{\partial v_x}{\partial y} \right) \right] = - \left( 1 + \lambda_1 \frac{\partial}{\partial t} \right) \frac{\partial p}{\partial x} \\ &+ \left( 1 + \lambda_2 \frac{\partial}{\partial t} \right) \left[ \frac{1}{R} \nabla^2 v_x + \frac{1}{3R} \frac{\partial}{\partial x} \left( \frac{\partial v_x}{\partial x} + \frac{\partial v_y}{\partial y} \right) \right], \end{aligned} \tag{10.9}$$

$$\begin{aligned} &\left( 1 + \lambda_1 \frac{\partial}{\partial t} \right) \left[ \rho \left( \frac{\partial v_y}{\partial t} + v_x \frac{\partial v_y}{\partial x} + v_y \frac{\partial v_y}{\partial y} \right) \right] = - \left( 1 + \lambda_1 \frac{\partial}{\partial t} \right) \frac{\partial p}{\partial y} \\ &+ \left( 1 + \lambda_2 \frac{\partial}{\partial t} \right) \left[ \frac{1}{R} \nabla^2 v_y + \frac{1}{3R} \frac{\partial}{\partial y} \left( \frac{\partial v_x}{\partial x} + \frac{\partial v_y}{\partial y} \right) \right], \end{aligned} \tag{10.10}$$



$$v_x = \mp k_n \frac{\partial v_x}{\partial y} \quad \text{at } y = \pm(1 + \eta),$$

$$v_y = \pm \frac{\partial \eta}{\partial t} \quad \text{at } y = \pm(1 + \eta), \quad \eta = [\epsilon \cos(\alpha(x - t))], \quad (10.11)$$

$$\left(1 + \lambda_1 \frac{\partial}{\partial t}\right) \frac{\partial}{\partial x} \left[ m \frac{\partial^2}{\partial t^2} + \frac{d}{R} \frac{\partial}{\partial t} + \frac{B}{R^2} \frac{\partial^4}{\partial x^4} - \frac{T}{R^2} \frac{\partial^2}{\partial x^2} + \frac{K}{R^2} \right] \eta$$

$$= \left(1 + \lambda_2 \frac{\partial}{\partial t}\right) \left[ \frac{1}{R} \left( \frac{\partial^2 v_x}{\partial x^2} + \frac{\partial^2 v_x}{\partial y^2} \right) + \frac{1}{3R} \frac{\partial}{\partial x} \left( \frac{\partial v_x}{\partial x} + \frac{\partial v_y}{\partial y} \right) \right]$$

$$- \left(1 + \lambda_1 \frac{\partial}{\partial t}\right) \left[ \rho \left( \frac{\partial v_x}{\partial t} + v_x \frac{\partial v_x}{\partial x} + v_y \frac{\partial v_x}{\partial y} \right) \right] \quad \text{at } y = \pm(1 + \eta), \quad (10.12)$$

in which the asterisks have been suppressed for simplicity.

## 10.2 Solution development

In the case of constant pressure gradient, the solution of Eq. (10.9) for steady flow is

$$u_0(y) = -\frac{R}{2} \frac{\partial p_0}{\partial x} (1 + 2k_n - y^2) \quad (10.13)$$

and for no-slip condition, we have  $k_n \rightarrow 0$  and so

$$u_0(y) = -\frac{R}{2} \frac{\partial p_0}{\partial x} (1 - y^2)$$

In perturbation solution, we have

$$P = \epsilon p_1 + \epsilon^2 p_2 + \dots,$$

$$v_x = \epsilon u_1 + \epsilon^2 u_2 + \dots,$$

$$v_y = \epsilon v_1 + \epsilon^2 v_2 + \dots,$$

$$\rho = 1 + \epsilon \rho_1 + \epsilon^2 \rho_2 + \dots, \quad (10.14)$$

Substituting Eq. (10.14) into Eqs. (10.7) – (10.12) and then taking into account

$$\begin{aligned}
u_1(x, y, t) &= U_1(y) e^{\iota\alpha(x-t)} + \bar{U}_1(y) e^{-\iota\alpha(x-t)}, \\
u_1(x, y, t) &= V_1(y) e^{\iota\alpha(x-t)} + \bar{V}_1(y) e^{-\iota\alpha(x-t)}, \\
p_1(x, y, t) &= P_1(y) e^{\iota\alpha(x-t)} + \bar{P}_1(y) e^{-\iota\alpha(x-t)}, \\
\rho_1(x, y, t) &= \chi P_1(y) e^{\iota\alpha(x-t)} + \chi \bar{P}_1(y) e^{-\iota\alpha(x-t)},
\end{aligned} \tag{10.15}$$

$$\begin{aligned}
u_2(x, y, t) &= U_{20}(y) + U_2(y) e^{2\iota\alpha(x-t)} + \bar{U}_2(y) e^{-2\iota\alpha(x-t)}, \\
v_2(x, y, t) &= V_{20}(y) + V_2(y) e^{2\iota\alpha(x-t)} + \bar{V}_2(y) e^{-2\iota\alpha(x-t)}, \\
p_2(x, y, t) &= P_{20}(y) + P_2(y) e^{2\iota\alpha(x-t)} + \bar{P}_2(y) e^{-2\iota\alpha(x-t)}, \\
\rho_2(x, y, t) &= D_{20}(y) + \chi D_2(y) e^{2\iota\alpha(x-t)} + \chi \bar{D}_2(y) e^{-2\iota\alpha(x-t)},
\end{aligned} \tag{10.16}$$

one has the following set of equations from the  $O(\epsilon)$  system as

$$-\gamma P_1(y) - \frac{\iota}{\alpha} (U_1''(y) - \beta^2 U_1(y)) = 0, \tag{10.17}$$

$$\begin{aligned}
-\iota\alpha(1 - \iota\alpha\lambda_1) V_1(y) &= -(1 - \iota\alpha\lambda_1) P_1'(y) + \frac{(1 - \iota\alpha\lambda_2)}{R} (V_1''(y) - \alpha^2 V_1(y)) \\
&+ \frac{(1 - \iota\alpha\lambda_2)}{3R} (V_1''(y) + \iota\alpha U_1'(y)),
\end{aligned} \tag{10.18}$$

$$(V_1''(y) - \beta^2 V_1(y)) = \gamma P_1'(y), \tag{10.19}$$

$$U_1(\pm 1) = \mp k_n U_1'(\pm 1), \quad V_1(\pm 1) = \mp \frac{\iota\alpha}{2}, \tag{10.20}$$

$$\begin{aligned}
(1 - \iota\alpha\lambda_2) U_1''(\pm 1) - \left[ \alpha^2 (1 - \iota\alpha\lambda_2) - \iota\alpha (1 - \iota\alpha\lambda_1) R + \frac{\alpha^2}{3} (1 - \iota\alpha\lambda_2) \right] U_1(\pm 1) \\
+ \frac{\iota\alpha}{3} (1 - \iota\alpha\lambda_2) V_1'(\pm 1) = (1 - \iota\alpha\lambda_1) R\delta,
\end{aligned} \tag{10.21}$$

$$\delta = -\frac{\iota\alpha}{2R^2} (-\alpha^2 T + \alpha^2 R^2 m + \iota\alpha R d - \alpha^4 B - K).$$

The  $O(\epsilon^2)$  system yields

$$-P'_{20}(y) + \frac{4}{3R}V''_{20}(y) = F(y), \quad U''_{20}(y) = RJ(y), \quad (10.22)$$

$$V'_{20}(y) = -\chi H(y), \quad D_{20}(y) = \chi P_{20}(y) + \chi^2 P_1(y) \bar{P}_1(y),$$

$$F(y) = \iota\alpha\chi P_1(y) \bar{V}_1(y) - \iota\alpha\chi \bar{P}_1(y) V_1(y) + V_1(y) \bar{V}'_1(y) + V'_1(y) \bar{V}_1(y) + \iota\alpha \bar{U}_1(y) V_1(y) - \iota\alpha U_1(y) \bar{V}_1(y), \quad (10.23)$$

$$J(y) = (\bar{U}_1(y) V_1(y) + U_1(y) \bar{V}_1(y))', \quad H(y) = (\bar{P}_1(y) V_1(y) + P_1(y) \bar{V}_1(y))',$$

$$U_{20}(\pm 1) \pm \frac{1}{2} [U'_1(\pm 1) + \bar{U}'_1(\pm 1)] = \mp k_n \left[ U'_{20}(\pm 1) \pm \frac{1}{2} (U''_1(\pm 1) + \bar{U}''_1(\pm 1)) \right], \quad (10.24)$$

$$V_{20}(\pm 1) \pm \frac{1}{2} [V'_1(\pm 1) + \bar{V}'_1(\pm 1)] = 0. \quad (10.25)$$

The solutions of Eqs. (10.17) – (10.21) after omitting details of calculations can be expressed as follows:

$$U_1(y) = j_1 C_1 \cosh \nu y + j_2 C_2 \cosh \beta y + \chi C_3, \quad (10.26)$$

$$V_1(y) = C_1 \sinh \nu y + C_2 \sinh \beta y, \quad (10.27)$$

$$C_1 = -R\delta \left( \frac{1 - \iota\alpha\lambda_1}{1 - \iota\alpha\lambda_2} \right) \frac{j_2 g_2}{G},$$

$$C_2 = R\delta \left( \frac{1 - \iota\alpha\lambda_1}{1 - \iota\alpha\lambda_2} \right) \frac{j_1 g_1}{G}, \quad C_3 = 0,$$

$$G = j_1 g_1 h_2 - j_2 g_2 h_1, \quad j_1 = \frac{\iota\alpha}{\nu}, \quad j_2 = \frac{\iota\beta}{\alpha}, \quad \nu^2 = \beta^2 - \frac{\beta^2 - \alpha^2}{\Gamma},$$

$$g_1 = \cosh \nu + k_n \nu \sinh \nu, \quad g_2 = \cosh \beta + k_n \beta \sinh \beta,$$

$$h_1 = \left[ \frac{\iota\alpha\nu}{3} + j_1 (\nu^2 - \omega) \right] \cosh \nu, \quad h_2 = \left[ \frac{\iota\alpha\beta}{3} + j_2 (\beta^2 - \omega) \right] \cosh \beta,$$

$$\omega = \frac{4\alpha^2}{3} - \iota\alpha R \left( \frac{1 - \iota\alpha\lambda_1}{1 - \iota\alpha\lambda_2} \right), \quad \Gamma = 1 - \frac{\iota\alpha\chi}{\gamma}, \quad \beta^2 = \alpha^2 - \iota\alpha R \left( \frac{1 - \iota\alpha\lambda_1}{1 - \iota\alpha\lambda_2} \right).$$

The solution of Eqs. (10.22) – (10.25) are developed as follows:

$$V_{20}(y) = -\chi (\bar{P}_1(y) V_1(y) + P_1(y) \bar{V}_1(y)) + D_1, \quad (10.28)$$

$$U_{20}(y) = RE(y) + D_2y + D_3, \quad (10.29)$$

$$P_{20}(y) = -\frac{4}{3R}\chi H(y) + D_4 - \int_{-1}^y F(r) dr, \quad (10.30)$$

$$D_1 = 0, \quad D_4 = P_{20}(-1) + \frac{4}{3R}\chi H(-1), \bar{\beta}$$

$$D_2 = -\frac{1}{2(k_n + 1)} \{k_n [R(g(1) + g(-1)) + \beta_3 + \beta_4] + R[E(1) - E(-1)] + \beta_1 - \beta_2\},$$

$$D_3 = -\frac{1}{2} \{k_n [R(g(1) - g(-1)) + \beta_3 - \beta_4] + R[E(1) + E(-1)] + \beta_1 + \beta_2\},$$

$$\beta_1 = \frac{1}{2} [U_1'(1) + \bar{U}_1'(1)], \quad \beta_2 = -\frac{1}{2} [U_1'(-1) + \bar{U}_1'(-1)],$$

$$\beta_3 = \frac{1}{2} [U_1''(1) + \bar{U}_1''(1)], \quad \beta_4 = -\frac{1}{2} [U_1''(-1) + \bar{U}_1''(-1)],$$

$$g(y) = \bar{U}_1(y) V_1(y) + U_1(y) \bar{V}_1(y),$$

$$\begin{aligned} E(y) = & j_1 C_1 \bar{C}_1 \left[ \frac{\cosh[(\bar{\nu} + \nu)y]}{(\bar{\nu} + \nu)} + \frac{\cosh[(\bar{\nu} - \nu)y]}{(\bar{\nu} - \nu)} \right] + j_2 \bar{C}_1 C_2 \left[ \frac{\cosh[(\bar{\nu} + \beta)y]}{(\bar{\nu} + \beta)} + \frac{\cosh[(\bar{\nu} - \beta)y]}{(\bar{\nu} - \beta)} \right] \\ & + j_1 C_1 \bar{C}_2 \left[ \frac{\cosh[(\bar{\beta} + \nu)y]}{(\bar{\beta} + \nu)} + \frac{\cosh[(\bar{\beta} - \nu)y]}{(\bar{\beta} - \nu)} \right] + j_2 \bar{C}_2 C_2 \left[ \frac{\cosh[(\bar{\beta} + \beta)y]}{(\bar{\beta} + \beta)} + \frac{\cosh[(\bar{\beta} - \beta)y]}{(\bar{\beta} - \beta)} \right] \\ & + \bar{j}_1 C_1 \bar{C}_1 \left[ \frac{\cosh[(\nu + \bar{\nu})y]}{(\nu + \bar{\nu})} + \frac{\cosh[(\nu - \bar{\nu})y]}{(\nu - \bar{\nu})} \right] + \bar{j}_2 C_1 \bar{C}_2 \left[ \frac{\cosh[(\nu + \bar{\beta})y]}{(\nu + \bar{\beta})} + \frac{\cosh[(\nu - \bar{\beta})y]}{(\nu - \bar{\beta})} \right] \\ & + \bar{j}_1 C_1 C_2 \left[ \frac{\cosh[(\beta + \bar{\nu})y]}{(\beta + \bar{\nu})} + \frac{\cosh[(\beta - \bar{\nu})y]}{(\beta - \bar{\nu})} \right] + \bar{j}_2 C_2 C_2 \left[ \frac{\cosh[(\beta + \bar{\beta})y]}{(\beta + \bar{\beta})} + \frac{\cosh[(\beta - \bar{\beta})y]}{(\beta - \bar{\beta})} \right] \end{aligned}$$

The axial velocity  $\langle v_x \rangle$  expression is given by

$$\langle v_x \rangle = \epsilon^2 U_{20}(y). \quad (10.31)$$

### 10.3 Graphical results and discussion

This section presents the graphical results in order to discuss the quantitative effects of the sundry parameters involved in the analysis. For this purpose, the mean velocity at the bound-

aries of the channel, the mean-velocity perturbation function, the time-averaged mean axial velocity distribution, the reversal flow and the critical values of the wall tension are calculated for various values of these parameters for the free pumping case ( $\partial p_0/\partial x = 0$ ). The variation of the mean velocity at the boundary  $D_{wall}$  ( $= U_{20}(1)$ ) with the wave number  $\alpha$  is plotted for different values of the compressibility parameter  $\chi$ , Knudsen number  $k_n$ , compliant wall parameters  $d$  and  $T$  and the relaxation  $\lambda_1$  and retardation  $\lambda_2$  times respectively in Figure 10.1(a – f). We observe from Figure 10.1a and Figure 10.1b that the mean velocity at the boundary  $D_{wall}$  increases when the compressibility parameter  $\chi$  and the Knudsen number  $k_n$  are increased. Figure 10.1c depicts that increasing the wall damping  $d$  decreases the mean velocity at the boundary. However it increases when the wall tension  $T$  is increased (Figure 10.1d). Figure 10.1e elucidates the variation of  $D_{wall}$  with  $\alpha$  for various values of the relaxation time  $\lambda_1$ . It is apparent from this Figure that  $D_{wall}$  decreases by increasing the value of relaxation time  $\lambda_1$ . The effect of  $\lambda_2$  on  $D_{wall}$  is quite opposite to that of  $\lambda_1$  on  $D_{wall}$  (Figure 10.1f). The mean-velocity perturbation function  $G(y)$  is defined as [7]

$$G(y) = -\frac{200}{\alpha^2 R^2} [E(y) - E(1)]. \quad (10.32)$$

The mean velocity perturbation function is plotted with  $\alpha$  for the various values of  $\chi$ ,  $k_n$ ,  $\lambda_1$ ,  $\lambda_2$  and  $d$  in Figures 10.2(a – e). It is obvious from these Figures that  $G(y)$  increases by increasing  $d$ ,  $k_n$ , and  $\lambda_1$ . However, it decreases by increasing  $\chi$  and  $\lambda_2$ . It is further noted from these Figures that  $G(y)$  is maximum near the centre of the channel and remains constant over a certain range of  $\alpha$ . Figure 10.3a examines the effects of  $\chi$  on the mean velocity distribution and reversal flow. It is observed that the mean flow first decreases by increasing  $\chi$  but increases when  $\chi \geq 0.5$ . However it increases with an increase in the Knudsen number  $k_n$  (Figure 10.3b). Figures 10.3c and 10.3d describe mean velocity distribution with  $y$  for different compliant wall parameters. Here mean flow decreases when  $d$  increases (Figure 10.3c) whereas it increases by increasing  $K$ . Mean flow also decreases when relaxation time  $\lambda_1$  increases (Figure 10.3e). It is found that the effects of  $\lambda_1$  and  $\lambda_2$  on mean velocity distribution are different (Figure 10.3f). Figures 10.4(a – f) sketched critical value of  $T$ . The critical value increases when there is an increase in  $R$ ,  $\chi$  and  $\lambda_2$ . However, it decreases by increasing  $k_n$  and  $\lambda_1$ . Also the critical value

of  $T$  is very high for small values of the wave number  $\alpha$  in comparison to the large ones. Figure 10.4f shows the variation of the critical values of  $T$  with the compressibility parameter  $\chi$  for different values of the wave number  $\alpha$ . It is observed from this Figure that the critical value of  $T$  decreases when  $\alpha$  is increased.

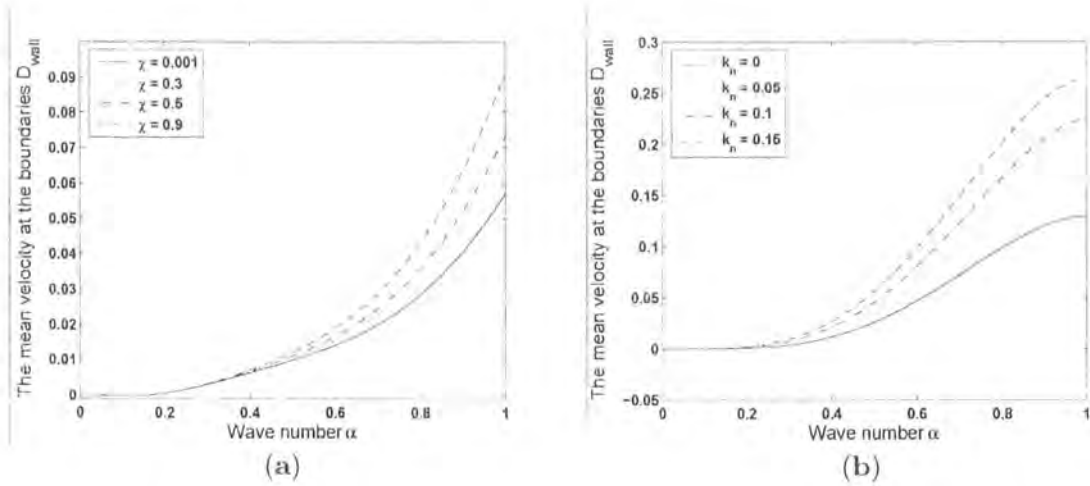


Figure 10.1a: The variation of  $D_{wall}$  with wave number  $\alpha$  for different values of compressibility parameter  $\chi$  when  $m = 0.01$ ,  $d = 0.5$ ,  $B = 2$ ,  $T = 30$ ,  $K = 1$ ,  $k_n = 0.2$ ,  $R = 15$ ,  $\lambda_1 = 1.2$  and  $\lambda_2 = 0.5$ .

Figure 10.1b: The variation of  $D_{wall}$  with wave number  $\alpha$  for different values of Knudsen number  $k_n$  when  $m = 0.01$ ,  $d = 0.05$ ,  $B = 2$ ,  $T = 10$ ,  $K = 0.2$ ,  $\chi = 0.001$ ,  $R = 1$ ,  $\lambda_1 = 0.4$  and  $\lambda_2 = 0.2$ .

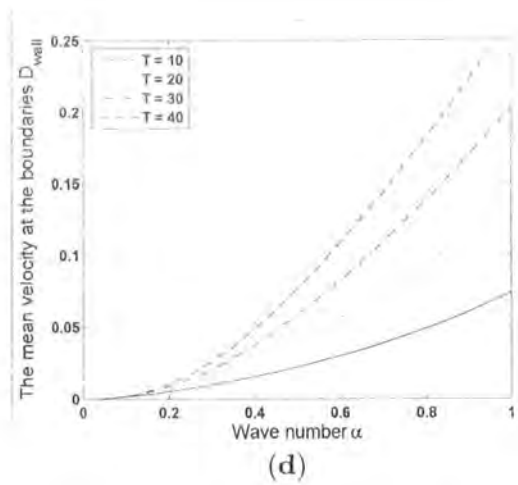
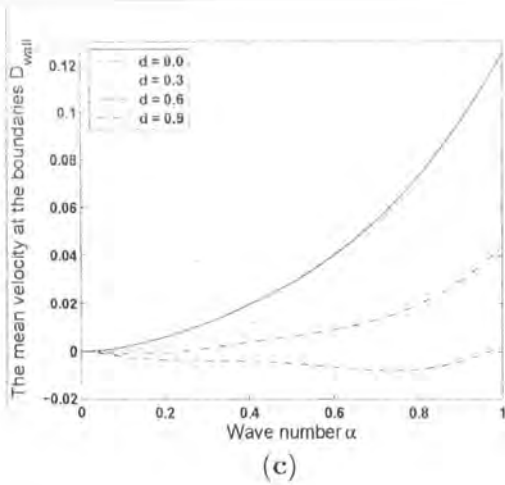


Figure 10.1c: The variation of  $D_{wall}$  with wave number  $\alpha$  for different values of wall damping  $d$  when  $m = 0.01$ ,  $\chi = 0.001$ ,  $B = 2$ ,  $T = 30$ ,  $K = 1$ ,  $k_n = 0.2$ ,  $R = 15$ ,  $\lambda_1 = 1.2$  and  $\lambda_2 = 0.5$ .

Figure 10.1d: The variation of  $D_{wall}$  with wave number  $\alpha$  for different values of wall tension  $T$  when  $m = 0.01$ ,  $d = 0.05$ ,  $B = 2$ ,  $K = 1$ ,  $k_n = 0.2$ ,  $R = 10$ ,  $\chi = 0.001$ ,  $\lambda_1 = 0.7$  and  $\lambda_2 = 0.3$ .

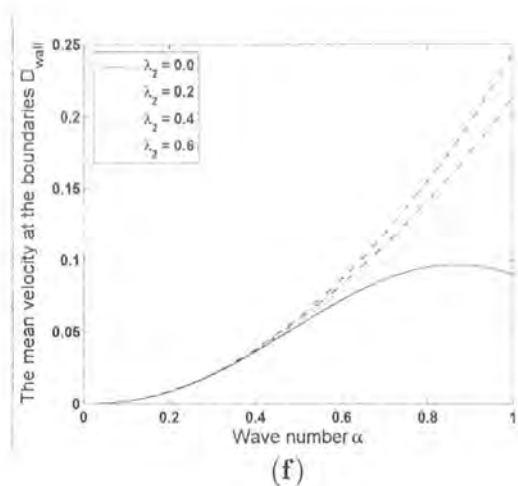
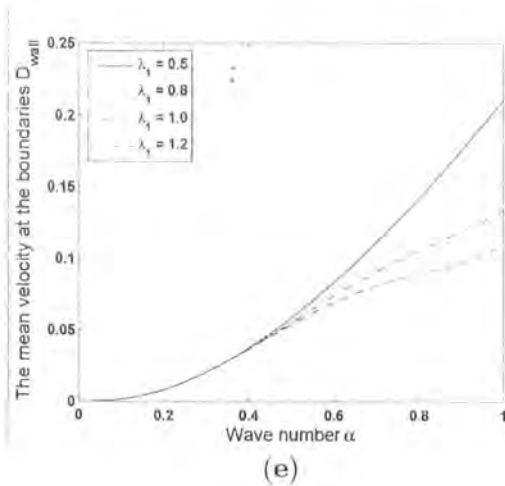


Figure 10.1e: The variation of  $D_{wall}$  with wave number  $\alpha$  for different values of relaxation time  $\lambda_1$  when  $m = 0.01$ ,  $d = 0.05$ ,  $B = 2$ ,  $K = 1$ ,  $T = 30$ ,  $k_n = 0.2$ ,  $R = 10$ ,  $\chi = 0.001$  and  $\lambda_2 = 0.2$ .

Figure 10.1f: The variation of  $D_{wall}$  with wave number  $\alpha$  for different values of retardation time  $\lambda_2$  when  $m = 0.01$ ,  $d = 0.05$ ,  $B = 2$ ,  $K = 1$ ,  $T = 30$ ,  $k_n = 0.2$ ,  $R = 10$ ,  $\chi = 0.001$  and  $\lambda_1 = 0.8$ .

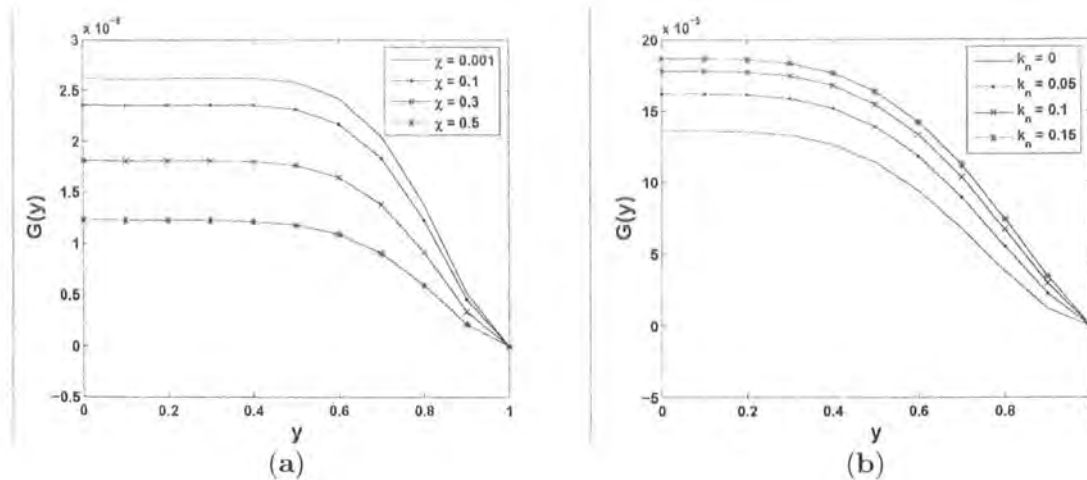


Figure 10.2a: The variation of mean-velocity perturbation function  $G(y)$  for different values of compressibility parameter  $\chi$  when  $m = 0.01$ ,  $\alpha = 0.5$ ,  $d = 0.5$ ,  $B = 2$ ,  $T = 30$ ,  $K = 1$ ,  $k_n = 0$ ,  $R = 100$ ,  $\lambda_1 = 0.7$  and  $\lambda_2 = 0.3$ .

Figure 10.2b: The variation of mean-velocity perturbation function  $G(y)$  for different values of Knudsen number  $k_n$  when  $m = 0.01$ ,  $\alpha = 0.5$ ,  $d = 0.5$ ,  $B = 2$ ,  $T = 10$ ,  $K = 0.1$ ,  $\chi = 0.001$ ,  $R = 10$ ,  $\lambda_1 = 0.7$  and  $\lambda_2 = 0.3$ .



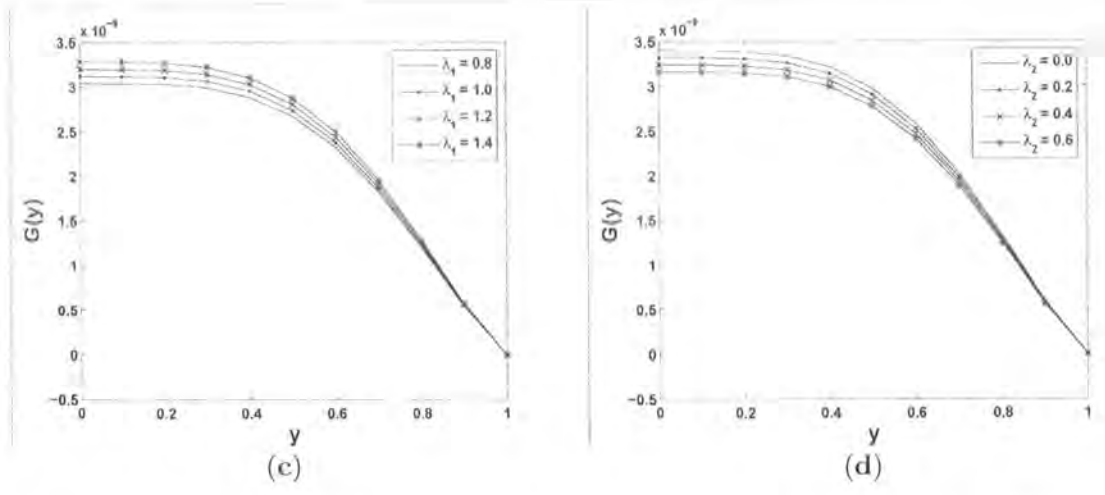


Figure 10.2c: The variation of mean-velocity perturbation function  $G(y)$  for different values of relaxation time  $\lambda_1$  when  $m = 0.01$ ,  $\alpha = 0.1$ ,  $d = 0.5$ ,  $B = 2$ ,  $T = 10$ ,  $K = 1$ ,  $k_n = 0.1$ ,  $R = 100$ ,  $\chi = 0.001$  and  $\lambda_2 = 0.5$ .

Figure 10.2d: The variation of mean-velocity perturbation function  $G(y)$  for different values of retardation time  $\lambda_2$  when  $m = 0.01$ ,  $\alpha = 0.1$ ,  $d = 0.5$ ,  $B = 2$ ,  $T = 10$ ,  $K = 1$ ,  $k_n = 0.1$ ,  $R = 100$ ,  $\chi = 0.001$  and  $\lambda_1 = 1.2$ .

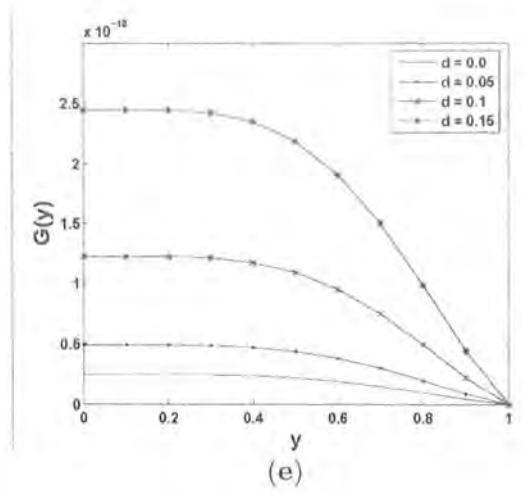


Figure 10.2e: The variation of mean-velocity perturbation function  $G(y)$  for different values of wall damping  $d$  when  $m = 0.01$ ,  $\alpha = 0.1$ ,  $\chi = 0.1$ ,  $B = 2$ ,  $T = 100$ ,  $K = 0.5$ ,  $k_n = 0.1$ ,

$R = 100$ ,  $\lambda_1 = 0.7$  and  $\lambda_2 = 0.4$ .

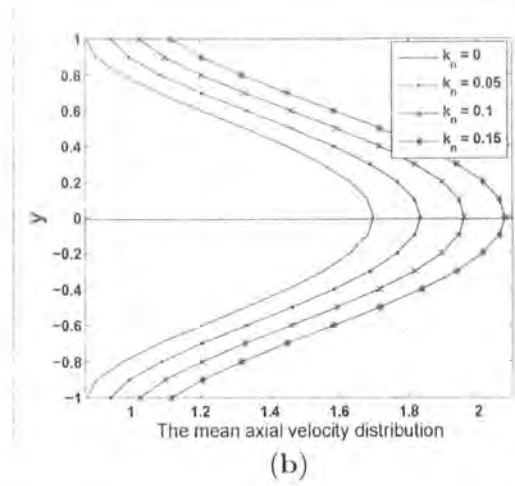
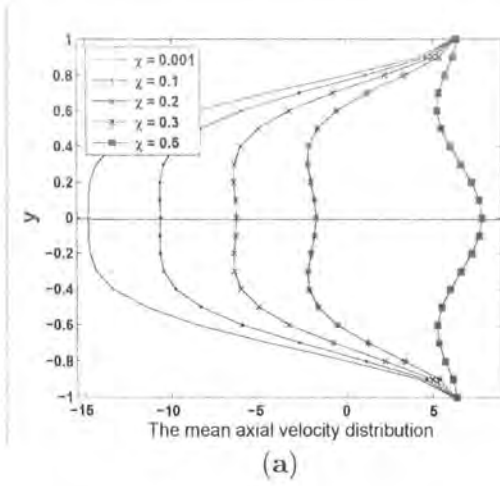


Figure 10.3a: The variation of mean-velocity distribution and reversal flow for different values of compressibility parameter  $\chi$  when  $m = 0.01$ ,  $d = 0.5$ ,  $\alpha = 0.5$ ,  $B = 2$ ,  $T = 10000$ ,  $K = 1$ ,  $k_n = 0$ ,  $R = 20$ ,  $\lambda_1 = 0.7$  and  $\lambda_2 = 0.4$ .

Figure 10.3b: The variation of mean-velocity distribution and reversal flow for different values of Knudsen number  $k_n$  when  $m = 0.01$ ,  $d = 0.1$ ,  $\alpha = 0.5$ ,  $B = 20$ ,  $T = 200$ ,  $K = 1$ ,  $\chi = 0.5$ ,  $R = 5$ ,  $\lambda_1 = 0.7$  and  $\lambda_2 = 0.4$ .

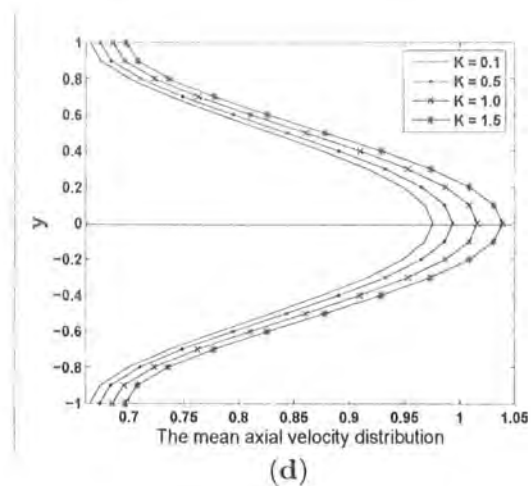
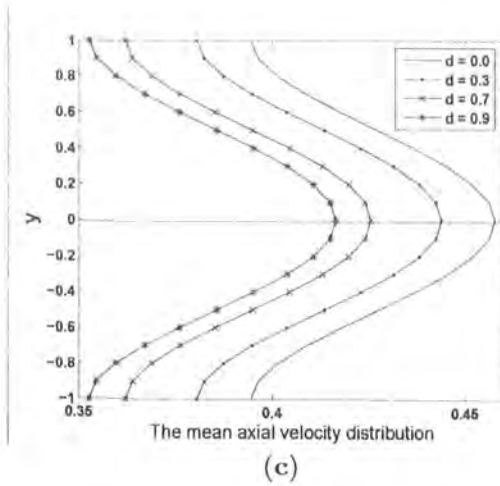


Figure 10.3c: The variation of mean-velocity distribution and reversal flow for different values of wall damping  $d$  when  $m = 0.01$ ,  $k_n = 0$ ,  $\alpha = 0.5$ ,  $B = 20$ ,  $T = 200$ ,  $K = 0.1$ ,  $\chi = 0.5$ ,  $R = 10$ ,  $\lambda_1 = 0.7$  and  $\lambda_2 = 0.4$ .

Figure 10.3d: The variation of mean-velocity distribution and reversal flow for different values of spring stiffness  $K$  when  $m = 0.01$ ,  $k_n = 0$ ,  $\alpha = 0.9$ ,  $B = 20$ ,  $T = 20$ ,  $d = 0.1$ ,  $\chi = 0.5$ ,  $R = 5$ ,  $\lambda_1 = 0.7$  and  $\lambda_2 = 0.4$ .

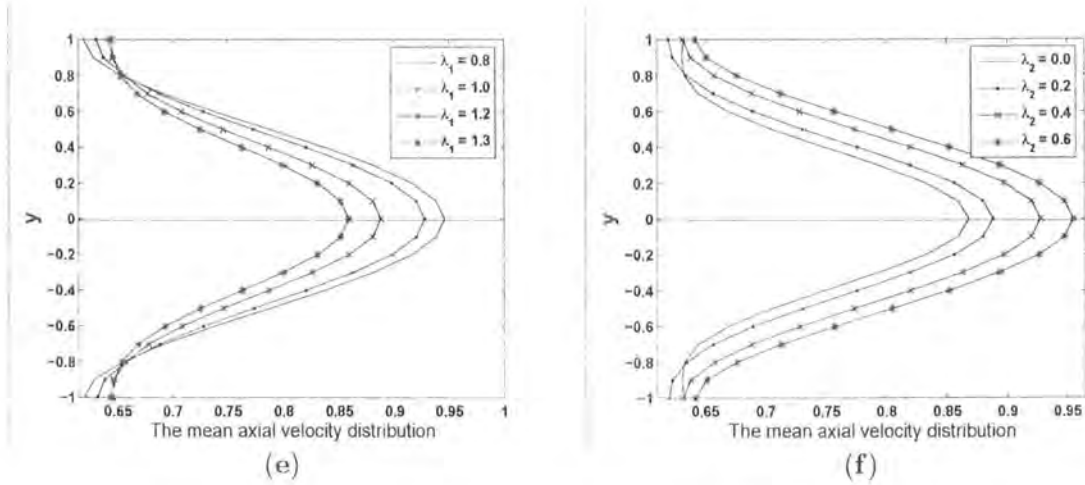
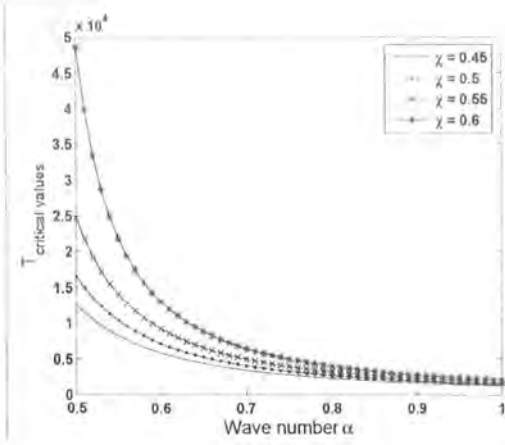
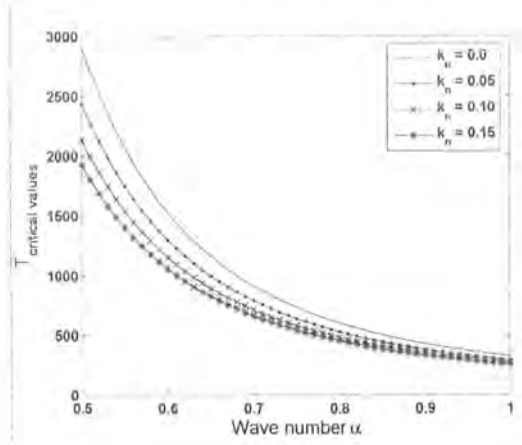


Figure 10.3e: The variation of mean-velocity distribution and reversal flow for different values of relaxation time  $\lambda_1$  when  $m = 0.01$ ,  $\alpha = 0.9$ ,  $d = 0.5$ ,  $B = 20$ ,  $K = 1$ ,  $T = 20$ ,  $k_n = 0$ ,  $R = 5$ ,  $\chi = 0.5$  and  $\lambda_2 = 0.4$ .

Figure 10.3f: The variation of mean-velocity distribution and reversal flow for different values of retardation time  $\lambda_2$  when  $m = 0.01$ ,  $\alpha = 0.9$ ,  $d = 0.5$ ,  $B = 20$ ,  $K = 1$ ,  $T = 20$ ,  $k_n = 0$ ,  $R = 5$ ,  $\chi = 0.5$  and  $\lambda_1 = 1$ .



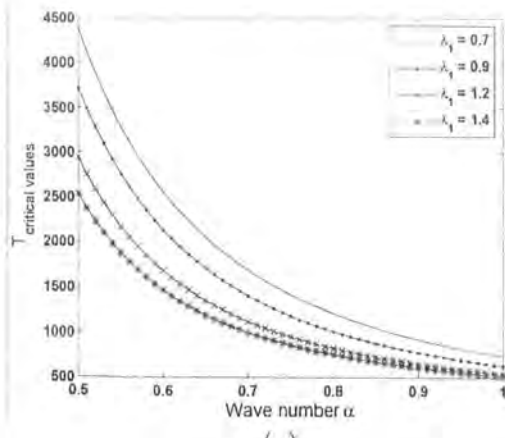
(a)



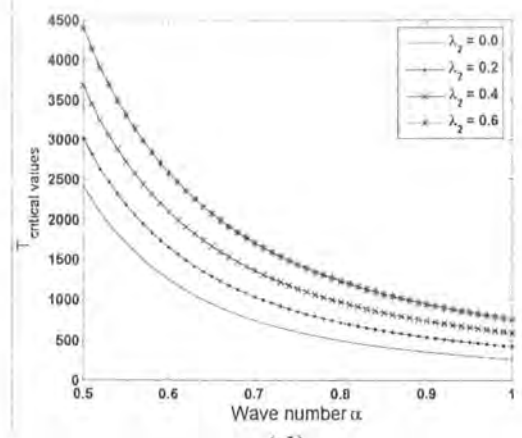
(b)

Figure 10.4a: The variation of critical values of the wall tension  $T$  for different values of compressibility parameter  $\chi$  when  $m = 0.01$ ,  $d = 0.5$ ,  $B = 2$ ,  $K = 1$ ,  $k_n = 0$ ,  $R = 30$ ,  $\lambda_1 = 0.7$  and  $\lambda_2 = 0.4$ .

Figure 10.4b: The variation of critical values of the wall tension  $T$  for different values of Knudsen number  $k_n$  when  $m = 0.01$ ,  $d = 0.5$ ,  $B = 2$ ,  $K = 1$ ,  $\chi = 0.001$ ,  $R = 20$ ,  $\lambda_1 = 0.7$  and  $\lambda_2 = 0.4$ .



(c)



(d)

Figure 10.4c: The variation of critical values of the wall tension  $T$  for different values of

relaxation time  $\lambda_1$  when  $m = 0.01$ ,  $d = 0.5$ ,  $B = 2$ ,  $K = 1$ ,  $k_n = 0$ ,  $R = 30$ ,  $\chi = 0.001$  and  $\lambda_2 = 0.5$ .

Figure 10.4d: The variation of critical values of the wall tension  $T$  for different values of retardation time  $\lambda_2$  when  $m = 0.01$ ,  $d = 0.5$ ,  $B = 2$ ,  $K = 1$ ,  $k_n = 0$ ,  $R = 30$ ,  $\chi = 0.001$  and  $\lambda_1 = 0.8$  and  $\lambda_2 = 0.4$ .

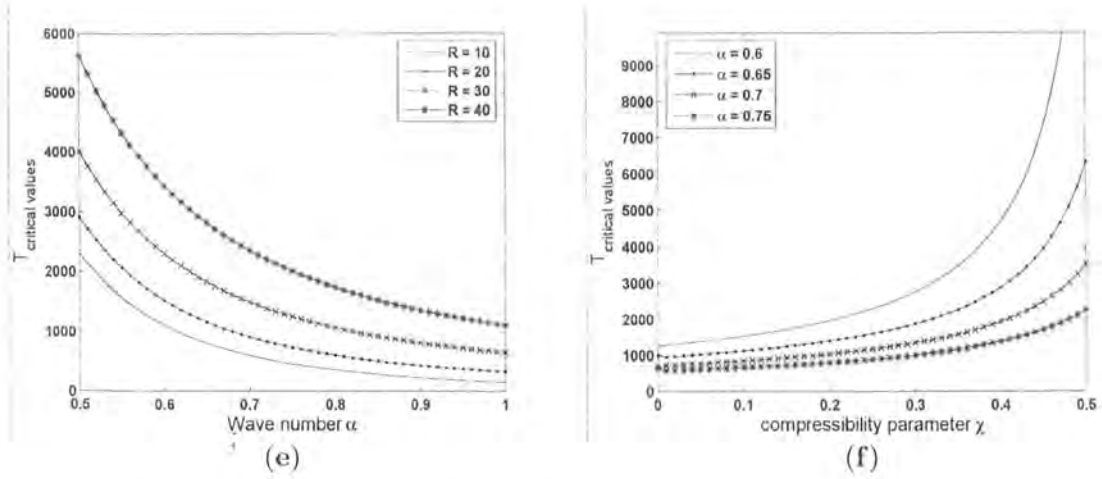


Figure 10.4e: The variation of critical values of the wall tension  $T$  for different values of Reynolds number  $R$  when  $m = 0.01$ ,  $\chi = 0.001$ ,  $B = 2$ ,  $d = 0.5$ ,  $K = 1$ ,  $k_n = 0$ ,  $\lambda_1 = 0.7$  and  $\lambda_2 = 0.4$ .

Figure 10.4f: The variation of critical values of the wall tension  $T$  for different values of wave number  $\alpha$  when  $m = 0.01$ ,  $R = 18$ ,  $B = 2$ ,  $d = 0.5$ ,  $K = 1$ ,  $k_n = 0$ ,  $\lambda_1 = 0.7$  and  $\lambda_2 = 0.3$ .

## 10.4 Conclusions

We have computed the peristaltic flow of a compressible Jeffrey fluid in a channel with compliant walls. The important points are described as follows:

- The constant  $D_{wall}$  decreases with an increase in  $d$  and  $\lambda_1$  and increases by increasing  $\chi$ ,  $k_n$ ,  $T$  and  $\lambda_2$ .
- The mean-velocity perturbation function  $G(y)$  increases by increasing  $d$ ,  $k_n$  and  $\lambda_1$ . How-

ever  $G(y)$  decreases when  $\chi$  and  $\lambda_2$  are increased.

- The mean flow is an increasing function of  $k_n$ ,  $K$  and  $\lambda_2$ . The mean flow decreases by increasing  $\chi$ ,  $d$  and  $\lambda_1$ .
- The results of viscous compressible fluid can be obtained by choosing  $\lambda_1 = \lambda_2 = 0$  [103].

# Bibliography

- [1] F. Kill, The function of the ureter and the renal pelvis. Saunders: Philadelphia (1957).
- [2] S. Boyarsky, Surgical physiology of the renal pelvis, Monogr. Surg. Sci. 1 (1964) 173–213.
- [3] R. C. Graves and T. M. Davidoff, Studies on ureter and bladder, with especial reference to regurgitation of vesical contents, J. Urology 10 (1923) 185 – 231.
- [4] T. W. Latham, Fluid motion in a peristaltic pump, MIT Cambridge MA (1966).
- [5] A. H. Shapiro, Pumping and retrograde diffusion in peristaltic waves, Proceedings. Workshop on ureteral reflux in children, National Academy of Science (Natural Research Council) (1967) 109 – 126.
- [6] J. C. Burns and T. Parkes, Peristaltic motion, J. Fluid Mech. 29 (1967) 731 – 743.
- [7] Y. C. Fung and C. S. Yih, Peristaltic transport, J. Appl. Mech. 35 (1968) 669 – 675.
- [8] A. H. Shapiro, M. Y. Jaffrin and S. L. Wienberg, Peristaltic pumping with long wavelengths at low Reynolds number, J. Fluid Mech. 37 (1969) 799 – 825.
- [9] M. Hanin, The flow through a channel due to transversely oscillating walls, Israel J. Technol. 6 (1968) 67 – 71.
- [10] R. J. Meginniss, An analytic investigation of flow and hemolysis in peristaltic-type blood pumps, Cambridge, MA, Massachusetts Institute of Technology 1970.
- [11] S. L. Weinberg, A theoretical and experimental treatment of peristaltic pumping and its relation to ureteral function, Ph. D Thesis, M. I. T, Cambridge.

- [12] E. C. Eckstein, Experimental and theoretical pressure studies of peristaltic pumping, M. S. Thesis, Department of Mech. Eng., M. I. T, Cambridge.
- [13] T. F. Zein and S. Ostrach, A long wave approximation to peristaltic motion, *J. Biomech.* 3 (1970) 63 – 75.
- [14] Y. C. Fung, Peristaltic pumping; a bioengineering model, published in *Proc. Workshop Hydrodynam. Upper Urinary tract*, National Academy of Science, Washington, D. C. (1971) 177 – 198.
- [15] P. S. Lykoudis, Peristaltic pumping; a bioengineering model, published in *Proc. Workshop Hydrodynam. Upper Urinary tract*. National Academy of Science, Washington, D. C. (1971).
- [16] M. Y. Jaffrin and A. H. Shapiro, Peristaltic pumping, *Ann. Rev. Fluid Mech.* 3 (1971) 13 – 36.
- [17] T. K. Mitra and S. N. Prasad, Interaction of peristaltic motion with Poiseuille flow, *Bull. Math. Bio.* 36 (1974) 127 – 141.
- [18] D. E. Wilson and R. L. Panton, Peristaltic transport due to finite amplitude bending and contraction waves, *J. Fluid Mech.* 90 (1979) 145 – 159.
- [19] C. Barton and S. Raynor, Peristaltic flow in tubes, *Bull. Math. Bio-Phys.* 30 (1968) 663 – 680.
- [20] C. C. Yin and Y. C. Fung, Peristaltic wave in circular cylindrical tubes, *J. Appl. Mech.* 36 (1969) 579 – 587.
- [21] C. H. Li, Peristaltic transport in circular cylindrical tubes, *J. Biomechanics* 3 (1970) 513 – 523.
- [22] T. S. Chow, Peristaltic transport in a circular cylindrical pipe, *Trans. ASME J. Appl. Mech.* 37 (1970) 901 – 906.
- [23] H. S. Lew and Y. C. Fung, A study on the low Reynolds number flow in a valved vessel, *J. Biomechanics* 4 (1971) 85 – 94.



- [24] P. Tong and D. Vawter, An analysis of peristaltic pumping, *J. Appl. Mech.* 39 (1972) 857 – 862.
- [25] M. J. Manton, Long-wavelength peristaltic pumping at low Reynolds number, *J. Fluid Mech.* 68 (1975) 467 – 476.
- [26] B. B. Gupta and V. Seshadri, Peristaltic pumping in non-uniform tubes, *J. Biomechanics* 9 (1976) 105 – 109.
- [27] N. Liron, On peristaltic flow and its efficiency, *Bull. Math. Bio.* 38 (1976) 573 – 596.
- [28] H. J. Rath, Peristaltic flow through a lobe-shaped tube, *Int. J. Mech. Sci.* 24 (1982) 359 – 367.
- [29] L. M. Srivastava and V. P. Srivastava, Interaction of peristaltic flow with pulsatile flow in a circular cylindrical tube, *J. Biomechanics* 18 (1985) 247 – 253.
- [30] C. Pozrikidis, A study of peristaltic flow, *J. Fluid Mech.* 180 (1987) 515 – 527.
- [31] S. Takabatake, K. Ayukawa and A. Mori, Peristaltic pumping in circular cylindrical tubes; a numerical study of fluid transport and its efficiency, *J. Fluid Mech.* 193 (1988) 267 – 283.
- [32] S. Takabatake and K. Ayukawa, Numerical analysis of two-dimensional peristaltic flows, *J. Fluid Mech.* 122 (1982) 439 – 465.
- [33] O. Eytan and D. Elad, Analysis of intrauterine fluid motion induced by uterine contractions, *Bull. Math. Bio.* 61 (1999) 221 – 238.
- [34] M. Mishra and A. R. Rao, Peristaltic transport of a Newtonian fluid in an asymmetric channel, *Z. Angew. Math. Phys.* 54 (2004) 532 – 550.
- [35] A. R. Rao and M. Mishra, Nonlinear and curvature effects on peristaltic flow of a viscous fluid in an asymmetric channel, *Acta Mech.* 168 (2004) 35 – 59.
- [36] Kh. S. Mekheimer, Peristaltic transport of a Newtonian fluid through a uniform and non-uniform annulus, *Arab. J. Sci. Eng.* 30 (2005) 69 – 83.

- [37] K. K. Raju and R. Devanathan, Peristaltic motion of a non-Newtonian, part-I, *Rheol. Acta* 11 (1972) 170 – 178.
- [38] R. G. Devi and R. Devanathan, Peristaltic transport of micropolar fluid, *Proc. Indian Acad. Sci.* 81(A) (1975) 149 – 163.
- [39] G. Radhakrishnamacharya, Long wave length approximation to peristaltic motion of a power law fluid, *Rheol. Acta* 21 (1982) 30 – 35.
- [40] G. Bohme and R. Friedrich, Peristaltic flow of viscoelastic liquids, *J. Fluid Mech.* 128 (1983) 109 – 122.
- [41] L. M. Srivastava and V. P. Srivastava, Peristaltic transport of blood: Casson model II, *J. Biomechanics* 17 (1984) 821 – 829.
- [42] L. M. Srivastava and V. P. Srivastava, Peristaltic transport of a non-Newtonian fluid: Applications to the vas deferens and small intestine, *Ann. Biomedical Eng.* 13(1985) 137 – 153.
- [43] A. M. Siddiqui and W. H. Schwarz, Peristaltic motion of a third order fluid in a planar channel, *Rheol. Acta*, 32 (1993) 47 – 56.
- [44] A. M. Siddiqui and W. H. Schwarz, Peristaltic flow of a second-order fluid in tubes, *J. Non-Newtonian Fluid Mechanics* 53 (1994) 257 – 284.
- [45] S. Usha and A. R. Rao, Peristaltic transport of two-layered power-law fluids, *J. Biomech. Eng.* 119 (1997) 483 – 488.
- [46] E. F. El Shehawey, A. M. El Misery and A. E. H. Abd El Naby, Peristaltic motion of generalized Newtonian fluid in a non-uniform channel, *J. Phys. Soc. Japan* 67 (1998) 434 – 440.
- [47] E. F. El Shehawey and A. M. Sobh, Peristaltic viscoelastic fluid motion in a tube, *Int. J. Math. Sci.* 26 (2001) 21 – 34.
- [48] A. E. Hakeem, A. E. Naby and A. E. M. Misery, Effects of an endoscope and generalized Newtonian fluid on peristaltic motion, *Appl. Math. Comp.* 128 (2002) 19 – 35.

- [49] Kh. S. Mekheimer, Peristaltic transport of a Couple-Stress fluid in a uniform and non-uniform channels, *Biorheology* 39 (2002) 755 – 765.
- [50] T. Hayat, Y. Wang, A. M. Siddiqui and K. Hutter, Peristaltic motion of a Johnson-Segalman fluid in a planar channel, *Math. Prob. Eng.* 1 (2003) 1 – 23.
- [51] T. Hayat, Y. Wang, K. Hutter, S. Asghar and A. M. Siddiqui, Peristaltic transport of an Oldroyd-B fluid in a planar channel, *Math. Prob. Eng.* 4 (2004) 347 – 376.
- [52] K. Vajravelu, S. Sreenadh and V. R. Babu, Peristaltic pumping of a Herschel-Bulkley fluid in a channel, *Appl. Math. Comp.* 169 (2005) 726 – 735.
- [53] K. Vajravelu, S. Sreenadh and V. R. Babu, Peristaltic transport of a Herschel-Bulkley fluid in an inclined tube, *Int. J. Nonlinear Mech.* 40 (2005) 83 – 90.
- [54] M. H. Haroun, Effect of Deborah number and phase difference on peristaltic transport of a third-order fluid in an asymmetric channel, *Comm. Nonlinear Sci. Numer. Simul.* 12 (2007) 1464 – 1480.
- [55] V. K. Stud, G. S. Sephon and R. K. Mishra, Pumping action on blood flow by a magnetic field, *Bull. Math. Bio.* 39 (1977) 385 – 390.
- [56] L. M. Srivastava and R. P. Agrawal, Oscillating flow of a conducting fluid with a suspension of spherical particles, *J. Appl. Mech.* 47 (1980) 196 – 199.
- [57] H. L. Agrawal and B. Anwaruddin, Peristaltic flow of blood in a branch. *Ranchi Univ. Math.* 15 (1984) 111 – 121.
- [58] Kh. S. Mekheimer, Peristaltic flow of blood under effect of a magnetic field in a non-uniform channel, *Appl. Math. Comp.* 153 (2004) 763 – 777.
- [59] E. E. Tzirtzilakis, A mathematical model for blood flow in magnetic field, *Phys. Fluids.* 17 (2005) 077103 – 077117.
- [60] T. Hayat and N. Ali, Peristaltically induced motion of a MHD third grade fluid in a deformable tube, *Physica A.* 370 (2006) 225 – 239.

- [61] M. Kothandapani and S. Srinivas, Peristaltic transport of a Jeffrey fluid under the effect of magnetic field in an asymmetric channel, *Int. J. Nonlinear Mech.* 43 (2008) 915 – 924.
- [62] E. F. El Shehawey, Kh. S. Mekheimer, S. F. Kaldas and N. A. S. Affi, Peristaltic transport through a porous medium, *J. Biomath.* 14 (1999).
- [63] E. F. El Shehawey and S. Z. A. Husseny, Effects of porous boundaries on peristaltic transport through a porous medium, *Acta Mech.* 143 (2000) 165 – 177.
- [64] E. F. El Shehawey, A. M. Sobh and E. M. El Barbary, Peristaltic motion of a generalized Newtonian fluid through a porous medium, *J. Phys. Soc. Japan* 69 (2000) 401 – 407.
- [65] E. F. El Shehawey and S. Z. A. Husseny, Peristaltic transport of magneto-fluid with porous boundaries, *Appl. Math. Comp.* 129 (2002) 421 – 440.
- [66] A. M. Sobh, Peristaltic transport of a magneto-Newtonian fluid through a porous medium, *Int. J. Islamic Uni. Gaza* 12 (2004) 37 – 49.
- [67] T. Hayat, N. Ali and S. Asghar, Hall effects on peristaltic flow of a Maxwell fluid in a porous medium, *Phys. Lett. A* 363 (2007) 397 – 403.
- [68] M. Kothandapani and S. Srinivas, Non-linear peristaltic transport of Newtonian fluid in an inclined asymmetric channel through a porous medium, *Phys. Lett. A* 372 (2008) 1265 – 1276.
- [69] G. Radhakrishnamacharya and V. R. Murty, Heat transfer to peristaltic transport in a non-uniform channel, *Defence Sci. J.* 43 (1993) 275 – 280.
- [70] K. Vajravelu, G. Radhakrishnamacharya and V. Radhakrishnamurty, Peristaltic flow and heat transfer in a vertical porous annulus, with long wave approximation, *Int. J. Nonlinear Mech.* 42 (2007) 754 – 759.
- [71] Kh. S. Mekheimer and Y. Abd Elmaboud, The influence of heat transfer and magnetic field on peristaltic transport of a Newtonian fluid in a vertical annulus: Application of an endoscope, *Phys. Lett. A* 372 (2008) 1657 – 1665.

- [72] S. Srinivas and M. Kothandapani, Peristaltic transport in an asymmetric channel with heat transfer-A note, *Int. Comm. Heat Mass Transfer* 34 (2008) 514 – 522.
- [73] S. Srinivas and R. Gayathri, Peristaltic transport of a Newtonian fluid in a vertical asymmetric channel with heat transfer and porous medium, *Appl. Math. Comp.* 215 (2009) 185 – 196.
- [74] T. Hayat, M. U. Qureshi and Q. Hussain, Effect of heat transfer on the peristaltic flow of an electrically conducting fluid in a porous space, *Appl. Math. Model.* 33 (2009) 1862 – 1873.
- [75] Kh. S. Mekheimer, S. Z. A. Husseny and Y. Abd Elmaboud, Effects of heat transfer and space porosity on peristaltic flow in a vertical asymmetric channel, *Num. Meth. Partial Diff. Eqs.* 26 (2010) 747 – 770.
- [76] T. Hayat, Q. Hussain and N. Ali, Influence of partial slip on the peristaltic flow in a porous medium, *Physica A: Statistical Mechanics and its Applications* 387 (2008) 3399 – 3409.
- [77] N. Ali, Q. Hussain, T. Hayat and S. Asghar, Slip effects on the peristaltic transport of MHD fluid with variable viscosity, *Phys. Lett. A* 372 (2008) 1477 – 1489.
- [78] A. Ebaid, Effects of magnetic field and wall slip conditions on the peristaltic transport of a Newtonian fluid in an asymmetric channel, *Phys. Lett. A* 372 (2008) 4493 – 4499.
- [79] T. Hayat, S. Hina and N. Ali, Simultaneous effects of slip and heat transfer on the peristaltic flow, *Comm. Nonlinear Sci. Numer. Simul* 15 (2010) 1526 – 1537.
- [80] A. Yıldırım and S. A. Sezer, Effects of partial slip on the peristaltic flow of a MHD Newtonian fluid in an asymmetric channel, *Math. Comp. Model.* 52 (2010) 618 – 625.
- [81] H. Sato, T. Kawai, T. Fujita and M. Okabe, Two dimensional peristaltic flow in curved channels, *Trans. Jpn. Soc. Mech. Eng. B* 66 (2000) 679 – 685.
- [82] N. Ali, M. Sajid and T. Hayat, Long wavelength flow analysis in a curved channel, *Z. Naturforsch.* 65a (2010) 191 – 196.

- [83] N. Ali, M. Sajid, T. Javed and Z. Abbas, Heat transfer analysis of peristaltic flow in a curved channel, *Int. J. Heat and Mass Transfer* 53 (2010) 3319 – 3325.
- [84] N. Ali, M. Sajid, Z. Abbas and T. Javed, Non-Newtonian fluid flow induced by peristaltic waves in a curved channel, *European Journal of Mechanics - B/Fluids* 5 (2010) 387 – 394.
- [85] T. K. Mitra and S. N. Prasad, On the influence of wall properties and Poiseuille flow in peristalsis, *J. Biomechanics* 6 (1973) 681 – 693.
- [86] G. Camenschi, The motion of a Newtonian viscous fluid through thin pipe with thin linear elastic wall, *Letters in Appl. Eng. Sc.* 5 (1977) 447 – 455.
- [87] G. Camenschi and N. Sandru, A model of a viscous fluid motion through an axisymmetrical deformable pipe with thin linear elastic wall, *Roum. Math. Pures Et Appl.* 24 (1979) 719 – 724.
- [88] E. O. Carew and T. J. Pedley, An active membrane model for peristaltic pumping: part 1-Periodic activation waves in an infinite tube. *Trans. ASME J. Biomech. Eng.* 119 (1997) 66 – 76.
- [89] C. Davies and P. W. Carpenter, Instabilities in a plane channel flow between compliant walls, *J. Fluid Mech.* 352 (1997) 205 – 243.
- [90] P. Muthu, B. V. Rathish Kumar and P. Chandra, Peristaltic motion in circular cylindrical tubes: Effect of wall properties, *Indian J. Pure Appl. Math.* 32 (2001) 1317 – 1328.
- [91] M. H. Haroun, Effect of wall compliance on peristaltic transport of a Newtonian fluid in an asymmetric channel, *Math. Prob. Eng.* 2006 (2006) 1 – 19.
- [92] G. Radhakrishnamacharya and Ch. Srinivasulu, Influence of wall properties on peristaltic transport with heat transfer, *Comptes Rendus Mécanique* 335 (2007) 369 – 373.
- [93] M. Kothandapani and S. Srinivas, On the influence of wall properties in the MHD peristaltic transport with heat transfer and porous medium, *Phys. Lett. A* 372 (2008) 4586 – 4591.

- [94] P. Muthu, B. V. Rathish Kumar and P. Chandra, Peristaltic motion of micropolar fluid in circular cylindrical tubes: Effect of wall properties, *Appl. Math. Model.* 32 (2008) 2019 – 2033.
- [95] M.A. Abd Elnaby and M. H. Haroun, A new model for study the effect of wall properties on peristaltic transport of a viscous fluid, *Comm. Non-Linear Sci. Numer. Simul.* 13 (2008) 752 – 762.
- [96] N. Ali, T. Hayat and S. Asghar, Peristaltic flow of a Maxwell fluid in a channel with compliant walls, *Chaos Solitons Fractals* 39 (2009) 407 – 416.
- [97] S. Srinivas, R. Gayathri and M. Kothandapani, The influence of slip conditions, wall properties and heat transfer on MHD peristaltic transport, *Comp. Phys. Comm.* 180 (2009) 2115 – 2122.
- [98] T. Hayat and S. Hina, The influence of wall properties on the MHD peristaltic flow of a Maxwell fluid with heat and mass transfer, *Nonlinear Analysis: Real World Applications* 11 (2010) 3155 – 3169.
- [99] T. Hayat, S. Hina and N. Ali, Simultaneous effects of slip and heat transfer on the peristaltic flow, *Comm. Non-Linear Sci. Numer. Simul.* 15 (2010) 1526 – 1537.
- [100] D. Tsiklauri and I. Beresnev, Non-Newtonian effects in the peristaltic flow of a Maxwell fluid, *Phys. Rev. E* 64 (2001) 036303 – 036331.
- [101] T. Hayat, N. Ali and S. Asghar, An analysis of peristaltic transport for flow of a Jeffrey fluid, *Acta Mech.* 193 (2007) 101 – 112.
- [102] E. F. Elshehawey, A. El-Saman, M. El-Shahed and M. Dagher, Peristaltic transport of compressible viscous liquid through a tapered pore, *Appl. Math Comp.* 169 (2005), 526 – 543.
- [103] Kh. S. Mekheimer and A. N. Abdel-Wahab, Effect of wall compliance on compressible fluid transport induced by a surface acoustic wave in a microchannel, *Numerical Methods for Partial Differential Equations* DOI 10.1002/num.20542.